R-10-67

Long Term Sorption Diffusion Experiment (LTDE-SD)

Performance of main *in situ* experiment and results from water phase measurements

Henrik Widestrand, Johan Byegård, Kersti Nilsson,
Susanne Höglund, Erik Gustafsson
Geosigma AB

Magnus Kronberg, Svensk Kärnbränslehantering AB

December 2010

Svensk Kärnbränslehantering AB
Swedish Nuclear Fuel
and Waste Management Co

Box 250, SE-101 24 Stockholm
Phone +46 8 459 84 00

ISSN 1402-3091
SKB R-10-67

Long Term Sorption Diffusion Experiment (LTDE-SD)

Performance of main *in situ* experiment and results from water phase measurements

Henrik Widestrand, Johan Byegård, Kersti Nilsson,
Susanne Höglund, Erik Gustafsson
Geosigma AB

Magnus Kronberg, Svensk Kärnbränslehantering AB

December 2010

Keywords: Crystalline rock, Epoxy, Fractured rock, Matrix rock, Transport properties, Sorption, Diffusion, *In situ* measurements, Modelling, Radionuclides, Tracers, Porosity, Groundwater.

Abstract

The LTDE-SD experiment, (Long Term Sorption Diffusion Experiment) aimed at increasing the scientific knowledge of sorption and diffusion under *in situ* conditions and to provide data for performance and safety assessment calculations. Performance and results of the *in situ* experiment phase are presented in the report. In total, 21 radionuclide trace elements and one stable trace element were injected, circulated and sampled for ~6.5 months in a closed borehole section. The trace elements represented non-sorbing tracers and sorbing tracers for which the sorption was dominated by a cation exchange mechanism, a surface complexation mechanism, or dependent on an electrochemical reduction in order to reach the tetravalent state (oxidation state IV) considered very strongly sorbing. The borehole section in contact with the tracer labelled groundwater consisted in part of a natural fracture surface and a borehole section in the unaltered matrix rock, devoid of natural fractures. Water samples were regularly extracted and analysed for trace element concentration and a few ion exchange speciation and filtered samplings were also conducted. Independent colloid filtering and chemical speciation calculations were performed in support the evaluation.

Sorption was demonstrated for a series of elements present in the experiment. The amounts lost of the different respective tracers from the aqueous phase follow very well the general understanding of the relative sorption strength of the tracers, as inferred from e.g. batch sorption experiments and dynamic *in situ* tracer experiments.

The chemical speciation calculations of the different tracers were in line with the results of the ion exchange speciation performed during the experiment. With the exception of UO_2^{2+} carbonate complexes formed, no strong indications were obtained that aqueous complexation prevents adsorption under the chemical conditions of the experiment.

The 20 nm filtered sampling indicated that radionuclide sorption to colloids in the aqueous phase was of minor importance. Furthermore, the measurements performed after a general colloid filtration showed no significant concentrations of inorganic colloids.

The natural redox conditions were difficult to maintain during the experiment. Therefore the experiment was performed under the oxidizing conditions (E_h ~470 mV) that was obtained during the circulation of the gorundwater. Sorption occurred on equipment during the experiment, in particular for some surface complexation sorbing tracers, possibly due to iron-oxy-hydroxides formed on equipment surfaces. Quantification was made of the amount of sorption on the equipment in order to enable corrections in the evaluation procedures. The sorption occurring for ion-exchange sorbing tracers was concluded to predominately be an effect of interaction with the geologic material since the sorbed amount on the equipment was found to be insignificant.

Natural pressure conditions were maintained throughout the experiment time and consequently penetration into the rock matrix must be considered as a result only of diffusion since no advection could have been involved.

Modelling in order to determine sorption coefficients (K_a, K_d) was performed using a homogeneous porosity sorption-diffusion model using fixed data for porosity and matrix diffusivity from laboratory investigations on LTDE-SD core materials. For the ion-exchange sorbing tracers, the *in situ* evaluated K_d was in the range of the batch sorption results or near the highest values (fracture material) from the batch sorption results. This indicates that a sorption-diffusion model can describe the concentration losses reasonably well for the ion-exchange sorbing tracers. However, due to the sorption on equipment, one should treat these results with care and consider the analysis of the sampled rock material before any definitive conclusions can be made based on the actual penetration profiles of the rock.

Sammanfattning

LTDE-SD-experimentet syftar till att öka den vetenskapliga förståelsen av sorption och diffusion under *in situ*-förhållanden, samt att förse de säkerhetsanalytiska beräkningarna med data. Specifika mål är att erhålla data för processer (sorption och diffusion) för enskilda nuklider på naturliga sprickytor och på innerytor i bergmatrisen, samt att undersöka omfattningen av diffusion in i bergmatrisen under naturliga bergsspänningsförhållande, hydrauliskt tryck och grundvattenkemi.

Innevarande rapport presenterar utförande och resultat från *in situ*-experimentets olika faser. 21 radionuklider samt ett stabilt ämne injicerades som spårämnen, vilka cirkulerade inuti den tillslutna borrhålssektionen och provtogs under ~6,5 månader. Spårämnena bestod av både icke-sorberande ämnen samt olika sorberande ämnen med varierande sorptionsmekanismer (katjonbyte, ytkomplexering samt ett antal spårämnen som är beroende av elektrokemisk reduktion för att nå den starkt sorberande tetravalenta nivån (oxidationstal IV). Den borrhålssektion som stod i kontakt med det spårämnesinjicerade grundvattnet bestod av en isolerad del av en naturlig sprickyta samt en borrhålssektion i det bakomvarande berget vilket representerade det icke omvandlade berget. Vattenprover togs regelbundet ut och analyserades med avseende på spårämeskoncentrationer. Ett antal jonbytesspecieringar liksom provtagningar genom filtrering utfördes också. En oberoende kolloidfiltrering och kemisk specieringsberäkning utfördes för att ge understöd vid utvärdering av resultaten.

Sorption påvisades för ett antal av de spårämnen som användes i experimentet. Förlusterna i vattenfasen för de olika spårämnen överensstämde mycket bra med den allmänna kunskapen om sorptionsstyrkan för spårämnena; kunskap som baseras på t.ex. sorptionsförsök och dynamiska *in situ*-spårförsök.

De kemiska specieringsberäkningarna av de olika spårämnena ligger i linje med resultaten av de jonbytesspecieringar som utfördes under försöket. Med undantag av den beräknade förekomsten av karbonatkomplex av UO_2^{2+}, kunde inga starka indikationer påvisas av att komplexbildning i vattnet förhindrar adsoption under de kemiska förhållandena i experimentet.

Provtagning med 20 nm-filter indikerade att sorption av radionuklider till kolloider i vattenfasen var av mindre betydelse. Den utförda kolloidfiltreringen visade också att den allmänna kolloidkoncentrationen var i ungefärlig nivå med grundvatten i Laxemarområdet vid SKB platsundersökning.

Det visade sig vara svårt att behålla naturliga redox-förhållanden under experimentet. På grund av detta fick experimentet utföras under oxiderande förhållanden (Eh ~470 mV). Det förekom sorption på utrustningen under experimentet, speciellt för vissa ytkomplexerande sorberande spårämnen, vilket förmodligen berodde på järn-oxy-hydroxider som bildats på utrustningens ytor. En kvantifiering av den sorberade mängden på utrustningen utfördes för att möjliggöra korrigeringar under utvärderingsprocessen. Sorptionen av jonbytessorberande spårämnen ansågs dock huvudsakligen vara en effekt helt orsakad av interaktionen med det geologiska materialet, detta eftersom mängden sorberat på utrustningen var obetydlig.

Naturliga tryckförhållanden bibehölls under hela experimenttiden och därför kan inträngning i bergmatrisen betraktas som ett resultat av enbart diffusion eftersom ingen advektion kan ha förekommit.

Modellering i syfte att bestämma sorptionskoefficienter (K_a, K_d) utfördes med hjälp av en sorption-diffusions-modell med homogen porositetsfördelning. I dessa modelleringar användes porositets- och diffusionsdata bestämda i laboratoriemätningarna av kärnmaterial från LTDE-SD. För de jonbytessorberande spårämnena låg de utvärderade *in situ* K_d inom intervallet för batch sorptions-resultaten eller nära de högsta värdena (sprickmaterial) från batch sorptions-resultaten. Detta indikerar att sorption-diffusions-modellen tämligen väl kan beskriva koncentrationsförluster för jonbytessorberande spårämnen. På grund av sorption på utrustning, bör man dock behandla dessa resultat med försiktighet och överväga analys av uttagna prover på bergmaterialet innan några definitiva slutsatser kan göras utifrån de faktiska inträngningsprofilerna i berget.

Acknowledgement

We appreciate the cooperation and help from the radiation protection staff at Clab throughout the course of the project. The good cooperation with the Swedish Research and Defence Institute, CBRN Defence and Security Division including skilful experimental and method development work is gratefully acknowledged.

Finally we are very grateful for the in depth and constructive review that was provided by Bill Wallin, Geokema AB, and Anders Winberg, Conterra AB.

Contents

1 Introduction

The Long Term Sorption Diffusion Experiment (LTDE-SD) is one of the experiments within the Natural Barriers research programme at the SKB Äspö Hard Rock Laboratory (HRL), the goal of which is to increase the scientific knowledge of the safety margins of the final repository for spent nuclear fuel and to provide data for performance and safety assessment calculations.

Transport of radionuclides in water-conducting rock fractures over 5–50 m distances has been studied within the Tracer Retention and Understanding Experiments (TRUE) experimental programme since the late 90's /Winberg et al. 2000, Andersson et al. 2002/. Advection, dispersion, sorption and diffusive mass transfer are relevant processes of which dispersion and diffusive mass transfer can be difficult to distinguish by modelling alone of concentration-time curves.

Because the evaluation of the results of the TRUE experiment /Winberg et al. 2002/ identified diffusion processes as an important retention mechanism, a demand for extended knowledge of diffusion and sorption processes over longer time scales in a controlled rock volume was identified. A sorption-diffusion experiment without advection and dispersion effects, LTDE-SD, was consequently set up. The LTDE-SD experiment aims at increasing knowledge of sorption and diffusion under *in situ* conditions and to provide data for performance and safety assessment calculations, i.e.:

- To obtain data on sorption properties and processes of individual radionuclides on natural fracture surfaces and inner surfaces in the rock matrix.
- To investigate the magnitude and extent of diffusion into matrix rock from a natural fracture *in situ* under natural rock stress and hydraulic pressure and groundwater chemical conditions.
- To compare laboratory derived diffusion constants and sorption coefficients for the investigated rock with the sorption behaviour observed *in situ* at natural conditions, and to evaluate if laboratory scale sorption results are representative also for *in situ* conditions.

The main *in situ* experiment was performed from September 2006 through April 2007. During this time period of ~7 months, radionuclide tracers were circulated, sampled and monitored in the test section of borehole KA3065A03 (see Section 2.1.1). Following the termination of the *in situ* experiment, the target rock volume was over-cored by drilling of a 300 mm diameter borehole which was subsequently sampled, geologically characterised and analysed for trace element concentration profiles within the rock.

A laboratory program was performed in parallel to the *in situ* experiment and the subsequent analysis of the in rock material. The aim of the laboratory experiments was to produce site-specific laboratory derived retention parameters (e.g. diffusivity and sorption distribution coefficients) for which the applicability to the actual *in situ* experiment results later can be tested. The laboratory experiments were performed with material from the exploration borehole KA3065A02, the core of the 36 mm extension borehole and fracture material from the opposite side of the stub surface in KA3065A03. A common tracer solution was prepared and divided for use *in situ* and in the laboratory experiments.

1.1 Scope

This report describes the main experiment with radioactive tracers, which was performed from September 2006 through April 2007. The report is focused on presentation of the performance and analysis results in the form of groundwater tracer concentrations and monitoring of other parameters (such as Eh, pH, pressure etc). The results are evaluated using a surface sorption model and a one-dimensional diffusion-sorption model.

1.2 LTDE-SD-reports

This particular report, R-10-67, constitutes one in a suit of three SKB R-reports presenting the performance, results and conclusions of the LTDE-SD laboratory and *in situ* experiment.

- R-10-66 /Widestrand et al. 2010/. The report covers the performance and results of laboratory sorption and diffusion experiments and porosity investigations, using geologically and mineralogical characterised site-specific crushed and intact rock materials.
- R-10-67, i.e. this report, covers the performance of the main *in situ* experiment and results from water phase measurements. Sorption coefficients were determined from tracer declining concentration time curves by applying a surface sorption model and a one-dimensional diffusion-sorption model.
- R-10-68, /Nilsson et al. 2010/. The report covers the performance and results of over-core drilling of the *in situ* experiment target rock volume, subsequent sampling, geological characterisation and analysis of radionuclide penetration and distribution in the rock. The report is focused on evaluation and modelling of the penetration profiles as well as the distribution of the radionuclides between fracture minerals and matrix rock. Results are compared to sorption and diffusion coefficients determined in the supporting laboratory experiments (R-10-66) and from the water phase measurements (R-10-67) of the *in situ* experiment.

The preparations for the LTDE-SD experiments included geological and hydrogeological characterisation of the site at Äspö HRL, as well as supporting laboratory tests and a functionality test with short lived radionuclides. These preparatory activities are presented in a set of reports.

/Winberg et al. 2003/ describes in detail the geologic features of the rock matrix in the vicinity of the test area. Borehole imaging by BIPS (Borehole Image Processing System) and core logging in the two boreholes were used to correlate fractures in the two holes. The correlation was substantiated by mineralogical and geochemical studies including stable isotopes.

Within the framework of collaboration between SKB and Ontario Power Generation's (OPG) Nuclear Waste Management Division, supporting laboratory experiments on core samples from the LTDE-SD borehole KA3065A03 were performed by /Vilks et al. 2005/. The experimental programme consisted of porosity measurements, diffusion cell experiments, radial diffusion experiments and permeability measurements.

During 2004, *in situ* pre-tests including hydraulic testing (flow logging, interference and pressure build-up tests) and non radioactive tracer tests (dilution test and leakage testing) were performed by /Wass 2005/.

Installation and installation tests of the experimental set up at LTDE-SD were finalized during 2005.

During September to October 2005 a functionality test with short lived radionuclides was conducted /Widestrand et al. 2006/. The functionality test was the final preparation for the main experiment and it showed that concentration-time curves based on sampling and on-line measurements of the radioactivity in the test section could be produced with the experimental set-up used. The successively decreasing concentrations with time for the sorbing tracers showed that sorption processes in the test section could be studied at the LTDE-SD site. Only minor sorption on tubings could be measured for the most strongly sorbing tracers, which indicated that the sorption mainly occurred on the stub and 36 mm section rock surfaces. It was concluded that sampling and on-line measurements complemented each other and that both should be used in the main *in situ* experiment.

1.3 Site overview

The LTDE-SD site is located in the niche NASA 3067A at Äspö HRL tunnel section 3,065 m at a depth of approximately –410 masl, see Figure 1-1. KA3065A03 is the experimental borehole and KA3065A02 served as pilot borehole to find a suitable target structure on which to perform the experiment. A structural model of the target rock volume is shown in Figure 1-2.

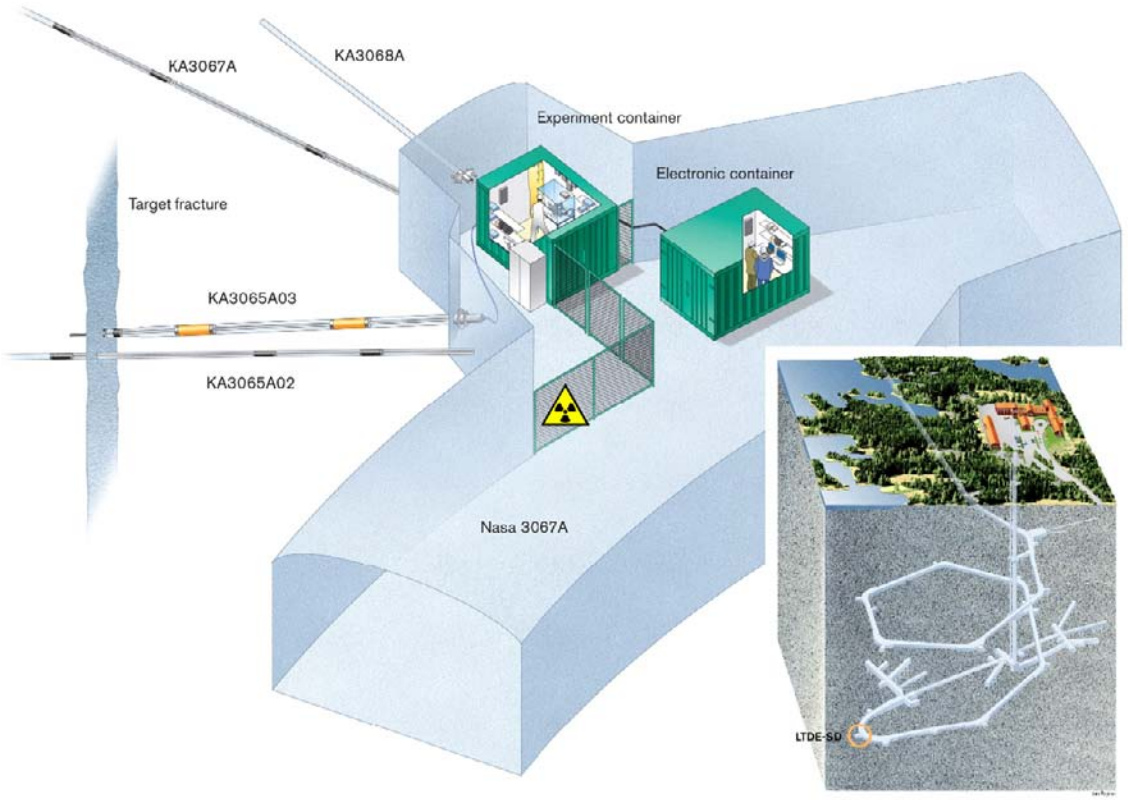

Figure 1-1. *Overview of the niche in the Äspö HRL. The LTDE-SD experimental borehole was KA3065A03 and the pilot borehole was KA3065A02. The area with the experiment container (Container 1) and borehole installations was controlled for radioactivity and fenced off towards the tunnel.*

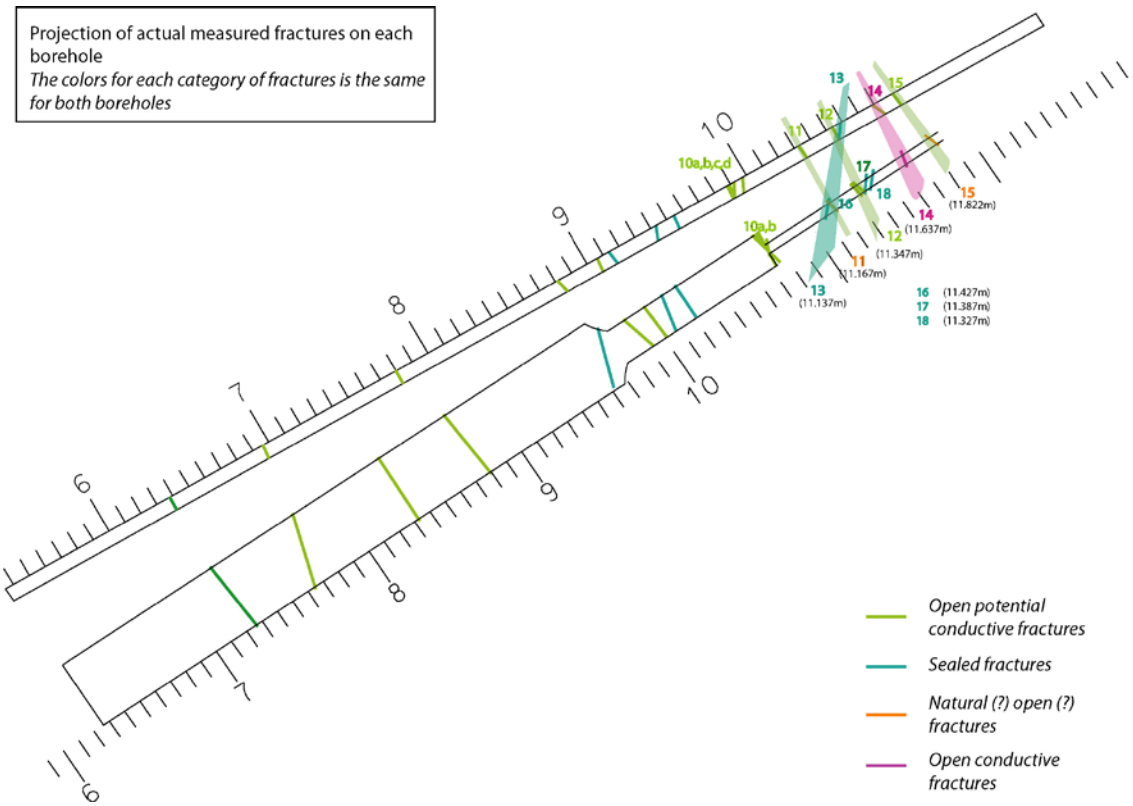

Figure 1-2. *Basic structural model of the LTDE-SD rock volume. The telescoped large diameter (300/197 mm) experimental borehole KA3065A03 is shown with the small diameter (36 mm) extension and the pilot borehole KA3065A02 above /Winberg et al. 2003/.*

The LTDE-SD area is surrounded by two dominant conductive structures, NW-2 and NW-3. The conclusion from the hydraulic pre-tests /Wass 2005/ was that the NW-2, NW-3 and related structures are of vital importance for the hydraulic pressure in the LTDE-SD boreholes, therefore no drilling or opening of boreholes were allowed in these structures during the course of the *in situ* experiment.

The 197 mm drilling of KA3065A03 was stopped ~14 cm behind the target fracture #10 at ~10.7 m depth, leaving a 177 mm diameter "stub" with the fracture surface intact and exposed towards the borehole collar as illustrated in Figure 1-3. In early versions of the test design only the stub itself was planned to be used for the matrix diffusion study. However, to enable studies of the diffusion in non-decompressed rock, without open fractures, a small diameter (36 mm) borehole of approximately one meter length, was drilled in the centre of the stub providing radial access to an essentially non-fractured matrix rock.

The geologic features of the site are described in /Winberg et al. 2003/ and in more detail for the rock relevant for the *in situ* tests in /Widestrand et al. 2010/ and /Nilsson et al. 2010/. The unaltered matrix rock in the experiment section of KA3065A03, as well as rock material from KA3065A03 analyzed by /Vilks et al. 2005/ and from KA306502 reported in /Widestrand et al. 2010/, is interpreted to be Ävrö granodiorite based on mineralogical observations and density data (average 2.66 g/cm^3).

Figure 1-3. *Illustration of the ~14cm long and 177 mm diameter core stub in Ävrö granodiorite exposing a natural fracture surface in borehole KA3065A03. The fracture surface is partly covered by relative thin layers of calcite (white) and chlorite (green) /Nilsson et al. 2010/. The 36 mm borehole is indicated in the centre of the stub. Illustration from /Winberg et al. 2003/.*

2 Performance

2.1 Equipment

2.1.1 Borehole KA3065A03

The experimental set-up consisted of a telescoped large-diameter borehole (KA3065A03) that intercepted a previously identified fracture. Further, the large diameter borehole outside the stub was packed off with mechanical and inflatable packers to avoid effects of the acting hydraulic gradient. A schematic diagram of the packer system used to complete the LTDE-SD borehole installation is shown in Figure 2-1. The experimental setup is illustrated in Figure 2-2 and an expansion of the inner experimental section is given in Figure 2-3.

The exposed part of the fracture was packed off using a special “packer” which sealed around the developed core stub. The packer consisted of a polyurethane rubber cylinder and a polyether ether ketone (PEEK) lid. The PEEK lid was equipped with two 1/8” PEEK tubes for circulation or pressure monitoring. A solution of tracers could thus be injected and circulated in the isolated section between the fracture surface and the PEEK lid, the so-called “stub section”. The aperture between the fracture surface and the PEEK lid was designed to be about 3 mm. In order to achieve the 3 mm distance over the irregular fracture surface, the PEEK lid was manufactured using parallel cutting technique where a gypsum cast of the stub surface in KA3065A03 was used as a model.

A small diameter (36 mm) borehole, approximately one meter long, was drilled in the centre of the stub and a 300 mm section of the small diameter borehole was packed off and installed with a PEEK dummy to minimize the section volume. This section is referred to as the “slim hole section”. The slim hole section and the stub section were connected by a tube so that the two sections constituted the section KA3065A03:1, which hereafter is referred to as the “test section”. The slim hole section was also equipped with a 1/8” PEEK tube for external circulation or pressure monitoring. Consequently, the test section as a whole had three 1/8” tubes of which two could be used for circulation and one for pressure monitoring. The circulation could be switched so that either the full section or only the stub surface was circulated. The stub section was circulated for shorter periods of time according to a routine in order to improve the mixing in this planar section. This was considered more important at early times after the injection than later in the experiment, especially for the more strongly sorbing tracers.

Besides these two experimental sections, a “guard section” was also obtained by isolating the water volume between the sealing and the mechanical packer. This guard section (KA3065A03:2) was aimed for sampling for radioactivity control measurements, i.e. to be able early detect any leakage from the experimental sections.

A collection of photographs showing the borehole installations are presented in Appendix 1.

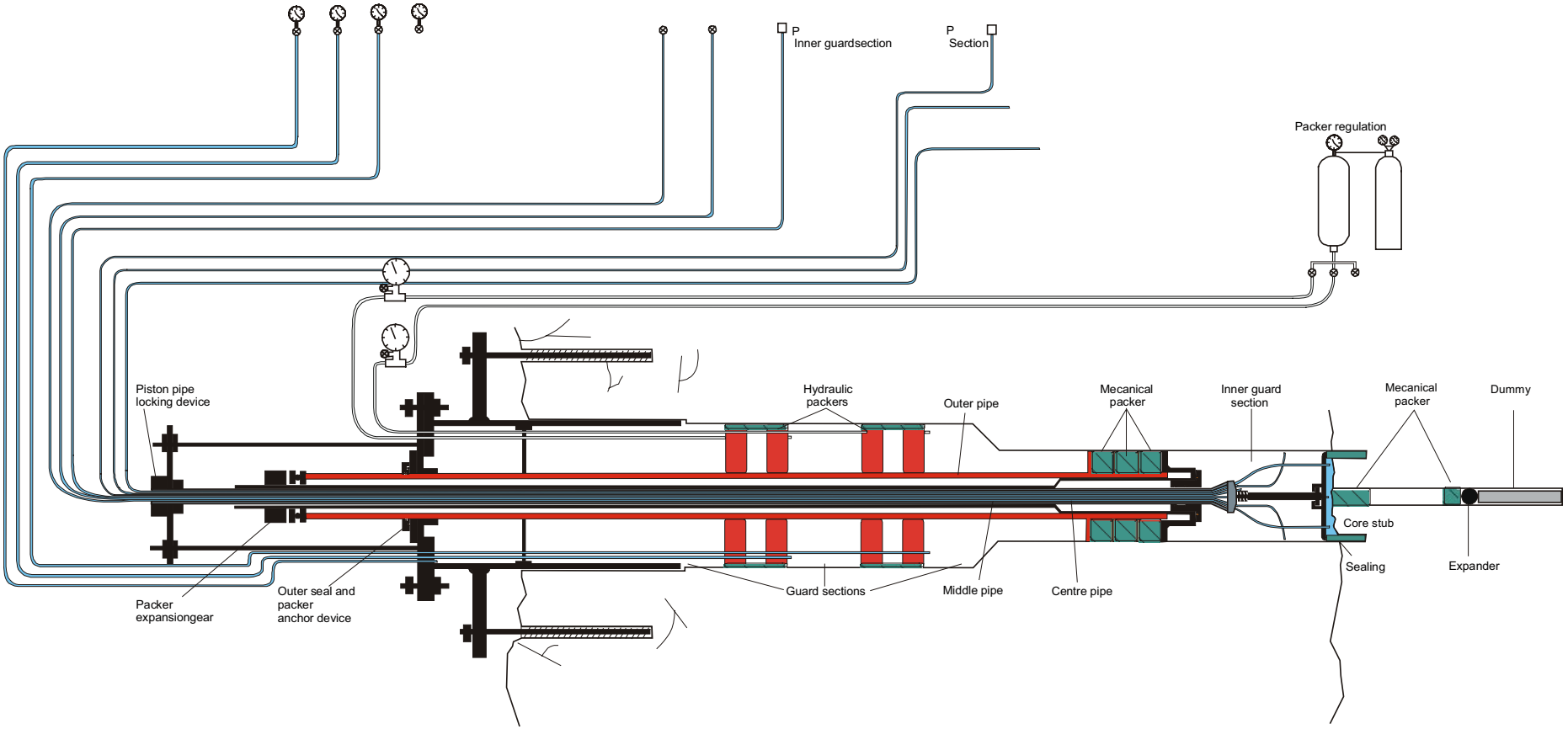

Figure 2-1. *Schematic diagram of the borehole casing and packer system used to complete the LTDE-SD borehole installation in KA3065A03 with 36 mm diameter extension.*

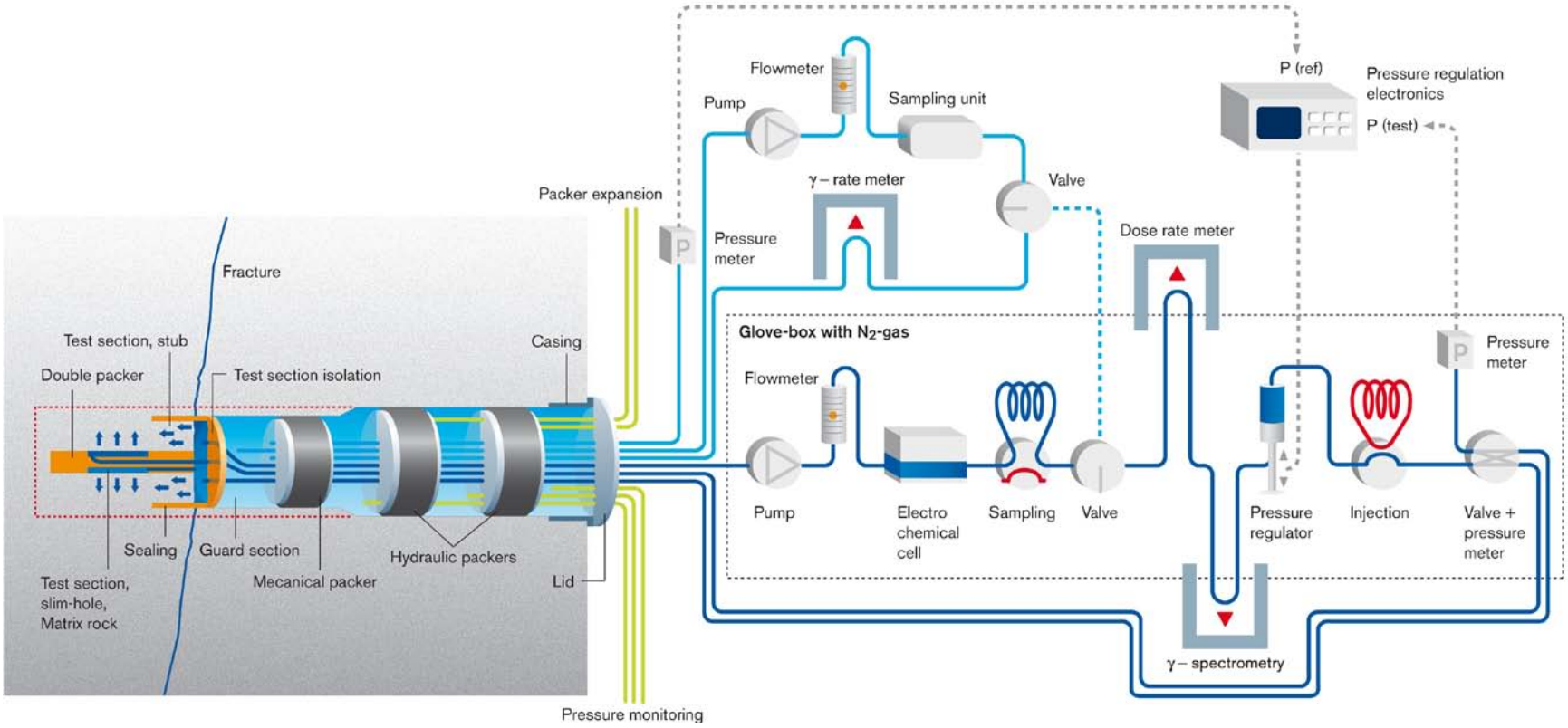

Figure 2-2. *Illustration of borehole instrumentation and test section design in KA3065A03, including circulation equipment, pressure regulation, on-line measurement of γ-emitting tracers, and injection/sampling possibilities. A close-up of the test sections in front of the natural fracture (Test section stub) and in matrix rock (Test section slim-hole) is shown in Figure 2-3.*

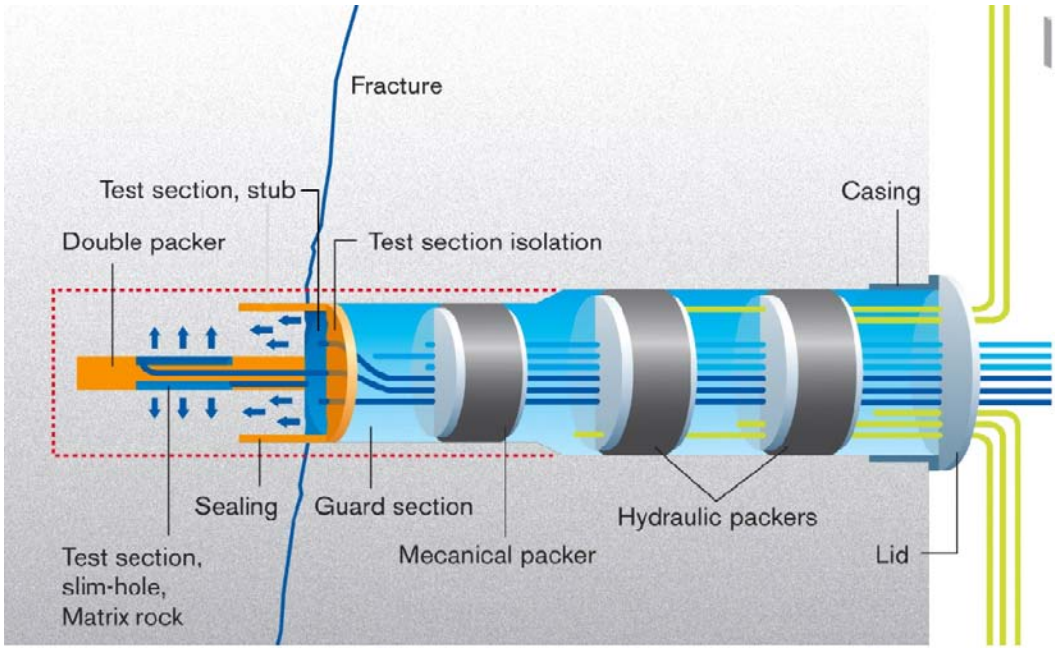

Figure 2-3. *Close-up of borehole instrumentation and test section design in KA3065A03, as presented in Figure 2-2, showing the ~3 mm wide and 177 mm diameter stub section in front of the natural fracture and the 300 mm long and 36 mm diameter slim hole section in matrix rock. The rock volume enclosed by the red dotted line was extracted by over-core drilling at termination of the experiment.*

2.1.2 Circulation equipment in KA3065A03:1 (test section)

All equipment in the circulation system in the test section (section 1) of KA3065A03 such as a magnetically coupled rotor pump (Microtech), inductive flow meter (Promag 33) and on-line measurement of radioactivity and electrochemical flow cell were placed in boxes with a through-flow of nitrogen gas, shown in Figure 2-4 and Figure 2-5. The flow could be regulated in the interval of c. 5–50 ml/min and the experiment was run with a continuous flow of 20–30 ml/min. The boxes were flushed with nitrogen gas of industrial quality (<500 ppm oxygen) in order to reduce the oxygen content in the test section groundwater. Thermoelectric coolers were installed in the inert gas boxes in order to compensate for heat generated by other equipment. All equipment parts in contact with the circulated groundwater were constructed in PEEK material. 3 mm PEEK tubing was used. An illustration of the circulation set-up with connection to the borehole is shown in Figure 2-6.

All equipment parts were attached to the circulation system using 6-port valves in PEEK (Upchurch Scientific, Injection Valve V-540) as shown in Figure 2-6. The flow could be directed through the external unit attached to ports 1 and 4, or it could be by-passed to the next valve according to Figure 2-6. When the valve was in its by-pass position, the external units could be flushed using water from the guard section (Figure 2-2). The flushing was done through ports 2 and 3 in order to fill up and pressurise the unit with groundwater prior to connecting it to the circulation.

2.1.3 On-line monitoring equipment in KA3065A03:1

γ-spectrometry

The radioactivity concentration in the test section groundwater was measured on-line by an HPGe-detector, (GEM10P4, ORTEC, relative efficiency ~10%). This detector failed a couple of days into the main experiment and was replaced (GEM20180P ORTEC, relative efficiency ~20%). The detectors were electrically compressor cooled (XCooler, ORTEC). A digital multi-channel analyser (DigiDart, ORTEC) was connected to a computer through an USB interface. In order to avoid ground loop disturbances, a fibre optic converter (OPTICIS optical USB extension cable M2-100) was placed between the DigiDart and the computer to create a galvanic isolation of the two units. The γ-spectra were collected and analysed using the software GammaVision 5.31 (ORTEC).

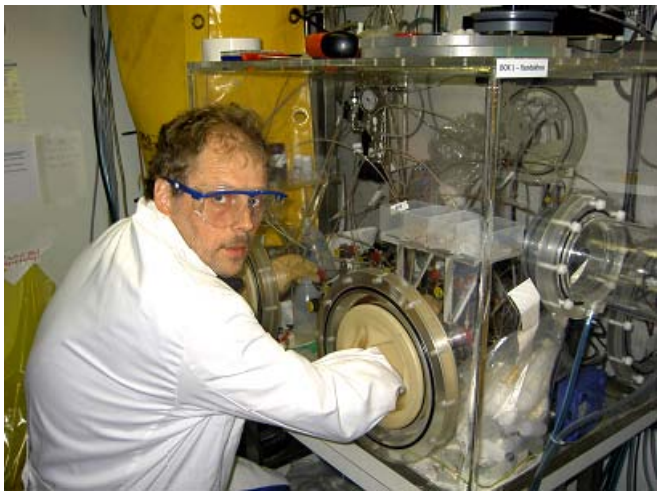

Figure 2-4. *Inert gas glove box for all circulation equipment excluding the pressure regulator which is contained in a separate inert gas box and the dose rate and γ-spectrometry to which tubing loops are mounted in lead shields outside of the glove box.*

Figure 2-5. *Inert gas box for the pressure regulator piston. The pressure regulator consists of a step motor (lower picture) which operates a piston in a PEEK mantled cylinder (upper picture). The motor is controlled by a separate electronic unit. The desired difference pressure between the test section (KA3065A03:1) and the reference section (guard section KA3065A03:2) is set using the control unit.*

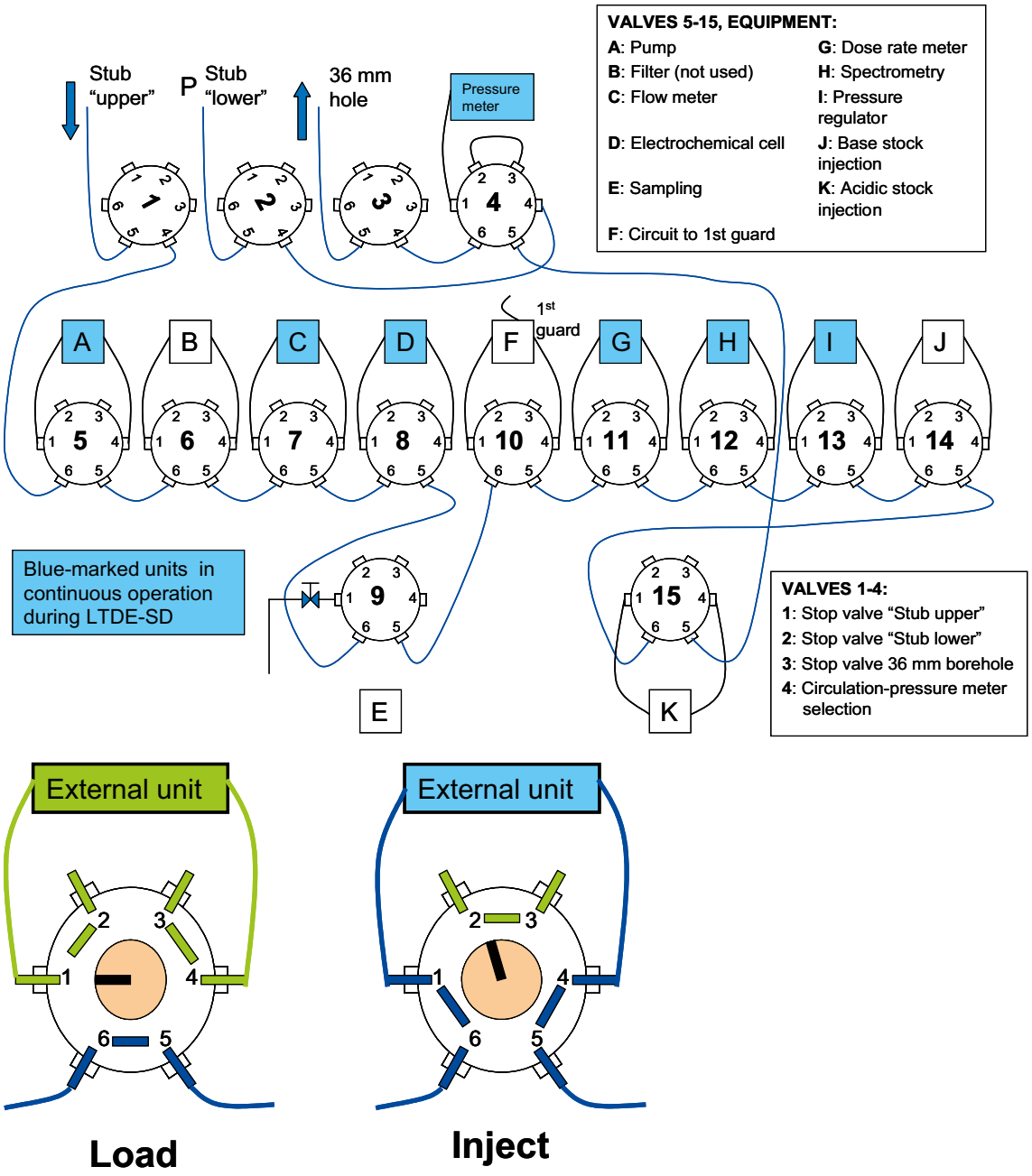

Figure 2-6. *Schematic diagram of the circulation set-up during the tests (top) and connection diagram of the 6-port valves used for connections of equipment to the circulation line (bottom).*

The circulation tubing was mounted in front of the detector through a loop, two tubes using the GEM10P4 detector and one tube using the GEM20180P detector. The loops were arranged so that the volume of the tubes exposed to the detector was about 0.6 ml and 0.3 ml, respectively. The distance between the detector end cap and the tube was approximately 1–2 cm. The calibration is described in Section 2.3.6. A picture of the lead shield and parts of the detector is shown in Figure 2-7.

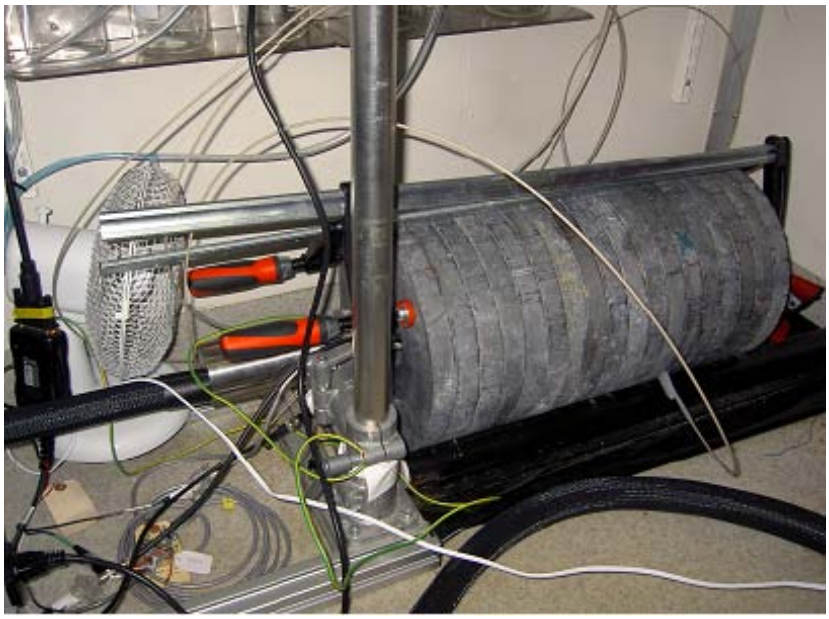

Figure 2-7. *Lead shield with PEEK tubing and parts of the HPGe-detector used for on-line radioactivity concentration measurements. The fan was installed to avoid condensation on the detector's heat exchanger.*

Test section dose rate equivalent (µSv/h)

The dose rate equivalent (µSv/h) was monitored in a separate tubing loop of the test section (~35 ml volume) using a GM-probe connected to a RNI-10SR instrument (RNI AB) in a separate lead shield. The RNI-instrument connected to a computer through a RS-232 interface. The software RNICom was used to collect and display data from the instrument. This monitoring was used to follow the total concentration of radioactivity in the system, especially during the injection procedure and to give alarm if a sudden decrease in the dose rate of the test section loop should occur as a result of a leakage in the test section. A picture of the lead shield and the back part of the probe is shown in Figure 2-8.

Figure 2-8. *Lead shield and back part of the GM-probe used for on-line dose rate monitoring.*

Electrochemical flow cell

A flow-cell and a measurement system were developed for continuous measurements of pH and E_h at high pressures. Figure 2-9 shows the flow-cell, which is made entirely in PEEK. The electrodes mounted in the flow-cell are two glass electrodes, a platinum electrode (Pt), a gold electrode (Au) and a reference electrode (Ag, AgCl). The pH and reference electrodes are specially designed for measurements at high pressure. Calibrations were performed by circulation of calibration solutions (pH 4+quinhydrone, pH 7+quinhydrone and pH 10). Data were transferred to a computer via a mulitplexer and serial interface. Calculation of calibration constants and recalculation of primary measurement data given in mV was done manually.

2.1.4 Other equipment

Dose rate equivalent at bounding fence and in Container 1

The dose rate equivalent (in units of µSv/h) at the fence towards the tunnel and in Container 1 (the experiment container) was monitored using RNI 10/SR-instruments (RNI AB). The data were collected through a computer interface in the same way as described for the test section dose rate monitoring above.

Monitoring of radioactivity in the guard section (KA3065A03:2)

The guard section KA3065A03:2 (Figure 2-2) had a circulation equipment placed in a cabinet outside of Container 1. The radioactivity in the groundwater of the guard section was monitored using a one inch plastic scintillator probe connected to a RNI-instrument. The probe was placed within a loop of the guard tubing in a separate lead shield. The volume of the loop was approximately 85 ml.

Radiation shielding

Lead mats were used to reduce the personal doses from the volume inside the pressure regulator cylinder which initially contained about 400 ml of the total 1,140 ml tracer solution.

Figure 2-9. *Electrochemical flow cell used for on-line measurements of pH and E_h.*

Other equipment

- Leak indicators were placed inside the inert gas boxes, on the floors of the containers and in the cabinet for the guard section and pilot borehole circulations equipment.
- Difference pressure transmitters monitored the pressure in the inert gas boxes.
- Three network cameras were used for remote observations of Container 1 and the area outside of the borehole.
- Temperature sensors monitored the temperature in the experimental borehole, at a number of different positions in the experimental set-up and in the tunnel on the site.
- Pressure monitors from all borehole sections and surrounding boreholes were located in a separate cabinet.
- All monitoring equipment was connected to the InTouch monitoring and control software in the computer LTDE2 through a PLC (Program Logic Control) interface in Container 2 (the work container for electronic equipment). Automatic security functions in the PLC were applied in order to prevent spreading of radioactivity in case of a malfunction in the experiment system.
- Groups of transmitters in InTouch were connected to the alarm system Alpha at Äspö HRL, which in turn is connected to Clab (Central interim storage facility for spent nuclear fuel, located near the Oskarshamn Nuclear Power Plant OKG) control room for 24h monitoring.
- In order to keep the temperature to about 20°C in Container 1, an air-conditioning unit was installed.
- The electrical power supplies for critical equipment were backed up with several universal power supplies (UPS).

2.1.5 Experimental conditions

Low redox potentials could not be established at the LTDE-SD site during the pre-test experiment /Widestrand et al. 2006/. In an attempt to locate possible leakages the entire circulation and all components were checked with a gas mixture of nitrogen and hydrogen using a portable hydrogen leak detector. The circulation was found to be absolutely tight. Repeated flushing campaigns with water from the guard section (of low redox potential) were performed and initially low redox potentials could be achieved after each flushing. However after each of these campaigns, within a few days the redox potential slowly started to increase to higher levels again. A possible explanation for the oxygen transport into the system may be diffusion through the PEEK-tubing from oxygen in the tunnel atmosphere or the nitrogen flushed glove boxes (<500 ppm O_2).

Eventually it was decided to start the main experiment including redox sensitive tracers despite the high redox potentials. The motivation was that even though redox sensitive tracers would be present in their oxidized form, a redox front may exist in the rock. This would imply that the natural reducing conditions might have been preserved e.g. some mm in to the rock and diffusion enrichment of the redox-sensitive tracer may occur at that place. In addition, sorption data even for oxidizing *in situ* conditions are scarce in the literature. Nevertheless, one has to consider that the experiment was performed in a groundwater that was under reducing conditions during the inlet but then became oxidized; conditions that is likely to produce e.g. iron precipitations which could influence the sorption conditions during the experiment.

2.2 Main experiment tracers

Both sorbing and non-sorbing tracers were used in the experiment. The radionuclides that were used are summarised in Table 2-1. The use of the different radionuclides aims at studying different retardation processes, e.g. sorption and diffusion. The radionuclides have been categorised in two groups after their primary usage:

A. Non-sorbing tracers, i.e. tracers that mainly due to their negative charge are assumed to diffuse without retardation due to sorption onto mineral surfaces. The group consists of $^{36}Cl^{-}$, $^{35}SO_4^{2-}$ and $^{75}SeO_4^{2-}$; however, with the two latter possible to reach lower redox states under reducing conditions, see below.

B. Sorbing tracers, i.e. tracers that are retarded by adsorption onto mineral surfaces. These tracers are aimed to help assess the impact of sorption on the penetration into the rock. The proposed tracers can be divided into three different subcategories within this group:

1. Tracers for which the sorption is dominated by a cation exchange mechanism, considered as a fast reversible process:
   i. Monovalent alkaline metal, i.e. $^{22}Na^{+}$ and $^{137}Cs^{+}$
   ii. Divalent alkaline earth metals, i.e. $^{85}Sr^{2+}$, $^{133}Ba^{2+}$ and $^{226}Ra^{2+}$.

   Furthermore, the cation exchange sorbing tracers have been used in several dynamic tracer experiments, e.g. the TRUE experiment series at Äspö HRL /Winberg et al. 2000, Andersson et al. 2002/ so the use of them in the present experiment is also motivated for purposes of obtaining mechanistic data for interpreting *in situ* experiments.
2. Tracers for which the sorption is dominated by a surface complexation mechanism:
   i. Monovalent transition metals. i.e. $^{110m}Ag^{+}$
   ii. Divalent transition metals, i.e. $^{57}Co^{2+}$, $^{63}Ni^{2+}$, $^{102}Pd^{2+}$ and $^{109}Cd^{2+}$
   iii. Trivalent lanthanide, i.e. $^{153}Gd(III)$
   iv. Different tetravalent compounds, i.e. $^{95}Zr(IV)$, $^{113}Sn(IV)$ and $^{175}Hf(IV)$
   v. Different pentavalent compounds, i.e. $^{95}NbO_2^{+}$ and $^{233}PaO_2^{+}$.
3. Tracers (i.e. $^{99}Tc(VII)O_4^{-}$, $^{236}U(VI)O_2^{2+}$ and $^{237}Np(VI)O_2^{2+}$) dependent of an electrochemical reduction in order to reach the respective tetravalent state (oxidation state IV) which is considered to be very strongly sorbing. The corresponding higher oxidation state for the respective tracer is thus considered to be weaker sorbing. To some extent also the anions $^{35}SO_4^{2-}$ and $^{75}SeO_4^{2-}$ are possible to reach lower oxidation states under reducing conditions; however, still maintaining negative net charge of their complexes.

The experiment also contains a demonstration aspect and the radioisotopes have also been chosen for the purpose of representing analogues and/or homologues to long-lived radioisotopes present in the spent nuclear waste. For that purpose, Table 2-1 also contains the specific information of which isotope and/or group of isotopes the particular tracer is meant to represent.

A main consideration of the experiment was of course to maintain natural chemical conditions in the experiment and that one therefore should avoid increasing the natural chemical concentration of the element used as tracers. For this reason, the use of radioactive isotopes of the different element aimed to be studied was a very suitable technique. By the use of radioisotopes with high specific activity, the combination of large amounts of radioactivity and low or no increase of the chemical concentrations could be achieved. The use of comparatively large amounts of radioactivity thus favoured the dynamic range of the tracer, i.e. the injected amount of activity given in relation to the detection limit.

However, avoiding increase of the natural concentration was not possible for every tracer element used; this mainly because of the cases when the element was not naturally present (or present in extremely low concentrations) in the groundwater. In addition, for some cases, avoiding an increase of the natural concentrations might have caused a low dynamic range (i.e. start concentration divided by the concentration for the detection limit). The following outline was therefore decided for the selection of chemical concentrations for the different tracers used:

- If possible, the addition of the tracer should not increase the natural concentration, i.e. the chemical concentration in the injection cocktail should be equal or below the natural elemental concentration.
- If not possible, the maximum elemental concentration of a trace element should be $1 \cdot 10^{-6}$ M.

Regarding the selection of non-sorbing tracers, the short-lived iodine tracer (^{131}I) used in the functionality test was indicated to be exposed to some form of adsorptive loss and the long-lived isotope ^{129}I was therefore rejected as an inert tracer for the main experiment. The selection of an inert tracer that could be analysed in the rock material after at least a year excluded some often used inert tracers. Tritiated water could not be used for rock analysis due to risk of evaporation during different procedures planned for the future outtake of the rock material and the radioactive bromide tracers are too short-lived. Fluorescent dye tracers and metal-complexes are undesired due to risk of

complexation of the other metal tracers with high charges (and could not meet the prerequisites of not changing the natural chemical conditions of the groundwater). Thus, ^{36}Cl proved to be the only reasonable choice, although it requires chemical separation procedures since it has no γ-emission that can be measured using γ-spectrometry.

The anionic tracer $^{35}SO_4^{2-}$ (and possibly also $^{75}SeO_4^{2-}$) could, based on its negative charges, be considered as potential inert tracers. However, both of them are subject to possible electrochemical reactions and/or precipitation reactions and there is no information in the literature of their use as groundwater tracers.

Table 2-1. Information on the radionuclide tracers used in the LTDE-SD experiment. The acronym ICP-SFMS stands for: Inductively Coupled Plasma – Sector field mass spectrometry.

Tracer	Amount	Half-life	Expected sorption mechanism	Analogue /Homologue radioistope present in nuclear waste	Analysis method
$^{22}Na^+$	3.2 MBq	2.6 y	Cation exchange		γ-spectrometry
$^{35}SO_4^{2-}$	13 MBq	87.5 d	Non-sorbing		Liquid scintillation counting after chemical separation, BaSO4(s) precipita
$^{36}Cl^-$	5.9 MBq	3.0E5 y	Non-sorbing	Cl-36 ($t_{½}$ = 3E5 y)	Liquid scintillation counting after chemical separation
$^{57}Co^{2+}$	19 MBq	272 d	Surface complexation	Co-60 ($t_{½}$ = 5.3 y)	γ-spectrometry, after cation exchange separation
$^{63}Ni^{2+}$	30 MBq	100 y	Surface complexation	Ni-59 ($t_{½}$ = 7.5E4 y) Ni-63 ($t_{½}$ = 100 y)	Liquid scintillation counting after chemical separation
$^{75}SeO_4^{2-}$	4.4 MBq	120 d	Non-sorbing	Se-79 ($t_{½}$ = 6.5E4 y)	γ-spectrometry, after cation exchange separation
$^{85}Sr^{2+}$	45 MBq	65 d	Cation exchange	Sr-90 ($t_{½}$ = 28.5 y)	γ-spectrometry
$^{95}Zr(IV)$	0.07 MBq	64 d	Surface complexation	Zr-93 ($t_{½}$ = 1.5E6 y)	γ-spectrometry, after cation exchange separation
$^{95}NbO_2^+$	0.03 MBq	35 d	Surface complexation	Nb-94 ($t_{½}$ = 2.0E4 y)	γ-spectrometry, after cation exchange separation
$^{99}TcO_4^-$	94 μg	2.1E5 y	Non-sorbing, redox sensitive	Tc-99 ($t_{½}$ = 2.1E5 y)	ICP-SFMS
$^{102}Pd^{2+}$	55 μg	Stable	Surface complexation	Pd-107 ($t_{½}$ = 6.5E6 y)	ICP-SFMS
$^{109}Cd^{2+}$	27 MBq	463 d	Surface complexation	Cd-113m ($t_{½}$ = 9E15 y)	γ-spectrometry, after cation exchange separation
$^{110m}Ag^+$	0.4 MBq	250 d	Surface complexation	Ag-108m ($t_{½}$ = 127 y)	γ-spectrometry, after cation exchange separation
$^{113}Sn(IV)$	0.09 MBq	115 d	Surface complexation	Sn-126 ($t_{½}$ = 1E5 y)	γ-spectrometry, after cation exchange separation
$^{133}Ba^{2+}$	1.8 MBq	10.5 y	Cation exchange		γ-spectrometry
$^{137}Cs^+$	8.8 MBq	30 y	Cation exchange	Cs-135 ($t_{½}$ = 3E6 y) Cs-137 ($t_{½}$ = 30 y)	γ-spectrometry
$^{153}Gd(III)$	4.3 MBq	240 d	Surface complexation	Analogue for all trivalent lanthanides and actinides	γ-spectrometry, after cation exchange separation
$^{175}Hf(IV)$	1.9 MBq	70 d	Surface complexation	Analogue for all tetravalent actinides	γ-spectrometry, after cation exchange separation
$^{226}Ra^{2+}$	0.15 MBq	1,600 y	Cation exchange	Ra-226 ($t_{½}$ = 1,600 y)	γ-spectrometry, after cation exchange separation (measured from its daughter radionuclide Bi-214)
$^{233}PaO(OH)_3$	5.7 MBq	27 d	Surface complexation	Pa-231 ($t_{½}$ = 3.3E4 y)	γ-spectrometry, after cation exchange separation
$^{236}UO_2^-$	57 μg	2.3E7 y	Surface complexation, redox sensitive	All uranium isotopes	ICP-SFMS
$^{237}NpO_2^+$	310 μg	2.1E6 y	Surface complexation, redox sensitive	All neptunium isotopes	ICP-SFMS

2.3 Performance of main experiment

The primary objective of the main experiment was to expose the available rock surfaces to the tracer solution so that a sorption and diffusion into the rock could take place. In a later stage, an overcoring would take place followed by measurements of the exposed rock material for its tracer content. Nevertheless, measurements of the aqueous phase were also performed during the main *in situ* experiment, this in order to study the time dependence of the sorption/diffusion process. Concentration versus time curves will thus be produced for the test section, with simultaneous circulation in the stub section and through the slim hole section. The concentration history will be used as an important input for modelling of the tracer penetration into the rock at a later stage.

A functionality test /Widestrand et al. 2006/ had been performed prior to the start of this main experiment. The functionality test proved the function of all crucial experiment components at the LTDE-SD site (e.g. the injection procedure, the circulation equipment, pressure regulator, sensors, monitoring system, alarms, remote access to computers and backup of data and sampling procedures).

2.3.1 Preparation of stock solutions

The radioactive tracers used were either obtained by delivery from different suppliers of radioactive isotopes or by neutron irradiation at the research reactor at Institute for Energy Technology, Kjeller, Norway, neutron flux $1.1 \cdot 10^{13}$ n/cm^2/s. Specifications of the different isotope enrichments are given in Table 2-2.

Table 2-2. Information on the stock solutions for the different radionuclide tracers used in the LTDE-SD experiment.

Tracer	Half-life	Stock solution	Supplier
$^{22}Na^+$	2.6 y	Aq >100 mCi/mg	GE Healthcare
$^{35}SO_4^{2-}$	87.5 d	Aq, carrier free	GE Healthcare
$^{36}Cl^-$	3.0E5 y	0.1–0.3 M HCl, >3 mCi/g	GE Healthcare
$^{57}Co^{2+}$	272 d	0.1 M HCl carrier free	GE Healthcare
$^{63}Ni^{2+}$	100 y	0.1 M HCl. 1–10 mCi/mg	GE Healthcare
$^{75}SeO_4^{2-}$	120 d		Irradiation of 0.11 mg Se-74 (78% enrichment, naturally 0.89%)
$^{85}Sr^{2+}$	65 d	0.5 M HCl, 360 MBq/mg	Perkin Elmer Life and Analytical Science
^{95}Zr(IV)	64 d		Irradiation of natural U, fission product separation by cation exchange
$^{95}NbO_2^+$	35 d		Ingrowth as from the deacy of its parent radionuclide Zr-95
$^{99}TcO_4^-$	2.1E5 y	0.1 M NH_3OH	Amersham (Isotrak)
$^{102}Pd^{2+}$	Stable		Stable isotope enrichment of 0.15 mg Pd-102 (78% enrichment, naturally 1.0%)
$^{109}Cd^{2+}$	463 d	0.1 M HCl, >50 uCi/ug	GE Healthcare
$^{110m}Ag^+$	250 d		Irradiation of 0.16 mg Ag-109 (99% enrichment, naturally 48%)
^{113}Sn(IV)	115 d		Irradiation of 0.17 mg Sn-112 (68% enrichment, naturally 0.96%)
$^{133}Ba^{2+}$	10.5 y		Amersham (Isotrak)
$^{137}Cs^+$	30 y	1 M HCl, 37–370 MBq/mg	Amersham Life Science
^{153}Gd(III)	240 d		Irradiation of Gd-152 0.03 mg (43% enrichment, naturally 0.2%)
^{175}Hf(IV)	70 d		Irradiation of 0.03 mg Hf-174 (19% enrichment, naturally 0.16%)
$^{226}Ra^{2+}$	1,600 y	1 M HCl, carrier free	AEA Technology (Isotrak)
$^{233}PaO(OH)_3$	27 d	Surface complexation	Irradiation of natural Th
$^{236}UO_2^-$	2.3E7 y	2 M HNO3, >99.9% U-236	AEA Technology (Isotrak)
$^{237}NpO_2^+$	2.1E6 y	0.1 M HCl	AEA Technology (Isotrak)

Irradiation

^{75}Se, ^{102}Pd, ^{110m}Ag, ^{113}Sn, ^{153}Gd and ^{175}Hf: Isotope enrichments (specified in Table 2-2 were purchased from Oak Ridge National Laboratory, USA, and were dissolved in 0.5 ml of concentrated nitric acid into individual batches. The appropriate amounts (i.e. 15–85 µl) of the individual batches were extracted and were treated with Na_2CO_3 and $MgCl_2$ to form a 30 mg $Na/MgCO_3$ co-precipitation in a quartz test tube. This test tube was sealed and was irradiated for one month.

^{95}Zr: 50 mg of uranium (taken from a uranium atomic absorption standard solution, Fluka) was co-precipitated together with 50 mg of Mg to form a $UO_2/MgCO_3$ precipitation which was irradiated for 14 days. ^{95}Zr is produced as one of the major products from the fission of ^{235}U.

^{233}Pa: 90 mg of thorium (taken from a thorium atomic absorption standard solution, Fluka) precipitated to form a $Th/MgCO_3$ precipitation which was irradiated for one month. In this irradiation, the neutron of the ^{232}Th isotope produces ^{233}Th ($t_{½}$=22.3 min) which decays to ^{233}Pa.

Preparation of tracers

For the vast majority of the tracers, appropriate amounts were simply extracted from the stock solutions and added to the tracer cocktail. However, for some of the tracers some more elaborate procedures had to be applied which are described below.

^{75}Se, ^{102}Pd, ^{110m}Ag, ^{113}Sn, ^{153}Gd and ^{175}Hf: The irradiated sample was dissolved in 10 ml 1 M HCl over night with low heating. When the volume had been reduced to 5 ml, the sample was filtered twice through syringe filters; first using a 0.2 µm filter and thereafter using a 0.02 µm filter. The solution was thereafter transferred to the main stock solution of the tracer cocktail.

^{95}Zr: The irradiated sample was left for cooling for 30 days; this mainly in order to reduce the radiation dose from the short-lived irradiation product of ^{239}Np (produced by neutron capture of ^{238}U to ^{239}U and the successive decay to ^{239}Np, $t_{½}$=2.36 days). The sample was thereafter dissolved in 1 M HCl and the solution was pored on a newly reconditioned 5 ml cation exchanger (Dowex 50WX4-50). The cation exchanger was then rinsed with 10 ml of distilled water and was thereafter treated with aliquots of 10 ml of successively increased concentrations of HCl/CaCl2 with the aim to first remove weakly bound elements such as $^{238}UO_2^{2+}$, $^{137}Cs^{+}$, $^{90}Sr^{2+}$, $^{140}Ba^{2+}$ and leaving the presumed strongly bound $^{95}Zr^{4+}$ to be selectively removed in a late stage with high concentrations of $HCl/CaCl_2$.

^{233}Pa: The irradiated $Th(CO_3)_2$ was dissolved in 10 ml 1 M HCl. A 5 ml cation exchanger Dowex 50WX4-50 was reconditioned and converted to its Na-form. The dissolved Th-solution was poured through the cation exchanger, a process in which the Th^{4+} was aimed to sorb on the cation exchanger while the PaO_2^{+} ion was aimed to pour through with only minor sorption. After the first cation exchange treatment, the solution was heated and concentrated to a 3 ml solution. The cation exchange treatment was repeated (on a new 5 ml cation exchanger, reconditioned and converted to its Na-form) and a final rinsing of the cation exchanger with 2×1 ml 0.01 M HCl was performed.

Solution 1 – acidic stock solution

Solution 1 comprised the tracers, prepared by sequential additions of separate acidic stock solutions for each tracer (described above). The volume injected was ~20 ml. When all tracers had been added to the cocktail, the acidity of this solution was adjusted to 0.1 M HCl solution; this (as described below) in order to avoid sorption on the equipment during the injection.

Solution 2 – NaOH solution, used to neutralise the first acidic injection.

Solution 2 was prepared by using deionized water and NaOH (Millipure). This solution was aimed to exactly neutralize the acid content of solution 1 during the injection. The strength of this solution was therefore set from the result of a separately performed titration of a small aliquot sampled from the stock solution. The volume injected was ~20 ml.

2.3.2 Injections

Principle for injection

The first injection (solution 1) was done in acidic solution in order to avoid a risk for precipitation in the stock solution of some tracers (mainly Hf and Gd) and to minimise sorption on equipment before the tracers reached the test section. The second injection (solution 2) was injected in order to neutralise the first acidic injection, i.e. to regain the natural pH in the test section.

The principle for the injection was to inject the tracers as pulses with a plug flow with short but sufficient time spacing between the two injections. The acidic pulse would thus reach the test section a short time before the basic pulse and the water would be pH-equilibrated to a large extent by the mixing in the first passage of the pulses in the stub section; the circulation was run in the stub section for the first two hours after which it was switched to the 36 mm borehole section. If precipitation or strong sorption would occur immediately following neutralisation, this procedure would at least make it occur mainly on the exposed fracture in the stub section and not on the tubing. A schematic picture of the serial pulse injections is shown in Figure 2-10. Figure 2-11 illustrates the flow paths when the pulses reached the test sections.

The injection valves used were placed as the last equipment part before the exiting outflow to the borehole sections (see Figure 2-6). This was done in order to minimise the volume available for mixing of the pulses with stagnant water before entering the borehole sections.

Performance of injection

At the LTDE-SD test site the stock solutions were entered through the airlock into the glove box. The injection loops were preinstalled behind extra lead protection inside the glove box. The specific tube volumes required were determined by the volumes of the stock solutions. The stock solution and the alkaline solutions were transferred to the two different injection loops with the help of syringes. First a small amount of synthetic groundwater was filled into the loop, thereafter the stock solution/alkaline solution and finally a small amount of synthetic groundwater. A detailed description of the transfer and injection procedure is given in Appendix 2. This procedure enabled the residual of the stock solution to remain in the vessel, which facilitated easy transfer to Baslab (Radiochemical laboratory within the Clab facility, serving the experiment) for sampling and determination of the non-injected amount of radioactivity.

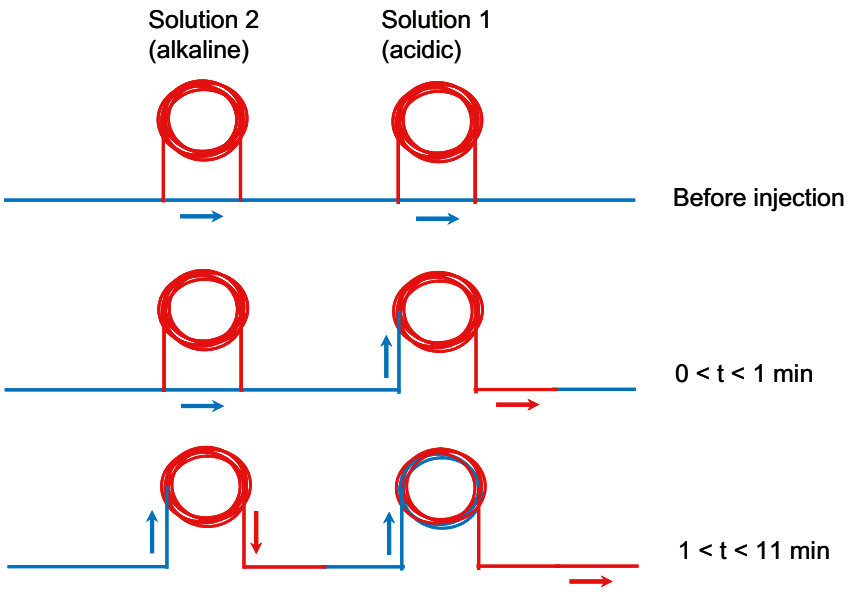

Figure 2-10. *Principle of injection procedure. At time t=0 the tubing loop containing the acidic stock solution 1 is connected to the circulation and at time t=1 min the alkaline solution 2 is connected to the circulation.*

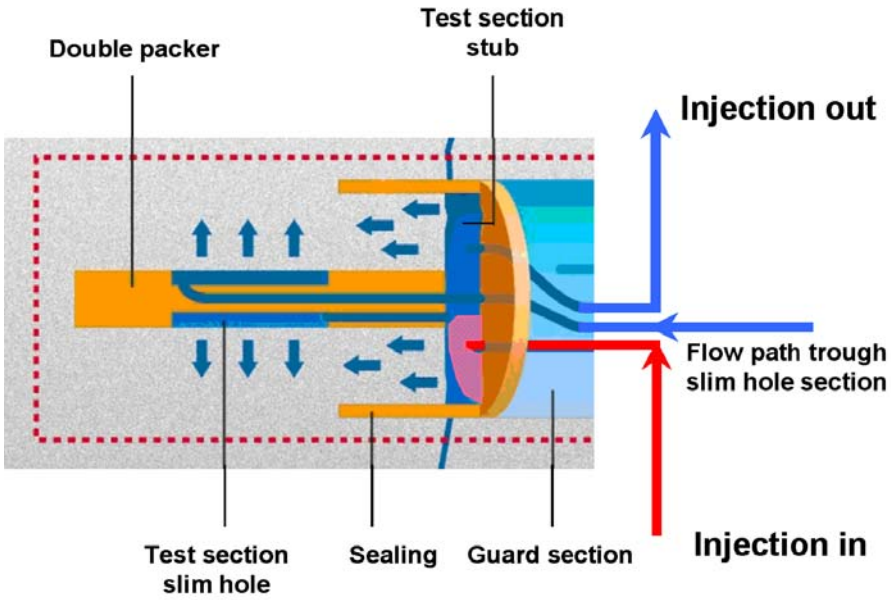

Figure 2-11. *Schematic figure illustrating the injection moment. Two hours after injection valve four, cf. Figure 2-6, was shifted changing the flow path to the 36 mm borehole section. Acidic stock solution is illustrated as red.*

2.3.3 Circulation

As stated earlier the injection procedure was performed with the circulation in front of the stub section only and after 2 hours the circulation was shifted to pass also through the slim hole section (including the stub section) for the first time. Circulation through the 36 mm section and the stub section constituted the main flow path during the experiment. However, to ensure proper mixing in the stub section the circulation was shifted regularly to this flow path for shorter time periods throughout the experiment.

On the day of the injection and the two following days the circulation was shifted several times to ensure a homogenous solution in both test sections. After this the time-wise spacing between flow path changes were increased to approximately two times each week with some longer periods during the holidays. A detailed account of the circulation scheme is given in Appendix 3.

The experiment lasted for approximately 196 days and during this period the circulation was run for 176 days through the slim hole section and 20 days using the flow path only using the stub section, cf. Figure 2-11.

2.3.4 Sampling

Test section

In addition to the on-line HPGe measurements of the circulation loop, sampling of small volumes of water was done for subsequent analysis at Baslab. The samples are presented in Appendix 4.

A total number of 26 test section samples were taken throughout the experiment. Two of these were filtered using 20 nm filters to investigate if some of the injected tracers were circulating in a colloidal bound form.

Two samples were also passed through a cation resin and one was sampled through an anion resin in order to enable a simple speciation study.

A detailed description of the sampling procedure is given in Appendix 2.

Guard section and pilot borehole

KA3065A03:2, the “guard” section, and the pilot borehole KA3065A02 was sampled in regular intervals for control of leakages. 250 ml samples were taken for γ-spectrometry analysis at Baslab.

Microbe sampling

A mechanism that possibly could interfere with the presumed natural processes aimed to study in this experiment was a non-natural increase in microbe growth; e.g. causing microbial interaction with the radionuclides and therefore giving erroneous sorption results. For this reason, the test section (section 1) was sampled for bacterial analysis just prior to the start of the experiment. The samples were preserved in formalin and analyzed for ATP (adenosine triphosphate) content which is proportional to bacterial cell concentration.

pH-control sample

A pH-control was performed on the test section KA3065A03:1 two months into the experiment. A small sample (4.5 ml) was withdrawn into a centrifuge tube according to normal sampling procedure and was transported as fast as possible to Baslab for analysis. The sample was kept closed in and only opened when the pH-electrode was put into the solution, hence a N_2-gas environment was maintained for as long as possible.

The sample was analysed 75 minutes after sampling by use of a PHM220 Lab pH meter (Radiometer, Copenhagen) with a Jenway A04 924005 electrode. The equipment was pre-equilibrated using the same type of centrifuge tube.

Colloid filtering

The guard section (KA3065A03:2) was sampled for inorganic (Mätsystem-beskrivning för kolloidfiltreringssystem, SKB MD 431.04) in special sample containers immediately prior to the termination of the LTDE-SD experiment. The colloid filtering equipment was adapted to the sample containers and consists of holders for two sample containers, a separate tube and valve system for water and gas, a filter holder package for five filters, and a collecting container. The pore sizes of the five connected filters were 2.0, 2.0, 0.4, 0.2 and 0.05 μm and the filtered water volume was 322 ml Figure 2-12 shows the equipment set-up. Data on performance of the filtration run is given in Table 2-3.

The major equipment features are:

- Filtering is performed in a closed system under argon atmosphere, thus avoiding the risk of iron precipitation due to contact between the groundwater sample and air.
- Filtering is performed at a pressure similar to that of the groundwater in the borehole section. The system is adjusted to create a pressure difference between the inlet of the filter package and the outlet side. The pressure difference drives the sample water through the filters.
- The design of the sample containers, and the mounting with the outlet at the top, prevents migration of larger particles that may clog the filters. Furthermore, clogging is prevented by the first two filters with pore sizes 2.0 μm which are mounted in parallel.

The analyses of water and filter samples were performed using ICP-AES (Inductively coupled plasma – atomic emission spectroscopy or ICP-SFMS (Inductively coupled plasma – sector field mass spectrometry) and the filters were dissolved in a microwave oven in $HNO_3 + H_2O_2$ in closed teflon containers prior to analysis.

Table 2-3. Colloid filtration, data on performance.

Section / date	Entering pressure [bar]	Max. differential pressure over filter package [bar]	Temp. [°C]	Filtering time [min]	Filtered volume [ml]	Comments
10.39–10.70 m /20070411	~36	3.0	~13	25	322	Leakage test performed prior to filtration. No leakage was noticed. No broken filters

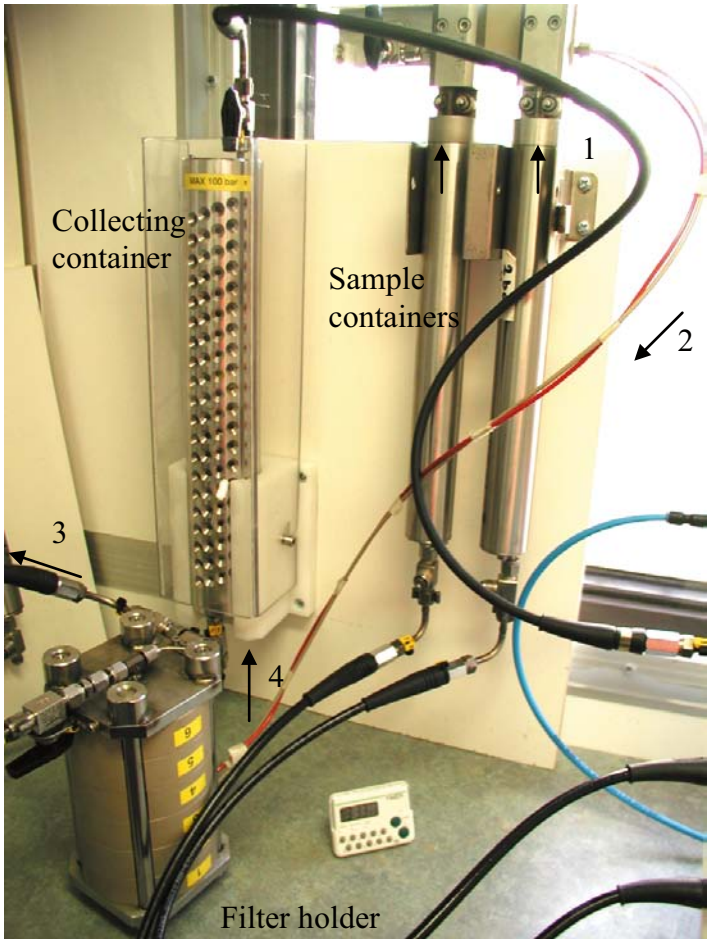

Figure 2-12. *The colloid filtering equipment including the sample containers, the filter holder package and the collecting container. The black arrows, 1 to 4, show the flow direction of the sample water through the system.*

2.3.5 Laboratory separations and analysis of tracers

For the analysis of the different tracers, γ-spectrometry, liquid scintillation counting (LSC) and ICP-SFMS (Ionic coupled plasma sector field mass spectrometry) where applied; specification of which method that were applied for each tracers is given in Table 2-1. The separation and analysis scheme was the following:

1. For analysis of the γ-emitting tracers present in the highest activity (^{22}Na, ^{57}Co, ^{75}Se, ^{109}Cd, ^{133}Ba and ^{137}Cs) γ-spectrometry was performed on an acidified groundwater sample, without any other pretreatment).
2. The stable isotope (^{102}Pd) and the isotopes with very low specific activity (^{99}Tc, ^{236}U and ^{237}Np) were analysed using ICP-SFMS by Swedish Research and Defence Institute, CBRN Defence and Security Division, FOI, in Umeå.
3. Removal of small sample parts for chemical separation of ^{63}Ni, ^{36}Cl and ^{35}S and subsequent LSC analysis.
4. A low amount of complexing agent (DTPA) and NaOH is added to the acidified groundwater sample. Thereafter, the solution is poured through a cation exchanger (Dowex 50WX4-50) in order to significantly reduce the concentrations of mainly ^{137}Cs, ^{22}Na, ^{133}Ba and ^{226}Ra (elements that are not complexed by DTPA and therefore adsorbed in the cation exchanger). Thereby, the Compton background in the γ-measurements is decreased which favours the measurement conditions of some radionuclides which due to sorption losses are present at low concentrations, e.g. ^{175}Hf and ^{153}Gd. The method was applied for analysis of ^{95}Zr, ^{110m}Ag, ^{113}Sn, ^{153}Gd, ^{175}Hf and ^{233}Pa.

5. The ion exchanger is left for one month in a closed vessel in order to equilibrate ^{226}Ra with ^{226}Rn and its short-lived daughters, ^{214}Bi and ^{214}Pb which are analysed using γ-spectrometry. ^{226}Ra concentration is calculated based on the ^{214}Bi and ^{214}Pb results.

γ-spectrometry

The radioactivity concentrations of the γ-emitting radionuclides ^{22}Na, ^{57}Co, ^{75}Se, ^{85}Sr, ^{109}Cd, ^{133}Ba and ^{137}Cs were measured using a high purity germanium, HPGe-detector (ORTEC, relative efficiency 35%). A sample exchanger capable of loading 12 samples was used. In each batch 10 samples were loaded together with one standard solution and one empty vessel for background control. A 5 ml vessel geometry was used. Gamma Vision 5.31, (ORTEC), was used to determine the efficiency of the detectors and for measurements and evaluation of sample spectra.

Liquid scintillation counting

^{63}Ni, ^{36}Cl and ^{35}S were separated from the groundwater samples using specifically developed separation methods /Nilsson et al. 2010/. A Wallac Guardian 1414 liquid scintillation counter was used for analysis of separated samples.

ICP-SFMS

The analyses of ^{99}Tc, ^{102}Pd, ^{236}U and ^{237}Np were performed by the Swedish Research and Defence Institute, CBRN Defence and Security Division, FOI, in Umeå.

2.3.6 Calibration of detectors

The HPGe-detector at Baslab was calibrated with an Amersham QCY44 standard solution. 5 ml vial geometry was used for calibration and sample measurements.

Standard solutions of ^{63}Ni, ^{36}Cl and ^{35}S were used for the calibration of the LSC.

Prior to the start of the on-line measurements the on-line detector was calibrated with a mixed radionuclide standard solution, Amersham QCY44. The solution was sucked into a PEEK tube using a syringe and the tubing was placed in front of the detector at the position of the circulation tubing. The calibration measurements on the HPGe detectors were evaluated with the program package Gamma Vision 5.31, (ORTEC), which also was used to determine the efficiency of the detectors and for measurements and evaluation of sample spectra.

2.3.7 Environmental monitoring

The effective dose rates at the fence and in Container 1 were monitored using RNI-instruments according to the description in 2.1.4. The test section (KA3065A03:1) and the guard section (KA3065A03:2) were monitored as described in Sections 2.1.3 and 2.1.4 in order to detect sudden decreases of radioactivity in the test section or slow increases of radioactivity in the guard section (which is adjacent to the test section, cf. Figure 2-11), respectively. Furthermore, the guard section was manually sampled to check for leakage from the test section, this was done throughout the experiment with a total number of 20 samples. The pilot bore hole (KA3065A02:3) was also sampled 16 times throughout the experiment.

At the end of the experiment the sections KA3065A03:3 and KA3065A03:4, located at larger distances from the test section, were sampled.

In addition to the KA3065A03 and A02-samples 9 different sampling points immediately off the site and in the open sewage system down stream were chosen and sampled at two occasions, prior to the initial injection and after the Epoxy injection (cf. Section 2.4.2) at the end of the experiment.

2.4 Termination of experiment in borehole KA3065A03:1

Following the *in situ* experiment, the experimental section was emptied from trace elements by rinsing the system with isopropyl alcohol. Thereafter an Epoxy resin was injected in order to increase the mechanical strength of the rock prior to over-coring and to protect the stub and slim hole test section water-rock interface from flushing water used for over-core drilling. The objective of the 300 mm diameter over-core drilling was to extract the core stub and the rock surrounding the slim hole test section. The core was subsequently sampled an analysed for trace element concentration profiles within the rock. Over-core drilling and subsequent analysis is further described in /Nilsson et al. 2010/.

2.4.1 Removal of tracer solution and additional sampling

The experiment was planned to be finished approximately 6 months after injection by a final sampling, closing of the circulation and emptying of the system. The system was emptied first by turning the pressure regulator to its minimum volume and next the equipment loops (see Figure 2-2) were emptied one by one by flushing with guard water into separate vials that were subsequently sampled and analysed for its tracer contents.

The HPGe tubing was also exchanged with groundwater and a control measurement was thereafter performed in order to check for activity on the tubing surfaces.

The electrochemical flow cell was calibrated after the exchange of the tracer solution.

2.4.2 Exchange of test section groundwater to isopropyl alcohol and Epoxy injection

The remaining tracer solution in the system was exchanged with isopropyl alcohol and samples were taken for analysis of its tracer contents. The exchange to isopropyl alcohol was done in order to improve the adhesion to the rock surfaces of the subsequently injected Epoxy resin. The isopropyl alcohol exchange was monitored using the HPGe-detector in order to ensure a high exchange yield of the tracers before termination of the isopropyl alcohol pumping.

In the following step, valves were connected to the tubing at the borehole collar, still maintaining the natural pressure. Epoxy resin (EpoTek 301 labelled with 11,200 ppm of EpoDye ©, a yellow fluorescent dye) was injected through the valves until curing stopped the pumping. Sampling of iso propyl alcohol-Epoxy solutions leaving the borehole during the injection was performed as in the previous cases.

2.4.3 Dismantling and overcore drilling

The dismantling and overcore drilling operations are described briefly regarding tracer losses and are further described in /Nilsson et al. 2010/.

2.5 Speciation calculations using PHREEQC

The ability of an element/tracer to sorb onto a mineral surface depends among other things on its chemical form in the aqueous phase. The element can be present as a bare $M^{n+/-}$ ion or as a complex being negatively or positively charged and/or as uncharged. To investigate the chemical form, or speciation, of the tracers in the present *in situ* experiment basic speciation calculations were performed with the geochemical program PHREEQC /Parkhurst and Appelo 1999/ using with the thermodynamic database LLNL that comes with the PHREEQC package /Parkhurst and Appelo 1999/.

3 Results and interpretations

First in this chapter the results of the speciation calculations are presented since interpretations of the experimental outcome are done in relation to these results. Next the experimental procedures, groundwater sampling and analysis and environmental monitoring are presented in order to give a covering of the experimental conditions. Thereafter the results and interpretation of the tracer experiment is described.

3.1 Speciation calculations

3.1.1 Experimental/Calculation

The natural groundwater composition used in the chemical speciation calculations is given in Table 3-1. These data originate from the borehole section KA3065A03;3, sampling date 2006-06-20, prior to the start of the *in situ* experiment. The water sample had a pH of 7.34. A more elaborate description of the groundwater composition is found in Appendix 5.

The elements and the tracer/isotope used in the *in situ* experiment together with the tracer concentrations are presented in Table 3-2. These concentrations corresponds to the compositions of the water at the injection moment, i.e. before any sorption had taken place.

The aim of the LTDE-SD *in situ* experiment was of course to establish natural conditions, e.g. with respect to the redox potential, which was measured at –90 mV 2006-06-20 when flushing the experiment volume with natural groundwater from the pilot borehole. However, these conditions were (as discussed previously) later shown not be possible to maintain during the circulation of the natural groundwater in the experiment loop; the value raised within some days to +470 mV which remained stable throughout the experiment. This latter value was used in the first case (oxidized condition) of the speciation calculations which thus is highly relevant for the interpretation of the tracers in the actually obtained experimental conditions. In the second case (reduced condition) of the calculations, the system redox potential was set to the presumably natural conditions of –90 mV; conditions that may be relevant for e.g. the rock matrix pores in the case that the induced oxidized conditions may not have had time enough to fully influence the rock matrix.

Table 3-1. Groundwater composition used in the speciation calculations together with pH=7.34.

Element/ Compound	Concentration (mg/L)	Element/ Compound	Concentration (mg/L)
Na	1,930	Cl	5,810
K	11.5	S(6)	443
Ca	1,710	S(–2)	0.009
Mg	60.9	Mn	0.359
HCO_3	35.9	Br	31.8
Si	6.68	F	1.42
Fe(II)	0.69	NH_4	0.115
Fe(III)	0.02	P	0.00153
Rb	0.0337	Li	1.23

Table 3-2. Tracers/Isotopes and their concentration used in the speciation calculations. In the last column comments on the justification of the used concentration for the different elemnets are given.

Element	Isotope	Concentration (mol/L)	Comments
Na	Na-22	7.4E–2	The added amount of tracer did not affect the measured natural concentration, cf. Appendix 5.
S	S-35	3.7E–3	The added amount of tracer did not affect the measured natural concentration, cf. Appendix 5.
Cl	Cl-36	1.6E–1	The added amount of tracer did not affect the measured natural concentration, cf. Appendix 5.
Co	Co-57	2.6E–11	Added tracer concentration, no or negligible background concentration is assumed.
Ni	Ni-63	9.9E–7	Added tracer concentration, no or negligible background concentration is assumed.
Se	Se-75	6.6E–7	Added tracer concentration, no or negligible background concentration is assumed.
Sr	Sr-85	3.5E–4	The added amount of tracer did not affect the measured natural concentration, cf. Appendix 5.
Zr	Zr-95	7.4E–8	Carrier free. Calculations were performed using the Hf(IV) concentration, based on a hypothesis that a co-precipitation of the two tetravalent elements are likely to occur.
Tc	Tc-99	1.0E–6	Added tracer concentration, no or negligible background concentration is assumed.
Cd	Cd-109	1.1E–8	Added tracer concentration, no or negligible background concentration is assumed.
Pd	Pd-102	6.6E–7	Added tracer concentration, no or negligible background concentration is assumed.
Ag	Ag-110	6.6E–7	Added tracer concentration, no or negligible background concentration is assumed.
Sn	Sn-113	6.6E–7	Added tracer concentration, no or negligible background concentration is assumed.
Ba	Ba-133	4.8E–7	The added amount of tracer did not affect the measured natural concentration, cf. Appendix 5.
Cs	Cs-137	2.0E–8	The added amount of tracer did not affect the measured natural concentration, cf. Appendix 5.
Gd	Gd-153	8.7E–8	Added tracer concentration, no or negligible background concentration is assumed.
Hf	Hf-175	7.4E–8	Added tracer concentration, no or negligible background concentration is assumed.
Ra	Ra-226	3.2E–8	Added tracer concentration, no or negligible background concentration is assumed.
Pa	Pa-233	3.2E–11	Added tracer concentration, no or negligible background concentration is assumed.
U	U-236	4.6E–7	Added tracer concentration, no or negligible background concentration is assumed.
Np	Np-237	1.0E–6	Added tracer concentration, no or negligible background concentration is assumed.

3.1.2 Results

Two speciation calculations were performed, one with a redox potential of 470 mV and one with –90 mV. A temperature of 15ºC was used in both calculations. The results from the speciation calculations are presented in Table 3-3 and Table 3-4. Table 3-3 shows the speciation of elements that were unaffected of the redox potentials used, while Table 3-4 shows results for the elements that were affected by the redox potentials.

Significant differences in the results can be seen for the redox sensitive elements Np, Se, Tc and U. Depending on the redox potential, different aqueous species were formed. The calculations yields that at oxidized conditions (i.e. the conditions under which the *in situ* experiment was performed) uranium is dominated by negatively charged complexes of the uranyl ion (UO_2^{2+}) with carbonates and hydroxides while Np exists dominantly as the non-complexed neptunyl ion (NpO_2^{+}). Under reducing conditions, they are both expected to exist as the hydrolysed tetravalent species of $Np(OH)_4(aq)$ and $U(OH)_4(aq)$, respectively.

Se and Tc are expected to exist as oxyanions (SeO_4^{2-} and TcO_4^{-}, respectively) at oxidized conditions. Under reducing conditions, Se is likely to form the monoprotonated form of the Se^{2-} ion, i.e. HSe^{-}, while Tc formed is expect to exist as a hydrolysed tetravalent complex of $TcO(OH)_2(aq)$.

Although Sn is redox-sensitive; it should according to the speciation calculation be present as an uncharged Sn(IV)-hydroxide complex in both the calculated cases, i.e. none of the cases are reducing enough to allow a reduction forming any species of the Sn(II) ion.

Table 3-3. Results from the speciation calculations performed for the tracers used in the LTDE-SD *in situ* experiment. In the table, tracers that were unaffected by the redox potentials are presented. Hence, no difference in speciation could be observed for these tracers. The aqueous species are expressed as a percentage of total concentration of the tracer. Only species with a percentage equal to or above one have been considered. The calculations were performed with the program PHREEQC using the data base LLNL, accompanying the PHREEQC package /Parkhurst and Appelo 1999/.

Speciation calculations performed valid for both E_h = 470 mV and E_h = –90 mV					
Tracer	**Species**	**%**	**Tracer**	**Species**	**%**
Ag	$AgCl_2^-$	74	**Hf**	$Hf(OH)_5^-$	100
	$AgCl_3^{2-}$	21	**Na**	Na^+	98
	$AgCl_{(aq)}$	4		$NaCl_{(aq)}$	1
	$AgCl_4^{3-}$	1	**Ni**	Ni^{2+}	96
Ba	Ba^{2+}	99		$NiSO_{4(aq)}$	3
	$BaCl^+$	1	**Pd**	$PdCl_4^{2-}$	77
Cd	$CdCl^+$	71		$PdO_{(aq)}$	22
	$CdCl_{2\ (aq)}$	25		$PdCl_3^-$	1
	Cd^{2+}	3	**Ra**	Ra^{2+}	100
	$CdCl_3^-$	1	**S**	SO_4^{2-}	60
Cl	Cl^-	99		$CaSO_{4(aq)}$	29
	$NaCl_{(aq)}$	1		$NaSO_4^-$	9
Co	$HCoO_2^-$	71		$MgSO_{4(aq)}$	3
	Co^{2+}	27	**Sn**	$Sn(OH)_{4(aq)}$	100
	$CoCl^+$	2	**Sr**	Sr^{2+}	94
Cs	Cs^+	95		$SrSO_{4(aq)}$	4
	$CsCl_{(aq)}$	5		$SrCl^+$	2
Gd	$GdCO_3^+$	59	**Zr**	$Zr(OH)_{4(aq)}$	100
	Gd^{3+}	26			
	GdF^{2+}	9			
	$Gd(CO_3)_2^-$	3			
	$GdCl^{2+}$	1			
	$GdOH^{2+}$	1			

Table 3-4. Results from the speciation calculations performed for the tracers used in the LTDE-SD *in situ* experiment. In the table, tracers that were affected by the redox potential are presented. Hence, difference in the speciation could be observed due to the redox potential. The aqueous species are expressed as a percentage of total concentration of the tracer. Only species with a percentage equal to or above one have been considered. The calculations were performed with the program PHREEQC together with the data base LLNL, accompanying the PHREEQC package /Parkhurst and Appelo 1999/.

Tracer	**E_h = 470 mV**		**E_h = –90 mV**	
	Specie	**%**	**Specie**	**%**
Np	NpO_2^+	96	$Np(OH)_{4(aq)}$	100
	$NpO_2Cl_{(aq)}$	2		
	$NpO_2OH_{(aq)}$	1		
Se	$Se(IV)O_3^{2-}$	7	HSe^-	100
	$HSe(IV)O_3^-$	2		
	$Se(VI)O_4^{2-}$	91		
U	$UO_2(CO_3)_3^{4-}$	34	$U(OH)_{4(aq)}$	100
	$UO_2(OH)_{2(aq)}$	30		
	$UO_2(CO_3)_2^{2-}$	23		
	$(UO_2)_2CO_3(OH)_3^-$	5		
	$UO_2CO_{3(aq)}$	2		
	$UO_2(OH)_3^-$	1		
Tc	TcO_4^-	100	$(TcO(OH)_2)_{2(aq)}$	52
			$TcO(OH)_{2(aq)}$	48

Concerning the tracers that were not expected to be influenced by the redox conditions, the speciation calculation of the elements Hf and Zr also showed dominance of hydrolysed tetravalent hydroxide complexes, Zr as a non-charged tetrahydroxide complex and Hf as a negatively charged pentahydroxide complex. Furthermore, the speciation of Ag, Cd and Pd were found to be dominated by different form of chloride complexes. The redox insensitive elements Ba, Cs, Na, Ni, Ra, and Sr all had the bare ion as the dominating species. Co was according to the speciation calculations expected to form a $HCoO_2^-$ complex at both redox conditions.

As the LLNL database did not include thermodynamic data for Pa, the database developed by the Radionuclide Migration Research Group, Geological Isolation Research Unit, Geological Isolation Research and Development Directorate, Japan Atomic Energy Agency (JAEA) was used in the speciation calculations for Pa (database version:100331c1.tdb) /Kitamura et al. 2010, Kitamura and Yoshida 2010/. At both redox conditions the aqueous species $PaO(OH)_3$ was found to be the dominating species (100%). Hence, Pa showed a redox insensitive behavior. It should be noted that the elements Gd and Hf were not included in this database. However, this fact did not affect the results for Pa.

Additional calculations were done to investigate if the natural water composition were affected by the addition of the tracers used in the experiment, i.e. the earlier described calculations were compared to the results of calculations in which no addition of the radioactive tracers had been performed. The results clearly show that the speciation of major and minor elements in the aqueous phase was not affected by the addition of tracers.

In addition to the speciation calculations described above, investigations were also performed in order to determine the possibilities of the different tracers forming insoluble compounds that could precipitate from the groundwater. This entity is presented as the saturation index SI=log IAP – log K, where IAP is the ion activity product of the soluble species forming the solid and K is the solubility product of the solid phase. Solid phases with a SI>0 imply that the product of the activities (in this context, corresponding to concentration) of the species forming the solid is higher than the solubility product and a precipitation is likely to occur (supersaturation). On the other hand, a SI<0 indicates that the aqueous concentrations of the species are lower than the solubility product and precipitation does not occur (undersaturation).

The solid phases containing a tracer are presented in Table 3-5 together with the saturation index, SI. The solid phases presented are obtained for the calculation with E_h= 470 mV, i.e. the redox conditions under which the experiment was performed. Further, the presented solids were chosen from the results as follows:

i) All solid phases that contains any of the tracer used in the experiment and where SI>0, i.e. tracers which according to the calculations are potential subject for precipitation.

ii) For the tracers where no supersaturation is indicated, the saturation index is presented for the solid phase that is closest to saturation, i.e. SI=0.

iii) For some tracers where the highest saturation index is obtained when combining the tracer with a groundwater component in very low concentrations (e.g. ^{153}Gd which according to the calculations should be precipitated as a phosphate complex $GdPO_4 \cdot 10H_2O$) precipitations can be argued to be kinetically unfavorable. Therefore, some alternative solid phases are given as well.

iv) For three components not used as tracers but considered to be of importance for the general water chemistry (i.e. Ca, Mn and Fe) results are also presented.

As a general comment to the saturation calculations, it is obvious that the oxidizing conditions have caused a supersaturation of different Fe(III) complexes, with e.g. the Fe_2O_3 compound having a saturation index of 13. Besides the general risk of obtaining a precipitation of strongly sorptive iron oxides, one obtains from the calculated saturation indexes of $CoFe_2O_4$ and $NiFe_2O_4$ (15 and 11, respectively) an indication that supersaturation of phases can occur where different cationic tracers can be co-precipitated into iron oxides-hydroxides.

It is shown in the calculations that the carbonate and sulfate complexes of the alkaline earth metals (i.e. Ca, Sr and Ba) are close to saturation and in some cases even slightly over the saturation index. However, none of these compounds are increased compared to the natural chemical concentration in the experiment so the slight supersaturation thus refers to the natural conditions. One must thus

speculate of the possibility that the calculated supersaturation is influenced by uncertainty in the solubility products used and/or the measured concentrations.

Although used in very low concentrations (sub-μM) indications with respects to the different oxides are obtained for all the tetravalent tracers used in the experiment (i.e. Zr, Sn and Hf). For Zr, supersaturation with respect to the silicate is also obtained. The trivalent Gd used indicate undersaturation for the hydroxide complexes; however, the results of the calculations states that the very minor amount of phosphate present in the groundwater (total phosphate concentration of $5 \cdot 10^{-8}$ M) should cause supersaturation.

Supersaturation is furthermore indicated for different poly-nuclear silicate compounds of uranyl.

An interesting observation is that the tetravalent oxide form of Np (NpO_2) has a saturation index only 2.3 units from saturation, i.e. comparatively minor changes in pH, redox potential and/or total Np concentration could cause a supersaturation of this solid. This is interesting to compare to the aqueous speciation which show a more than 99% dominance of pentavalent species which is good illustration of how the low solubility of NpO_2 at least theoretically should cause reduction/precipitation of Np in comparatively mildly reducing conditions of a groundwater.

The detailed results of the aqueous speciation and the results of the saturation calculations with the implication to the behavior of the different tracers in the experiment are further discussed in Section 3.5.2.

Table 3-5. Saturation indices for tracer containing solid phases calculated for the redox conditions measured during the experiment, i.e. E_h=470 mV. See text above for more details.

Element	Tracer	Element conc. (M)	Supersaturated solids		Undersaturated solids	
			Solid Phase	SI	Solid Phase	SI
Na	Na-22	7.4E–2			NaCl	–3.7
S	S-35	3.7E–3			$CaSO_4$	–0.5
Cl	Cl-36	1.6E–1			NaCl	–3.7
Co	Co-57	2.6E–11	$CoFe_2O_4$	15	$Co(OH)_2$	–9.3
Ni	Ni-63	9.9E–7	$NiFe_2O_4$	11	$Ni(OH)_2$	–5.2
Se	Se-75	6.6E–7			$CaSeO_3 \cdot 2H_2O$	–5.3
					$CaSeO_4$	–5.6
Sr	Sr-85	3.5E–4	$SrCO_3$	0.1	$SrSO_4$	–1.4
Zr	Zr-95	7.4E–8	$ZrSiO_4$	6.0		
			ZrO_2	2.1		
Tc	Tc-99	1E–6			$KTcO_4$	–7.2
Pd	Pd-102	6.6E–6			PdO	–4.8
Cd	Cd-109	1.1E–8			$CdCO_3$	–4.4
Ag	Ag-110m	6.6E–7			AgCl	–0.8
Sn	Sn-113	6.6E–7	SnO_2	1.5		
Ba	Ba-133	4.8E–7	$BaSO_4$	0.3		
			$BaCO_3$	0.2		
Cs	Cs-137	2.0E–8	No relevant solid phases within the database used			
Gd	Gd-153	8.7E–8	$GdPO_4 \cdot 10H_2O$	1.5	$Gd(OH)_3$	–2.4
Hf	Hf-175	7.4E–8	HfO_2	1.4		
Ra	Ra-226	3.2E–8			$RaSO_4$	–0.4
Pa	Pa-233	3.2E–11			Pa_2O_5	–5.0
U	U-236	4.6E–7	$Ca(UO_2)_2(Si_2O_5)_3 \cdot 5H_2O$	3.0	$CaUO_4$	–0.5
			$(UO_2)_2SiO_4 \cdot 2H_2O$	2.6		
Np	Np-237	1.0E–6			NpO_2[A)]	–2.3
Major groundwater components, not used as tracers in the experiment						
Ca		4.3E–2	$CaCO_3$	0.0		
Mn		6.5E–6			MnO(OH)	–1.2
Fe		1.3E–5	Fe_2O_3	13		

[A)] The original data of the solubility of NpO2 in the LLNL database was replaced with data proposed by /Guillaumont et al. 2003/.

3.2 Experimental results

3.2.1 Tracer injection

The injections were executed in accordance with the planned procedure described in Section 2.3.2 with start time for the acidic stock solution injection 2006-09-27 19:00. One minute later the neutralizing base solution was injected. The on-line HPGe measurement shortly after injection is presented in Figure 3-1 for ^{22}Na, ^{57}Co and ^{175}Hf. During the first two hours, the section was circulated only in the stub section and substantial losses of the more strongly sorbing tracers from the groundwater had occurred already at this point. This means that a lower activity concentration entered the 36-mm section compared to the stub surface section for the strongly sorbing tracers. A complete mixing was achieved within approximately 4 hours after the injection.

The RNI-instrument measuring the activity in the test section showed a similar course of events, however with an impact of the background variation since it had a thinner lead shielding than the HPGe-detector.

3.2.2 Circulation

During the experiment groundwater was circulated in the test section (KA3065A03:1), guard section (KA3065A03:2) and in section 3 of the pilot borehole (KA3065A02:3) which is in contact with the same fracture as in the guard section. The circulation operated well and at relatively constant volumetric flow rate, see Table 3-6 for typical flow. A full graph of the circulation flows is presented in Appendix 6.

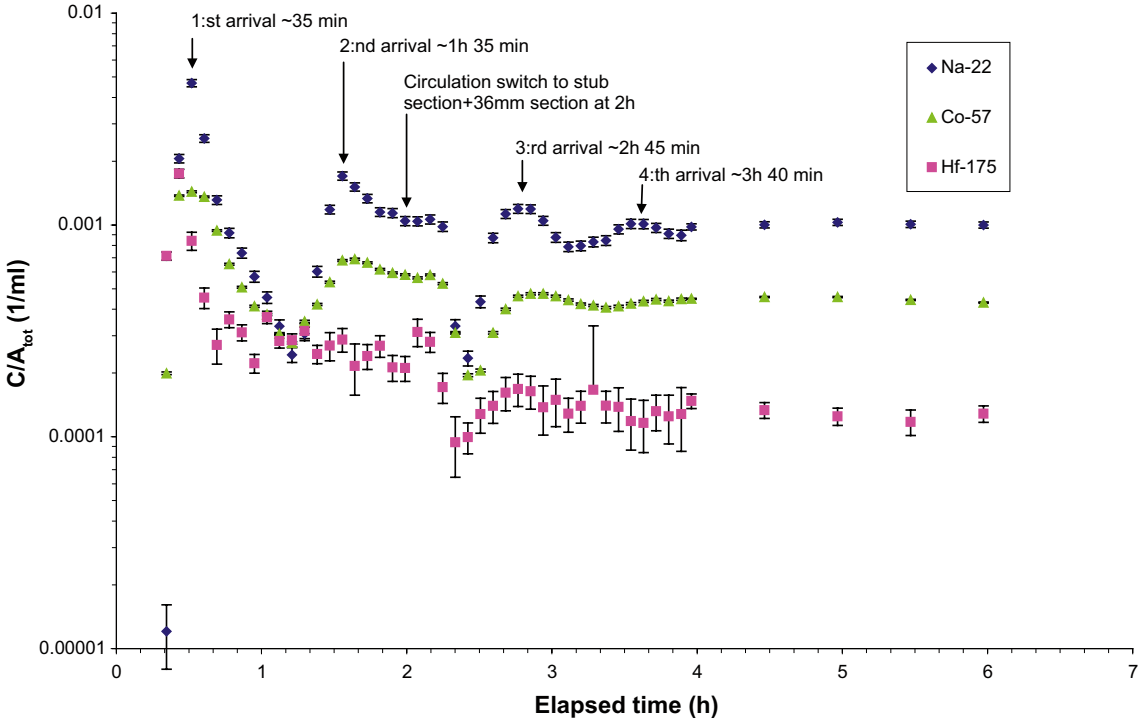

Figure 3-1. *On-line HPGe measurement presented as 5 minute average values for the first six hours following injection for ^{22}Na, ^{57}Co and ^{175}Hf. 20 minutes after the injection, the tracers return and give an increased dose rate which peaks after ~35 minutes. When entering the second lap, the relatively large volume in the pressure regulating cylinder (~400 ml of total ~1,150 ml) is passed and the second lap takes about 1 hour, i.e. it is obtained after 1 hour and 35 minutes. After two hours the circulation is changed to include the slim hole section which causes the dip at ~2.5 hour after the injection. Stable values are obtained for non-sorbing tracers after ~4 hours circulation, indicating that the system is well mixed at this time. Note that ~50% of ^{57}Co and ~80% of ^{175}Hf were sorbed in the system at 2 h time when the circulation was changed to also include the 36-mm section. The sorbed % values may be underestimated since sorption on the detector tubing may have occurred already at this point.*

Table 3-6. Typical volumetric flow rate (ml/min) in the circulated sections.

Test section KA3065A03:1	Guard section KA3065A03:2	Pilot borehole section 3 KA3065A02:3
15	90	160

The test section volume was calculated based on equipment data to 1,150±50 ml at the start of the experiment (i.e. with the pressure cylinder at piston position 50 mm).

3.2.3 Sampling

A total of 25 samplings of groundwater were done in the test section according to the procedure described in Appendix 2. The sampling times are presented in Appendix 4. The method worked as planned with limited pressure disturbances (see Section 3.4.1). In addition, a number of control samples were collected from the guard section and the pilot borehole and at some control points in the tunnel.

3.2.4 Removal of tracer solutions and isopropyl alcohol exchange in the test section

The progress of the removal of the tracer solution from the test section involving the isopropyl alcohol exchange cf. Section 2.4, was followed closely with online HPGe and RNI measurements. The HPGe-results for ^{57}Co, ^{85}Sr, ^{137}Cs and ^{22}Na are presented in Figure 3-2.

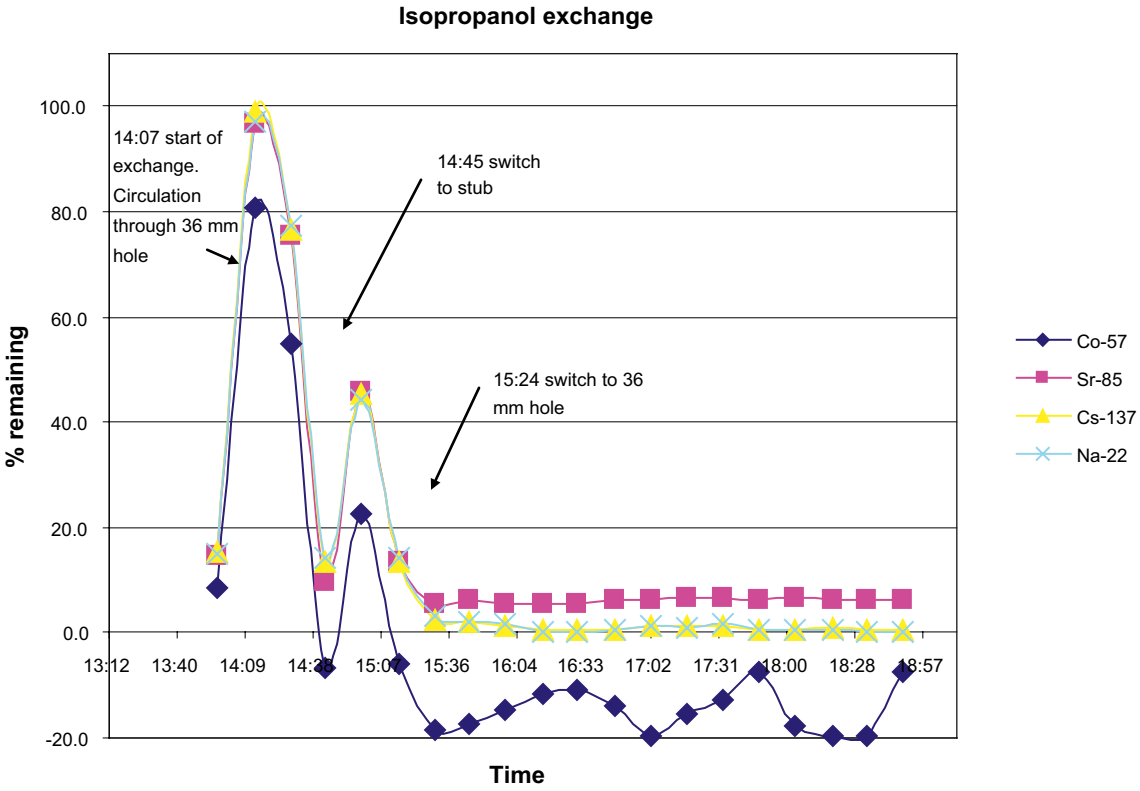

Figure 3-2. *Remaining ^{57}Co, ^{85}Sr, ^{137}Cs and ^{22}Na relative to the concentrations just prior to the exchange. Activity resulting from ^{57}Co adsorbed on the tubes has been subtracted.*

A considerable part of the ^{57}Co was shown to remain in the online measurement after the tracer solution had been removed; this indicated that an adsorption had occurred of the ^{57}Co on the tubing of the measurement cell. Hence, this level of ^{57}Co activity remaining in the measurements after the tracer solution had been removed was defined as a "background" activity which was subtracted when evaluating the ^{57}Co activity in the water measurement performed thereafter. However, as can be seen in Figure 3-2, a majority of these background corrected measurements came to show negative values, indicative of a ^{57}Co desorption from the tubing of the measurement cell taking place due to isopropyl alcohol contact.

Approximately 5 litres of isopropyl alcohol was used during the exchange corresponding to roughly five test section volumes. The last HPGe-measurement made prior to the exchange was used to calculate starting concentrations. ^{22}Na- and ^{137}Cs-values stabilized below 1% of their initial concentration after approximately 2.5 litres of isopropyl alcohol had been injected. At this point the ^{85}Sr levels were still at 6%. After 5 litres had been injected, the strontium seemed to have stabilized at around 6% of its initial concentration, this posed the question whether this was caused by contamination on the tubing in front of the detector or due to desorption within the test section. It was decided to stop the exchange at this point based on the sodium and cesium results.

To try to clarify the issues with strontium the HPGe-loop was filled with water from the guard section after the exchange and analysed. The results indicated that there was no contamination on the tubing in front of the detector. This indicates that during the isopropyl alcohol exchange, a considerable part of strontium is desorbed somewhere in the system, most likely from the rock surfaces in the experimental section. The reason for this is not fully understood, there is e.g. no obvious cation exchange component in the isopropyl alcohol that should compete with Sr in the cation exchange process. One could speculate of a solid phase, e.g. amorphous iron oxy hydroxides and/or any carbonate phase which might be dissolved by the isopropyl alcohol and that Sr adsorbed on or co-precipitated in that mineral is released in that process. The absence of similar release of any other of the strongly sorbing tracers contradicts such a desorption mechanism.

The cyclic pattern corresponds well with the changes made in flow paths, the first series of points are taken with water from the guard section standing in the HPGe-loop prior to the exchange. Immediately after the start of the exchange at 14:07, mainly original tracer solution was passing through the detector loop. The activity then dropped until approximately 15:00 when it again began to rise due to a switch of the circulation flow to the flow path through the slim hole section (cf. Figure 2-11) and the test section water from the slim hole section and corresponding tubing was forced to leave the system. After this the activity dropped again and began to stabilize. The RNI-instrument measuring the total activity of the γ-emitting tracers showed the similar cyclic pattern as the nuclide specific HPGe measurements.

The flow rate during the isopropyl alcohol injection was initially about 9 ml/min but was increased to 15 ml/min after half an hour. At 14:48 the flow rate dropped to 5 ml/min and the pressure increased. The flow rate was restored to approximately 17 ml/min by opening the needle valve further. After this a rather stabile flow rate was maintained.

3.2.5 Epoxy injection

The Epoxy injection was started 2007-04-12 20:50 after cutting the tubes under pressure as close to the borehole as possible using a specially developed technique. At 23:48 a clearly noticeable Epoxy front was noticed in the outgoing tube. At this point approximately 300 ml of easy flowing liquid had been collected averaging about 1.7 ml/min. At 01:30 the Epoxy injection was stopped as the flow rate was close to zero due to the Epoxy having started to cure. The total amount of Epoxy injected was 364 ml. A photograph of the ongoing Epoxy injection is shown in Figure 3-3.

3.2.6 Dismantling

During dismantling of the borehole equipment 2007-04-17 water samples were taken for HPGe-analysis (Figure 3-4). Some low levels of ^{22}Na (hardly visible in most spectra), ^{57}Co, ^{85}Sr, ^{133}Ba and ^{137}Cs were detected but naturally occurring Rn daughters dominated the radioactivity.

Figure 3-3. *The yellow coloured Epoxy resin being injected at the borehole collar.*

Figure 3-4. *Dismantling of borehole equipment showing water collection container below the borehole collar where water was sampled and monitored for γ-radiation. The hydraulic packer is being dismantled.*

A scintillation contamination detector was also used to measure the activity during the procedure, with most borehole equipment showing no rise above the background (between 10–15 cps).

The hydraulic packers and supporting steel plate for the PEEK lid, (cf. Section 2.1.1 and Appendix 1, Figure A1-4) gave a small increase above the background values (about 20–25 cps). This may be a result of extra Rn daughters accumulating on the borehole walls sticking to these larger objects as they were slowly hauled out of the borehole. The smaller pipes that did not touch the borehole wall gave lower count rates.

Scanning of surfaces made by Clab radiation personnel cleared the entire equipment for storage. This supports that the slight increase in radiation may have been due to Rn and its daughters.

A RNI-instrument with external plastic scintillating probe (1.5”×1.5”) was used to monitor the γ-radiation in the water flowing from the borehole and the data are presented in Figure 3-5.

3.2.7 Over core drilling

Over core drilling was performed during the period 2007-04-24 to 2007-05-02. Preparation of the drilling machine is shown in Figure 3-6. The rock volume that was extracted by the over-core drilling, i.e. the core stub and the rock surrounding the slim hole test section, is outlined in Figure 2-3. An unexpected release of the PEEK-disc and injected Epoxy resin at the interface between the resin-rock surface occurred during the over core drilling. In combination with a failure of an evacuation pump that was keeping the borehole dry, the stub rock surface was flushed with natural groundwater for a maximum of three days. Low levels of ^{22}Na (observed in one sample only), ^{57}Co, ^{85}Sr, ^{133}Ba and ^{137}Cs were detected but naturally occurring Rn daughters dominated. ^{137}Cs was the radionuclide that was observed giving the highest activity releases during the dismantling and overcoring, the other radionuclides were below detection limits in most samples.

The maximum amount of tracer that was removed from the KA3065A03 borehole during the whole dismantling and drilling procedure was estimated to be <0.9 MBq for ^{137}Cs which gave the highest activity concentrations in the borehole water (at maximum ~25 Bq/L at the moment when the release occurred). This estimation is based on measured concentration in the borehole water and applicable detection limits (~2 Bq/L). For ^{22}Na, no tracer in the borehole water was detected except for the first sample and the estimated maximum amount based on detection limits was <0.4 MBq. A compilation of sample analysis results for ^{22}Na and ^{137}Cs during dismantling and over core drilling is given in /Nilsson et al. 2010/.

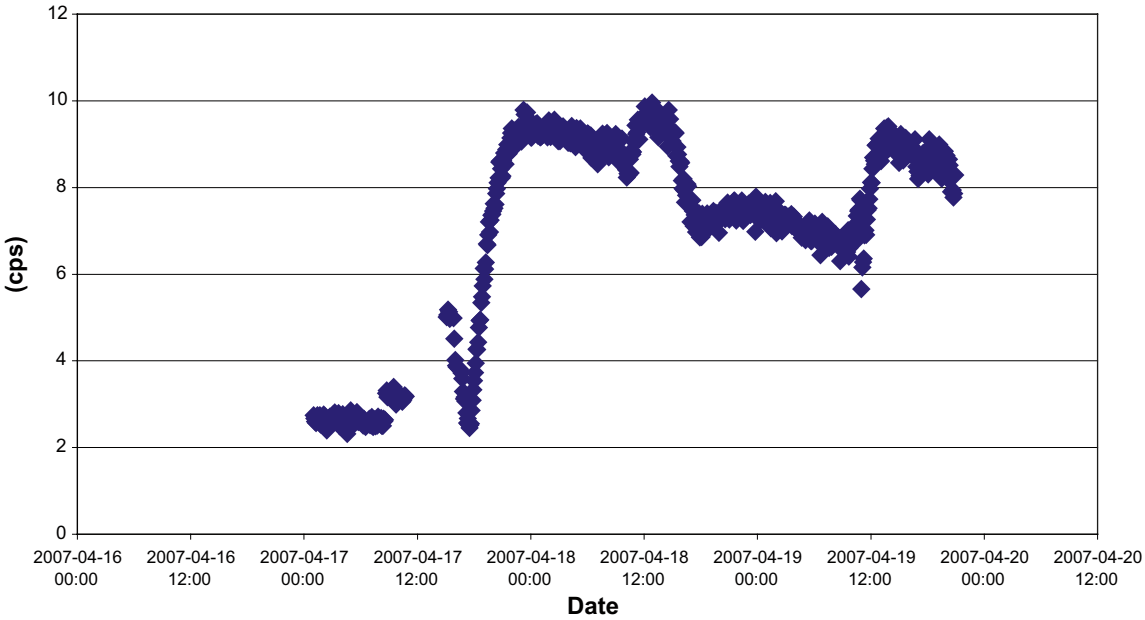

Figure 3-5. *RNI γ-radiation measurement count rate (cps = counts per second) during dismantling. After a couple of hours from the dismatling 2007-04-17 the count rate stabilized at approximately 9–10 cps. HPGe-analysis during this time period showed that this is a result of an increase in Rn daughters. When all equipment had been removed and the borehole was sealed at 2007-04-18 14:37 the instrument measured a stable water volume circulated in an open vessel, consequently the count rate dropped as a result of Rn leaving the water. When the borehole was opened for sampling at 2007-04-19 09:50 the count rate again increased to about 9 cps due to an increase in Rn and its daughters.*

Figure 3-6. *Drilling machine is prepared for 300 mm diameter over-core drilling at experimental borehole KA3065A03. Drill bit with core barrel in centre of photo. Open vessel for collecting drilling fluid beneath borehole collar.*

3.3 Groundwater characterization

3.3.1 Chemical composition

The rationale of the LTDE experiment was to perform experiment under as natural site conditions as possible. Consequently, the water that was let into the isolated borehole section was water naturally present in the surrounding fracture and no address of the impact of any changed water composition was performed within the project.

The groundwater in the guard section (connected to the test section during sampling) was sampled 2006-06-20 for chemical analysis, including trace elements and a few heavy isotopes. The results (in Sicada as SKB sample number 6918) are presented in Appendix 5. The groundwater composition is practically unchanged relative to that of previous measurements. The water is a sulphate rich sodium-calcium-chloride type of water, Na-Ca-(Mg)-Cl-SO4-(HCO3), with a Cl content of 5,810 mg/L. It is a Transition type of water between Brackish Glacial and Brackish Non-marine groundwater, with a component of Brackish Marine (Littorina) water. Water of this type is found at 100–600 m depths at Äspö HRL /Laaksoharju and Wallin 1997/ and at 350 to 550 m depth interval at Laxemar site /Laaksoharju et al. 2009/, as well as at Forsmark site at about 300–600 m depth /Laaksoharju et al. 2008/.

Laboratory batch sorption experiments were carried out within the SKB site investigation programme to determine bedrock transport properties at sites Laxemar /Selnert et al. 2009/ and Forsmark /Byegård et al. 2008/. The water sampled from the LTDE-SD test section fall in with water types II (Brackish groundwater with marine character) and III (Brackish groundwater of dominantly non-marine origin) used for Laxemar site. The LTDE-SD water also fall in with water types II (Brackish/marine character) and III (Brackish/saline), used for Forsmark site.

3.3.2 E_h measurements

For a view of the E_h conditions during the injection of the radionuclides, see Figure 3-7. The injection gave a very slight drop in redox potential and the potential was about 400 mV the hours after injection.

However, the redox potential was in the range of 450–500 mV during the major part of the experiment, see Appendix 7. However, some interference of the measurements during October 9 to October 20 has caused lack of credible experimental data during this period, including some less severe disturbances at the shift between September and October. The reason for the disturbances has not been elucidated. The data peak from November 22 is caused by a control of the functioning of the electrodes.

The reason for the high E_h-value has not been explained. Discussions of possible causes consider the fact that the borehole remained open for a long time after the drilling. During this time the stub was submerged in water flowing out of fractures at reducing conditions but in contact with air at the water surface. Therefore the surfaces, mainly the one on the stub surface, may have oxidized resulting in a low reduction capacity in the system. The oxygen that potentially penetrates parts of the circulation loops, especially through the valves, would then be sufficient to counteract the possibility of attaining a low redox potential.

The judgment during the experiment was that no efforts of reducing the E_h value should be made, as the following calculations and modelling would be very difficult if the redox potential would have a slow transient course towards a lower E_h-value.

3.3.3 pH measurements

The on-line measurement of the pH was in operation during the whole experiment. For a view of pH during the injection of the radionuclides, see Figure 3-8.

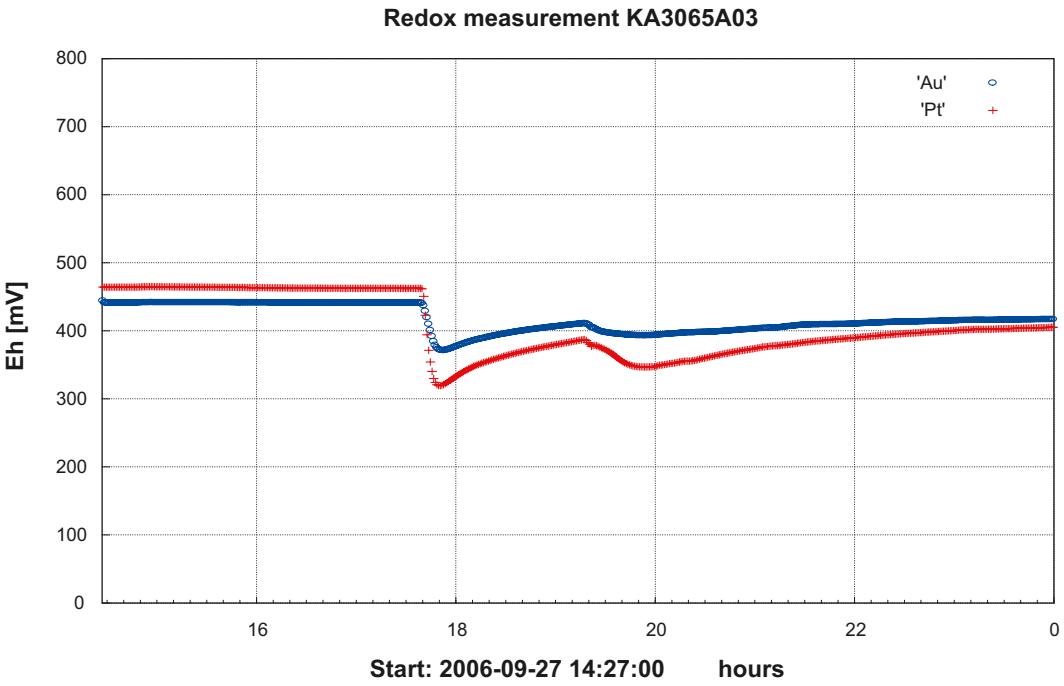

Figure 3-7. *E_h (mV) during the hours prior to and after the injection at 2006-09-27 19:00. At 17:40 the circulation was switched to the stub surface only which lead to a slight drop in redox potential which however increased somewhat before the time of the injection. A further slight drop is noticed after injection followed by a slow increase to about 400 mV.*

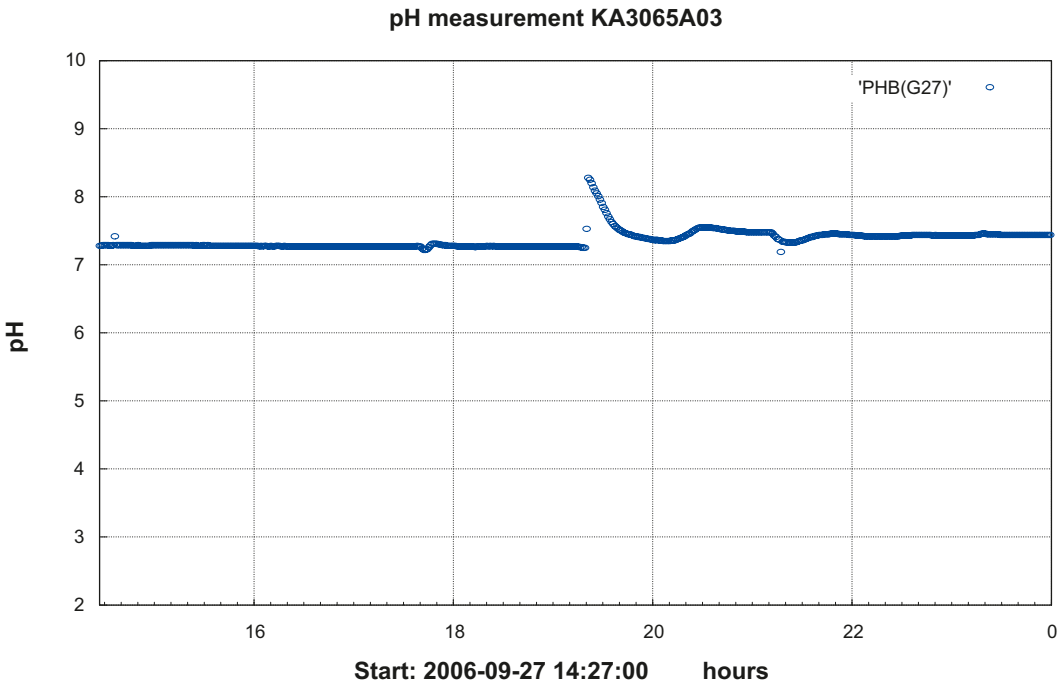

Figure 3-8. *pH during the hours prior to and after the injection at 19:00 hours. A pH increase with peak ~8.3 is seen shortly after injection approximately at the time of the first return of the radionuclides. A small pH drop is seen after the circulation is switched at 21:00 and pH stabilizes at about 7.4 after 22:00.*

However, some unidentified interference to the measurements during October 9 to October 20 has caused lack of experimental data also for pH during this period. One of the pH-electrodes was malfunctioning already since the calibration prior to the start of the experiment. However, a decision was made to continue using only one electrode due to risks with disturbances of the experiment and risks of leakages in connection with an electrode switch. The pH value has been quite stable and slightly decreasing from 7.3 to 6.9 by the end of the experiment see Appendix 7.

A sample for manual measurement of pH was taken 2006-11-30 in order to verify the functionality of the on-line measurement. It was closed in the inert gas (nitrogen) and transported quickly to the laboratory where pH was analyzed directly in the test tube. The equipment was pre-equilibrated in the same type of tube. The pH was 7.4 which can be compared with the actual on-line value at the time of sampling which was 7.2 The agreement must be considered as satisfactory taking the pressure difference of almost 3,600 kPa and the time delay to analysis in the laboratory into account. The result is also in good agreement with earlier pH-measurements in the same borehole. The results from manual sampling and measurements are presented in Table 3-7.

Table 3-7. pH measurement in samples from KA3065A03.

Date	Time	Action	pH
2006-11-30	13:40–13:42	Sampling	–
2006-11-30	14:55	Analysis	7.39
Earlier measurements:	*SKB No.:*		
2000-02-07	3049	–	7.40
2003-06-25	6046	–	7.73
2004-01-21	6253	–	7.34
2006-06-20	6918	–	7.34

3.3.4 Microbes

A groundwater sample collected 2006-06-25 was analysed for ATP (adenosine triphosphate). ATP transports chemical energy within cells for cell metabolism and is used here for estimation of the groundwater microbe content. The ATP concentration was $(7.2\pm1.1)\cdot10^{-11}$ mol/L which roughly corresponds to a total number of cells concentration (TNC) of $\sim1.2\cdot10^{5}$ cells/ml according to a relationship between ATP and TNC established in the Laxemar Site Investigation /Hallbeck and Pedersen 2008, Figure 1-3/. This is a relatively high value for deep groundwaters but within the range found in the Laxemar Site Investigations. It is somewhat lower than the measurement at LTDE-SD in 2005 that was $3.3\cdot10^{5}$ cells/ml /Widestrand et al. 2006/.

3.3.5 Inorganic colloids

The results from the inorganic colloid filtration for the section 10.39–10.70 m in KA3065A03 are presented in Table 3-8 and in figures in Appendix 8. The analysed elements are re-calculated to amounts of their most probable mineral phases (K- Mg- illite, iron hydroxide, and silica). The results from the corresponding blank filter samples (the same procedure performed with deionised water) have been subtracted, as these were rather high. The figures presented in Appendix 8 are not corrected for high blank samples.

The bars in the figures in Appendix 8 represent amounts (µg) of aluminium, iron, silicon and manganese, entering the filter package, accumulated on each filter and present in the collecting container. Calcium, manganese and sulphur were not detected on the filters. The amounts are calculated assuming that the water volume passing through the filters and into the collecting container is equal to the filtrate volume. This is not quite the case, as up to ten millilitres will be left in cavities in the filter holder package, in the tubing and in valves. Further, a small volume of about 0.01 to 0.06 mL is left in each filter after the filtration and its salt content is included in the analysis.

The presented input amounts in the figures in Appendix 8 represent the sample taken on-line just before opening the sample containers (“alternative input concentration” in Table 3-9).

The concentrations in blank samples (rinsing water), sample containers, collecting container and pumped groundwater are given in Table 3-9. The remaining water in the sample containers after filtration was contaminated by aluminium and iron.

The following conclusions may be drawn from the colloid filtration results:

- The amount of aluminum and iron in the filters and found in the collecting container does not balance the input amount when the results are compared with the results from the rest volume in the sample container. Therefore, the results are presented with the results from the collected water as the input concentration in Appendix 8.
- Compared with previous results from colloid filtration tests in the Laxemar area, the amounts of inorganic colloids are equal or lower with some exceptions /Bergelin et al. 2008a, b, c/.
- The applied method for analysis of colloids does not comprise analysis of organic constituents. No analysis of organic colloids (Mätsystembeskrivning för fraktionering av humus- och fulvosyror. SKB MD 431.043) has been performed, as previous results from the Laxemar Site (with some exceptions) have shown that in general the dominant organic fraction consists of low molecular organic acids which are not considered to behave as colloids. Later results from analyses of organic material in groundwater from Äspö HRL have shown that the vast majority is present as low molecular acids (Sara Holmström, Department of Geological Sciences, Stockholm University, 2010, pers. comm.).

Table 3-8. Colloid concentrations measured in the sample from section 10.39–10.70 m in KA3065A03.

Filtration through a series of connected filters						
Idcode/secup/ filter pore size (µm)	Filtrate volume (ml)	Element content/mineral phase on each filter per litre of water (µg/L)			Mineral phases (µg/L)	
		Al	Fe	Si	Total/ filter*	Sum**/ three filters
KA3065A03/10.39/0.4	322	0.65/9.3	5.0/9.6	<0.5/1.1	19	
KA3065A03/10.39/0.2	322	<0.01/<0.1	1.3/2.5	<0.5/1.1	2.5	
KA3065A03/10.39/0.05	322	<0.01/<0.1	0.37/0.71	<0.5/1.1	0.71	41

* Total content on each filter. Aluminium is calculated as 2.3 Al in K- Mg- illite (383.9 g/ mol) iron is calculated as $Fe(OH)_3$ (106.8 g/mol) and Si as silica (60.1 g/mol).

** Sum of content (mineral phases) on the three filters (0.4, 0.2 and 0.05 µm).

Table 3-9. Element concentrations in blank water, remaining water in sample container, collected output water from filter system and in pumped water that has not passed the filter system.

Section m	Sample origin	Al µg/L	Fe mg/L	Si mg/L	Mn µg/L	Ca mg/L	S mg/L
10.39–10.70	Blank, deionised water	5.25	0.0053	<0.03	9.19	<0.1	<0.2
	Rest volume sample container (input conc)	27.6	0.118	6.48	246	741	93.8
	Collecting container	6.4	0.0197	6.52	228	756	94.0
	Collected water (alt. input conc)	3.20	0.0132	6.56	227	768	95.0

Blank, deionised water = Deionised water from the tap, input concentration in leakage test.
Rest volume sample container = remaining water in the sample container after filtering experiment.
Collecting container = water that has passed the filter system.
Pumped water = regular sample collected at the surface and not *in situ* in the borehole section.

3.4 Environmental monitoring

3.4.1 Pressure

All packed off borehole sections involved in the LTDE-SD project are connected to the Hydro Monitoring System (HMS) for pressure monitoring.

The LTDE-SD area is surrounded by two dominant conductive structures, NW-2 and NW-3. The conclusion from the hydraulic pre-tests /Wass 2005/ was that the NW-2, NW-3 and related structures are of vital importance for the hydraulic pressure responses in the LTDE-SD boreholes.

In Appendix 9 an overview of the pressure in some of the LTDE-SD borehole sections is presented. The experimental hydraulic conditions were stable according to monitoring of pressure, apart from short pressure disturbances. The pressure in the test section varied between 3,580 to 3,600 kPa during normal circulation. Most of the disturbances, seen particularly in the test and guard sections in KA3065A03, are due to injection and sampling occasions in the borehole.

A small disturbance occurred on October 11, 2006, when the pressure decreased ~8 kPa in the innermost sections in KA3065A03, including the test section and reference fracture in the guard section. The same day the pressure also decreases with ~8 kPa in the entire closest surrounding rock volume (KA3065A02, KA3067A, KA3068A, SA3045A, KA2050A), except in KA3010A where the pressure drop is larger, ~15 kPa. In the area outside of the immediate vicinity the pressure dropped 1–5 kPa (KA3005A, KA3105A and KXTT1–5). Probably some activity occurred in KA3010A which affected the pressure in this borehole and the surrounding rock. The pressure is decreased

equally in all boreholes and sections, i.e. in the fracture system of the entire rock volume in the vicinity of LTDE-SD. Consequently, the hydraulic gradients remained unchanged and the pressure changes that occurred are not assessed to influence the experimental result of the *in situ* experiment. As a comparison to the pressure dip on October 11, the daily oscillation due to tidal effects is within 2–3 kPa in the LTDE-SD area and the large-scale variations are even larger than that.

The pressure regulator was in stable operation without failures during the experiment period September to April, see Appendix 6. Prior to the start of the experiment the cylinder was filled up with groundwater by running the piston backwards to a position of about 50 mm (maximum 500 mm) in order to allow for outtake of sampling volumes during the tests and still to enable pressure regulation to lower pressures if needed. The piston position was stable between sampling occasions, indicating that the system was tight.

More detailed plots over the pressure in the test and guard sections in borehole KA3065A03 during injection and sampling procedures for the initial 2 hours are shown in Figure 3-9. The first injection (acidic injection, valve 15) was made at 19:00 and is only slightly visible in the pressure plot. The second injection (basic injection, valve 14) was made at 19:01. The pressure dip associated with the second injection at 23:56 was caused by compression of nitrogen gas trapped in the injection loop. The following drawdowns around 20:00 and 21:00 are sampling occasions.

Short, small pressure responses in the guard section (KA3065A03:2) are noticed at several occasions in conjunction with pressure changes due to sampling or injections in the test section. It can be seen in Figure 3-9 (lower figure) that the response in the guard section appears both in the beginning and at the end of a drawdown in the test section. It is observed as a pressure decrease following the opening of the test section and as a pressure build-up when the pressure is restored by piston movement. The reason for this behaviour is likely due to responses through the rubber-cylinder seal at the stub. The pressure in the test section was restored quickly by the pressure regulator after sampling and injections as can be seen in Figure 3-9.

Altogether, the overall results indicate that the attempts to maintain natural pressure conditions seem to have worked out well. One can therefore assure that any penetration into the rock matrix must be considered as a result only of diffusion and that no advection was involved.

3.4.2 Temperature

Temperature data are presented in Appendix 6. Initially, the temperature in Container 1 was set to approximately 18ºC as a compromise between dry conditions for electronic equipment and near the rock temperature. However, this lead to problems with condensation on the HPGe-detector and the temperature had to be increased during October 2006. After preventive measures the temperature in Container 1 was kept at ~22ºC.

Coolers inside the inert gas boxes reduced the temperature relative to that of the container air, most efficient in the pressure regulating box since the heat generation was lower in that box than in the glove box with the circulation pump. During October, the water temperature in the flow cell (inside the glove box) was elevated to <21 ºC and for the remaining period the maximum water temperature outside of the borehole was <19 ºC, i.e. a 4 ºC increase relative to the rock temperature in KA3065A03, see Appendix 6, Figure A6-4. The temperature at 10 m in the borehole was steady around 15 ºC. Table 3-10 presents the temperatures in different equipment parts 2006-12-14. A diagram showing temperatures versus time is presented in Appendix 6, Figure A6-3.

Table 3-10. Temperature (ºC) in various circulation equipment parts 2006-12-14.

~10 m depth in borehole KA3065A03	Tunnel (air)	Container 1 (air)	Incoming circulation water to glove box	Glove box (atmosph.)	Flow cell water	Pressure cylinder inert gas box (atmosph.)
15.0	16.5	21.8	17.0	19.2	18.0–18.5	15.0

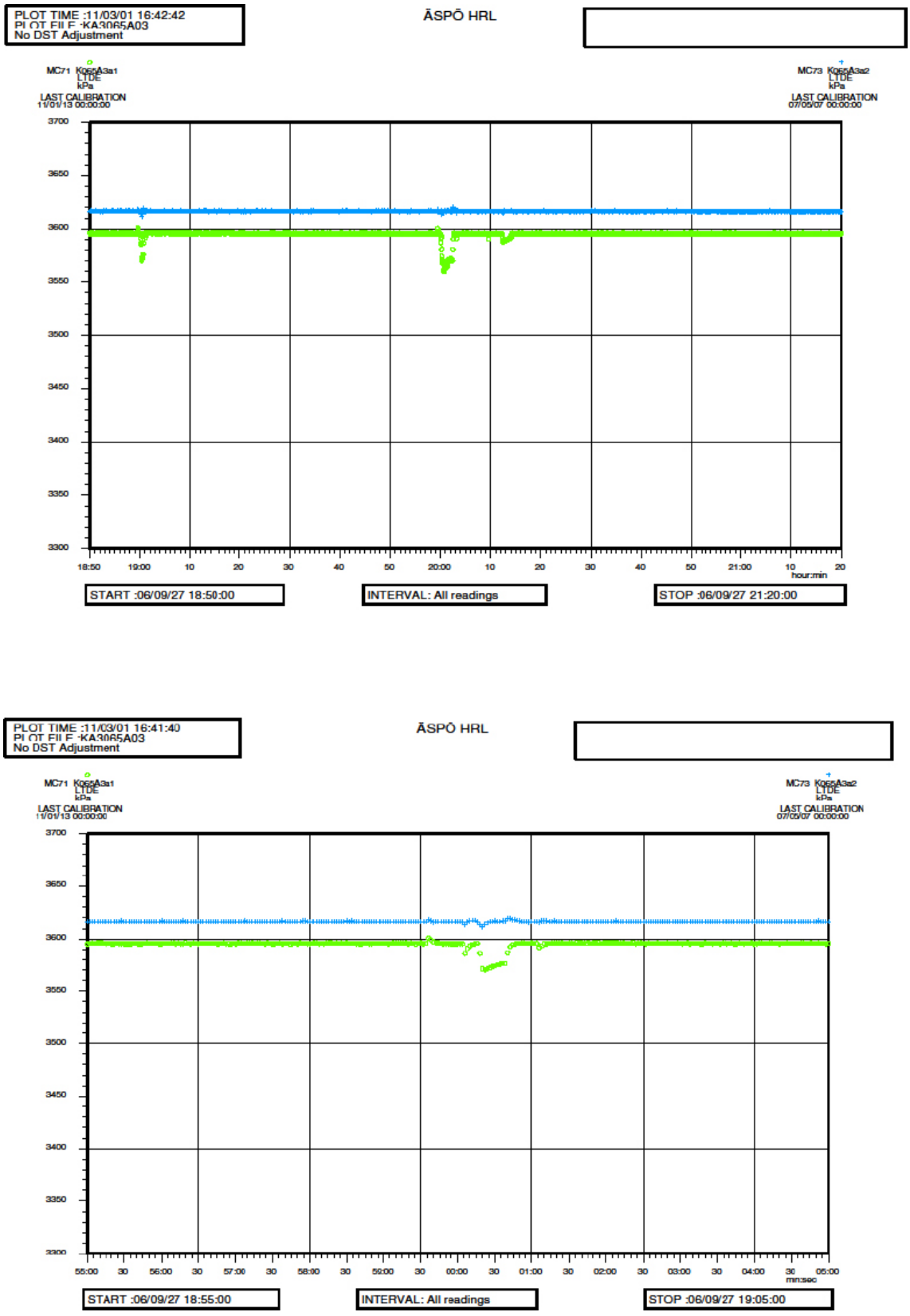

Figure 3-9. *Pressure in the test section (green) and the guard section (blue) between 18:50 and 21:20 (top figure) and 18:55 to 19:05 (lower figure) on the day of injection 2006-09-27. Y-axis scale is 3,300–3,700 kPa.*

3.4.3 Environmental radioactivity control

No experimentally related tracer radioactivity was detected in any of the guard section samples or pilot borehole samples taken during the course of the experiment phase. After completion of dismantling and over core drilling, tracer radioactivity was neither found in the pilot borehole, nor in the control points along the tunnel. The typical detection limit for ^{22}Na was 0.5 Bq/L in the environmental samples.

Dose rate monitoring was done continuously at the fence that restricts the controlled working area towards the tunnel and in the Container 1 near the glove box. A plot of the dose rates from these points is presented in Figure 3-10. The figure clearly shows an increased dose rate at the time of injection, a decreasing dose rate during the circulation phase and a return to normal background levels after termination of the experiment and full dismantling of the radioactive tubing etc in June/ July 2007.

The handling of radionuclides in the LTDE-SD *in situ* experiment is included in /Nilsson et al. 2010, Appendix 2/.

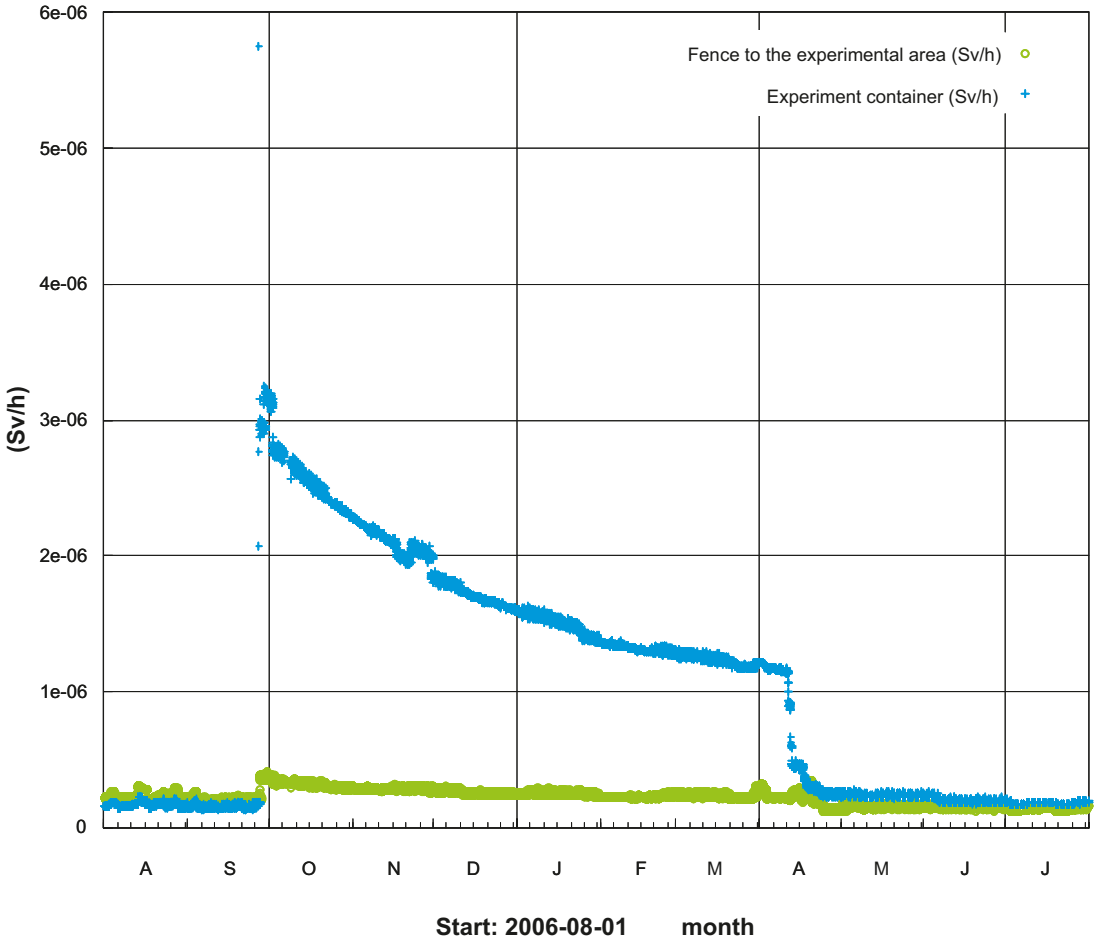

Figure 3-10. *Dose rate monitoring (in Sv/h) at the fence to the experimental area (green circles), and in the experimental container (blue crosses). An increased dose rate is observed at the time of injection, a decreasing dose rate during the circulation phase and a return to normal background levels after termination of the experiment and full dismantling of radioactive tubing etc in June/July 2007.*

3.5 Tracer concentration measurements in the water phase

3.5.1 Injected radioactivity

The injected amounts of the different tracers are presented in Table 2-1.

3.5.2 Tracer concentration-time curves

The on-line measurement loop was affected by sorption on the tubing as is shown and discussed further below. Consequently, only sample concentration measurements have been used for all tracer evaluations. The only exception is ^{233}Pa and ^{95}Nb for which the first few on-line results were used.

Below the tracer concentration versus time are presented for different groups of tracers. A summary of the part of the tracers that remained in the aqueous phase is given in Table 3-11. The results in the figures below are given as concentration of the tracer in the aqueous phase (C) divided by the total amount (A_{tot}) injected of that tracer. The concentration uncertainty was calculated based on the radiometric measurement uncertainty. The error bars are included but are relatively small compared to the size of the concentration points in most figures in this section.

Na^+ and Cl^-

Na^+ and Cl^- are the two tracers for which adsorption clearly can not visually be shown in the tracer concentration-time curves (Figure 3-11). From the results of the chemical speciation calculations, it is shown that these two elements are present in their ionic form (Na^+ and Cl^-, respectively). The low (if any) sorption of Cl^- is explained by the negative charge that causes electrostatic repulsion from negatively charged surfaces of the rock material. The Na^+ is expected to interact with these surfaces but due to the relatively high ionic strength of the groundwater, there is a pronounced competition for the relatively low number of cation exchange sites which causes the relatively weakly sorbing Na^+ to be outcompeted in the cation exchange process.

Based on the average of the 4 first ^{36}Cl measurements C/A_{tot}, an experimental volume of 1,140±60 ml was calculated using the assumption of no sorption of this tracer. This is in good agreement with the volume estimation performed using the equipment data to 1,150±50 ml.

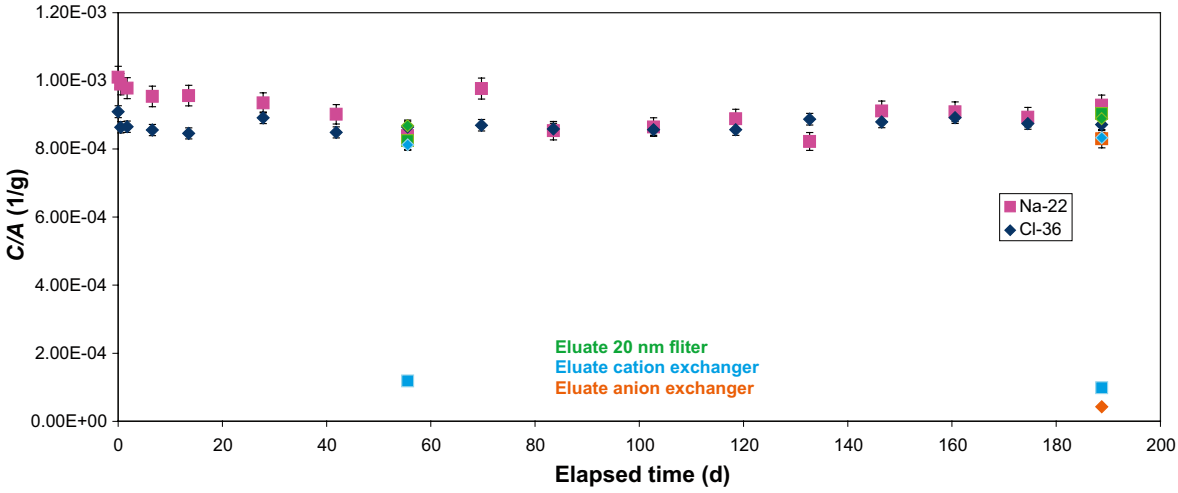

Figure 3-11. *Tracer concentration in C/A (1/g) where A is the injected radioactivity versus elapsed experiment time for ^{22}Na and ^{36}Cl.*

Cs^+

For the monovalent cation Cs^+ approximately 64% of the added tracer was sorbed at the end of the circulation phase of the experiment (Figure 3-12). As expected, the results of the chemical speciation calculation show a dominance of the non-complexed cation Cs^+, (95%); however, indications are obtained of some chloride complexation. The much stronger adsorption compared to the other monovalent alkaline cation is fully expected from the knowledge of sorption properties of cation exchange sorbing tracers in saline groundwater environment of e.g. /Byegård et al. 1998/.

Divalent alkaline earth metal cations Sr^{2+}, Ba^{2+}, Ra^{2+}

For the hard divalent cations (alkaline earth metals, expected to adsorb mainly by cation exchange) used in this investigation, the amount of adsorbed tracer varies from 18% (Sr) to 34% (Ba) and 52% (Ra). Their respective order in sorption strength is thus as expected from e.g. earlier investigations (e.g. /Andersson et al. 2002, Byegård et al. 1998/). The experiment results are presented in Figure 3-13.

The clear observation of a decrease in the Sr tracer content is somewhat unexpected. Based on earlier laboratory experiments (e.g. /Byegård et al. 1998/) batch sorption experiments performed in saline groundwater environment almost always show no decrease of the Sr tracer content in the water phase. A possible explanation for this could be sulfate and/or carbonate precipitation of Sr^{2+} and maybe also for Ba^{2+} and Ra^{2+}. However, the chemical speciation calculations do not clearly show that these solid phases should be supersaturated; saturation indices of up to 0.3 are obtained but it can not be ruled out that uncertainties in the concentration measurement and the solubility data may have had an impact on this. Since any increase of neither the metals nor the sulfates/carbonates should be obtained because of the tracer injection; the natural concentration of all these species should be obtained after the injection had been performed. Consequently, the supersaturation indicated by the speciation calculation is thus also obtained for a natural groundwater and they can therefore not easily be used for explaining the Sr loss observed.

However, one possible explanation to the Sr loss is that the sodium hydroxide injection (made in order to neutralize the acidified tracer cocktail, cf. Section 2.3.2) could have been poorly mixed, thus causing local pockets where carbonates precipitations could have occurred. Nevertheless, the on-line pH measurement shows very stable values and do not indicate any mixing problem.

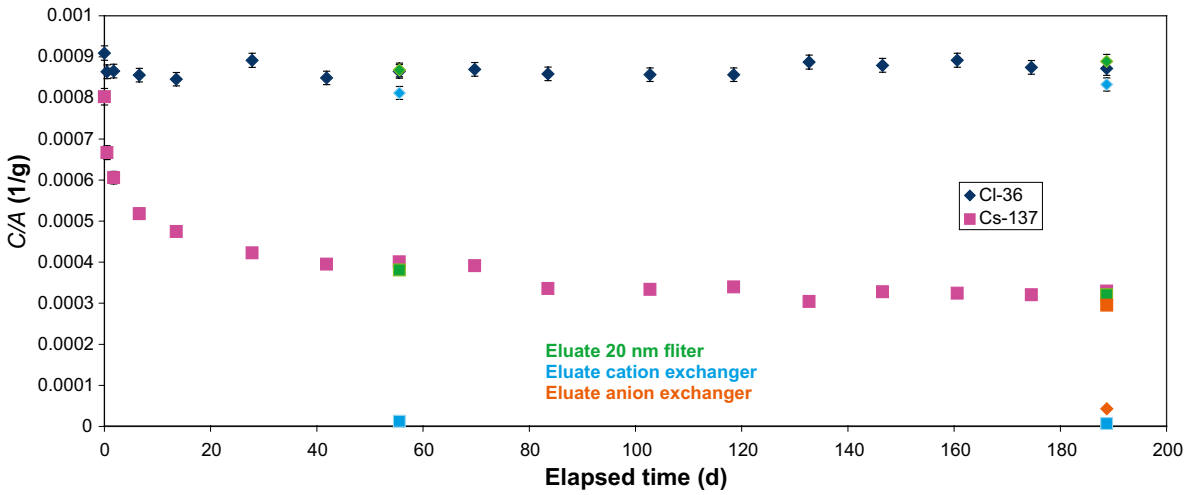

Figure 3-12. *Tracer concentration in C/A (1/g) where A is the injected radioactivity versus elapsed experiment time for ^{137}Cs. ^{36}Cl is included for comparison.*

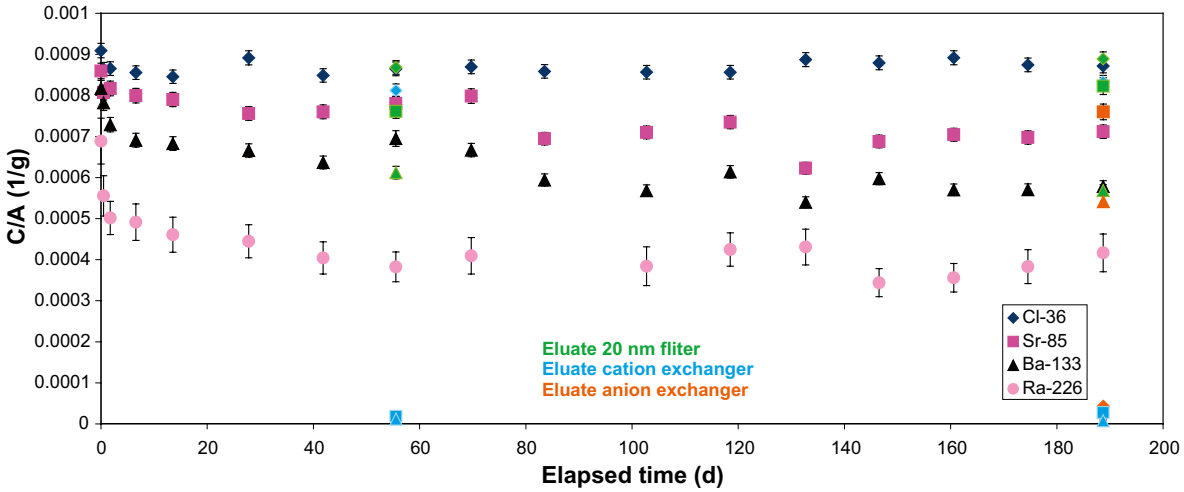

Figure 3-13. *Tracer concentration in C/A (1/g) where A is the injected radioactivity versus elapsed experiment time for ^{85}Sr, ^{133}Ba and ^{226}Ra. ^{36}Cl is included for comparison.*

SO_4^{2-} and SeO_4^{2-}

The experiment results are presented in Figure 3-14. The sorption studies indicate a loss of the divalent anions/oxy-anions of sulfur (29%) and selenium (42%). The chemical speciation indicates that by applying electrochemical conditions according to the measured Eh of +470 mV, they should be present as SO_4^{2-} and SeO_4^{2-}, respectively. However, the speciation calculations also yields that different species of $Se(IV)O_3^{2-}$ (9%) should be present in the solution. These species have been shown to strongly adsorb on different iron-oxyhydroxides (e.g. /Duc et al. 2003/) which through a coupled equilibrium therefore could explain the losses of ^{75}Se obtained in the beginning of the experiment. A similar mechanism for losses of ^{35}S by reduction to sulphite may therefore also be possible.

An alternative explanation for the losses could be an initial precipitation caused by a temporary oversaturation of Ca, Sr and/or Ba selenates and/or sulfates during the initial mixing process during the injection. However, the chemical speciation calculation shows no supersaturation with respect to any of the selenates which thus contradicts selenate formation as the reason for the loss of that tracer. Concerning the sulfates, the speciation calculation show supersaturation with respect to $BaSO_4$, but, as mentioned above, the injection actually give no increase of the chemical concentrations of neither sulfates nor the Ca, Sr and Ba cations.

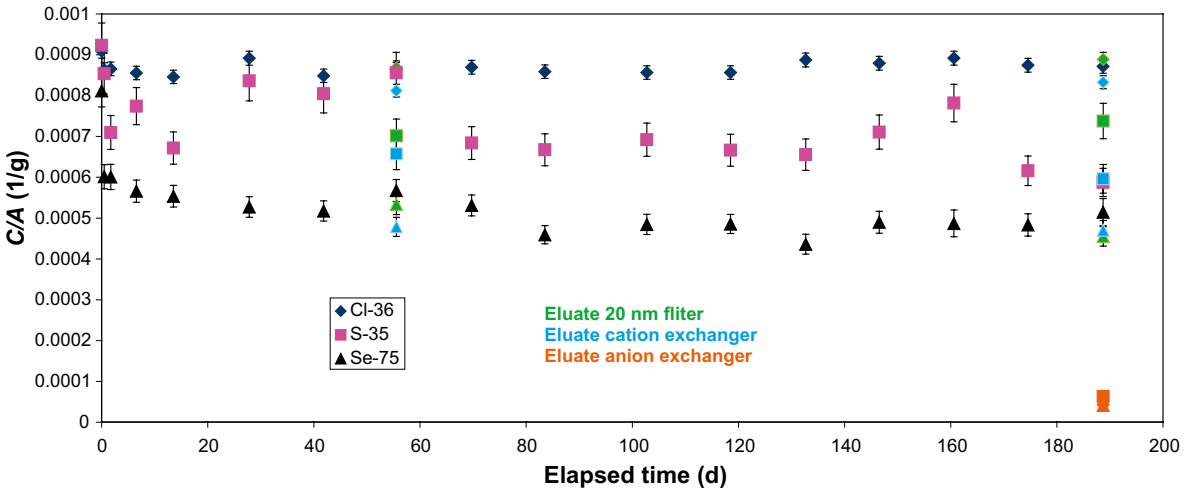

Figure 3-14. *Tracer concentration in C/A (1/g) where A is the injected radioactivity versus elapsed experiment time for ^{35}S and ^{75}Se. ^{36}Cl is included for comparison.*

Transition metals, monovalent cation, Ag

The tracer ^{110m}Ag is strongly adsorbed in the experiment, it can be shown that more than 99.5% of the added tracer is sorbed, see Figure 3-15. The chemical speciation calculations indicate that the high chloride concentration in the groundwater forces the ^{110m}Ag tracer to form negatively charged chloride complexes where the $AgCl_2^-$ complex should dominate. According to the speciation calculations, the combination of low Ag concentration and high chloride concentration causes formation of complexes that are strong enough to prevent precipitation of AgCl(s). However, the high sorption indicates that the complexation is not strong enough to prevent sorption of ^{110m}Ag to e.g. the rock surfaces.

Transition metals, divalent cations, Ni, Co, Cd and Pd

Concerning the different divalent transition metals included in this experiment, the adsorbed amount of tracer varies from 68% (Ni), 82% (Cd) and 99% (Co), see Figure 3-16 for the experiment results. The calculated chemical speciation yields somewhat opposite results; the strongly sorbing ^{109}Cd and ^{57}Co should be present in the aqueous phase as aqueous complexes ($CdCl^+$ and $HCoO_2^-$, respectively) while the somewhat more weakly sorbing ^{63}Ni should be present as non-complexed Ni^{2+}. It is therefore an indication that the aqueous complexation is not strong enough to offer any strong competition to the adsorption reaction for these elements.

The injected stable isotope ^{102}Pd, presented in Figure 3-16, was never detected in the sampled groundwater and the detection limits shows that more than 97% of the injected tracer was sorbed. The detection limits in the eluates from the cation exchanger is one order of magnitude lower; this probably since the eluate contains lower amounts of Sr; an element that interferes with the ICP-MS measurement of the ^{102}Pd. The chemical speciation calculation yields a dominance of a $PdCl_4^{2-}$ complex in the aqueous phase; a complexation that obviously is not strong enough to prevent sorption to the geologic material.

The chemical speciation calculations indicate a supersaturation for both Co and Ni as the solid phases $CoFe_2O_4$(s) and $NiFe_2O_4$(s), respectively. Formation of such polynucleus complexes with compounds in comparatively low concentrations must be considered as kinetically unfavorable within the time perspective of the experiment which raises some doubts of explaining the experimental results caused by precipitation reactions. Nevertheless, the results of the speciation calculations indicate that interaction with iron oxides might have an impact of the behavior of the divalent transition metals; an observation that is interesting to compare with the strong sorption observed for particularly ^{57}Co in this experiment.

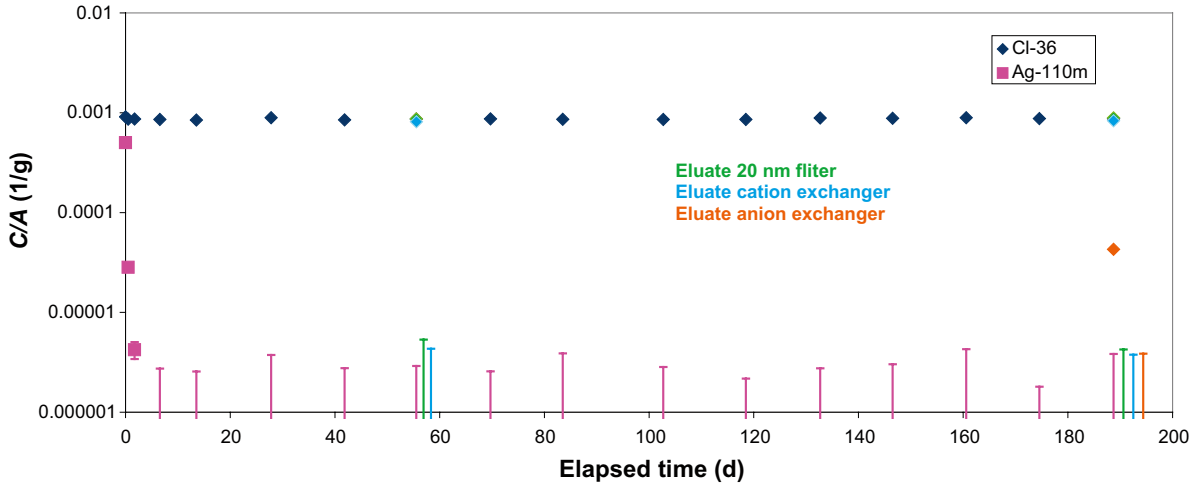

Figure 3-15. *Tracer concentration in C/A (1/g) where A is the injected radioactivity versus elapsed experiment time for ^{110m}Ag. ^{36}Cl is included for comparison. Error bars without concentration points from about 7 days and onwards represent the detection limit.*

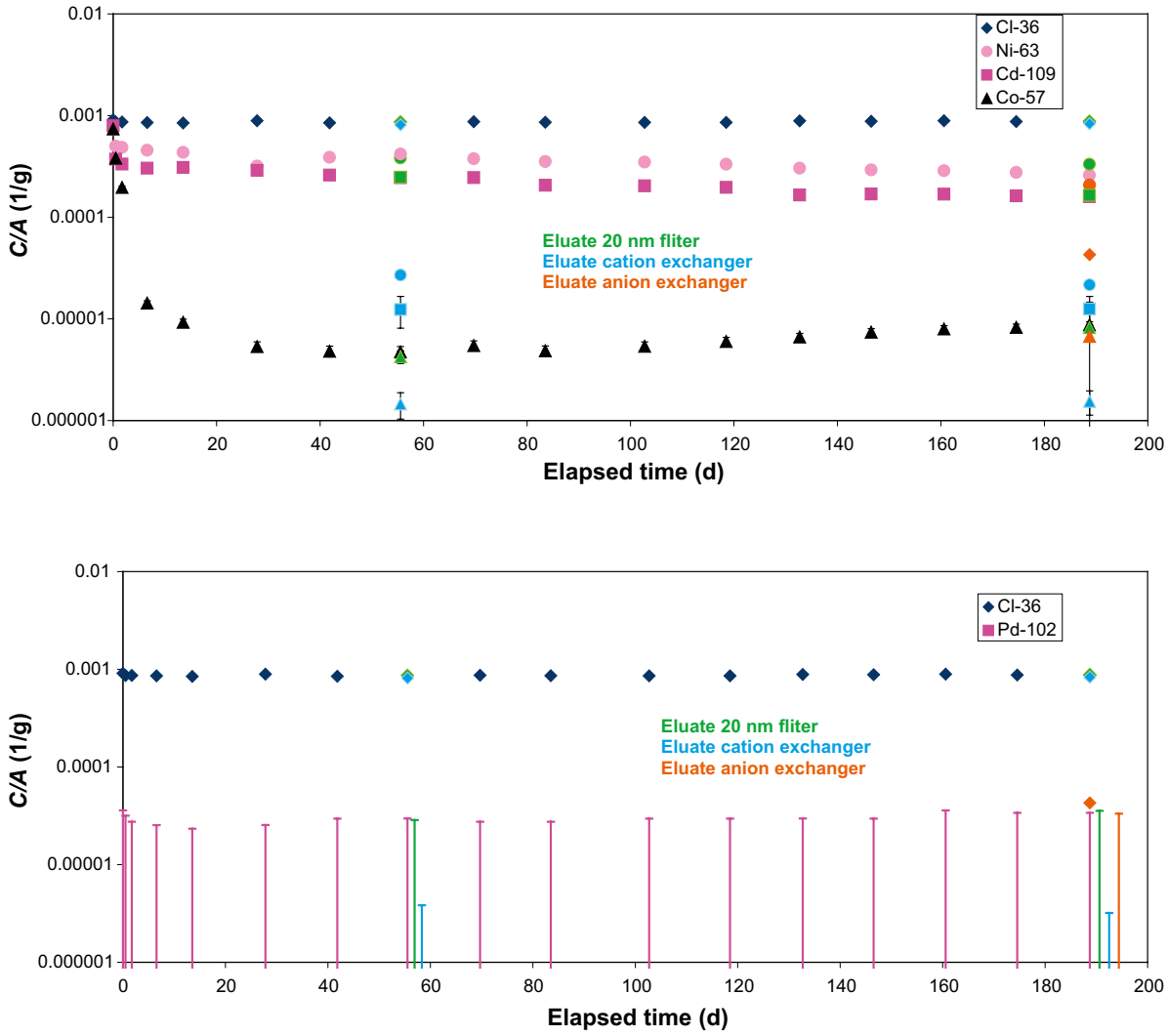

Figure 3-16. *Tracer concentration in C/A (1/g) where A is the injected radioactivity versus elapsed experiment time for ^{63}Ni, ^{109}Cd and ^{57}Co (upper figure) and ^{102}Pd (lower figure). ^{36}Cl is included for comparison. Error bars without concentration points represent the detection limit for ^{102}Pd.*

Redox sensitive elements U, Np and Tc

For the redox sensitive elements involved in this study, shown in Figure 3-17, the low adsorption indicates that no reduction to the presumed strongly sorbing tetravalent states amongst these elements. This is also in line with the measured redox potential and is also in agreement with the speciation calculations. The sorbed amount of the tracer ranges from 38% (Np), 22% (U) and 13% (Tc), however, with an uncertainty of approximately 10% for the individual tracer. The sorption for ^{237}Np is in the range for what could be expected for a monovalent cation which is also supported by the results of speciation calculations which shows a total dominance of the NpO_2^+ cation.

The indication of lower sorption for the divalent UO_2^{2+} ion compared to the monovalent NpO_2^+ could at a first glance appear somewhat inconsistent. However, since results of the ion exchange analyses support an anionic species in the groundwater and that the chemical speciation calculation show a dominance of negatively charged carbonate complexes, it is indicated that the low sorption could be a result of a aqueous carbonate complexation of UO_2^{2+} competing with sorption reactions between UO_2^{2+} and surface sites of the rock material.

The part of the results of the speciation calculation indicating supersaturation of UO_2^{2+} complexes with silicates is contradicted by the results; no indication of any loss of ^{236}U from the aqueous phase due to precipitation is obtained.

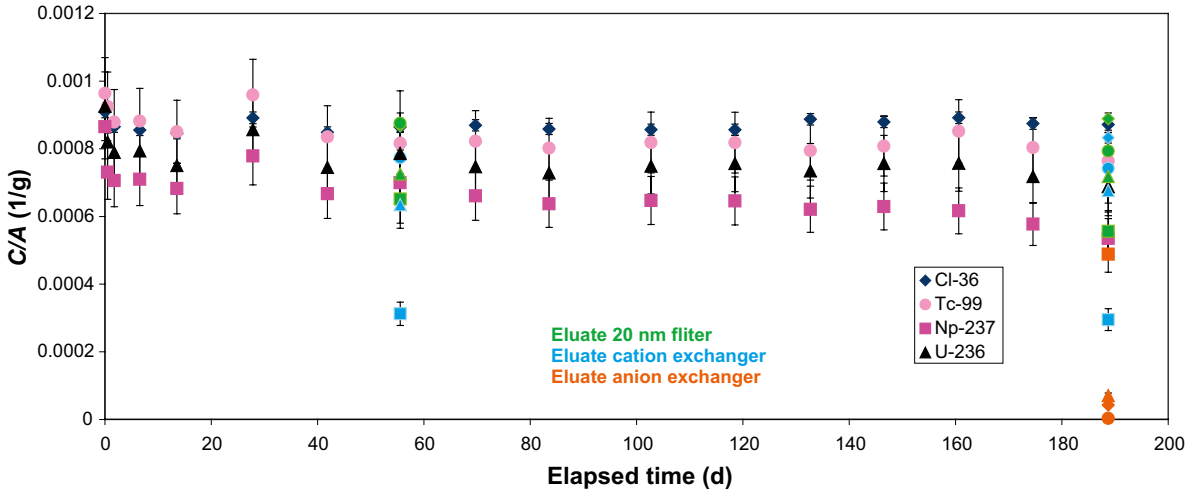

Figure 3-17. *Tracer concentration in C/A (1/g) where A is the injected radioactivity versus elapsed experiment time for ^{99}Tc, ^{237}Np and ^{236}U. ^{36}Cl is included for comparison.*

Regarding the ^{99}Tc, there is no reason to doubt the outcome of the chemical speciation that the TcO_4^- anion dominates the speciation and that no sorption of this anion can be proved, given the uncertainty in the measurements.

Trivalent lanthanide Gd, proposed analogue to trivalent actinides

The ^{153}Gd tracer (used mainly as a proposed chemical analogue to trivalent actinides and) is adsorbed to more than 99%, see Figure 3-18. The chemical speciation calculations yields that a positively charged complex of $GdCO_3^+$ dominates in the aqueous phase. It is nevertheless obvious that whatever the aqueous speciation of the Gd is, the sorption reactions will dominate.

The chemical speciation calculation furthermore indicates a supersaturation with respect to the phosphate phases. However, both Gd and phosphate are present in very low concentrations ($9 \cdot 10^{-8}$ M and $5 \cdot 10^{-8}$ M, respectively) so a formation of such a solid phase seem kinetically difficult. It seems more likely that, within these relatively short time perspectives, different sorption reactions (i.e. interaction with sorption sites of the rock material) will outcompete any phosphate formation.

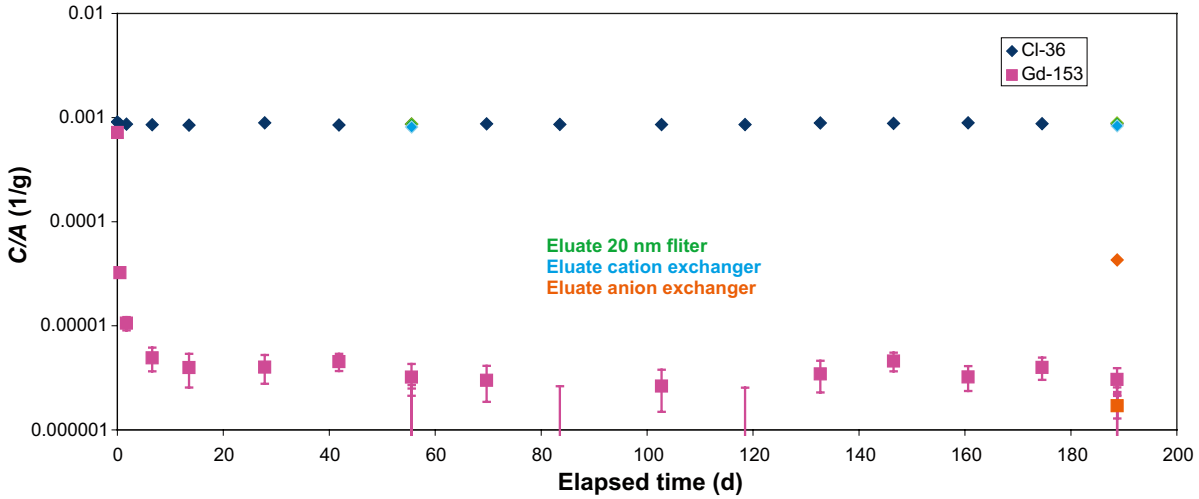

Figure 3-18. *Tracer concentration in C/A (1/g) where A is the injected radioactivity versus elapsed experiment time for ^{153}Gd. ^{36}Cl is included for comparison. Error bars without concentration points represent the detection limit for ^{153}Gd.*

Tetravalent Hf (Zr and Sn)

The best measurement of tetravalent compounds (potential analogues to tetravalent actinides) is obtained for the ^{175}Hf tracer for which a sorption of more than 99% of the added tracer amount is adsorbed (Figure 3-19). Other tetravalent elements used in this investigation are ^{95}Zr and ^{113}Sn; both of which are present as long-lived fission products in spent nuclear fuel. The latter tracers could only be measured in the first groundwater samples collected during the experiment; otherwise they were found to be below the detection limits. Due to short half-lives and comparatively low added amount of tracer, the measurements of these tracers are rather insensitive and the amounts of the tracer sorbed can only be approximated to be more than 90% for ^{95}Zr and more than 95% for ^{113}Sn.

The chemical speciation calculations yield that hydroxide complexes should dominate for these tetravalent compounds. For ^{95}Zr and ^{113}Sn the tetrahydroxide complex dominate ($Zr(OH)_4(aq)$ and $Sn(OH)_4(aq)$, respectively) while the negatively charged pentahydroxide complex ($Hf(OH)_5^-$ dominates for ^{175}Hf. However, the results seem to indicate that the complexation is not strong enough to prevent the tracers from sorption.

It must be added that the chemical speciation calculations indicate supersaturation for the oxide phases of all the tetravalent cations used, i.e. ZrO_2, SnO_2 and HfO_2. This is good illustration of the difficulties of doing experiment with elements with very low solubility; even with sub µ-molar concentrations the risk of obtaining supersaturation can not be ruled out. However, the relevance of a solid phase formation reaction of compounds in sub µ-molar concentration must be questioned, especially in an environment with availability of large amounts of surfaces where sorption reactions are more likely to take place.

Pentavalent non-redox sensitive elements, Nb and Pa

The elements expected to exist in their pentavalent state were difficult to measure in the experiment, this since they both were produced by the decay of their respective parent isotope:

- ^{95}Nb was a subject to in-growth during the experiment, this because of the decay of the ^{95}Zr isotope. Since they were not in equilibrium in the beginning of the experiment, the A_{tot} of ^{95}Nb. This in-growth has been compensated for when presenting the C/A_{tot}-values in Figure 3-20, i.e. the total amount of ^{95}Nb activity in the experimental section is expected to increase from both ^{95}Zr adsorbed and from ^{95}Nb in the aqueous phase. However, measurements of ^{95}Nb in the sampled water became useless since no ^{95}Zr was found above the detection limits and decay correction became impossible. Instead, the detection limits for ^{95}Nb was estimated from the on-line measurement which actually was shown to be more sensitive than the measurements on the samples.
- The relatively short half life of ^{233}Pa (27 d) resulted in quite low sensitivity for all but the five first of the measurements of the sampled groundwater. This occurred since they were measured too long time after the sampling; at this time a significant in-growth of ^{233}Pa from the decay of ^{239}Np in the same samples had taken place. For this reason, the detection limits in the late part of the curve instead origin from the on-line measurement and do therefore not offer as good sensitivity as the sample measurements.

Due to these circumstances, the sensitivity of the measurement of the pentavalent elements was not so good in this experiment. However, one could show that after 2 weeks of experiment time, more than 95% of the ^{233}Pa had undergone sorption. For ^{95}Nb, a minimum sorption of 75% could be shown from the results. A summary of the tracers that were not detected during the experiment or only detected shortly after injection is given in Table 3-11.

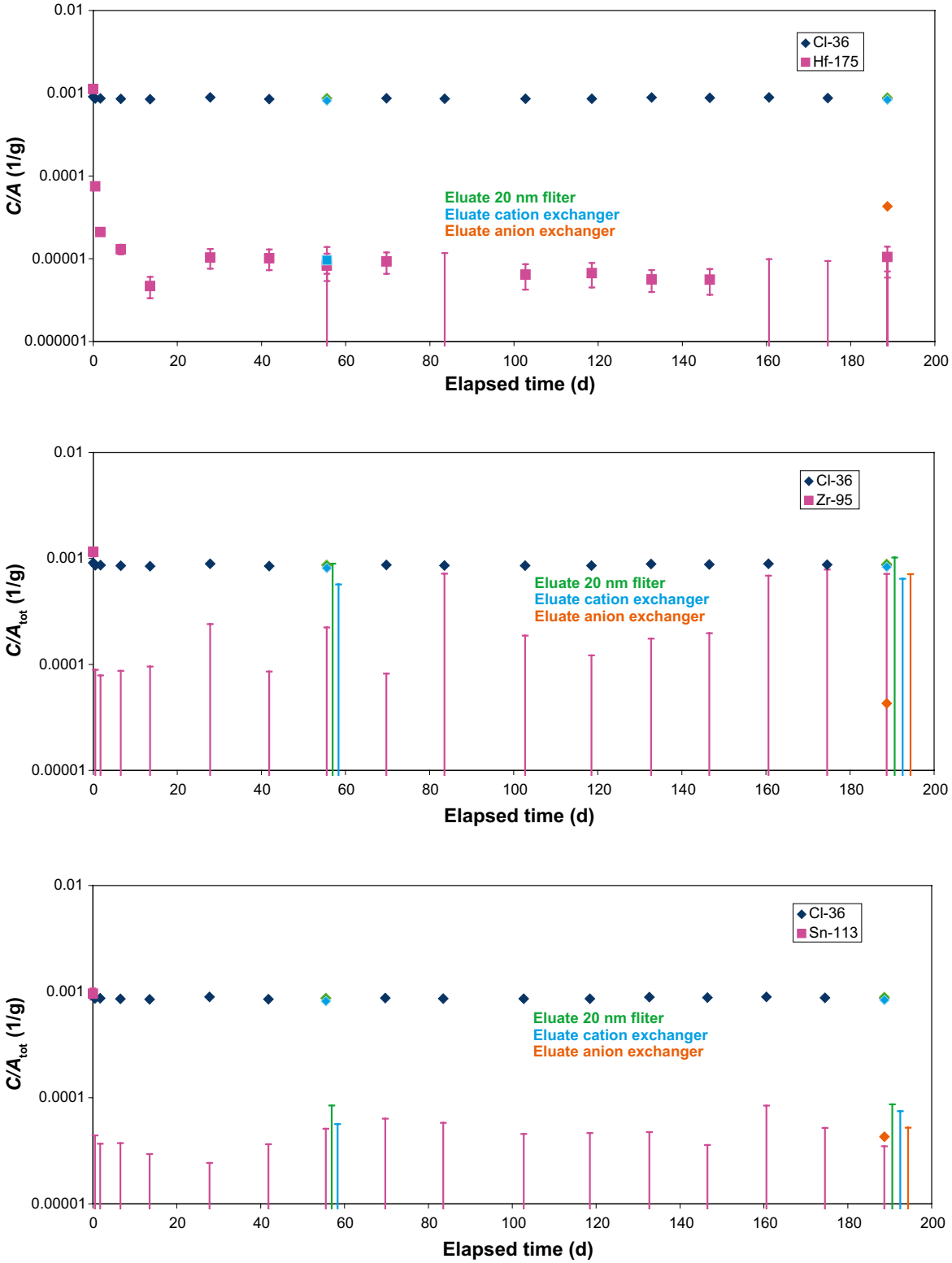

Figure 3-19. *Tracer concentration in C/A_{tot} (1/g) where A_{tot} is the injected radioactivity versus elapsed experiment time for ^{175}Hf (upper), ^{95}Zr (middle) and ^{113}Sn (lower figure). ^{36}Cl is included for comparison. Error bars without concentration points represent the detection limit.*

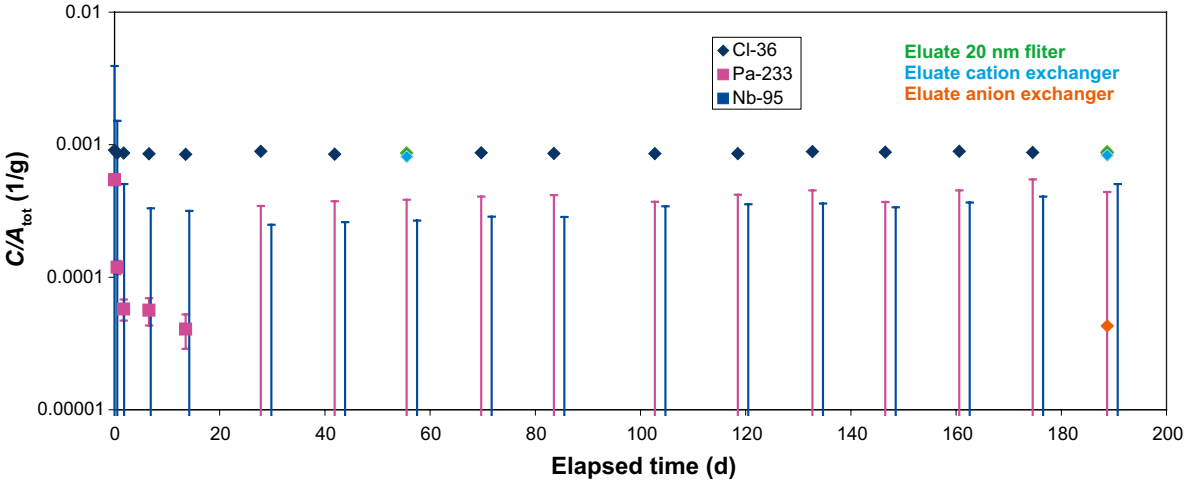

Figure 3-20. *Tracer concentration in C/A_{tot} (1/g) where A_{tot} is the injected radioactivity versus elapsed experiment time for ^{233}Pa and ^{95}Nb. ^{36}Cl is included for comparison. Error bars without concentration points represent the detection limit based on the on-line measurements.*

Table 3-11. Presentation of the amount of tracer remaining in the aqueous phase at the end of the circulation part of the experiment. Besides that, the percent that sorbed on PEEK tubing and the percent of the added tracer that was found in the excess of liquid Epoxy injected at the end of the experiment (Section 2.4.2 and 3.2.5) is also given.

	Remaining in aqueous phase at the end of the circulation experiment	Sorption on PEEK tubing	Desorbed by the excess of the liquid Epoxy injection
Cl-36	100±3%		
S-35	67±24%		
Se-75	57±4%	20%	3%
Na-22	104±4%	0.1%	4%
Sr-85	81±2%	0.7%	3%
Cs-137	37±1%	0.2%	2%
Ba-133	66±1%	3%	2%
Ra-226	48±7%		
Ag-110m	(<0.2%)[1]	11%	<0.1%
Co-57	1±0.1%	7%	0.1%
Ni-63	30±3%		
Pd-102	(<3%)[1]		
Cd-109	19±1%	6%	0.5%
Gd-153	0.4±0.1%	15%	<0.03%
Zr-95	(<8%)[1]	40%	<6%
Sn-113	(<3%)[1]	30%	<1%
Hf-175	1±0.1%	80%	<0.2%
Nb-95	(<30%)[1]		
Pa-233	(<5%)[1]		
Tc-99	87±10%	5%	2%
U-236	79±8%	10%	0.1%
Np-237	61±9%	16%	0.1%

[1] Not detectable at the end of the experiment. The values given refer to the highest proven adsorption (i.e. lowest detection limit for the aqueous phase measurement) during the experiment which, due to the radioactive decay, does not have to be at the end of the experiment.

3.5.3 Material balance and sorption on equipment

At the end of the experiment, all the remaining aqueous solutions in the experiment equipment were collected and were measured for their tracer content. The tracer content in the aqueous phase is thus calculated as the sum of the tracer content in the sampled water during the experiment and the water obtained during the exchange of the groundwater with isopropyl alcohol. During the filling of the experimental section with liquid Epoxy, a combined phase of isopropyl alcohol mixed with excess Epoxy was obtained as a last sample for which the results of the measurement of the tracer content is presented separately. Furthermore, the amount of tracer adsorbed in the PEEK tubing of the experiment has been measured.

The results for the different tracers are given in Figure 3-21, as the sum percentage of the amount of tracer added to the experiment (obtained as measurement of the tracer injection cocktail). One can thereby conclude that the gap between 100% and the sum of the staples represent the part of the tracers that is expected to have interacted with the geological material in the experimental section.

As can be seen, the results for the ^{22}Na tracer show a good match to 100% which is in agreement with the non-sorbing behaviour showed by the tracer time-concentration curve. When studying the similar results for the more strongly sorbing tracers (e.g. ^{85}Sr, ^{133}Ba, ^{137}Cs, ^{109}Cd and ^{57}Co), it is found that the gap to the 100% level increases in the same order that losses were obtained in the respective tracer time-concentration curve. This provides a general conceptual agreement of the experimental results; the results of the time-concentration curves are supported by the results of the material balances which shows that the losses obtained for these tracers during the circulation are obtained mainly because of interaction with the geologic material.

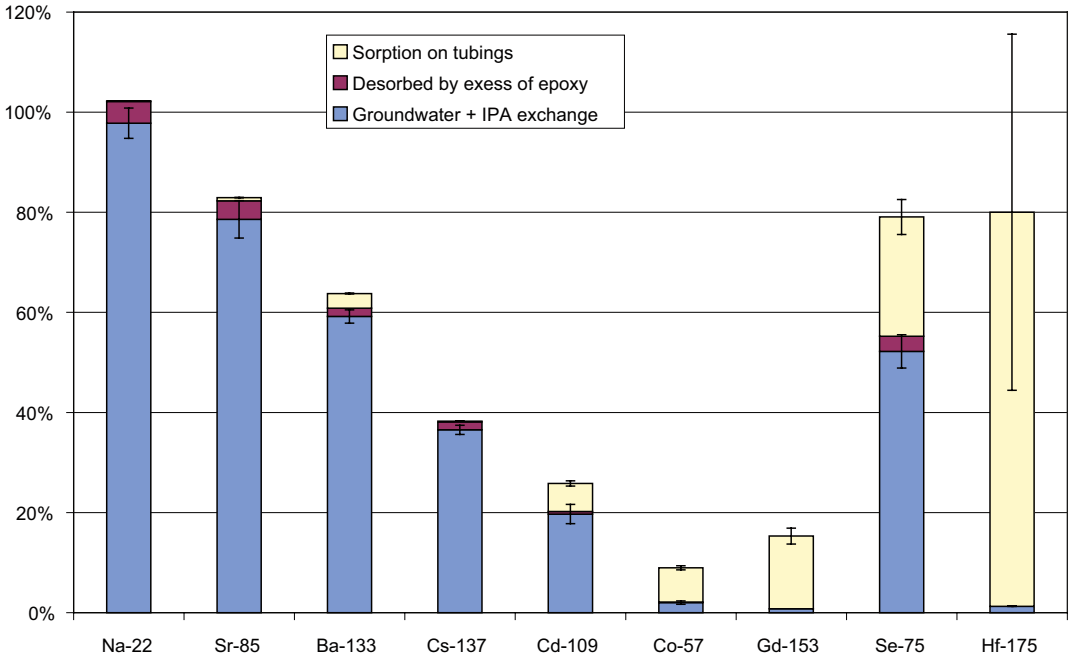

Figure 3-21. *Sum percentage of the amount of tracer added to the experiment (obtained as measurement of the tracer injection cocktail). The gap between 100% and the sum of the staples represent the part of the tracers that is expected to have interacted with the geological material in the experimental section.*

The results of the studies of the sorption on the PEEK tubing show that significant amounts of the tracers have interacted with the PEEK material (see Table 3-11). Especially the tetravalent ^{175}Hf show large amounts (~80%) sorbed on the tubings but also the tetravalent compounds (^{95}Zr and ^{113}Sn) as well as the trivalent ^{153}Gd show significant amounts sorbed. Concerning the divalent elements, the transition metals ^{57}Co and ^{109}Cd show 6–7% adsorbed and the alkaline earth metals ^{85}Sr and ^{133}Ba is only lost in amounts of 0.7% and 3%, respectively. The monovalent transition metal ^{110m}Ag was adsorbed on the equipment to an amount of 11% while only very minor parts of ^{22}Na and ^{137}Cs were adsorbed. The sorption characteristics for the PEEK surfaces indicate that elements expected to sorb by surface complexation are sorbed to significant amounts; an observation that suggests that the losses could mainly be explained by interaction with iron oxy-hydroxides that have attached on the PEEK surfaces due to the fact that the oxidized conditions causes iron to precipitate. This is furthermore supported by the results of the ^{75}Se; an anionic species known to adsorb by surface complexation on iron oxy-hydroxides (e.g. /Duc et al. 2003/). Consequently, elements expected to adsorb with cation exchange (e.g. ^{137}Cs) do not interact to any significant amount with the PEEK equipment.

During the filling of the experimental section with liquid Epoxy, a significant increase of the tracer concentrations was observed in the last batch of liquid extracted, i.e. the last injected volumes of isopropyl alcohol combined with the excess Epoxy. There are different possible explanations to this:

- The Epoxy contains amine groups, and it is possible that these groups can compete in cation exchange with the geologic material and therefore desorb different tracers.
- Alternatively, the injection of the liquid Epoxy of different viscosity may have introduced a different flowpath during the circulation, thereby reaching potential pockets of more stagnant water and mixing with them.

It is difficult to conclude which of these proposed explanations that are correct. Nevertheless, it must be acknowledged that the former explanation involves a possibility that the amount of tracer adsorbed in the experiment is underestimated due to desorption. If so, this may cause underestimation in the actual sorption established from the studies of the tracer amount in the rock material after the overcoring /Nilsson et al. 2010/.

3.6 Speciation of tracers by ion exchange resins

The results of the attempts to make an ion exchange speciation of the tracers involved in this experiment is presented below in Table 3-12 and is discussed in terms of groups of tracers.

^{22}Na, ^{85}Sr, ^{137}Cs, ^{133}Ba and ^{226}Ra: This group of alkaline and alkaline earth metal cations is more or less fully adsorbed by the cation exchanger and passes through the anion exchanger without any interaction. This is as expected from the results of the chemical speciation calculations which shows that they are almost only present in their non-complexed ionic form. The somewhat lower adsorption observed for especially ^{22}Na is probably explained by the fact that the cation exchanger was presaturated with Na^+ and that this presumably weakly sorbing tracer is to a comparatively large extent competed out when pouring through the natural groundwater with its e.g. high Ca^{2+} concentration. Therefore, a full adsorption of Na^+ is not obtained.

^{63}Ni: Ni^{2+} is a transition metal with a presumably larger influence of hydrolysis and surface complex formation than the previous group. Nevertheless, the chemical speciation calculation yields that the non-complexed aqueous form of Ni^{2+} dominates, (96%). This speciation is fully supported by the results of the behaviour of ^{63}Ni in the ion exchange speciation; it is fully adsorbed in the cation exchanger and is passed through the anion exchanger.

^{57}Co: According to the chemical speciation calculation, the negatively charged $HCoO_2^-$ (71%) should dominate the speciation, however with Co^{2+} (27%) also present. Nevertheless, the ion exchange speciation contradictorily shows that ^{57}Co is to the major part instead adsorbed in the cation exchanger (67–82%) and no interaction with the anion exchanger can be shown. This raises some doubts of the correctness of the thermodynamic database with respect to this ion and makes one suspect that the actual speciation instead should be described as dominance of the Co^{2+} ion.

One can possibly explain the strong interaction in the cation exchanger as a competition reaction in which the sulfonic groups of the cation exchanger competes out the oxy-hydroxy groups attached to the Co^{2+} ion, but the complete absence of interaction in the anion exchanger is more difficult to explain.

^{109}Cd: The chemical speciation calculation shows that different chloride complexes of Cd^{2+} should dominate; $CdCl^{+}$ (71%) and $CdCl_2$ (aq) (25%). However, the results of the ion exchange speciation show that ^{109}Cd is fully adsorbed in both the cation and the anion exchanger. The same results were obtained during the pre-test /Widestrand et al. 2006/. Possibly, the interaction between the sulfonic groups and the Cd^{2+} ion are strong enough to compete out the chloride complexation which therefore causes full adsorption in the cation exchanger. The full adsorption in the anion exchanger suggests that the chloride complexation in the groundwater is stronger than what the thermodynamic database indicates and that negatively charged complexes of $CdCl_3^-$ and/or $CdCl_4^{2-}$ actually dominate in groundwater. An alternative explanation could be that the adsorption of Cd^{2+} in the anion exchanger is occurring through a mechanism in which Cd^{2+} make use of to the Cl^- attached to the anion exchanger, i.e. the chloride anion acting as a bridge between th positively charged amine group of the anion exchanger and the Cd^{2+} cation. Nevertheless, the general conclusion of the ion exchange speciation of the ^{109}Cd must be that the there is an influence of chloride complexation, as was predicted by the chemical speciation calculation.

^{153}Gd: This trivalent element is, according to the chemical speciation calculations, present as $GdCO_3^+$ (59%) and Gd^{3+} (26%) as the dominating species. This is in agreement with the observation of the interaction in the cation exchanger where more than 50% of the tracer is adsorbed. This is also in agreement with the fact that no interaction with the anion exchanger can be shown. However, the large part of this tracer being lost during the filtration (i.e. more than 78%) could be an indication of a colloidal presence of this element. The proven interaction in the cation exchanger is nevertheless a stronger indication of cationic species dominating and that the interaction in the filter is more likely to be caused by adsorption of these cationic species on the surfaces of the filter.

^{175}Hf: This tetravalent element should according to the chemical speciation calculation be fully present as a negatively charged complex, $Hf(OH)_5^-$. No interaction of this tracer with the cation exchanger could be measured which can be regarded as a support of the results of the chemical speciation calculation. Unfortunately, the measurement on the anion exchanger was done at a time when this comparatively short-lived tracer had decayed and no relevant results are therefore available. However, the general conclusion for this tracer must be that there are no observations in the ion exchange analyses that contradict the results of the chemical speciation calculations.

^{237}Np: The chemical speciation calculation yields a total dominance of the NpO_2^+ complex in the groundwater. This result is consistent with the observation of sorption in the cation exchanger (42–52%) and no interaction being indicated for the anion exchanger. However, the relatively low amount adsorbed in the cation exchanger (e.g. much lower than for ^{22}Na) indicates that the selectivity for NpO_2^+ is low; alternatively, that there is a complexation of the ion that prevents it from being adsorbed.

^{236}U: The chemical speciation calculations yields that negatively charged carbonate complexes, $UO_2(CO_3)_3^{4-}$ (34%), $UO_2(CO_3)_2^{2-}$ (23%), should dominate the speciation of ^{236}U, although with some presence of other complexes, e.g. $UO_2(OH)_2$ (30%). These calculations are supported by the results of the ion exchange speciation which (given the uncertainties) suggests a negative net charge of the ^{236}U complex.

^{36}Cl: As expected, both chemical speciation calculations and ion exchange speciation shows a total dominance of the Cl^- anion.

^{35}S and ^{75}Se: As expected, both chemical speciation calculations and ion exchange speciation shows a total dominance of the SO_4^{2-} and SeO_4^{2-} anions, respectively.

Table 3-12. The results of the ion exchange sampling and filtered sampling.

	Dominating species according to PHREEQC	% in 20 nm filter		% in cation exchanger		% in anion exchanger
		56 d	189 d	56 d	189 d	189 d
Na-22	Na^+ (98%)	<0.06	<0.07	85±0.9	89±0.6	3±2
S-35	SO_4^{2-}	<15	<15	<16	<16	89±14
Cl-36	Cl^-	<4	<4	<6	<5	95±4
Co-57	$HCoO_2^-$ (71%), Co^{2+-} (27%)	0.4±0.2	<8	67±7	82±4	<0.2
Ni-63	Ni^{2+-} (96%)	<25	<25	92±23	91±23	<25
Se-75	SeO_4^{2-} (91%)	<0.08	<0.13	<0.5	5±3	91±2
Sr-85	Sr^{2+-} (94%)	<0.06		97.4±0.2		
Tc-99	TcO_4^- (100%)	<17	<17	<17	<17	>99
Cd-109	$CdCl^+$ (71%), $CdCl_2$ (aq) (25%)	0.4±0.1	0.7±0.2	94±2	92±3	>90
Ba-133	Ba^{2+} (99%)	0.7±0.1	0.7±0.1	98.1±0.4	98.6±0.3	<0.2
Cs-137	Cs^+ (99%)	<0.06	<0.04	96.7±0.2	97.8±0.2	<2
Gd-153	$GdCO_3^+$ (59%), Gd^{3+} (26%)	>78	>87	>50	>64	<27
Hf-175	$Hf(OH)_5^-$ (100%)	3±2		<27		
Ra-226	Ra^{2+-} (100%)	4±0.5	2±0.4	89±11	95±13	<2
U-236	$UO_2(CO_3)_3^{4-}$ (34%), $UO_2(OH)_2$ (30%) $UO_2(CO_3)_2^{2-}$ (23%)	<16	<16	<17	<17	89±15
Np-237	NpO_2^+ (96%)	<17	<17	52±9	42±8	<17

3.7 20 nm filtered sampling

The results of the analyses of filters exposed to the sampled groundwater (Table 3-12) indicates that more or less no indication is given of any tracer attached to any colloidal phase (which should not pass the 20 nm filter). The only tracer that is significantly adsorbed in the filters is the ^{153}Gd tracer for which >80–90% of the aqueous tracer is lost during the filtering. However, the combined observation of large parts of this tracer (>50–70%) also adsorbing on the cation exchanger indicates that the loss in the filter instead could be a result of a chemical adsorption of e.g. the dominating species $GdCO_3^+$ and Gd^{3+} on the surfaces of the filter.

Contrary to Gd, the strongly hydrolysed tetravalent element present in the investigation, Hf(IV), show very limited ability to interact with the filter; only 3% of the tracer amount is lost in the filter. One can speculate that this is in line with the result of the speciation calculation which states that this element should be present in a negatively charged $Hf(OH)_5^-$ complex which due to its charge may prevent it from interacting with the filter.

Indications are also obtained of small amounts of Ba^{2+} and Ra^{2+} (0.7 and 4%, respectively) interacting with the filter. This could be an effect of e.g. sulphate precipitation of these elements; an indication which however is somewhat contradicted by the speciation calculations that show no supersaturation of these elements. There is also a very slight concentration increase of Co and Cd in the filter.

However, as a summary it must be concluded that the results of the filter analyses contradicts any hypothesis of a strong colloidal impact on the tracer speciation. This observation is in good agreement with the colloid analysis which does not show any significant content of inorganic colloids in the sampled groundwater.

4 Estimation of transport parameters based on aqueous phase measurements

4.1 Introduction

The results from the *in situ* sorption diffusion experiment were evaluated regarding sorption and diffusion properties of the individual tracers. Below is a description of the parameters that were evaluated from the experimental data, the model used and simplifications made in connection with the modeling. The present modelling only utilizes the data from the aqueous concentration of the tracers; for the evaluation and modelling using the data from the rock phase measurements it is referred to /Nilsson et al. 2010/.

The loss of tracer from the aqueous phase was modelled with a simplified model where the diffusion into the rock pores of the stub fracture surface and across the 36 mm borehole mantle surface was approximated to occur in a one-dimensional mode coupled with matrix sorption and surface sorption. The model is based on an analytical solution for diffusion across a plane sheet proposed by /Crank 1975/. The calculation involves a least squares summation method. The model is further described in Appendix 10.

The indata in form of porosity, ε (–) and effective diffusivity (or matrix diffusivity) D_e (m^2/s), were assembled from laboratory investigations by /Vilks et al. 2005/ on non-altered rock material from the 300 mm core of KA3065A03. Diffusivity data for iodide in through diffusion cell experiments was used for calculation of the rock formation factor F_f (–). The matrix (effective) diffusivity coefficient D_e (m^2/s), is related to the water diffusivity, D_w, through the rock formation factor F_f as:

$$D_e = F_f \cdot D_w \qquad (4\text{-}1)$$

The rock formation factor depends only on the properties of the rock and not on the tracer or solute properties. Consequently, by using the rock formation factor together with tabulated water diffusivity of a specific tracer, the D_e for the tracer can be calculated.

The selective import of diffusion data from intact and non-altered rock can be argued to be an underestimation of the diffusion interaction in the modelling; the presumed faster interaction in the vicinity of the stub surface due to increased numbers of microfracture has not been addressed. However, this modelling using only the water phase data should only been considered as a preliminary exercise compared to the elaborate modelling which will be performed in a later stage /Nilsson et al. 2010/ when the analyses of the rock material has been done.

In this work, the D_e of the different tracers was calculated individually by use of formation factor determined from the matrix diffusivity of iodide (I^-) from /Vilks et al. 2005/ One case with F_f based on matrix diffusivity determined from through diffusion of H^3HO (tritiated water) /Widestrand et al. 2010/ (based on four samples from the 36 mm borehole and KA3065A02) is included as a comparison. Water diffusivities determined by /Li and Gregory 1974/ at 18°C were used for all tracers except H^3HO for which data from /Mills and Lobo 1989/ were used. The indata from /Vilks et al. 2005/ and /Widestrand et al. 2010/ are summarized in Table 4-1 below.

Table 4-1. Summary of input data. Diffusivities and formation factors are based on through diffusion experiments of non-altered rock material from the LTDE-SD site.

Mean value of water saturation porosity (–):	**3.0E–3**		**Vilks et al. 2005**
	D_e (m^2/s):	F_f (–):	
Max (I^-):	5.6E–12	3.3E–3	Vilks et al. 2005
Min (I^-):	4.4E–15	2.6E–6	Vilks et al. 2005
Mean (I^-):	1.7E–13	9.9E–5	Vilks et al. 2005
Mean (H^3HO):	4.6E–14	2.2E–5	Widestrand et al. 2010

Three different cases were applied in the modelling:

- Surface sorption model. As a first approach the loss of tracer from the aqueous phase was assumed to occur by way of surface sorption only. The surface sorption coefficient, K_a (m), was estimated, i.e. the sorption was assumed to take place only on the rock surfaces of the slim hole section and the stub section. Thus, no diffusion into the pores of the rock matrix was considered and the diffusivity and matrix sorption coefficient were set to zero. For this particular case, the model is equivalent to the simple batch sorption model used in the evaluation of the tracer pre-tests /Widestrand et al. 2006/.
- Matrix sorption (K_d). In this case the matrix sorption coefficient, K_d (m^3/kg), was estimated. No surface sorption was considered in estimating K_d, (i.e. that K_a=0). The porosity and mean diffusivity for iodide according to Table 4-1 were applied.
- Simultaneous estimation of surface sorption and matrix sorption. In addition to the estimations of K_d and K_a in separately, estimations were done where both parameters were allowed to vary simultaneously in the calculation. Also in this case, the porosity and mean diffusivity for iodide according to Table 4-1 were applied.

4.2 Estimation of surface sorption (K_a)

The results of the modelling (the calculated K_a values) are summarised in Table 4-2 below. For the low and non-sorbing tracers Cl and Na the sorption was so low that only detection limit-values for K_a could be produced from the estimations. Thus, the value reported for K_a should be regarded as a maximum value.

The very high values obtained for ^{233}Pa, ^{113}Sn, ^{95}Zr, ^{102}Pd, ^{57}Co, ^{110m}Ag, ^{153}Gd and ^{175}Hf may partly be influenced by sorption on the equipment as is discussed in Section 3.5.3.

As an example of fitting K_a to the measured data, the result for ^{137}Cs is shown in Figure 4-1. In accordance with the model and equilibrium assumption, no concentration-time dependence was obtained. Similar curve fitting results were obtained for all other tracers.

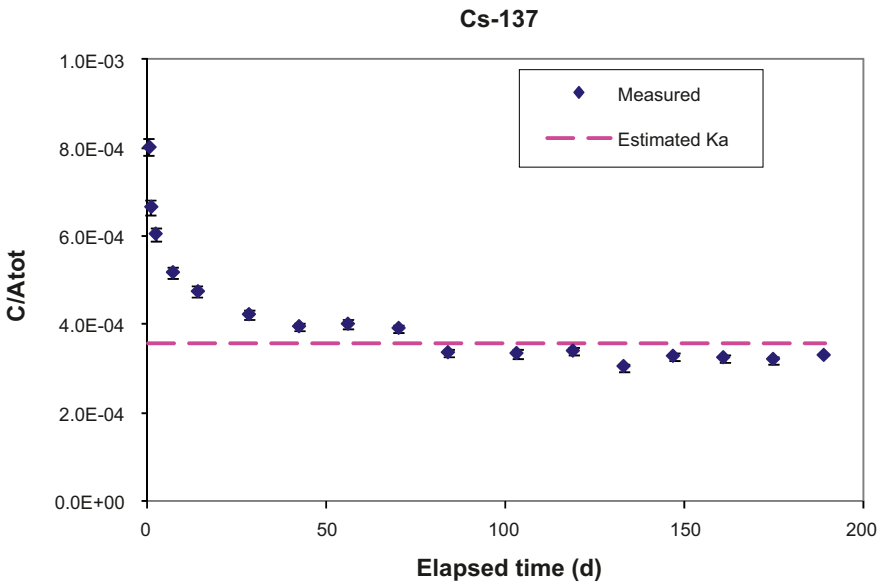

Figure 4-1. *Estimation of* K_a *for* ^{137}*Cs.*

4.3 Estimation of matrix sorption (K_d)

The results are summarised in Table 4-2 below. As in the case for the estimation of K_a, the K_d value obtained for Na and Cl should be regarded as a maximum values. The very high values obtained for ^{233}Pa, ^{113}Sn, ^{95}Zr, ^{102}Pd, ^{57}Co, ^{110m}Ag, ^{153}Gd and ^{175}Hf may partly be influenced by sorption on the equipment as is discussed in Section 3.5.3.

The resulting concentration-time curves together with the corresponding measured values are presented in Appendix 11, and are exemplified with ^{63}Ni, ^{137}Cs and ^{22}Na in Figure 4-2, Figure 4-3 and Figure 4-4, respectively. It can be seen that it is a fairly good agreement between measured and estimated values. For comparative purposes, the corresponding predicted penetration depth curves are also presented, provided as an indication of the predicted depth of interaction between the tracer and the rock sample.

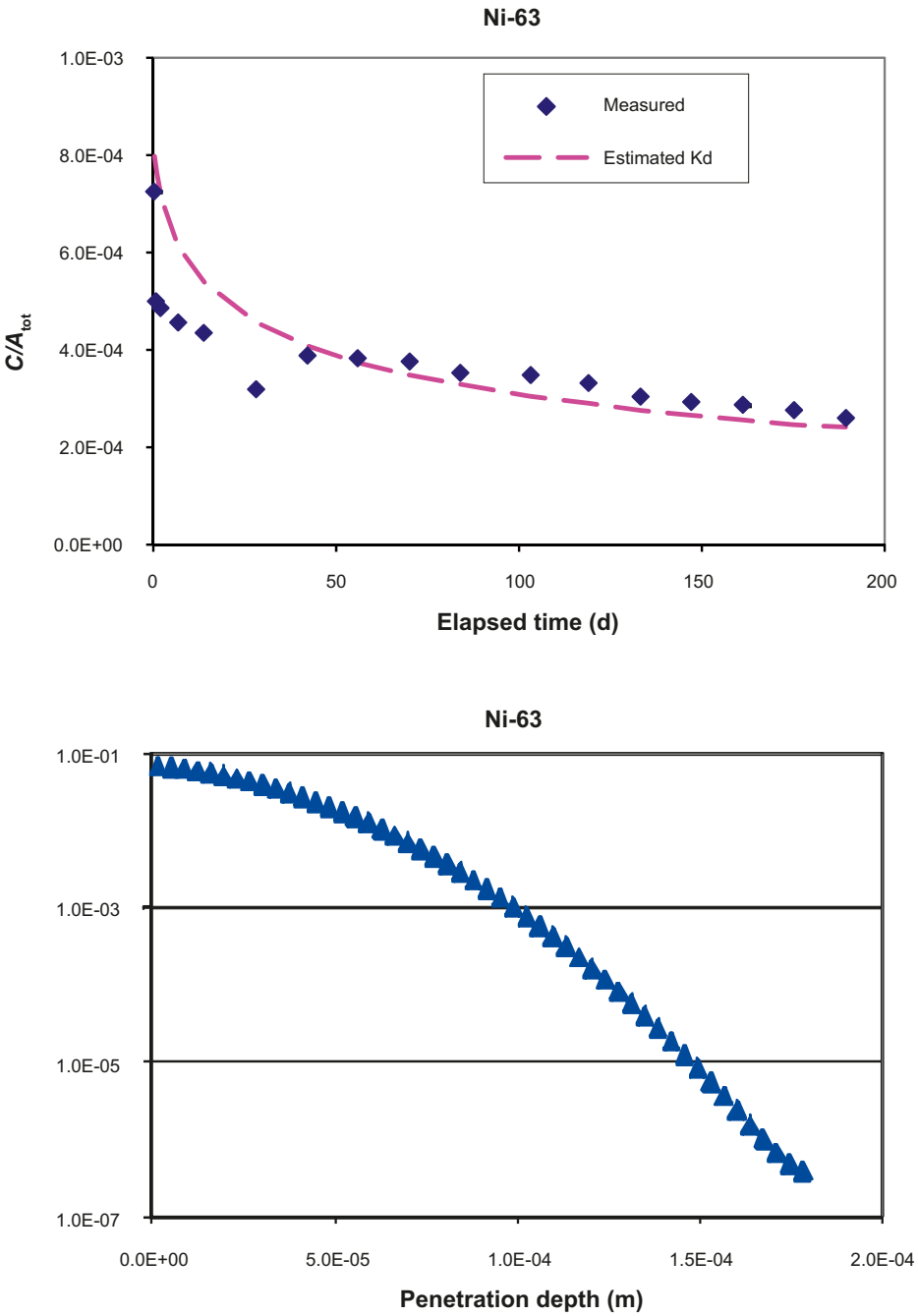

Figure 4-2. *Estimation results for ^{63}Ni and experimental data (top) and calculated penetration depth (bottom, y-axis represents the part of the added tracer present within the depth interval).*

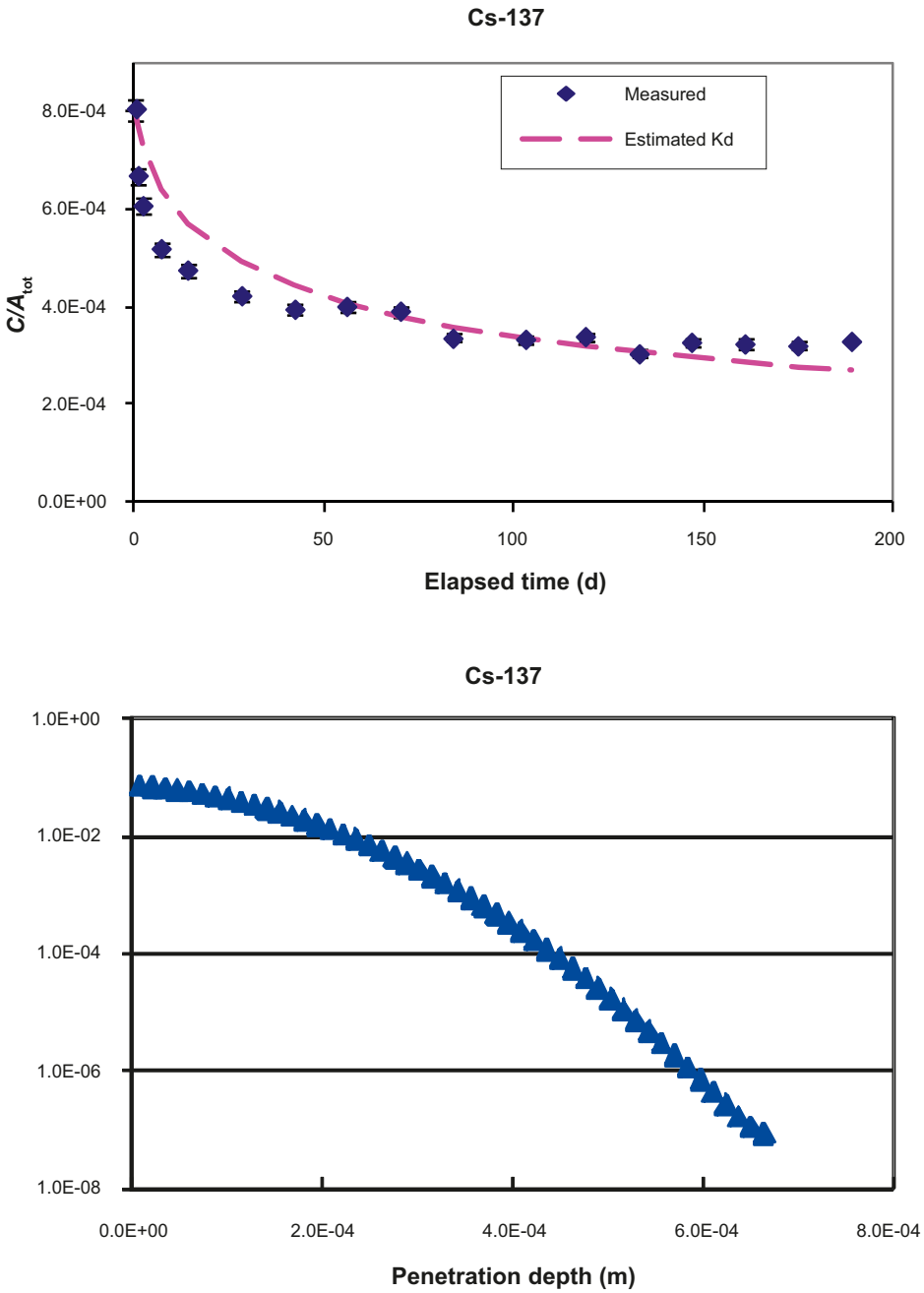

Figure 4-3. *Estimation results for ^{137}Cs and experimental data (top) and calculated penetration depth (bottom, y-axis represents the part of the added tracer present within the depth interval).*

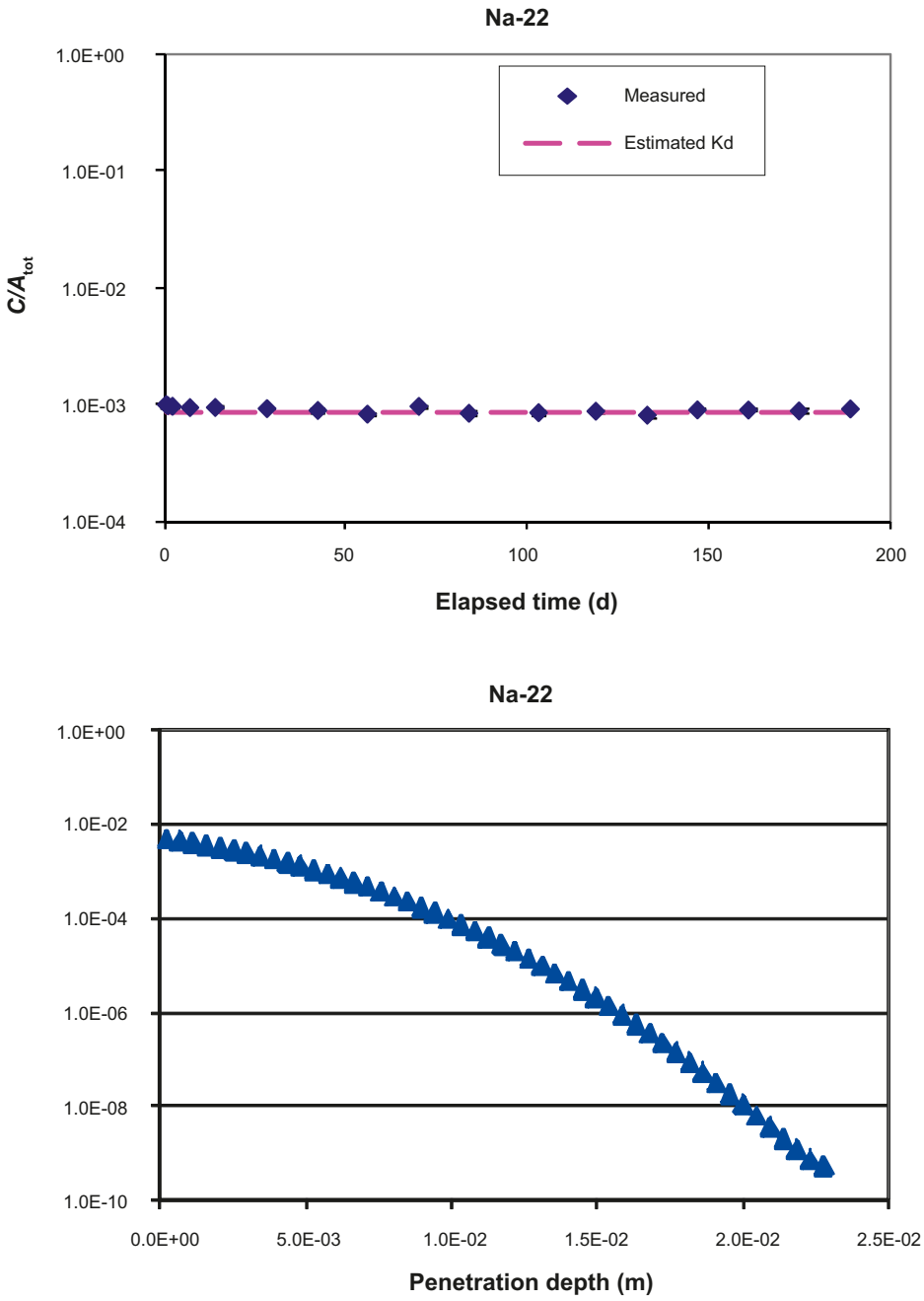

Figure 4-4. *Estimation results for ^{22}Na and experimental data (top) and calculated penetration depth (bottom, y-axis represents the part of the added tracer present within the depth interval).*

4.4 Simultaneous estimation of surface sorption (K_a) and matrix sorption (K_d)

In this calculation K_d and K_a were estimated simultaneously. The result is presented in Table 4-2. The same tendency as reported for the parameter estimates, reported above, can be seen for ^{233}Pa, ^{113}Sn, ^{95}Zr, ^{102}Pd, ^{57}Co, ^{110m}Ag, ^{153}Gd and ^{175}Hf, i.e. they appear affected by sorption on equipment parts.

4.4.1 Analysis of variation of matrix diffusivity on K_d estimation

Further estimation calculations were performed where the dependence of K_d on the diffusivity was analysed. Beside the geometric mean value on the diffusivity (Mean (I^-)) used as input data in the estimation calculations described above /Vilks et al. 2005/ also reported a maximum diffusivity, Max (I^-), and a minimum diffusivity, Min (I^-), cf. Table 4-1. Two further estimation calculations of K_d were performed with these two diffusivities (surface sorption was not considered i.e. K_a=0). Finally, a third estimation of K_d was performed at which a mean value from matrix diffusivity of H^3HO (tritium) was used, cf. Table 4-1. This value was determined from laboratory through diffusion experiments /Widestrand et al. 2010/. These additional three estimation calculations of K_d were carried out for the tracers ^{137}Cs and ^{153}Gd. The results are summarised in Table 4-3. For comparison, the estimated K_d calculated with Vilk's geometric mean diffusivity has been included in the table.

Table 4-2. Estimated values of K_a and K_d obtained from the estimation calculations described in Sections 4.2, 4.3 and 4.4. ε=3.0E–3 (–) and F_f=9.9E–5 (–) from /Vilks et al. 2005/ (geometric mean value from I^-).

Nuclide	Matrix sorption and diffusion case F_f = 9.9E–5 ε = 3.0E–3, K_a = 0	Surface sorption case F_f = 0, K_d = 0, ε = 0	Matrix sorption-diffusion and surface sorption F_f = 9.9E–5, ε = 3.0E–3	
	K_d[1] (m^3/kg)	K_a[2] (m)	K_d[3] (m^3/kg)	K_a[3] (m)
Ag-110m	1.13E+4[5]	5.05E+0[5]		
Ba-133	3.16E–2	8.41E–3	1.25E–2	3.41E–3
Cd-109	1.73E+0	6.59E–2	8.68E–1	2.07E–2
Cl-36	1.76E–5[4]	3.52E–4[4]		
Co-57	3.76E+3[5]	2.53E+0[5]	7.25E+2[5]	2.12E+0[5]
Cs-137	1.25E–1	2.83E–2	5.50E–2	1.04E–2
Gd-153	1.61E+4[5]	4.60E+0[5]	6.62E+2[5]	3.62E+0[5]
Hf-175	2.13E+4[5]	2.25E+0[5]	1.08E+3[5]	1.71E+0[5]
Na-22	7.48E–5[4]	3.75E–4[4]		
Ni-63	5.08E–1	3.28E–2	1.76E–1	1.44E–2
Np-237	3.82E–2	7.10E–3	2.01E–2	2.16E–3
Pa-233	6.44E+2[5]	2.35E–1[5]	6.44E+2[5]	3.20E–9[5]
Pd-102	2.57E+2[5]	5.25E–1[5]		
Ra-226	2.22E–1	2.28E–2	2.75E–2	1.53E–2
S-35	9.20E–3	4.93E–3	5.66E–3	2.70E–3[4]
Se-75	8.14E–2	1.44E–2	1.07E–2	9.57E–3
Sn-113	3.30E+1[5]	3.72E–1[5]		
Sr-85	8.36E–3	3.98E–3	5.61E–3	8.04E–4[4]
Tc-99	2.54E–4	1.02E–3	2.54E–4	4.48E–4
U-236	8.11E–3	3.17E–3	2.87E–3	1.39E–3
Zr-95	7.88E+1[5]	2.57E–2[5]		

[1] K_d fitted without considering K_a.
[2] K_a calculated without considering K_d.
[3] K_d and K_a fitted simultaneously in the calculation.
[4] Only a maximum value could be calculated.
[5] Probably overestimated due to sorption on the equipment.

Table 4-3. Estimated values of K_d (m^3/kg) calculated for various diffusivities and hence, for various formation factors, F_f(–). The mean value of water saturation porosity, $\varepsilon=3.0\cdot10^{-3}$(–) reported by Vilks was used in the estimations together with the water diffusivities as given in Section 4.1.

	D_e (m^2/s)	F_f (–)	K_d (m^3/kg)	
			Cs-137	Gd-153
Max (I^-)[1)]	$5.6\cdot10^{-12}$	$3.3\cdot10^{-3}$	$3.8\cdot10^{-3}$	$4.9\cdot10^{2}$
Min (I^-)[1)]	$4.4\cdot10^{-15}$	$2.6\cdot10^{-6}$	$1.3\cdot10^{-1}$	$1.6\cdot10^{4}$
Mean (I^-)[1)]	$1.7\cdot10^{-13}$	$9.9\cdot10^{-5}$	$4.8\cdot10^{0}$	$6.2\cdot10^{5}$
Mean (H^3HO)[2)]	$4.6\cdot10^{-14}$	$2.1\cdot10^{-5}$	$5.8\cdot10^{-1}$	$7.4\cdot10^{4}$

[1)] /Vilks et al. 2005/
[2)] /Widestrand et al. 2010/

The resulting aqueous concentration-time curves for ^{137}Cs together with the corresponding measured data are presented in Figure 4-5.

As can be seen in Figure 4-5, all the estimated concentration-time curves are identical. This result is attributed to K_d being correlated with the formation factor, F_f (and hence D_e). Figure 4-6 explains this correlation further.

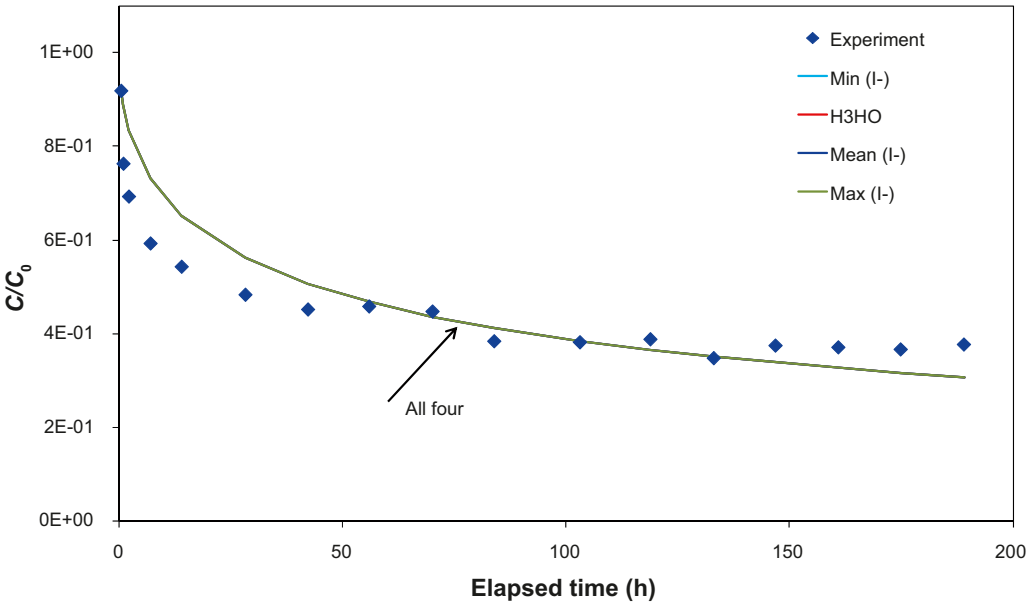

Figure 4-5. *Results from estimation calculations of K_d for ^{137}Cs for various F_f (D_e). The results are compared to experimental data.*

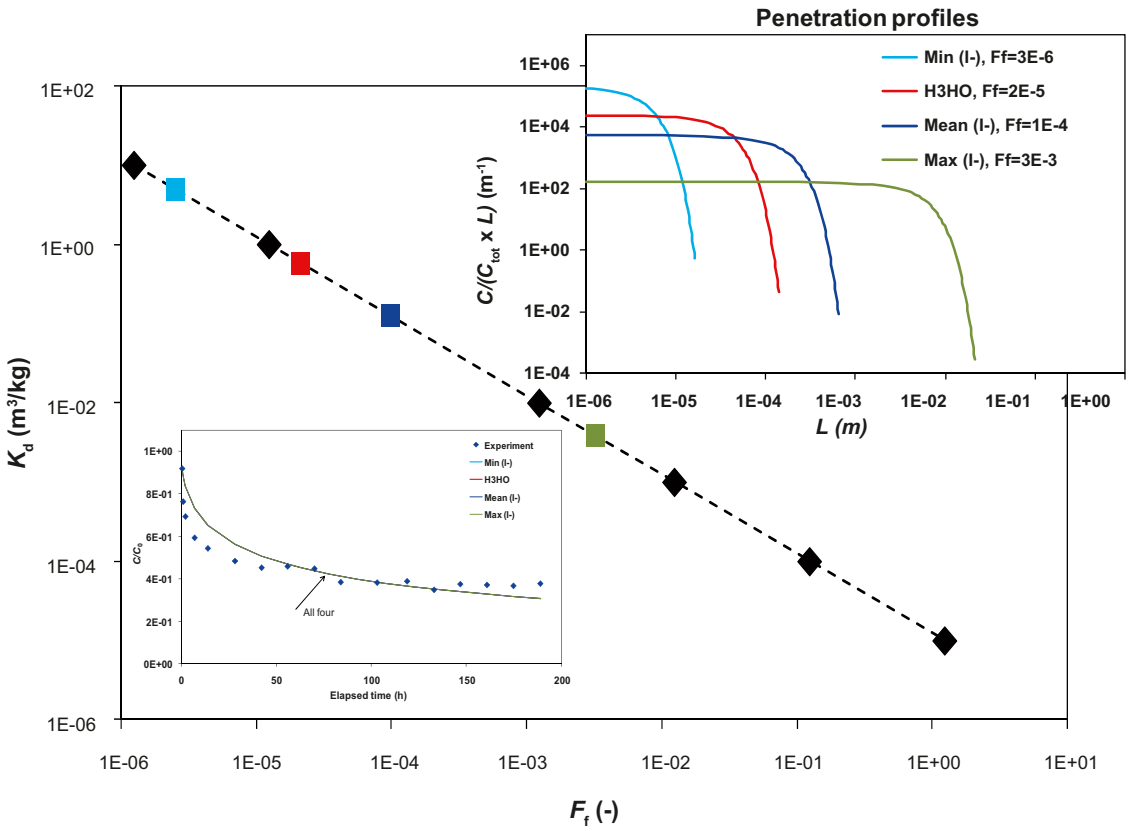

Figure 4-6. *Illustration of the dependence of the formation factor (F_f) on the K_d-value in the curve fitting procedure for the loss of Cs due to sorption on intact rock. The major figure shows that, within at least a range of 6 orders of magnitudes, the best fit can be obtained independently of the individually employed F_f and K_d, as long as their product remains constant (in this particular case $F_f K_d$=1E–5). However, as expected the penetration profiles differ strongly between the different cases which illustrate that penetration profile measurements are necessary in order to identify the individual values of F_f and K_d, respectively.*

5 Conclusions

In summary, the principal outcome and conclusions of the LTDE-SD *in situ* experiment is:

- *In situ* sorption has been demonstrated for a series of elements exclusively present in the LTDE-SD experiment, and also for some tracers which have been used in earlier performed dynamic *in situ* tracer experiments performed at the Äspö HRL. The amounts lost from the aqueous phase of the different tracers follow very well the general knowledge of the relative sorption strengths of the tracers; as established from previous laboratory batch sorption experiments and *in situ* dynamic tracer experiments at the Äspö HRL, i.e.:
  - Very low sorption is obtained for the cation exchange sorbing tracers Na^+ and Sr^{2+}, while the presumed stronger sorbing cation exchanging sorbing tracers Cs^+, Ba^{2+} and Ra^{2+} is lost to a higher extent.
  - Concerning the other cation tracers used, the Ni and Cd cations are lost to an extent of 68 and 82 percent extent, respectively. For the other cations used, i.e. the monovalent transition metal Ag^+, the divalent transition metals Co^{2+} and Pd^{2+}, the trivalent Gd(III), the tetravalent Zr(IV), Sn(IV) and Hf(IV) together with the pentavalent NbO_2^+ and PaO_2^+, very strong sorption is observed. For the radioistopes characterized with low detection limits, i.e. $^{57}Co^{2+}$, ^{153}Gd(III) and ^{175}Hf(IV), it can be shown that less than 1 percent remained in the water phase at the end of the experiment. For the other tracers mentioned, they were all below the detection limits at the end of the experiment.
  - The redox dependent tracers (i.e. ^{99}Tc(VII)O_4^-, ^{236}U(VI)O_2^{2+} and ^{237}Np(V)O_2^+, all expected to be reduced to strongly sorbing species of the oxidation state IV) are all behaving non- or very weakly sorbing. This is in line with the redox measurement performed during the experiment which shows that the reducing conditions shown in the inlet water in the beginning of the experiment were not possible to maintain during the tracer circulation phase.
  - The anions ^{35}S(VI)O_4^{2-} and ^{75}Se(VI)O_4^{2-} show some losses compared to the non-sorbing $^{36}Cl^-$, an observation that is not easily explained. For Se, the chemical speciation calculations show some presence of the Se(IV)O_3^{2-} species, a species that in literature is shown to sorb strongly on iron oxy-hydroxides.
- The attempt to inject tracer using a slightly acidified solution (in order to prevent adsorption already in the stock solution beaker of strongly sorbing tracers, e.g. tri- and tetravalent cations) appears to have worked out satisfactory. A slightly alkaline solution was injected immediately after the acidic solution (aimed to cause a neutralisation in the experimental section) and no significant pH-changes were noted as a result of this procedure. Furthermore, the success of this neutralisation procedure was supported by no visual observation of any precipitates in the sampled groundwater.
- The chemical speciation calculations performed using thermodynamic databases show a chemical speciation of the different tracers that is in agreement with the results of the ion exchange speciation performed during the experiment. However, with the exception of the UO_2^{2+} carbonate complexes, no strong indications were obtained that aqueous complexation prevents adsorption.
- The sampling of the experimental test section using 20 nm filtration show that only the trivalent tracer ^{153}Gd is strongly attached in the filter; all other tracers passes through without significant losses. This indicates that attachment to colloids in the aqueous phase appears to be a minor problem, if any, in this particular case. Additionally, the ^{153}Gd has also been shown to adsorb significantly on the cation exchanger; an observation that supports the hypothesis of this tracers being present in a non-colloidal state in the aqueous phase which can adsorb both on the cation exchanger and the filter surfaces. The independently performed analyses of inorganic colloids in the groundwater support this observation.
- It was shown difficult to maintain the natural redox conditions during the experiment. The low redox potential measured when natural groundwater from the fracture was pumped through the experimental section could be maintained for less than one week (as a maximum) after the

outflow had been changed to a circulation. This illustrates the general difficulties of performing a sorption diffusion experiment under ambient natural conditions.

- The observed difficulties in maintaining natural redox conditions in combination with the indications of sorption on the PEEK equipment, especially so for sorbing tracers expected to adsorb by surface complexation mechanism, lead to the suspicion that formation of oxidized iron oxy-hydroxides on surfaces (experimental material as well as the rock surfaces) may have occurred. This gives some indications that the sorption observed might have been influenced by mechanisms that are not present to the same extent in the natural conditions.
- The attempts to maintain natural pressure conditions seem to have worked out and one can assure that any penetration into the rock matrix must be considered as being a result of diffusion alone, and that no advection was involved.
- Modelling in order to determine sorption coefficients (K_d) has been performed. For the ion-exchange sorbing tracers, the *in situ* evaluated K_d was in the range of the highest values (fracture material) from the laboratory batch sorption results. This indicates that a sorption-diffusion model can describe the concentration losses reasonably well for the ion-exchange sorbing tracers. However, due to the observed sorption on equipment, one should relate to these results with care and consider the analysis of the sampled rock material based on penetration profiles before any definitive conclusions can be made.

References

Andersson P, Byegård J, Dershowitz B, Doe T, Hermanson J, Meier P, Tullborg E-L, Winberg A (ed), 2002. Final report of the TRUE Block Scale project. 1. Characterisation and model development. SKB TR-02-13, Svensk Kärnbränslehantering AB.

Bergelin A, Nilsson K, Lindquist A, Wacker P, 2008a. Oskarshamn site investigation. Complete chemical characterisation in KLX13A. Results from two investigated borehole sections: 432.0–439.2 m, 499.5–506.7 m. SKB P-07-149, Svensk Kärnbränslehantering AB.

Bergelin A, Nilsson K, Lindquist A, Wacker P, 2008b. Oskarshamn site investigation. Complete chemical characterisation in KLX17A. Results from two investigated borehole sections: 416.0–437.5 m, 642.0–701.9 m. SKB P-07-164, Svensk Kärnbränslehantering AB.

Bergelin A, Nilsson K, Lindquist A, Wacker P, 2008c. Oskarshamn site investigation. Complete chemical characterisation in KLX15A. Results from the investigated borehole section: 623.0 to 634.5 m. SKB P-08-69, Svensk Kärnbränslehantering AB.

Byegård J, Johansson H, Skålberg M, Tullborg E-L, 1998. The interaction of sorbing and non-sorbing tracers with different Äspö rock types. Sorption and diffusion experiments in the laboratory scale. SKB TR-98-18, Svensk Kärnbränslehantering AB.

Byegård J, Selnert E, Tullborg E-L, 2008. Bedrock transport properties, Data evaluation and retardation model. Site descriptive modelling, SDM-Site Forsmark. SKB R-08-98, Svensk Kärnbränslehantering AB.

Crank J, 1975. The mathematics of diffusion, 2nd edition, Oxford University press, London.

Duc M, Lefevre G, Fedoroff M, Jeanjean J, Rouchaud JC, Monteil-Rivera F, Dumonceau J, Milonjic S, 2003. Sorption of selenium anionic on apatites and iron oxides from aqueous solutions. Journal of Environmental Radioactivity, 70, pp 61–72.

Guillaumont R, Fanghänel T, Neck V, Fuger J, Palmer D R, Grenthe I, Rand M H, 2003. Chemical thermodynamics. Vol. 5. Update on the chemical thermodynamics of uranium, neptunium, plutonium, americium and technetium. Amsterdam: Elsevier.

Hallbeck L, Pedersen K, 2008. Explorative analyses of microbes, colloids, and gases together with microbial modelling. Site description model. SDM-Site Laxemar. SKB R-08-109, Svensk Kärnbränslehantering AB.

Kitamura A, Yoshida Y, 2010. Preparation of text files of JAEA-TDB for geochemical calculation programs. JAEA-Data/Code 2010-011, Japan Atomic Energy Agency.

Kitamura A, Fujiwara K, Yui M, 2010. JAEA thermodynamic database for performance assessment of geological disposal of high-level and TRU wastes: Refinement of thermodynamic data for trivalent actinoids and samarium. JAEA-Review 2009-047, Japan Atomic Energy Agency.

Laaksoharju M, Wallin B (eds), 1997. Evolution of the groundwater chemistry at the Äspö Hard Rock Laboratory. Proceedings of the second Äspö International Geochemistry Workshop, Äspö, Sweden, 6–7 June 1995. SKB HRL ICR 97-04, Svensk Kärnbränslehantering AB.

Laaksoharju M, Smellie J, Tullborg E-L, Gimeno M, Molinero J, Hallbeck L, Waber N, 2008. Bedrock hydrogeochemistry Forsmark. Site descriptive modelling, SDM-Site Forsmark. SKB R-08-47, Svensk Kärnbränslehantering AB.

Laaksoharju M, Smellie J, Tullborg E-L, Wallin B, Drake H, Gascoyne M, Gimeno M, Gurban I, Hallbeck L, Molinero J, Nilsson A-C, Waber N, 2009. Bedrock hydrogeochemistry Laxemar. Site descriptive modelling, SDM-Site Laxemar. SKB R-08-93, Svensk Kärnbränslehantering AB.

Li Y-H, Gregory S, 1974. Diffusion of ions in sea water and in deep sea sediments. Geochimca et Cosmochimica Acta, 38, pp 703–714.

Mills R, Lobo V M M, 1989. Self-Diffusion in electrolyte solutions: a critical examination of data compiled from the literature. Amsterdam: Elsevier. (Physical Sciences Data 36)

Nilsson K, Byegård J, Selnert E, Widestrand H, Höglund S, Gustafsson E, 2010. Äspö Hard Rock Laboratory. Long Term Sorption Diffusion Experiment (LTDE-SD). Results from rock sample analyses and modelling. SKB R-10-68, Svensk Kärnbränslehantering AB.

Parkhurst D L, Appelo C A J, 1999. User's guide to PHREEQC (version 2): a computer program for speciation, batch-reaction, one-dimensional transport, and inverse geochemical calculations. Water-Resources Investigations Report 99-4259, U.S. Geological Survey, Denver, Colorado.

Selnert E, Byegård J, Widestrand H, Carlsten S, Döse C, Tullborg E-L, 2009. Bedrock transport properties. Data evaluation and retardation model. Site descriptive modelling, SDM-Site Laxemar. SKB R-08-100, Svensk Kärnbränslehantering AB.

Vilks P, Miller N H, Stanchell F W, 2005. Laboratory program supporting SKB's Long Term Diffusion Experiment. Report 06819-REP-01200-10128-R00, Ontario Power Generation, Nuclear Waste Management Division, Canada.

Wass E, 2005. Äspö Hard Rock Laboratory. LTDE Long-Term Diffusion Experiment. Hydraulic conditions of the LTDE experimental volume – results from Pre-Tests 0.1-6. SKB IPR-05-25, Svensk Kärnbränslehantering AB.

Widestrand H, Byegård J, Börjesson S, Bergelin A, Wass E, 2006. LTDE Long-Term Diffusion Experiment. Functionality tests with short-lived radionuclides 2005. SKB IPR-06-05, Svensk Kärnbränslehantering AB.

Widestrand H, Byegård J, Selnert E, Skålberg M, Höglund S, Gustafsson E, 2010. Long Term Sorption Diffusion Experiment (LTDE-SD). Supporting laboratory program – Sorption diffusion experiments and rock material characterisation. With supplement of adsorption studies on intact rock samples from the Forsmark and Laxemar site investigations. SKB R-10-66, Svensk Kärnbränslehantering AB.

Winberg A, Andersson P, Hermanson J, Byegård J, Cvetkovic V, Birgersson L, 2000. Äspö Hard Rock Laboratory. Final report of the first stage of the tracer retention understanding experiments. SKB TR-00-07, Svensk Kärnbränslehantering AB.

Winberg A, Andersson P, Byegård J, Poteri A, Cvetkovic V, Dershowitz W, Doe T, Hermanson J, Jaime Gómez-Hernaández J, Hautojärvi A, Billaux D, Tullborg E-L, Holton D, Meier P, Medina A, 2002. Final report of the TRUE Block Scale project – 4. Synthesis of flow, transport and retension in the block scale. SKB TR-02-16, Svensk Kärnbränslehantering AB.

Winberg A, Hermanson J, Tullborg, E-L, Staub I, 2003. Äspö Hard Rock Laboratory. Long-Term Diffusion Experiment. Structural model of the LTDE site and detailed description of the characteristics of the experimental volume including target structure and intact rock section. SKB IPR-03-51, Svensk Kärnbränslehantering AB.

Appendix 1

Photographs of parts and installations in KA3065A03

Figure A1-1. *Polyurethane cylinder (mounted on lead-in equipment).*

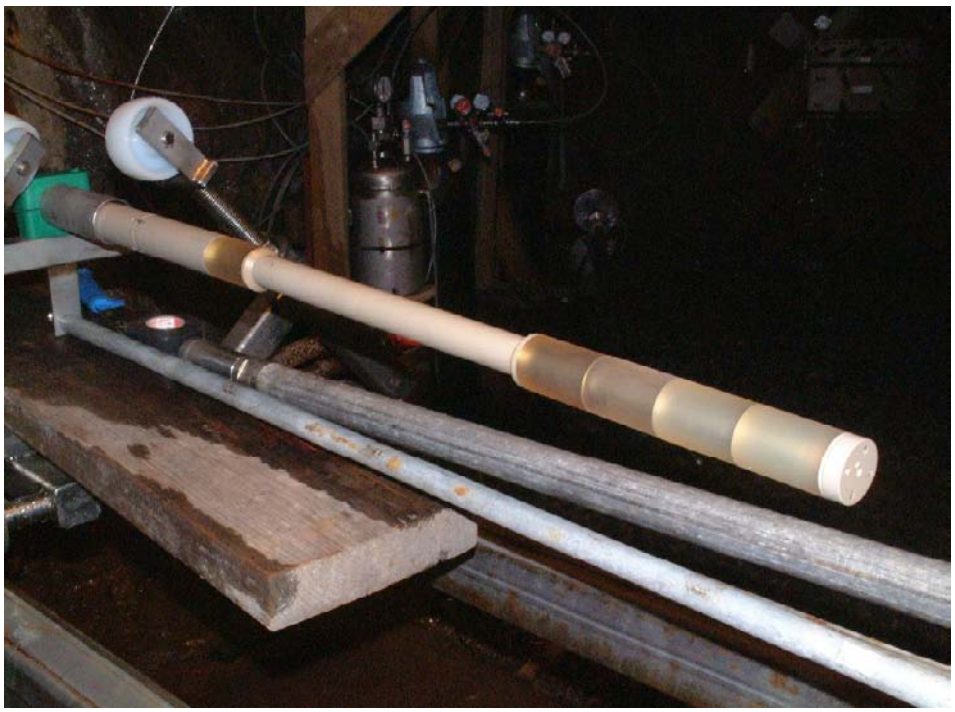

Figure A1-2. *36 mm borehole packer and dummy.*

Figure A1-3. *PEEK lid with connection to 36 mm borehole equipment.*

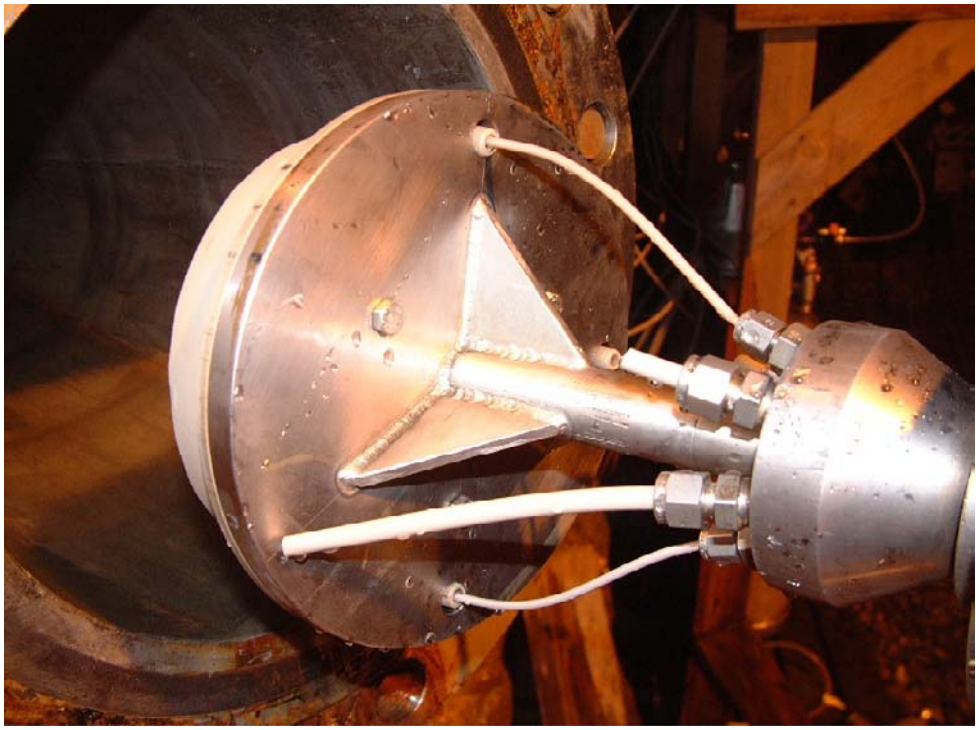

Figure A1-4. *Backside of PEEK lid, fixed to the supporting steel plate, where the 1/8" circulation tubing to the stub section is seen and the ¼" tubing for circulation of section 2 is seen.*

Figure A1-5. *Mounted PEEK lid, mechanical and hydraulic 300 mm packers.*

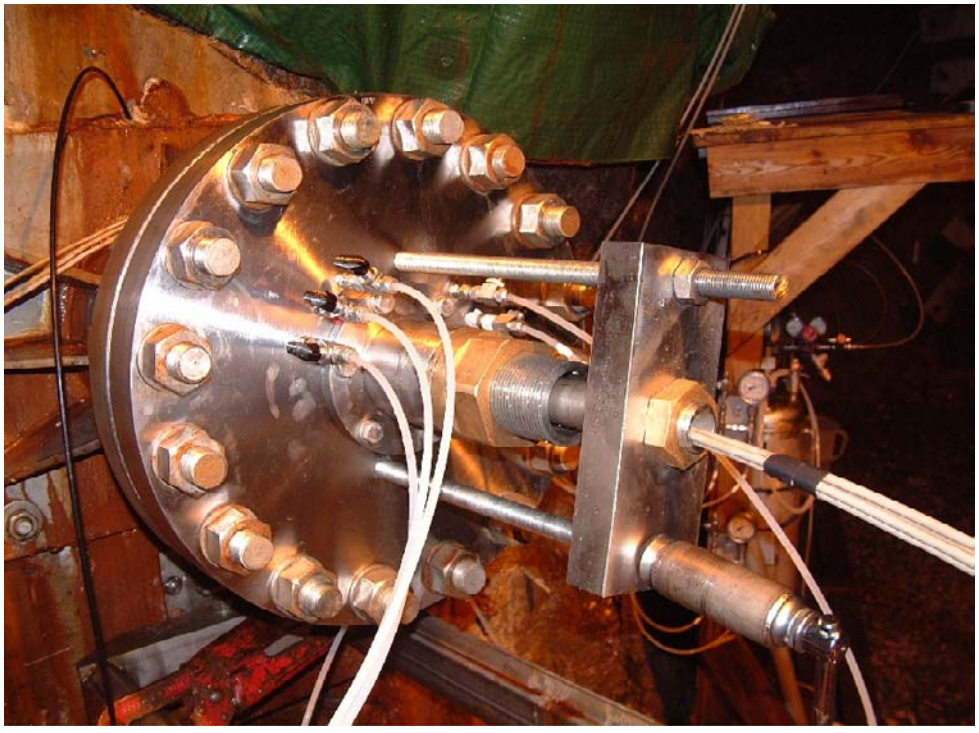

Figure A1-6. *Borehole collar after installation.*

Appendix 2

Injection and sampling procedure

A2.1 Injection procedure

Transfer of stock solution to tubing loop

The length of each loop was adjusted to, in addition to the stock solution, hold approximately 6–7 ml guard water. The purpose of having guard water in the beginning and in the end of each loop was to minimize the loss of tracer solution at the transfer of the stock solution from the glass vessel to the tubing loop.

The two empty loops were joined to injection valve 14 and 15, respectively, at ports 1 and 4, see Figure 2-6 and A2-1. The injection valves 14 and 15 were placed in series, 14 before 15. The injection loop joined to valve 14 was used for the alkaline stock solution while the acidic stock solution was joined to valve 15. In the following, the procedure to load the injection loop joined to valve 15 is outlined. The same is valid for loading of the injection loop joined to valve 14.

A syringe was joined to port 2 and a short tube was joined to port 3 of the injection valves. The tube had a length sufficient to reach down to the bottom of the vessel containing the stock solution. When the injection valve is in its "LOAD" position, ports 1 and 2 are connected as well as ports 3 and 4. This makes it possible, with the help of the syringe, to suck an aqueous solution, guard water or stock solution, into the loop. The tubing loop was filled in three steps as follows (see also Figure A2-1):

1) As a first step the short tube was immersed in a beaker with guard water. Approximately 3–4 ml was sucked into the syringe-injection loop-tube set-up.
2) Next, the tube was transferred to the glass vessel and immersed in the stock solution. The vessel was tilted to ensure that almost all of the stock solution was sucked into the tubing loop.
3) When almost all of the stock solution was sucked into the set-up, a small amount of guard water was added to the vessel. Suction with the syringe continued until small droplets of water could be seen in the inlet of the syringe, indicating the syringe-injection loop-tube set-up was filled with solution.

Thus, the stock solution was now transferred to the injection loop, ready to be connected to the circulation equipment. The only residual of the stock solutions were left in the vessels, and could easily be returned to Baslab and be sampled and measured to determine the non-injected amount of radioactivity

Injection

The injection was done by switching the valve to the "INJECTION" position, connecting ports 1 and 6 as well as ports 4 and 5. The stock solution in the injection loop was then transferred into the circulation loop as a flow pulse. It was desired that a pulse flow within the tubing should be obtained until the stock solutions would reach the experimental test section, in which mixing would occur and the two solutions would be pH-equilibrated. A photo of the equipment set-up is shown in Figure A2-2.

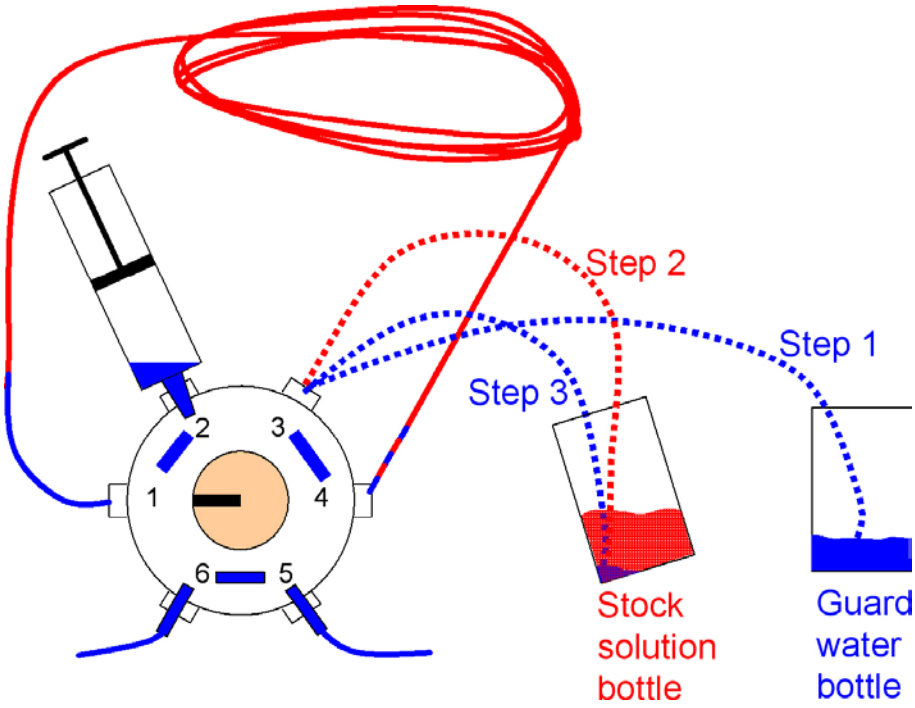

Figure A2-1. *Drawing of equipment set-up for controlled transfer of the stock solution to the injection loop. The three steps of filling the loop are described in the text above.*

Figure A2-2. *Injection valves photograph with tubes to stock solution bottles, syringes and one injection loop visible behind the left syringe. The photo is from a pre-test. In the LTDE-SD injection, 20 ml plastic vials were used for the stock solutions and the vials were placed in lead shields.*

A2.2 Sampling procedure

A short tube was connected to the outlet of the needle valve aimed to facilitate sampling in 20 ml plastic vials (scintillation vials).

A description of the sampling procedure is outlined below.

1. The circulation in the test section was shut down.
2. A scintillation vial was placed under the tube.
3. Valve 9 was switched into the “INJECT” position.
4. The needle valve was opened with precaution. A pressure drop less than 2–3 bar was desirable.
5. The valve 9 was switched to “LOAD” position when approximately 10 ml had been withdrawn from the test section.

Thereafter the needle valve was set to fully open allowing remaining solution to drop into the sample. To ensure that no solution will be left in the sampling equipment after each sampling a syringe was joined to port 2 on valve 9 and nitrogen was pressed, with the aid of the syringe, through port 2 and 1 to flush the needle valve and the tube.

Filtered samples

In order to be able to take filtered water samples the tube was replaced by a filter. To the filter a syringe was joined which was arranged to fit into a scintillation vial. The same sampling procedure as outlined above was used.

Appendix 3

Circulation scheme (KA3065A03:1)

The normal circulation was through both the 36 mm borehole section and the stub section. The time periods with circulation in the stub section only are presented below:

Circulation through lower part of stub (start)	Circulation through lower part of stub (stop)	Hours
2006-09-27 19:00	2006-09-27 21:03	2
2006-09-27 23:03	2006-09-28 00:31	1
2006-09-28 08:53	2006-09-28 11:04	2
2006-09-28 13:41	2006-09-28 15:09	1
2006-09-29 10:26	2006-09-29 13:39	3
2006-10-03 08:38	2006-10-03 17:08	8
2006-10-04 10:36	2006-10-04 13:52	3
2006-10-05 09:18	2006-10-05 14:19	5
2006-10-06 09:24	2006-10-06 15:14	6
2006-10-09 09:15	2006-10-09 15:56	7
2006-10-11 09:54	2006-10-11 17:53	8
2006-10-13 12:12	2006-10-13 13:55	2
2006-10-16 10:30	2006-10-16 16:26	6
2006-10-18 09:37	2006-10-18 15:18	6
2006-10-20 10:20	2006-10-20 16:05	6
2006-10-24 06:29	2006-10-24 18:22	12
2006-10-27 09:38	2006-10-27 15:00	5
2006-10-30 09:29	2006-10-30 16:23	7
2006-11-02 07:18	2006-11-02 12:05	5
2006-11-06 09:15	2006-11-06 19:01	10
2006-11-09 08:00	2006-11-09 19:05	11
2006-11-14 07:50	2006-11-14 18:51	11
2006-11-17 08:29	2006-11-17 17:26	9
2006-11-21 07:34	2006-11-24 07:22	72
2006-11-28 09:13	2006-11-28 18:05	9
2006-12-01 11:49	2006-12-01 15:07	3
2006-12-04 08:50	2006-12-04 16:14	7
2006-12-07 07:47	2006-12-07 17:47	10
2006-12-11 09:44	2006-12-11 16:28	7
2006-12-14 08:58	2006-12-14 18:31	10
2006-12-18 09:24	2006-12-18 17:15	8
2006-12-21 08:57	2006-12-21 14:37	6
2006-12-28 10:45	2006-12-28 15:25	5
2007-01-09 08:48	2007-01-09 15:33	7
2007-01-12 07:21	2007-01-12 13:44	6
2007-01-15 09:07	2007-01-15 16:27	7
2007-01-18 08:34	2007-01-18 19:37	11
2007-01-22 08:40	2007-01-22 18:08	9
2007-01-26 08:50	2007-01-26 15:25	7
2007-02-05 08:41	2007-02-05 15:04	6
2007-02-08 09:28	2007-02-08 16:53	7
2007-02-12 08:40	2007-02-12 17:08	8
2007-02-15 08:46	2007-02-15 16:20	8
2007-02-19 07:54	2007-02-19 15:12	7
2007-02-22 09:01	2007-02-22 15:40	7
2007-02-26 08:39	2007-02-26 17:10	9
2007-03-01 08:40	2007-03-01 15:35	7
2007-03-05 08:34	2007-03-05 16:14	8

Circulation through lower part of stub (start)	Circulation through lower part of stub (stop)	Hours
2007-03-07 11:19	2007-03-07 16:48	5
2007-03-12 07:22	2007-03-12 15:50	8
2007-03-15 08:57	2007-03-15 15:15	6
2007-03-19 08:36	2007-03-19 18:09	10
2007-03-22 09:15	2007-03-22 15:27	6
2007-03-26 08:47	2007-03-26 15:51	7
2007-03-29 08:40	2007-03-29 19:18	11
2007-04-02 08:48	2007-04-02 17:45	9
2007-04-05 08:35	2007-04-05 14:10	6
2007-04-10 09:01	2007-04-10 18:22	9
Total number of days with circulation through small hole	176	
Total number of days with circulation at lower stub part	20	

Appendix 4

Sampling in KA3065A03:1 and main events

Table A4-1. Sampling in KA3065A03:1 and selected main events.

Sample nr.	Date	Approx. Volym (ml)	Comment
1	2006-09-27	10	Background sample prior to injection.
	2006-09-27		19:00 Injection of acidic stock solution with tracers, circulation only in stub section.
	2006-09-27		19:01 Injection of base solution for neutralization.
2	2006-09-27	1	First radioactive sample, 1 hour after injection.
3	2006-09-27	10	Sampled two hours after injection. Circulation changed to 36-mm section and stub section.
4	2006-09-27	1	Sampled four hours after injection. Circulation changed to stub section only.
	2006-09-28		00:30 Circulation changed to 36-mm section and stub section.
5	2006-09-28	10	Sampled 14 hours after injection. Circulation changed to stub section for two hours, then normal circulation through and 36-mm section and stub section. This procedure was maintained throughout the experiment with regular intervals. Not further noticed in this table.
6	2006-09-29	10	
7	2006-10-04	10	
8	2006-10-11	10	
9	2006-10-25	10	
10	2006-11-08	10	
11	2006-11-22	10	
12	2006-11-22	5	Sampled in a syringe and filtered (0.020 micrometer filter).
13	2006-11-22	5	Sampled in a syringe passed through a cation resin.
–	2006-11-30	4	pH sample in centrifuge tube, not numbered or intended for tracer analysis.
14	2006-12-06	10	
15	2006-12-20	10	
16	2007-01-08	10	
17	2007-01-24	10	
18	2007-02-07	10	
19	2007-02-21	10	
21	2007-03-07	10	Sample vessels number 20 and 22 were never used due to an uncontrolled change in acid content.
23	2007-03-21	10	
24	2007-04-04	10	
25	2007-04-04	5	Sampled in a syringe and filtered (0.020 micrometer filter).
26	2007-04-04	5	Sampled in a syringe passed through a cation resin.
27	2007-04-04	5	Sampled in a syringe passed through a anion resin.
	2007-04-11		Pressure cylinder emptied to minimum volume, equipment loops disconnected from flow line and emptied. Circulation maintained with pressure regulation.
	2007-04-11		Colloid sampling from section KA3065A03:2.
	2007-04-12		Termination of experiment phase. Circulation stopped. Isopropyl alcohol exchange performed.
	2007-04-12		Epoxy injection performed.

Appendix 5

KA3065A03:1–2 groundwater sample 2006-06-20 analysis results

Table A5-1. Analysis results for groundwater sample 2006-06-20 in KA3065A03:1–2.

Idcode		KA3065A03	Section 1 and 2 connected
Secup	m	10.72	
Seclow	m	11.28	
Sample	No.	6918	
Sampling	date	2006-06-20	
Analysis of:	**Unit**	**Value**	**Note**
Ag	µg/L	<1	
Ba	µg/L	85.6	
Br	mg/l	31.8	
Ca	mg/L	1,710	
Cd	µg/L	<0.1	
Ce	µg/L	0.158	
Cl	mg/L	5,810	by titration
Cs	µg/L	2.72	
DOC	mg/L	1.6	
Drill water	%	0.07	
Dy	µg/L	<0.1	
Electr. Cond.	mS/m	1,640	
Er	µg/L	<0.1	
Eu	µg/L	<0.1	
F	mg/L	1.42	by potentiometric method
Fe2+	mg/L	0.68	
Fe-ICP	mg/L	0.708	
Fetot	mg/L	0.692	
Gd	µg/L	<0.1	
HCO3	mg/L	35.9	
Hf	µg/L	<0.1	
Hg	µg/L	<0.002	
Ho	µg/L	<0.1	
I	mg/l	0.191	
K	mg/L	11.5	
La	µg/L	0.241	
Li	mg/L	1.23	
Lu	µg/L	<0.1	
Mg	mg/L	60.9	
Mn	mg/L	0.359	
N	mg/L	0.14	
Na	mg/L	1,930	
Nb	µg/L	<0.02	
Nd	µg/L	<0.1	
NH4-N	mg/L	0.0896	
NO2-N	mg/L	0.0002	
NO2NO3-N	mg/L	0.0014	
NO3-N	mg/L	0.0013	
P	mg/L	0.0005	
Pa	µg/L	<0.0001	
Pd	µg/L	<0.5	
pH	pH unit	7.34	
PO4-P	mg/L	<0.0005	
Pr	µg/L	<0.1	
Ra-226	Bq/L	<0.015	
Rb	µg/L	33.7	

Idcode		KA3065A03	Section 1 and 2 connected
Secup	m	10.72	
Seclow	m	11.28	
Sample	No.	6918	
Sampling	date	2006-06-20	
Analysis of:	**Unit**	**Value**	**Note**
Rn-222	Bq/L	60±3	
S2	mg/L	0.009	
Sc	µg/L	<1	
Se	µg/L	<0.02	
Si	mg/L	6.68	
Sm	µg/L	<0.1	
Sn	µg/L	1.11	
SO4	mg/L	359	
SO4-S	mg/L	148	
Sr	mg/L	30.7	
Tb	µg/L	<0.1	
Th	µg/L	<0.4	
Tl*	µg/L	<0.1	
Tm	µg/L	<0.1	
U	µg/L	0.0959	
V	µg/L	0.418	
Y	µg/L	0.51	
Yb	µg/L	<0.1	
Zr	µg/L	<0.6	
Charge Balance	%	0.37	
Isotopes			
^{2}H	‰ dev SMOW	–90.3	Sampling 1999-04-20 in pilot borehole KA3065A03, Secup 8.80 m, Seclow, 11.20
^{3}H	TU	3.8	
^{18}O	‰ dev SMOW	–11.6	

Appendix 6

Circulation flow, temperatures and pressure regulator piston position

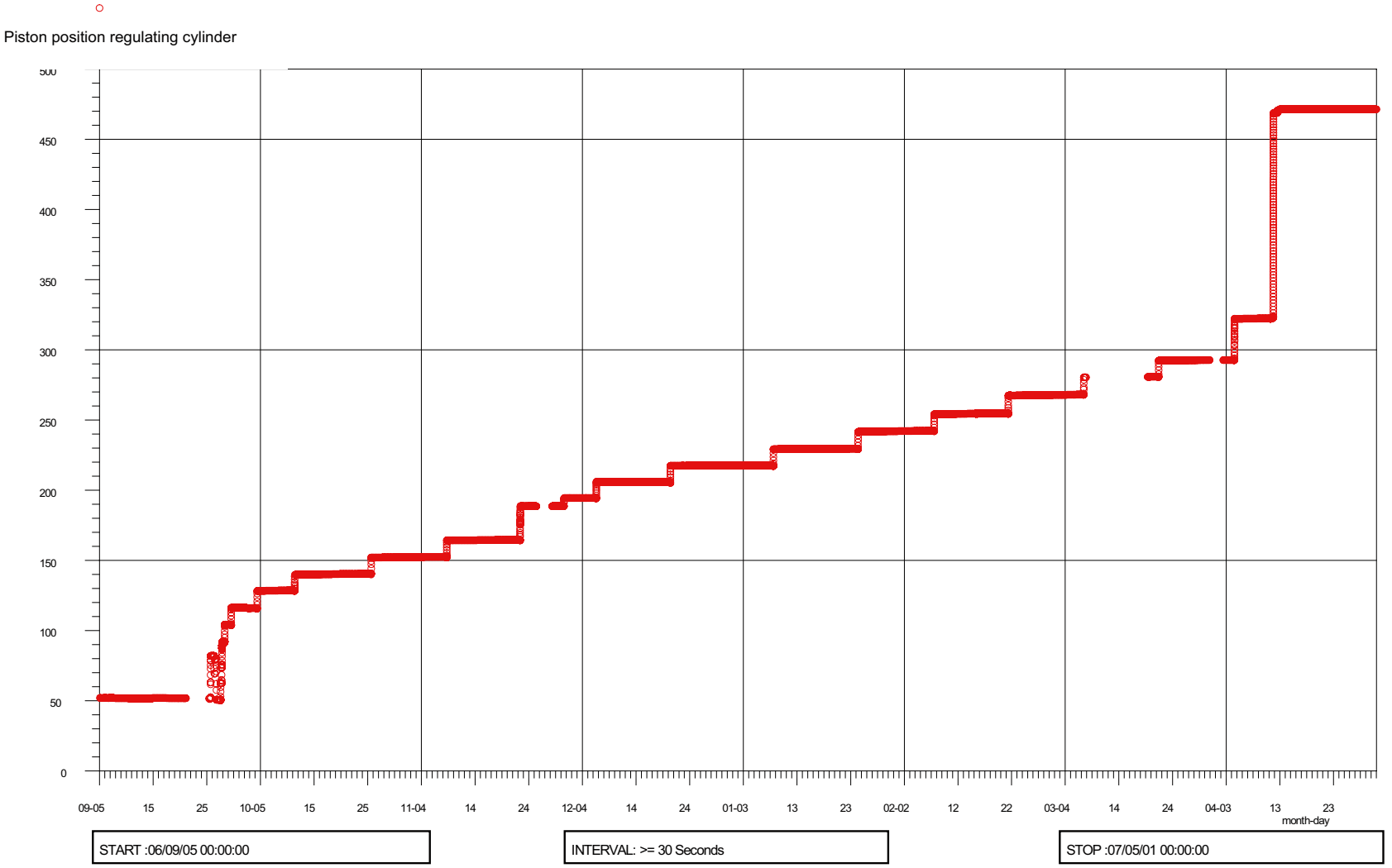

Figure A6-1. *Regulating cylinder piston position.*

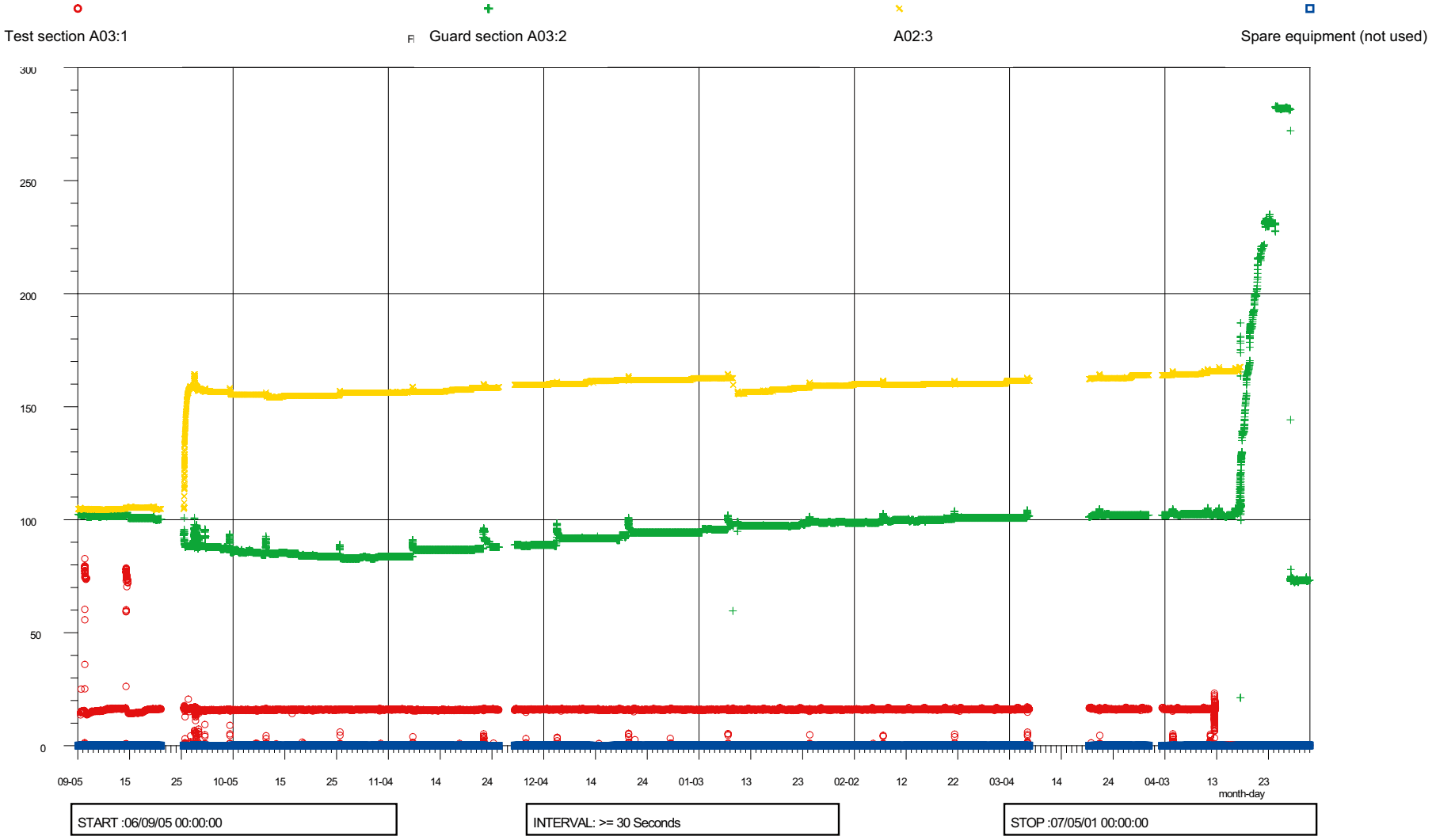

Figure A6-2. *Circulation flow (ml/min):*

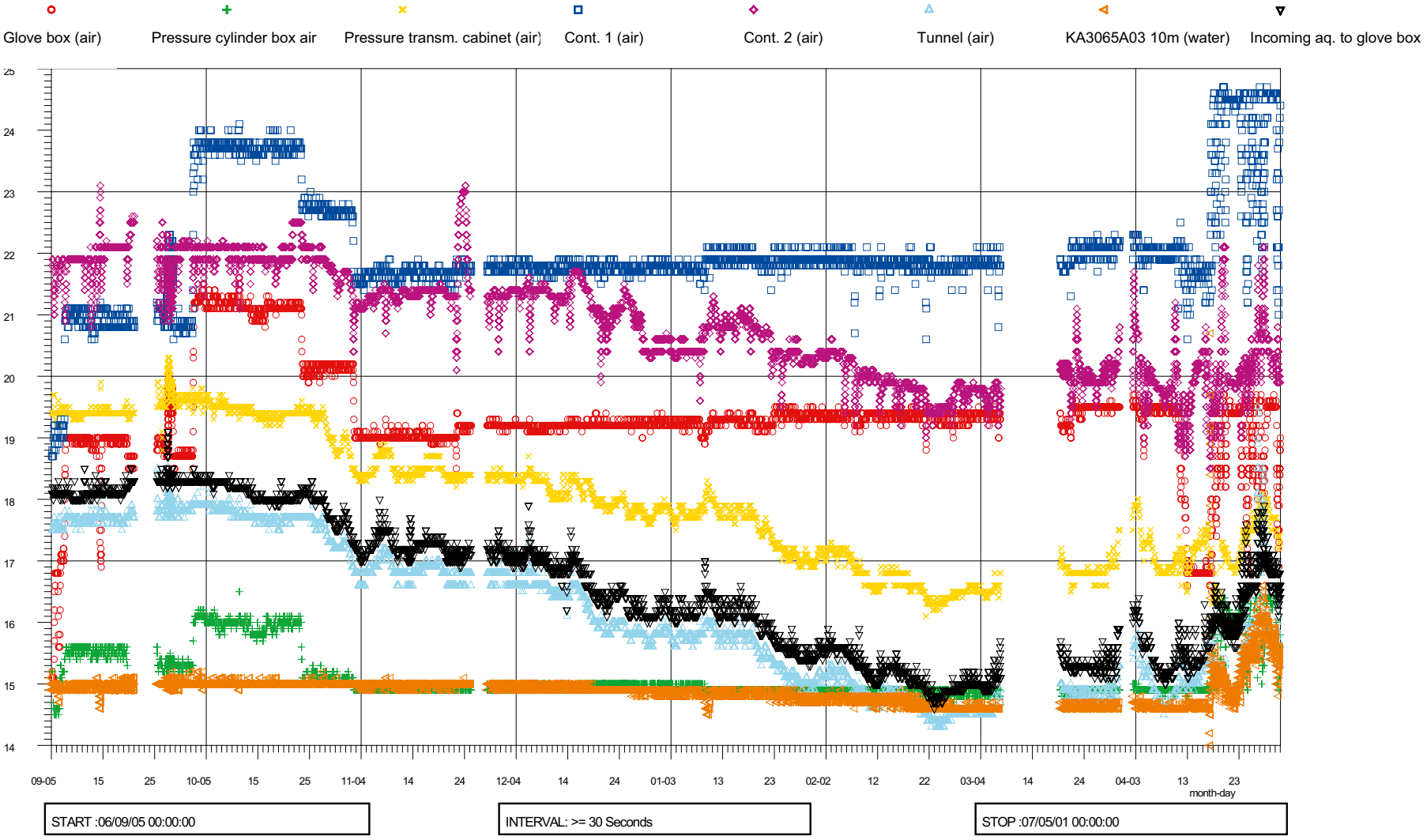

Figure A6-3. *Temperatures (°C).*

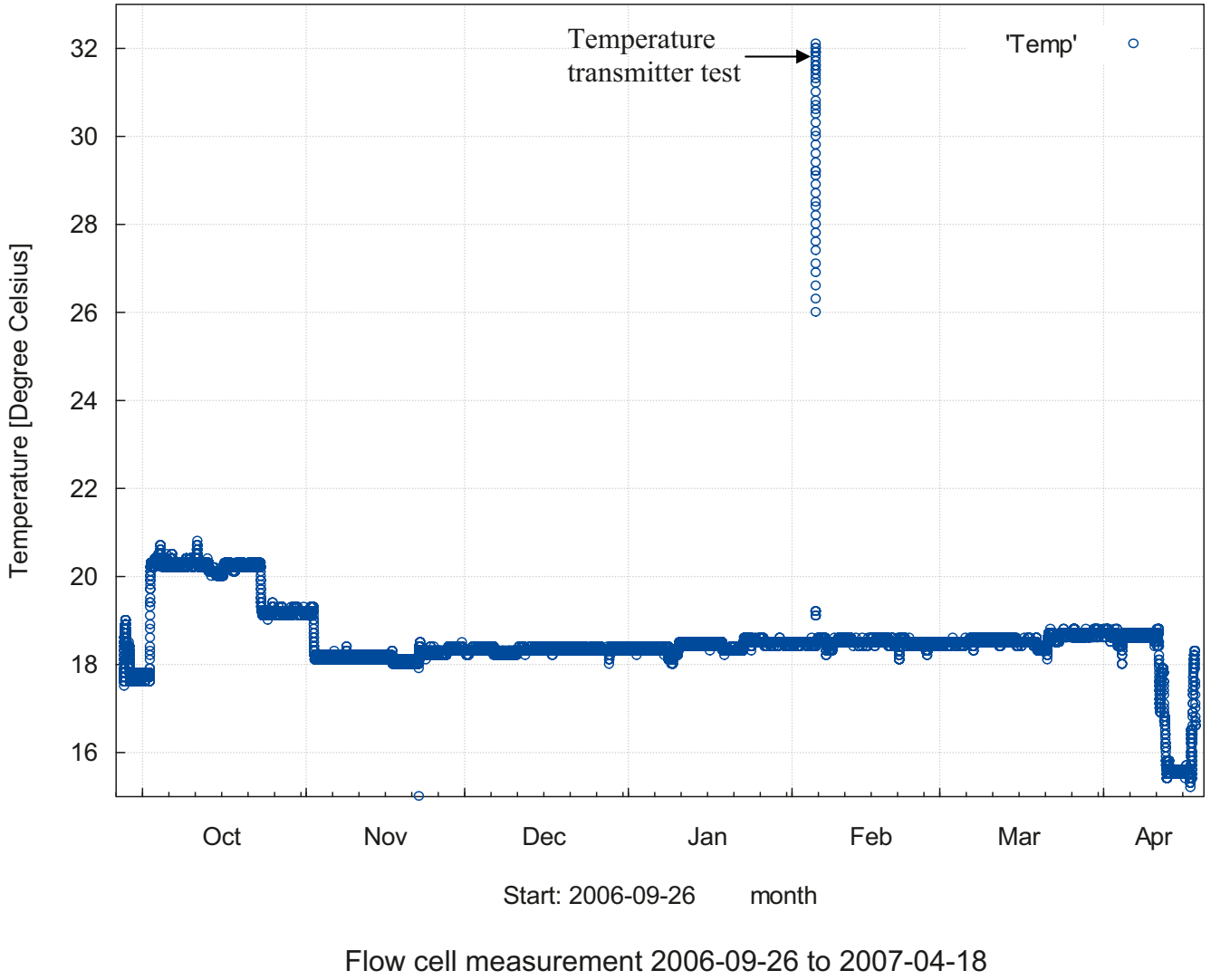

Figure A6-4. *Flow cell water temperature.*

Appendix 7

Eh and pH measurements on-line

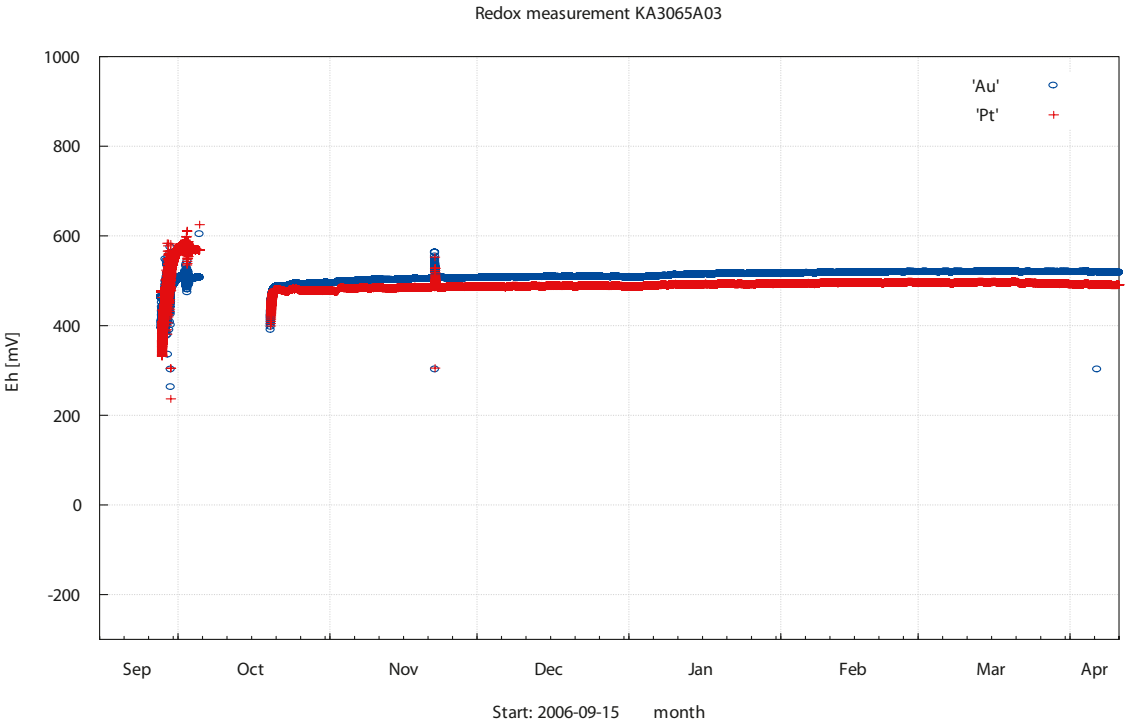

Figure A7-1. *Eh. On-line measurement of the redox potential in the groundwater of the test section loop throughout the LTDE-SD experiment. Two periods of disturbances occurred in the end of September and in early October and a more severe disturbance period from October 9 to October 20 has caused lack of credible experimental data during this period.*

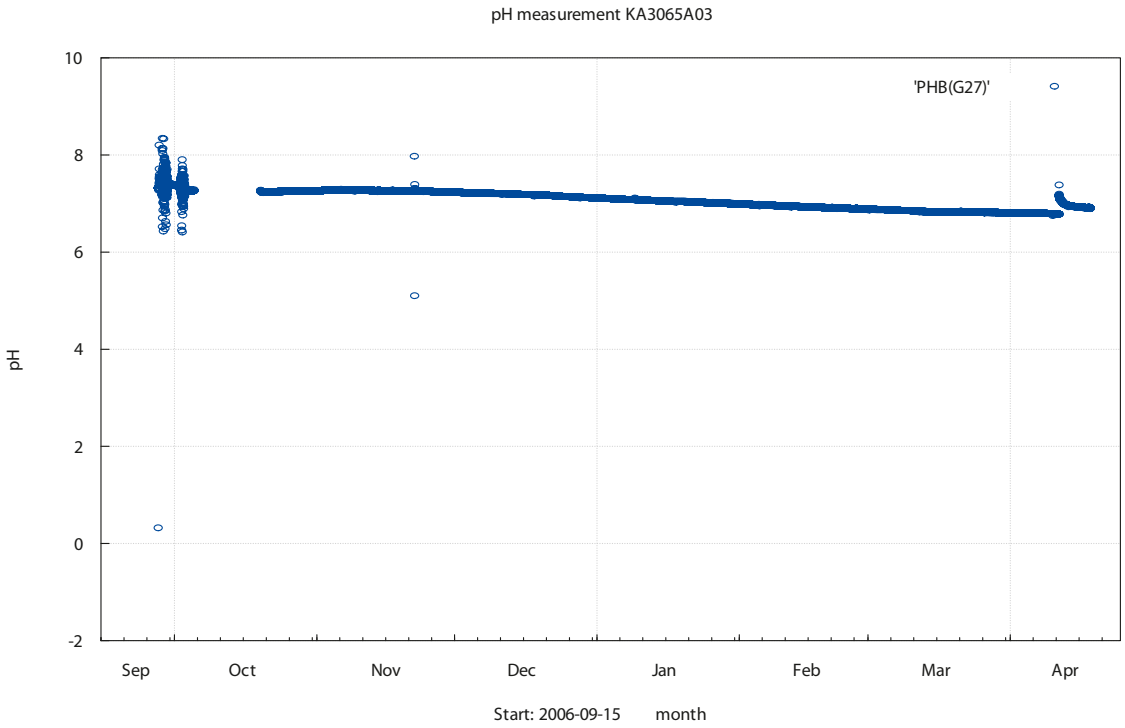

Figure A7-2. *pH. On-line measurement of the pH in the groundwater of the test section loop throughout the LTDE-SD experiment. Two periods of disturbances occurred in the end of September and in early October and a more severe disturbance period from October 9 to October 20 has caused lack of credible experimental data during this period.*

Appendix 8

Colloid filtration results

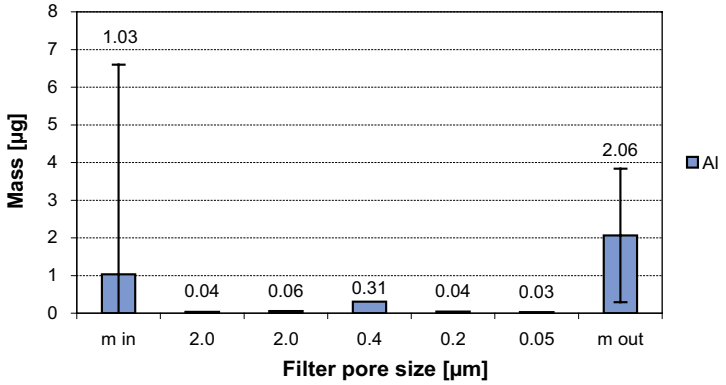

Figure A8-1. *Amount of aluminium entering the filter system (m in), in the filters and in the collecting container (m out).*

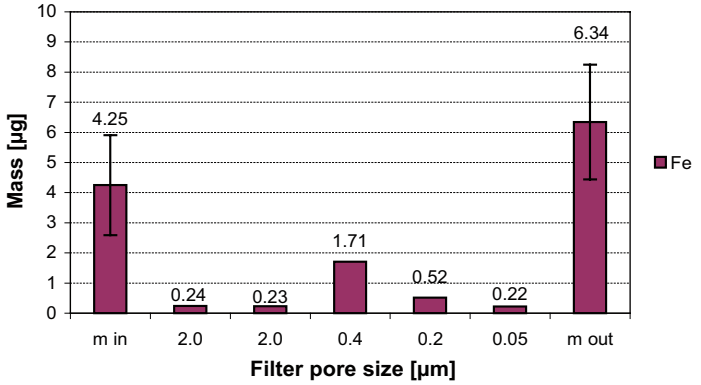

Figure A8-2. *Amount of iron entering the filter system (m in), in the filters and in the collecting container (m out).*

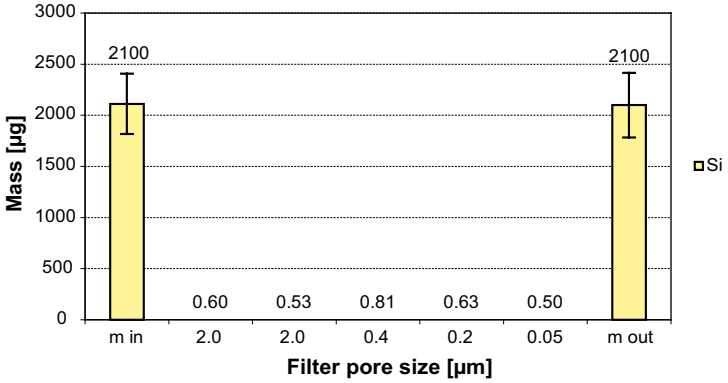

Figure A8-3. *Amount of silicon entering the filter system (m in), in the filters and in the collecting container (m out).*

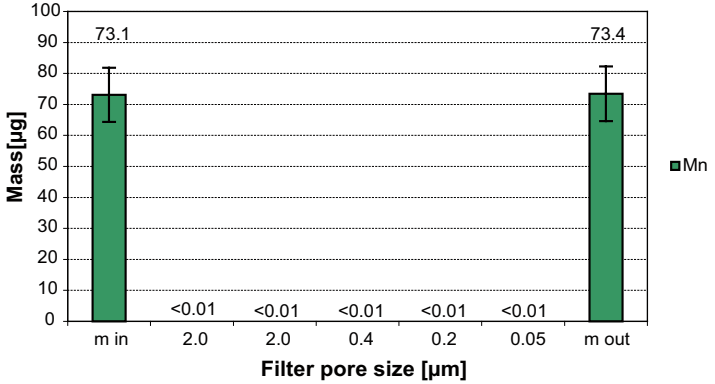

Figure A8-4. *Amount of manganese entering the filter system (m in), in the filters and in the collecting container (m out).*

Appendix 9

Pressure monitoring

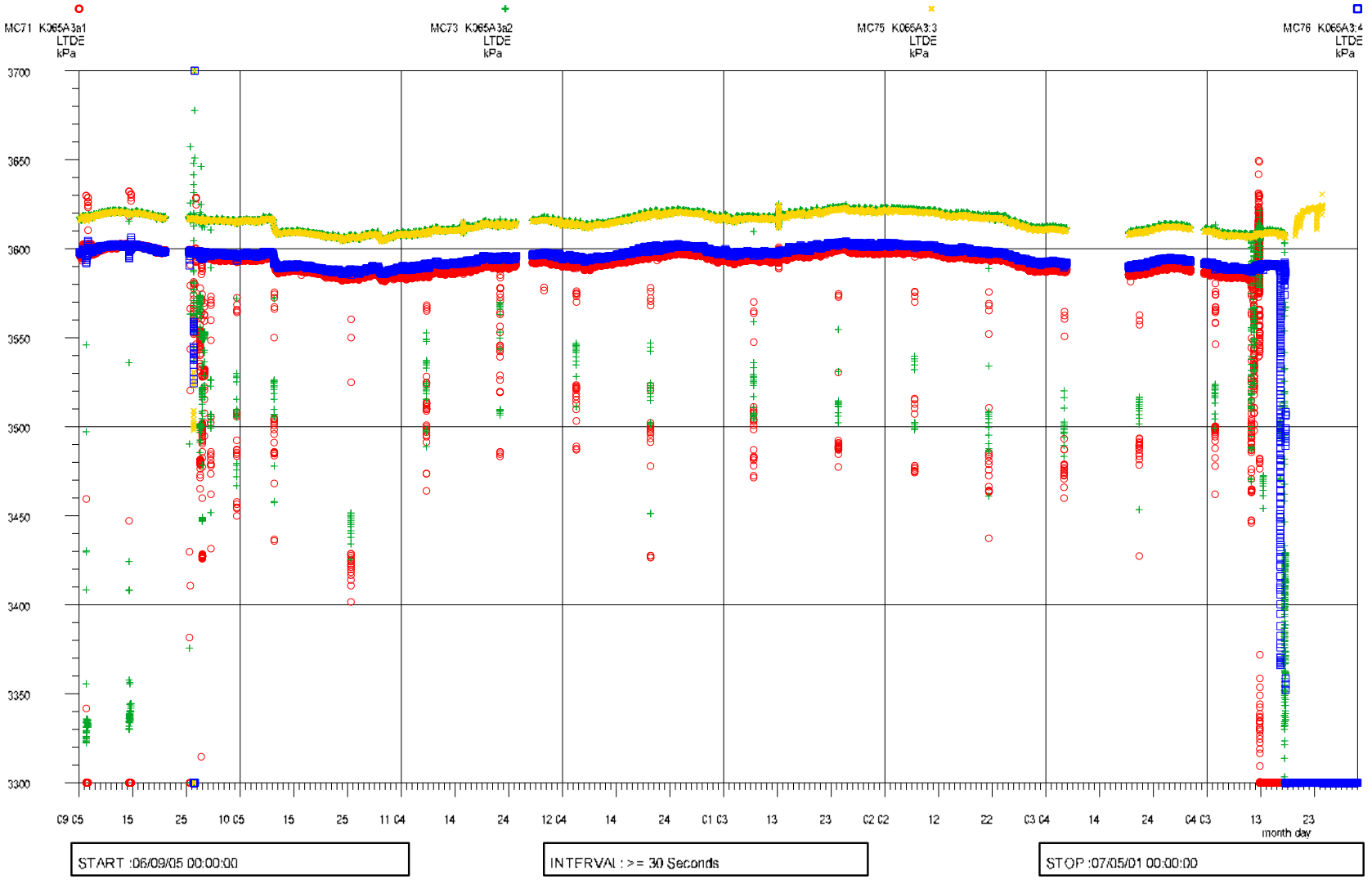

Figure A9-1. *Pressure in KA3065A03.*

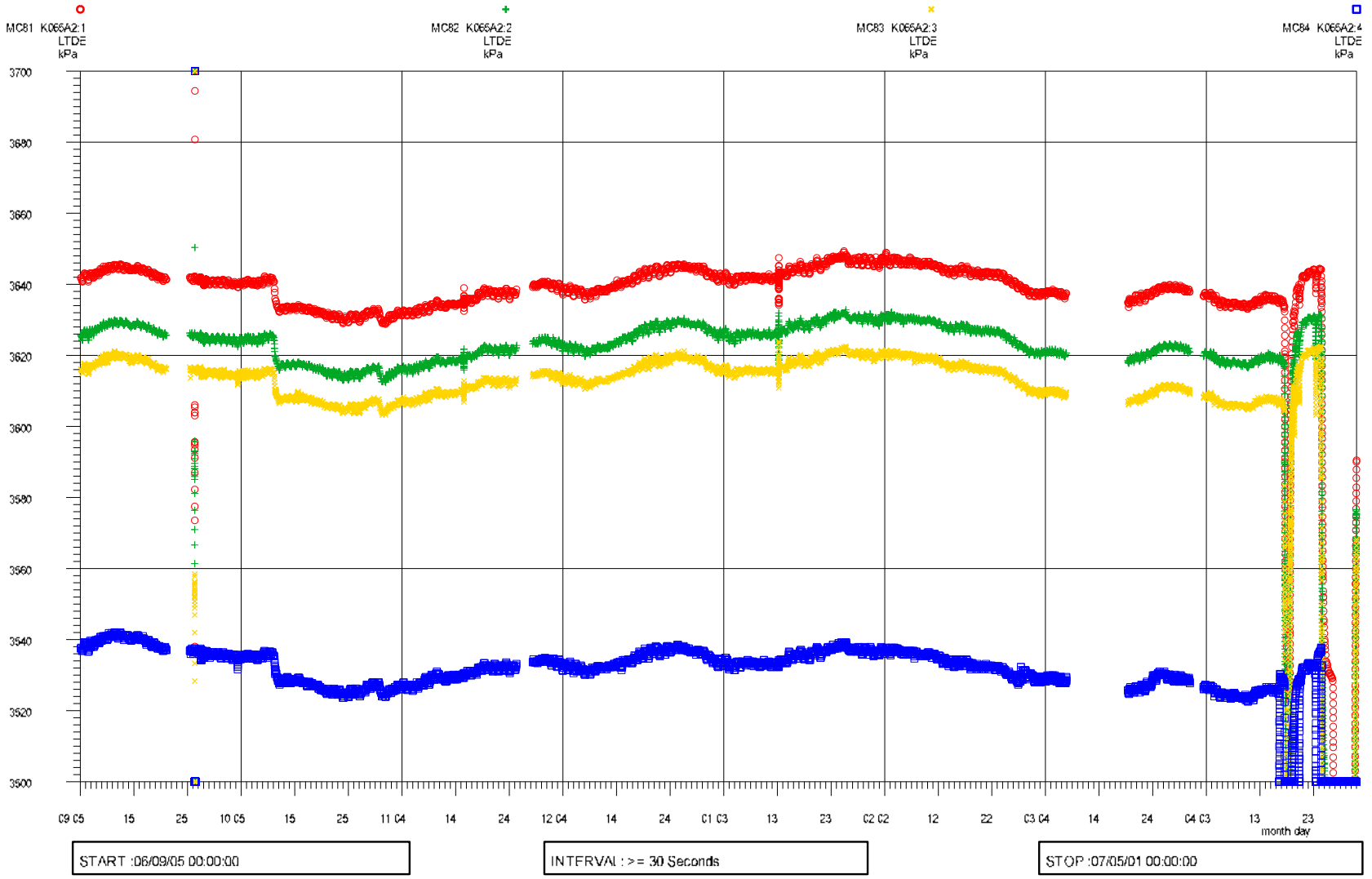

Figure A9-2. *Pressure in KA3065A02.*

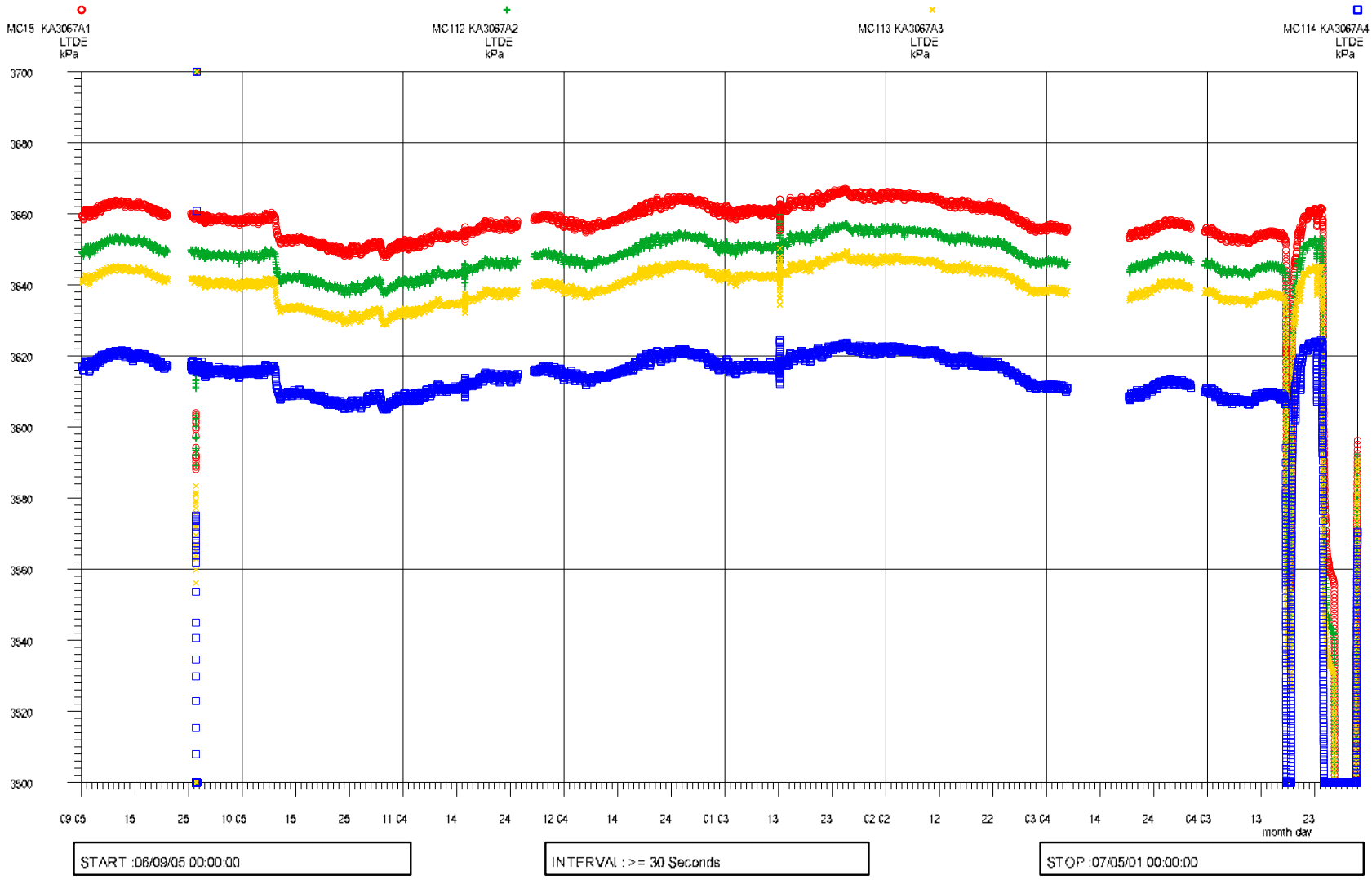

Figure A9-3. *Pressure in KA3067A.*

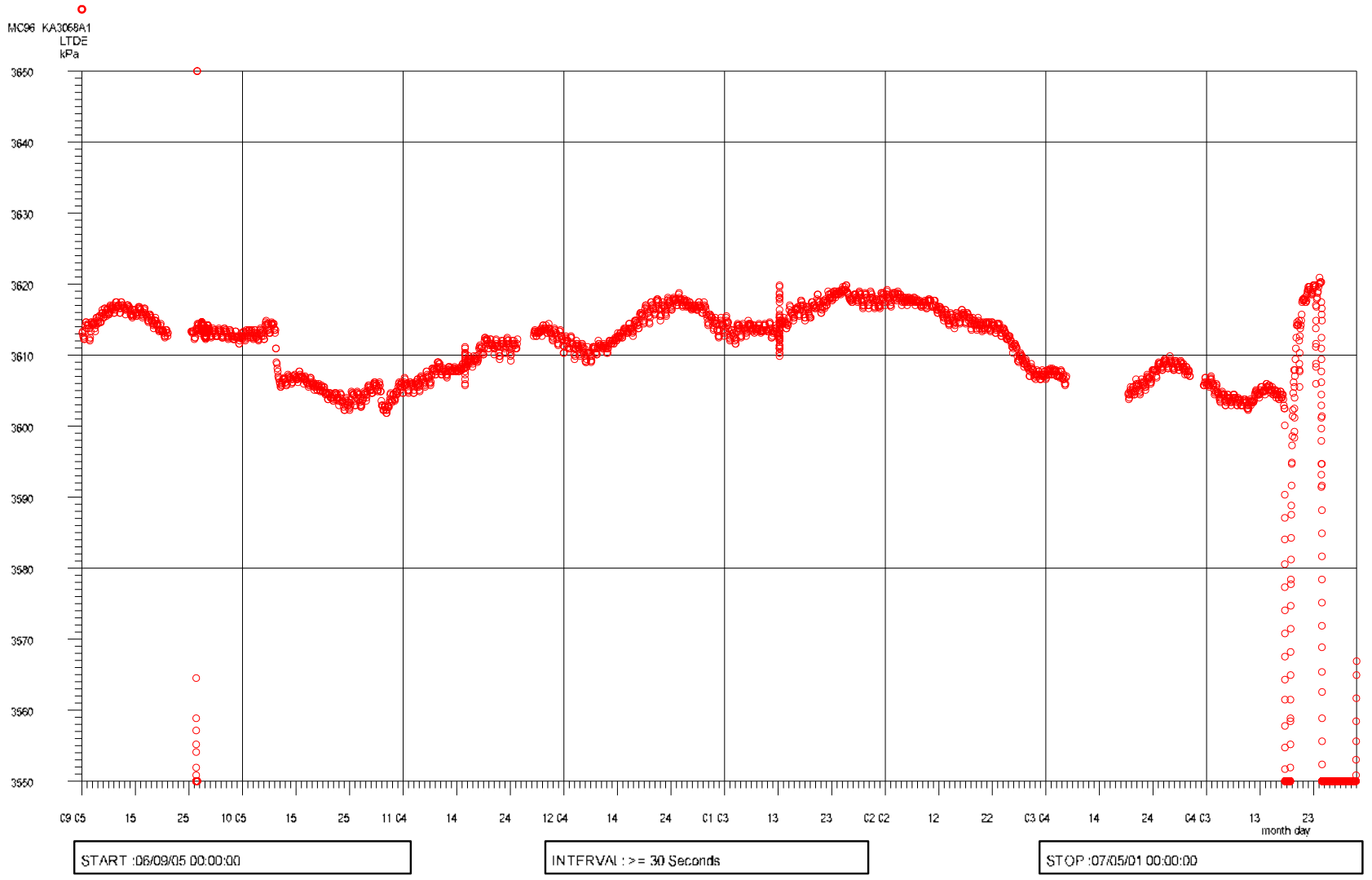

Figure A9-4. *Pressure in KA3068A.*

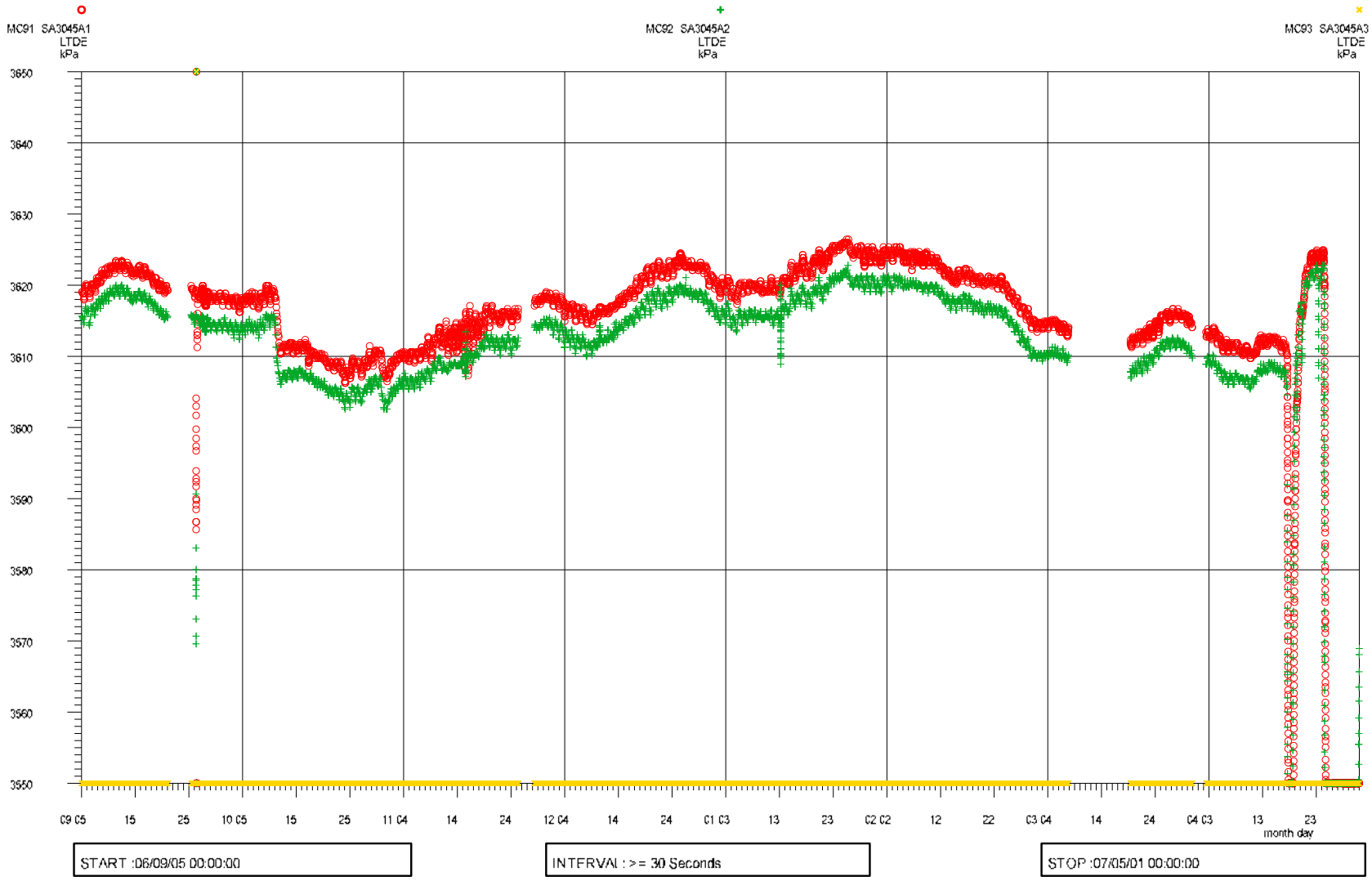

Figure A9-5. *Pressure in SA3045A.*

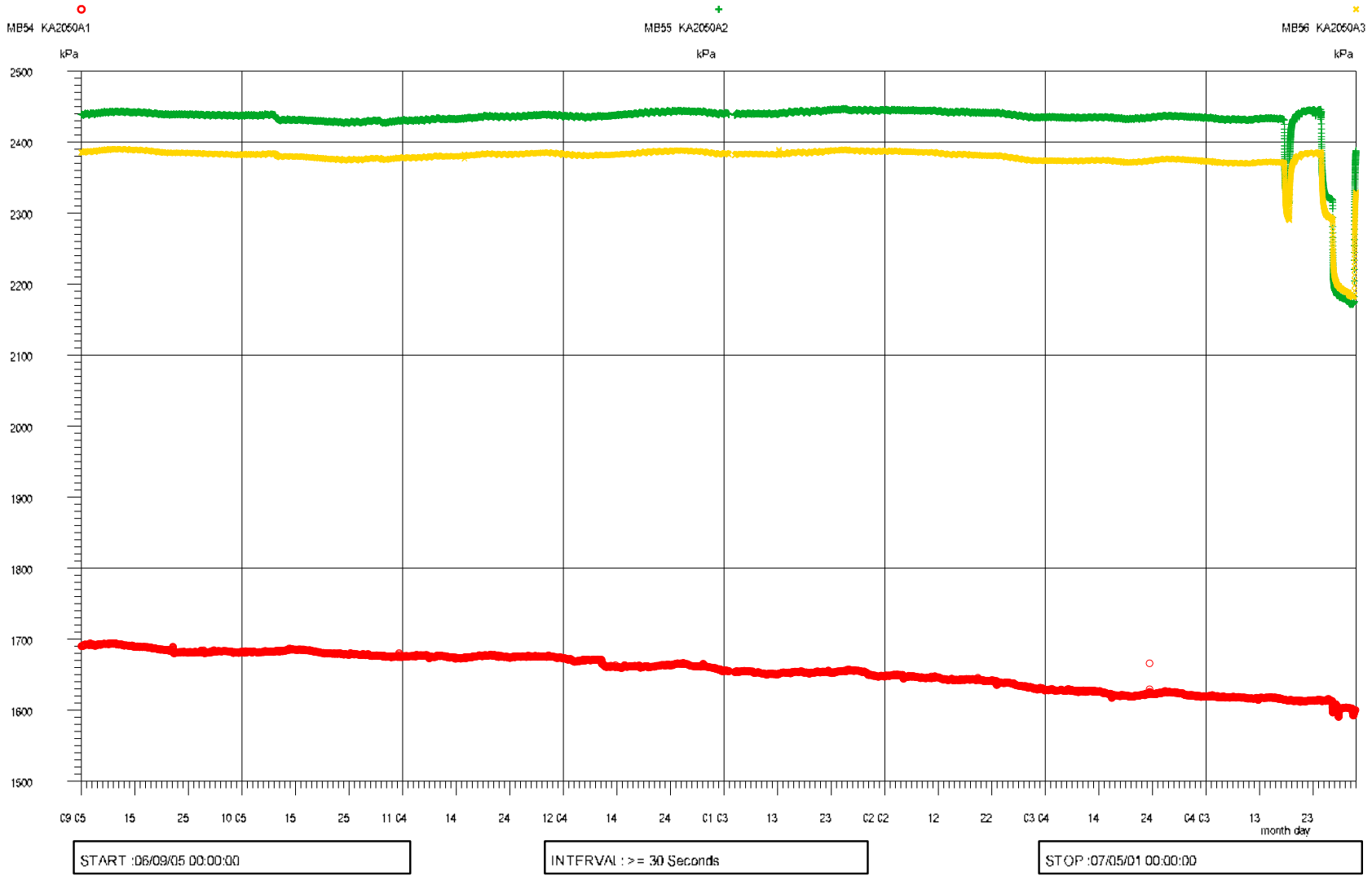

Figure A9-6. *Pressure in KA2050A.*

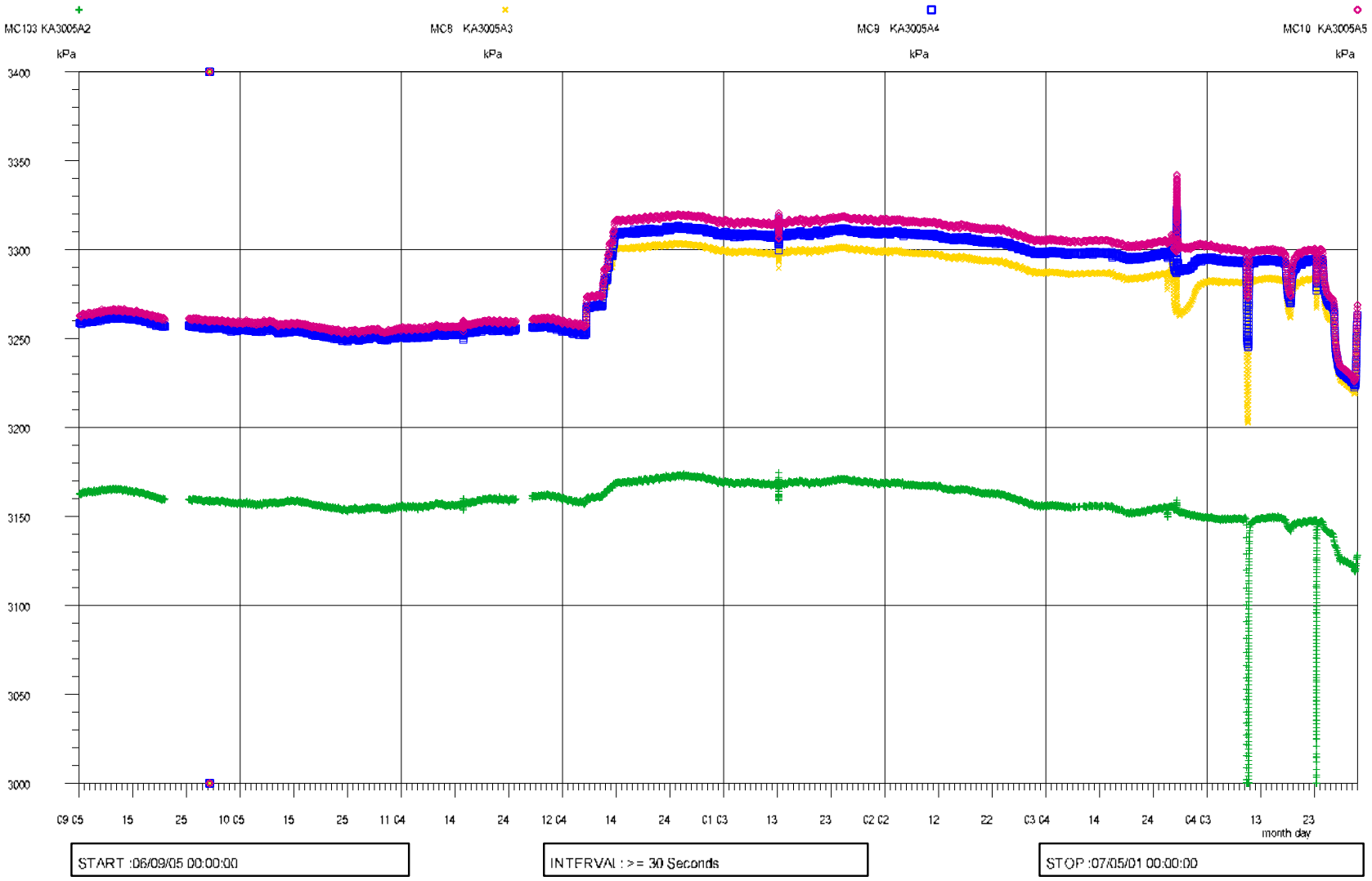

Figure A9-7. *Pressure in KA3005A.*

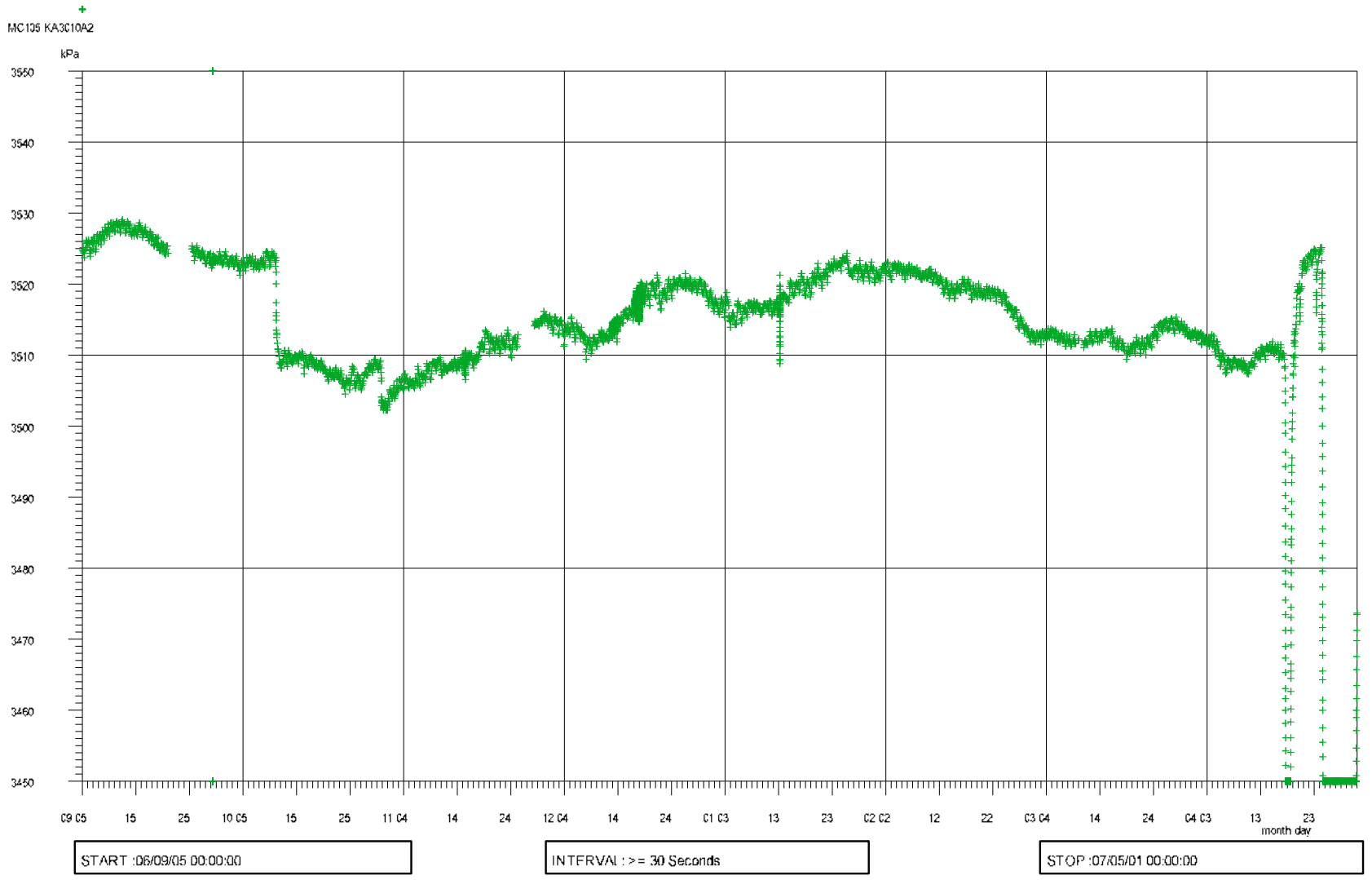

Figure A9-8. *Pressure in KA3010A.*

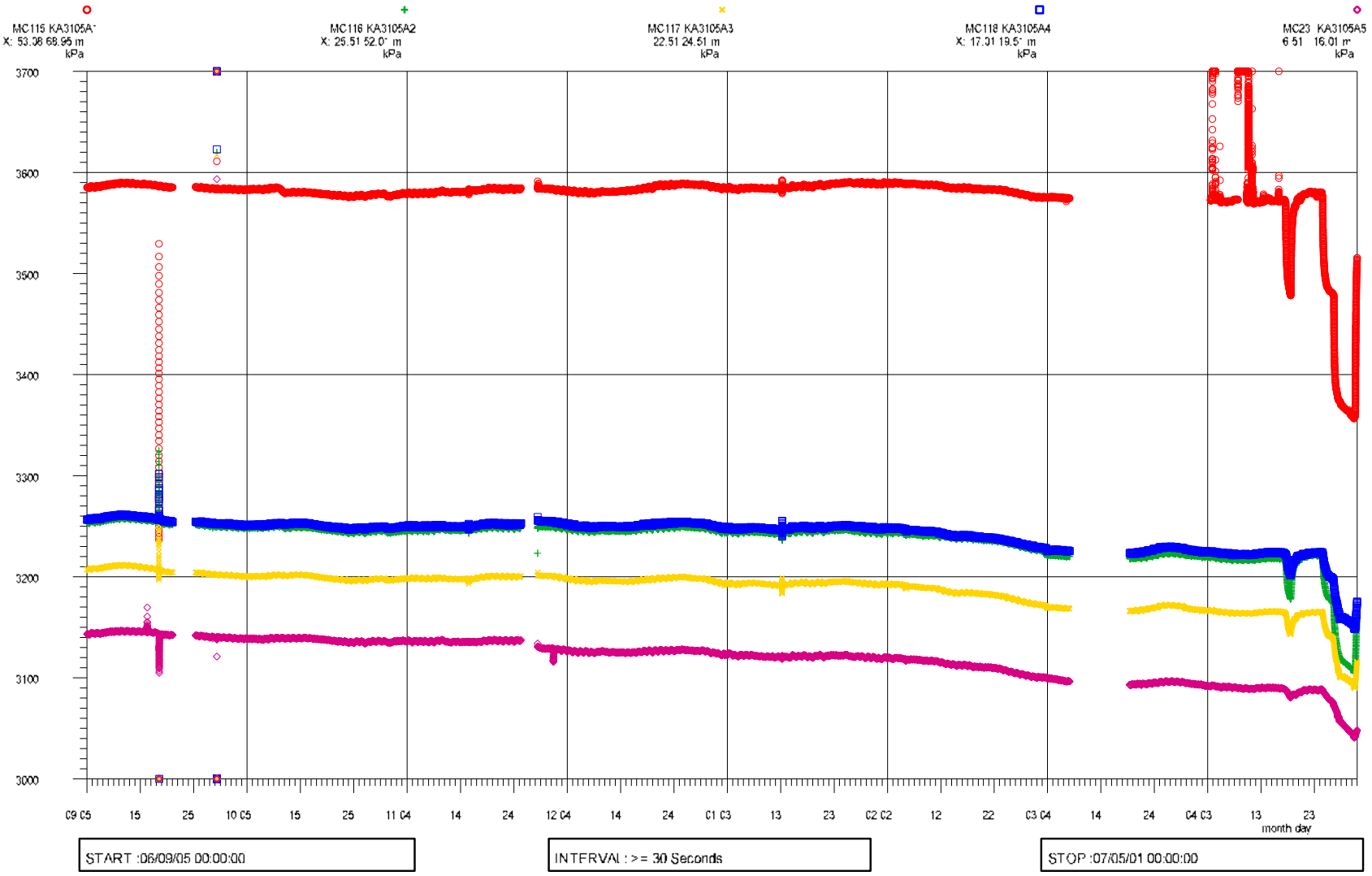

Figure A9-9. *Pressure in KA3105A.*

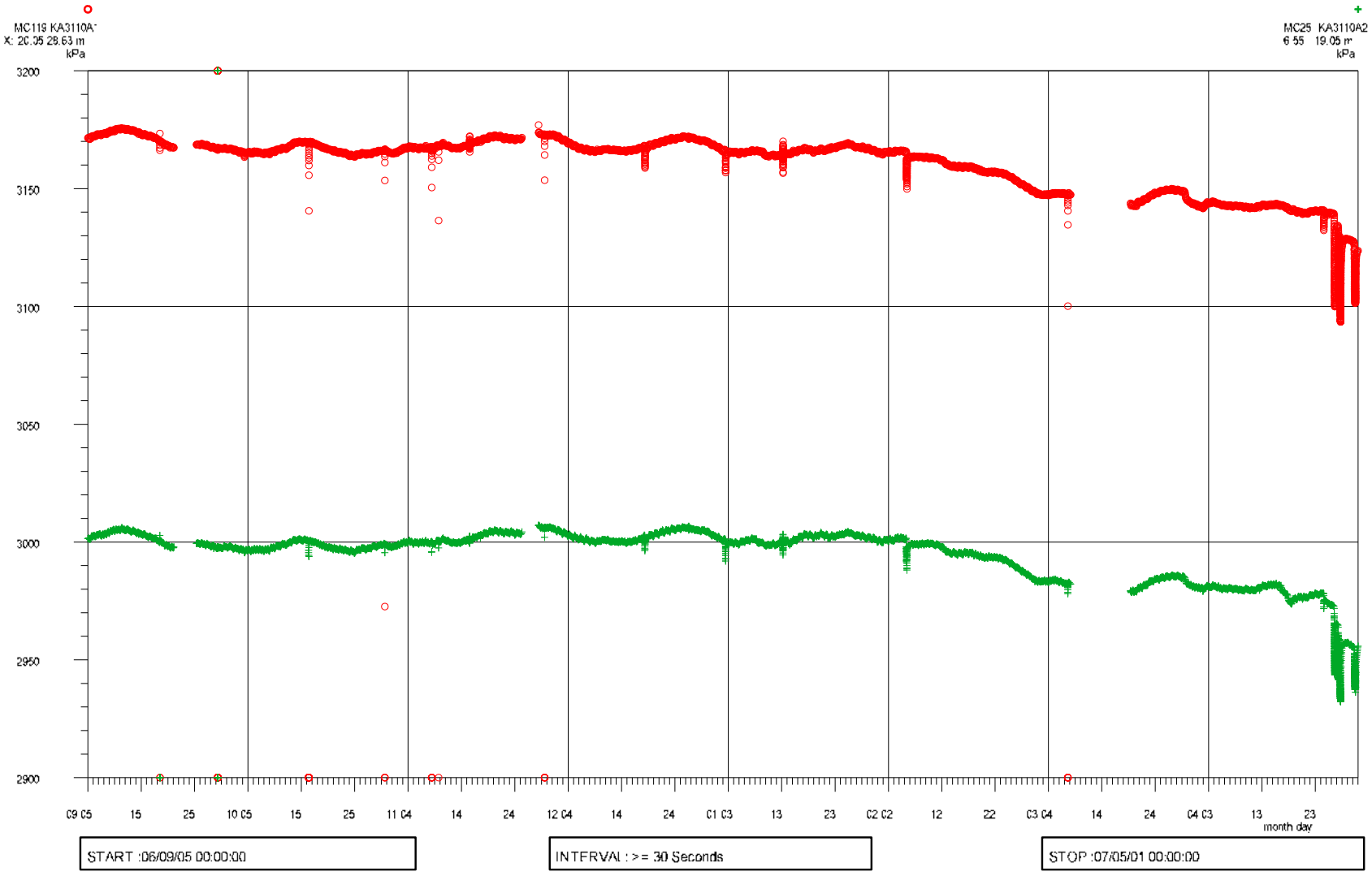

Figure A9-10. *Pressure in KA3110A.*

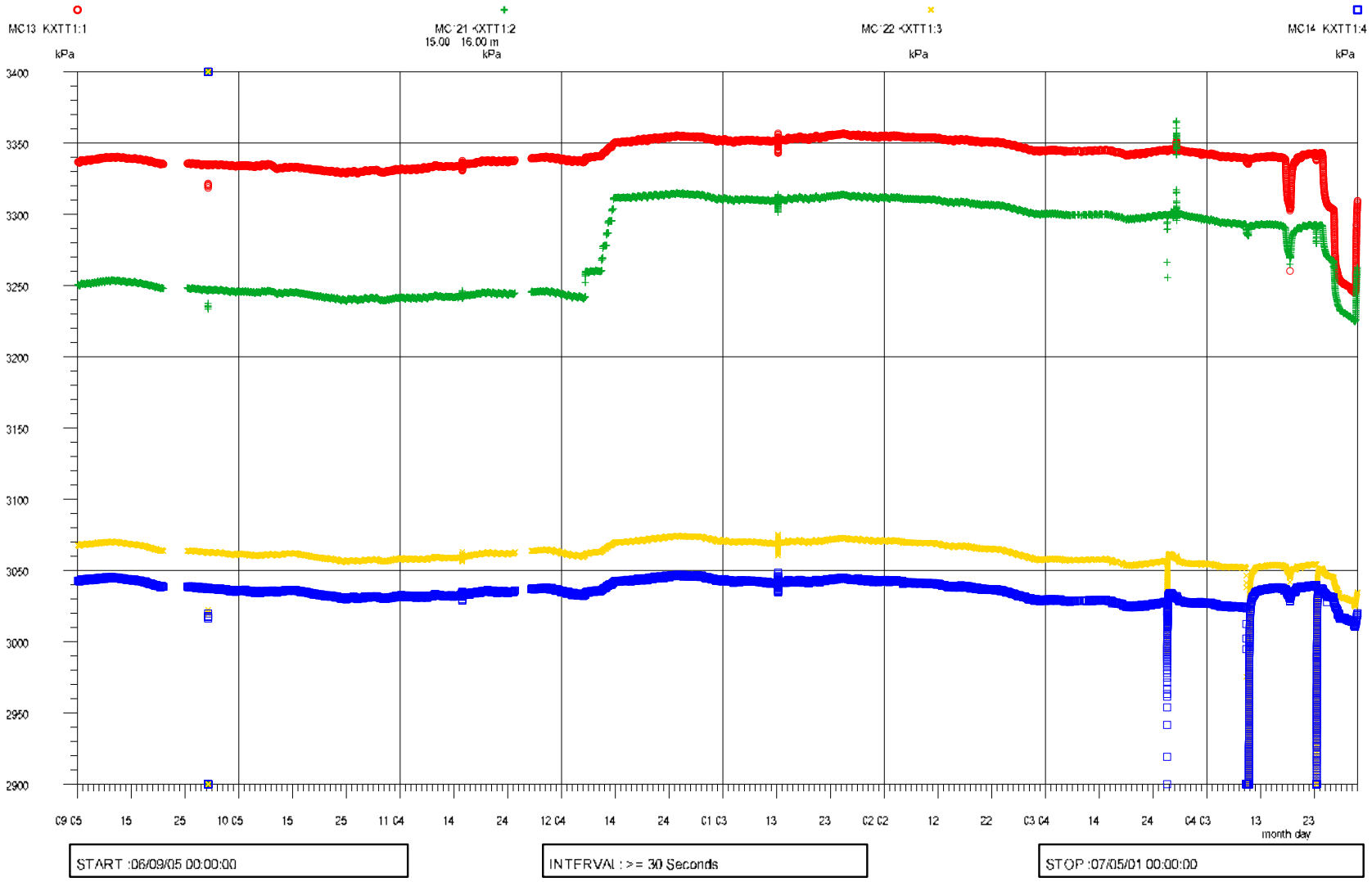

Figure A9-11. *Pressure in KXTT1.*

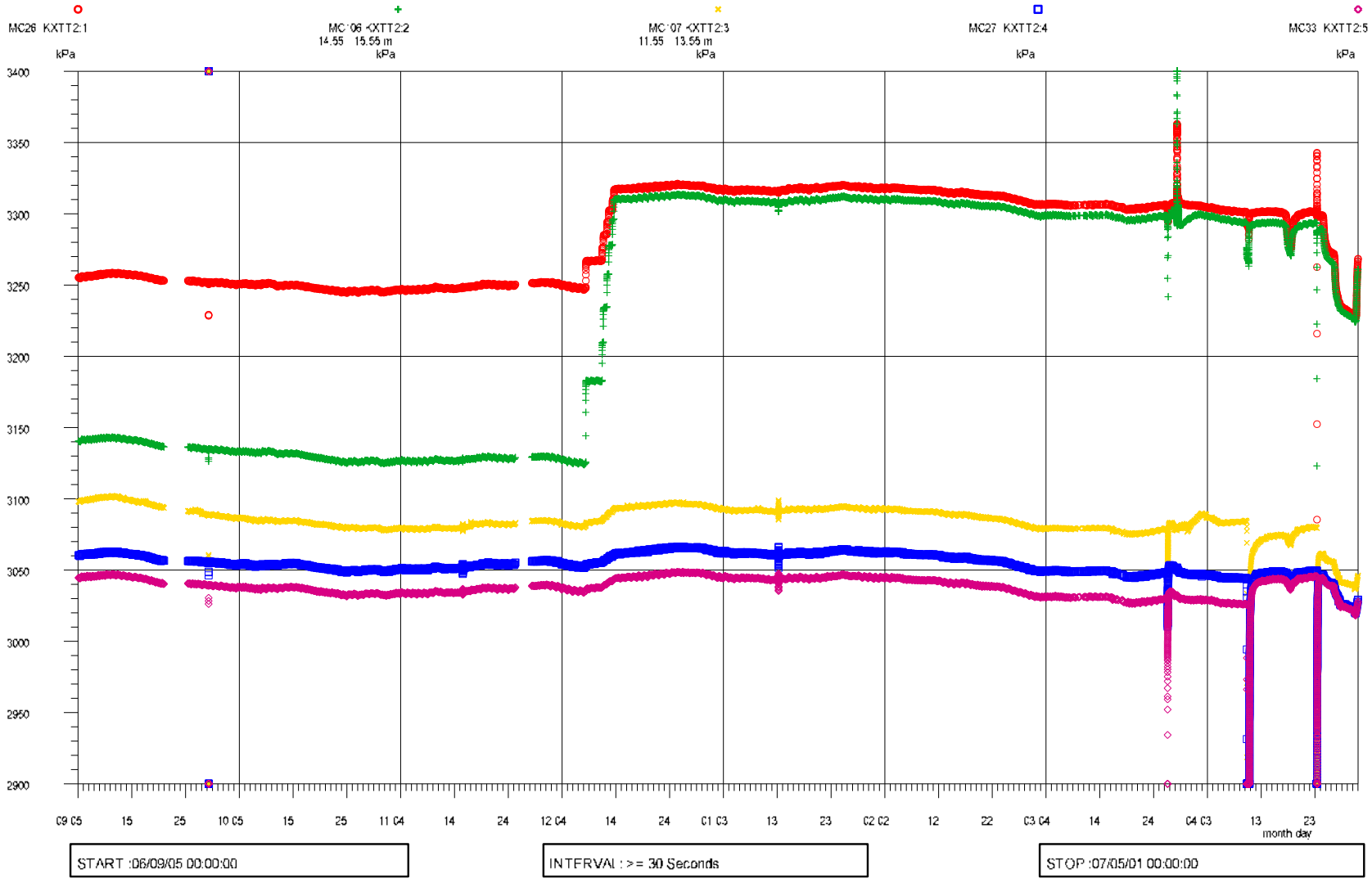

Figure A9-12. *Pressure in KXTT2.*

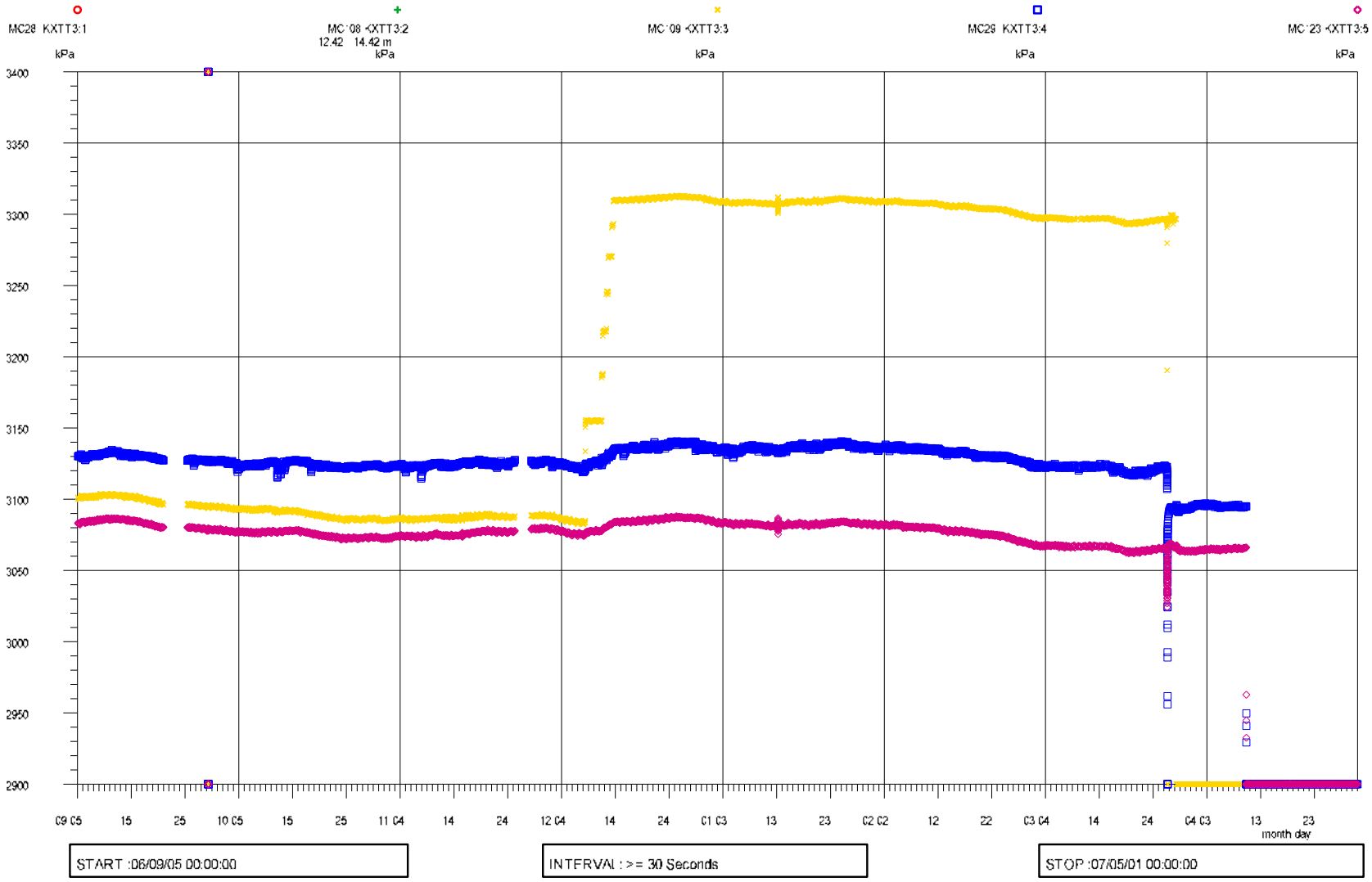

Figure A9-13. *Pressure in KXTT3.*

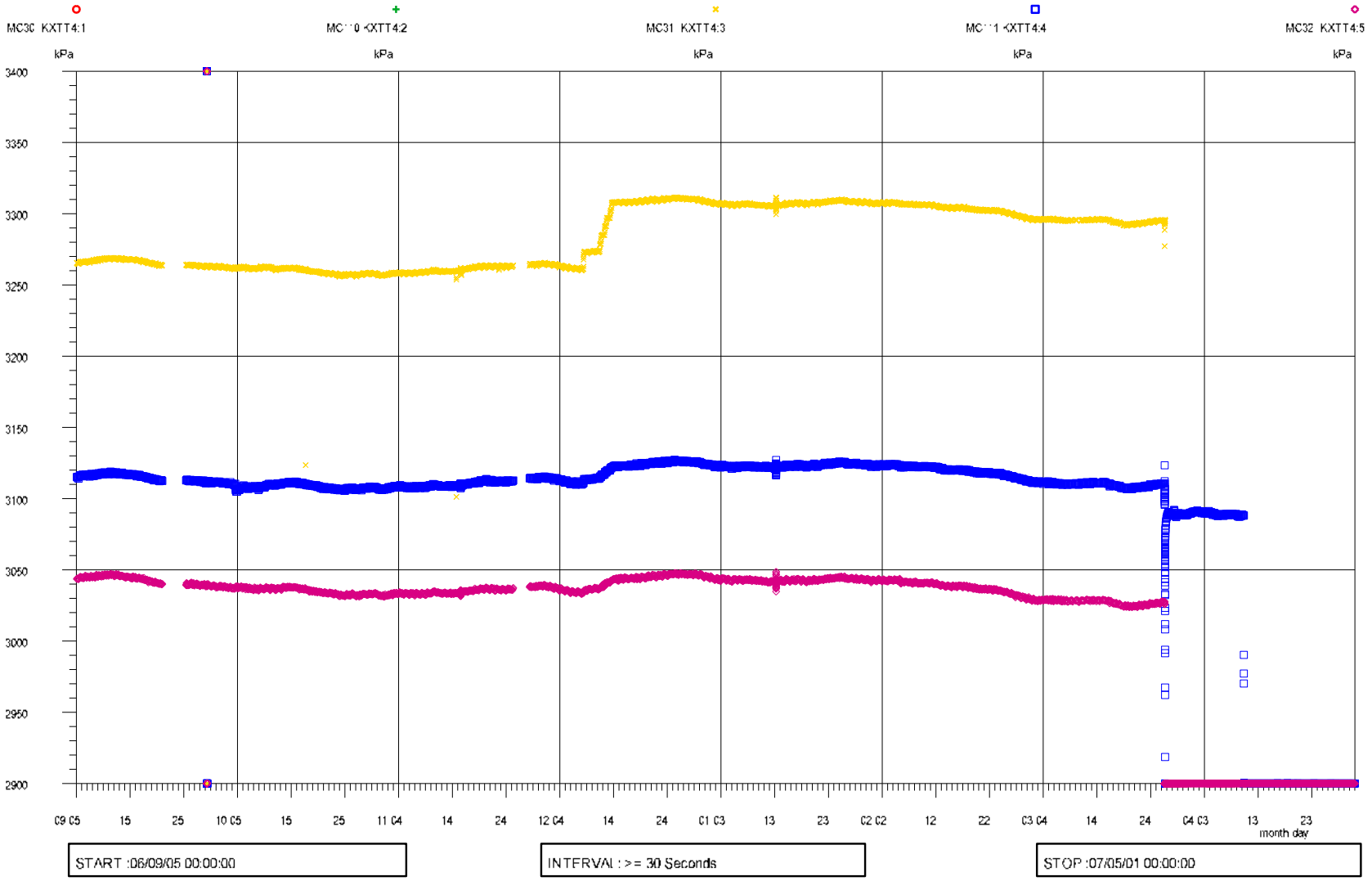

Figure A9-14. *Pressure in KXTT4.*

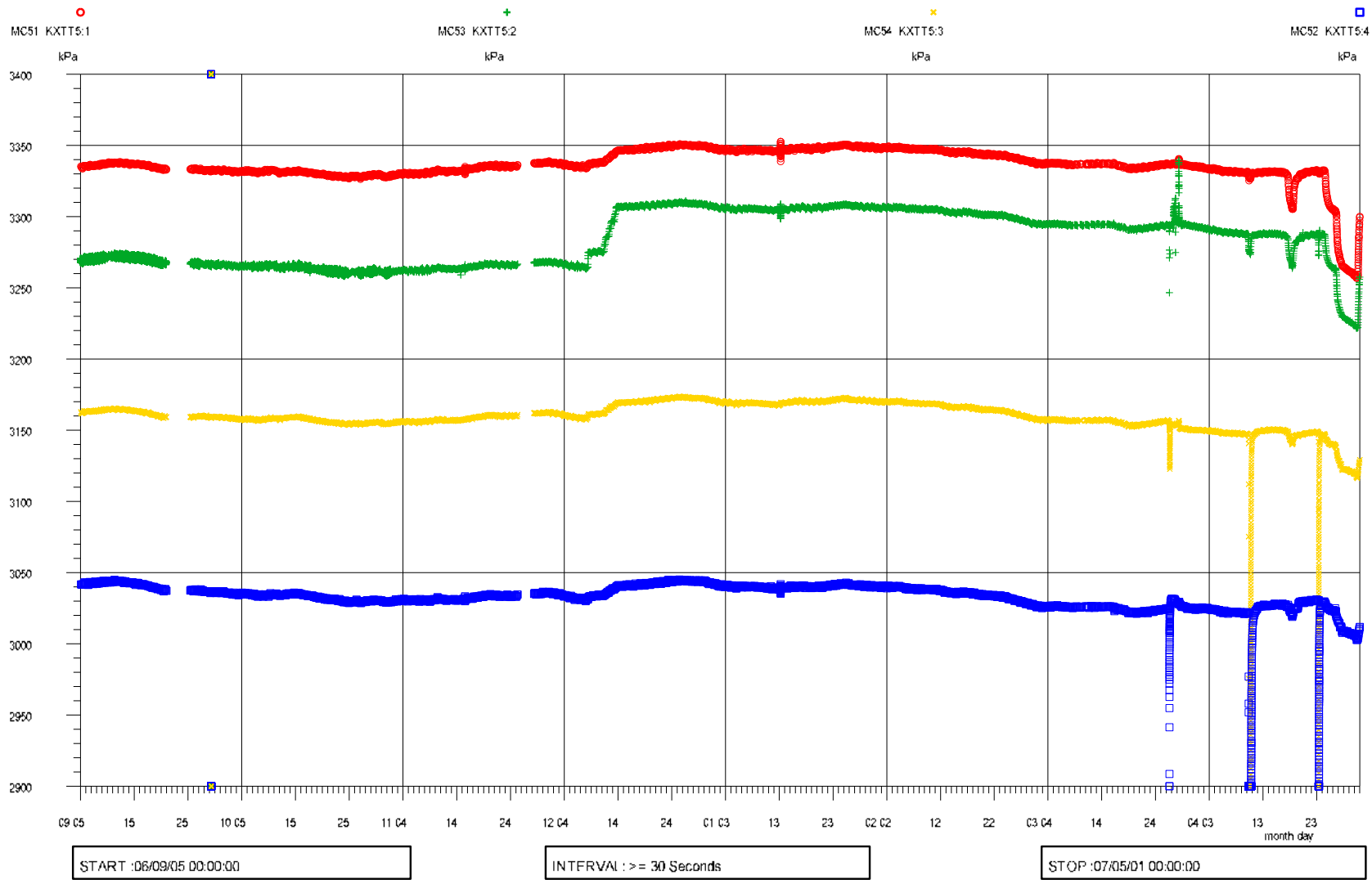

Figure A9-15. *Pressure in KXTT5.*

Appendix 10

One-dimensional diffusion model (slightly modified version of SKB PIR-04-16)

The general one dimensional diffusion equation is expressed by;

$$\frac{\partial C}{\partial t} = D\frac{\partial^2 C}{\partial x^2} \tag{1}$$

In the present situation the interaction can be regarded as diffusion from a stirred solution of limited volume into a plane sheet. In order to benefit from the analytical solution of this case given by /Crank 1975/, a case, where diffusion from both sides of the sheet occurs will be considered. The sheet occupies the space $-l \le x \le l$, while the solution is of limited extent and occupies the spaces $-l-a \le x \le -l$ and $l \le x \le l+a$. The occupation length of the water phase (a) is set to:

$$a = V / A + K_a \tag{2}$$

where V corresponds to the total volume used in the borehole experiment (i.e. both the volume in the borehole section and the volume of the circulation equipment) and A is the sum of the stub surface area and borehole wall area.

The length of the sheet (l) has no influence of the rate of the loss of tracer in the water phase as long as the contribution of tracer diffusing from one side to the other can be neglected. The length can therefore be set arbitrarily and in this particular case l has been set in order to obtain a tracer concentration in the middle of the sheet (x=0) that is at least 10^8 times lower than the tracer concentration in surface layer of the sheet (i.e. $x = l$ or $x = -l$).

The concentration of the solute in the solution is always uniform and is initially C_0, while the sheet initially is free from solute. The following boundary conditions therefore apply:

$$C = 0, \qquad a\frac{\partial C}{\partial t} = \pm D\frac{\partial C}{\partial x} \qquad -\mathrm{l} \le x \le \mathrm{l}, \qquad t = 0 \tag{3}$$

and

$$a\frac{\partial C}{\partial t} = \pm D\frac{\partial C}{\partial x}, \qquad x = \pm\mathrm{l}, \qquad t > 0 \tag{4}$$

The analytical solution to this problem has been given by /Crank 1975/. The total concentration within the sheet, C_x, (including both the pore water concentration and the mass sorbed on the rock) at the distance x at a given diffusion time of t is given by the expression:

$$C_x = C_\infty \left\{ 1 + \sum_{j=1}^{\infty} \frac{2(1+\alpha_r)\exp\left(-\frac{D_a q_j^2 t}{l^2}\right)}{1+\alpha_r+\alpha_r^{\,2} q_j^2} \frac{\cos\left(\frac{q_j x}{l}\right)}{\cos q_j} \right\} \tag{5}$$

where C_∞ is the concentration in the sheet after infinite time and the q_j values are the non-zero positive roots of:

$$\tan q_j = -\alpha_r q_j \tag{6}$$

and α_r is the ratio of the capacities of the rock and water phase, defined as;

$$\alpha_r = \frac{a}{l(\varepsilon + K_d \rho)} \tag{7}$$

Furthermore, the decrease of the concentration of tracer in the start cell, C_1, can be calculated according to:

$$C_1 = C_{1(0)} - \frac{C_\infty m}{V_1 \rho}\left\{1 - \sum_{j=1}^{\infty} \frac{2\alpha_r (1+\alpha_r)\exp\left(\frac{-D_a q_j^2 t}{l^2}\right)}{1+\alpha_r+\alpha_r{}^2 q_j^2}\right\} \quad (8)$$

where $C_{1(0)}$ corresponds to the initial concentration in the start cell.

By applying mass balance, C_∞ can be calculated according to:

$$C_\infty = \frac{C_0 a}{l + a/(\varepsilon + K_d \rho)} \quad (9)$$

However, for the present *in situ* experiment, the concentration profile within the rock will not be possible to measure. Instead, the decrease of the concentration in the water phase (caused by diffusion and/or sorption in the rock) will be the only available experimental parameter that can be measured. The analytical solution for calculating the total amount of tracer in the sheet (M_t) after a given experimental time (t) is expressed as:

$$\frac{M_t}{M_\infty} = 1 - \left\{\sum_{j=1}^{\infty} \frac{2\alpha_r (1+\alpha_r)}{1+\alpha_r+\alpha_r{}^2 q_j^2}\exp\left(\frac{-D_a q_j^2 t}{l^2}\right)\right\} \quad (10)$$

where M_∞ corresponds to the total amount of tracer in the sheet after infinite experimental time. Applying mass balance, M_∞ can be expressed as:

$$M_\infty = \frac{2aC_0}{1+\alpha_r} \quad (11)$$

where C_0 is the initial concentration of tracer in the water phase. Furthermore, M_t can be expressed as:

$$M_t = (M_0 - M_{aq(t)}) = a(C_0 - C_{aq(t)}) \quad (12)$$

where M_0 is the initial amount of tracer added to the system, $M_{aq(t)}$ is the amount of tracer in the water phase after an experimental time of t and $C_{aq(t)}$ is the corresponding concentration of tracer in the water phase.

By inserting (11) and (12) into (10) and by rearranging, the following expression is obtained:

$$\frac{C_{aq(t)}}{C_0} = 1 - \left\{\frac{1}{1+\alpha_r} - \sum_{j=1}^{\infty} \frac{2\alpha_r}{1+\alpha_r+\alpha_r{}^2 q_j^2}\exp\left(\frac{-D_a q_j^2 t}{l^2}\right)\right\} \quad (13)$$

References

Crank J, 1975. The mathematics of diffusion, 2nd edition, Oxford Univ. press, London.

Appendix 11

Estimation results

Table A11-1. Estimated K_d (m^3/kg) and K_a (m) results. K_d_max, K_d_min, K_a_max and K_a_min are values obtained when the uncertainty ranges in the corresponding parameter estimation has been taken into consideration.

Nuclide	Matrix diffusion-sorption only ($K_a = 0$) ε = 3.0E–3, F_f = 9.9E–5			Surface sorption only ($K_d = 0$, $F_f = 0$) ε = 3.0E–3, F_f = 0			Matrix diffusion-sorption and surface sorption ε = 3.0E–3, F_f = 9.9E–5					
	K_d[1] (m^3/kg)	K_d_max	K_d_min	K_a[2] (m)	K_a_max	K_a_min	K_d[3] (m^3/kg)	K_d_max	K_d_min	K_a[3] (m)	K_a_max	K_a_min
Ag-110m	1.13E+4[5]			5.05E+0[5]								
Ba-133	3.16E-2	4.19E–2	2.35E–2	8.41E–3	9.96E–3	7.03E–3	1.25E–2	1.66E–2	9.12E–3	3.41E–3	4.22E–3	2.65E–3
Cd-109	1.73E+0	2.41E+0	1.28E+0	6.59E–2	8.07E–2	5.49E–2	8.68E–1	9.92E–1	7.60E–1	2.07E–2	2.38E–2	1.78E–2
Cl-36	1.76E-5[4]			3.52E–4[4]								
Co-57	3.76E+3[5]	7.50E+3	2.25E+3	2.53E+0[5]	3.20E+0	2.09E+0	7.25E+2[5]			2.12E+0[5]	2.78E+0	1.69E+0
Cs-137	1.25E-1	1.64E–1	9.64E–2	2.83E–2	3.33E–2	2.42E–2	5.50E–2	6.42E–2	4.70E–2	1.04E–2	1.19E–2	9.04E–3
Gd-153	1.61E+4[5]	3.62E+4	9.08E+3	4.60E+0[5]	5.23E+0	4.11E+0	6.62E+2[5]	1.55E+3	2.11E+2	3.62E+0[5]	4.17E+0	3.18E+0
Hf-175	2.13E+4[5]	4.90E+4	1.18E+4	2.25E+0[5]	2.93E+0	1.82E+0	1.08E+3[5]			1.71E+0[5]	2.32E+0	1.31E+0
Na-22	7.48E-5[4]			3.75E–4[4]								
Ni-63	5.08E-1	7.40E–1	3.55E–1	3.28E–2	3.89E–2	2.79E–2	1.76E–1	2.32E–1	1.32E–1	1.44E–2	1.72E–2	1.19E–2
Np-237	3.82E-2	5.03E–2	2.84E–2	7.10E–3	8.71E–3	5.67E–3	2.01E–2	2.73E–2	1.43E–2	2.16E–3	3.02E–3	1.35E–3
Pa-233	6.44E+2[5]			2.35E–1[5]			6.44E+2[5]			3.20E–9[5]		
Pd-102	2.57E+2[5]			5.25E–1[5]								
Ra-226	2.22E-1	3.61E–1	1.38E–1	2.28E–2	2.57E–2	2.03E–2	2.75E–2	4.30E–2	1.63E–2	1.53E–2	1.73E–2	1.35E–2
S-35	9.20E-3	1.56E–2	4.89E–3	4.93E–3	6.78E–3	3.32E–3	5.66E–3	1.08E–2	2.45E–3	2.70E–3[4]		
Se-75	8.14E-2	1.25E–1	5.24E–2	1.44E–2	1.61E–2	1.28E–2	1.07E–2	1.64E–2	6.45E–3	9.57E–3	1.08E–2	8.43E–3
Sn-113	3.30E+1[5]			3.72E–1[5]								
Sr-85	8.36E-3	1.17E–2	5.71E–3	3.98E–3	5.08E–3	2.97E–3	5.61E–3	8.32E–3	3.54E–3	8.04E–4	1.53E–3	1.16E–4
Tc-99	2.54E-4	5.48E–4	7.74E–5	1.02E–3	1.74E–3	3.51E–4	2.54E–4	5.49E–4	7.74E–5	4.48E–4[4]		
U-236	8.11E-3	1.18E–2	5.24E–3	3.17E–3	3.90E–3	2.49E–3	2.87E–3	4.82E–3	1.47E–3	1.39E–3	1.96E–3	8.60E–4
Zr-95	7.88E+1[5]			2.57E–2[5]								

[1] K_d fitted without considering surface sorption. [2] K_a calculated without considering matrix diffusion and sorption. [3] K_d and K_a fitted simultaneously in the calculation. [4] Only a maximum value could be calculated. [5] Probably overestimated due to sorption on the equipment.

The figures below show the fit to the experimental data (upper) and the corresponding calculated penetration depth (lower). The legend shows if only K_d (with K_a=0) or K_d+K_a were estimated. The y-axis represents the part of the added tracer present within the depth interval.

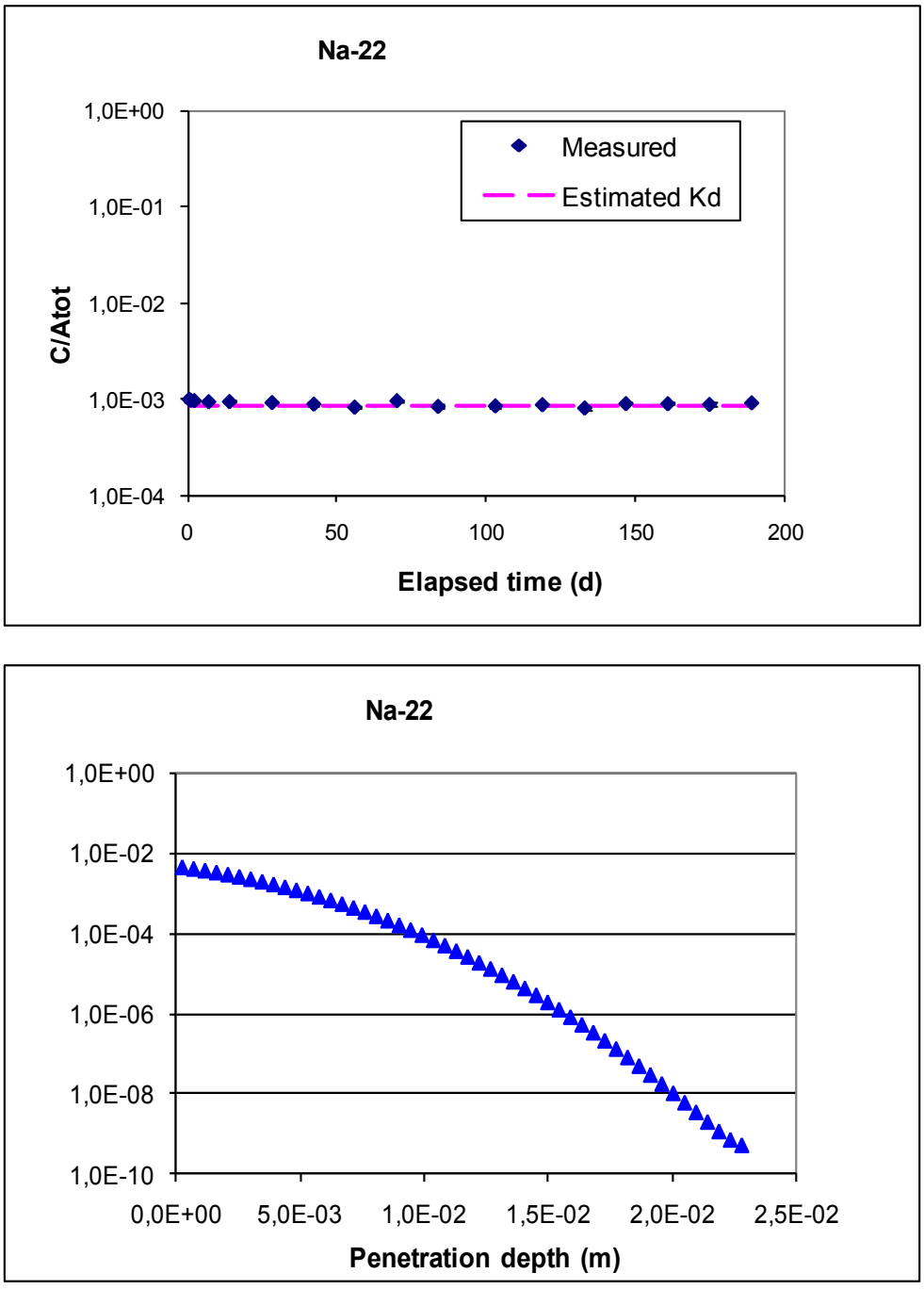

Figure A11-1. *^{22}Na estimations, sorption addressed by only using a K_d.*

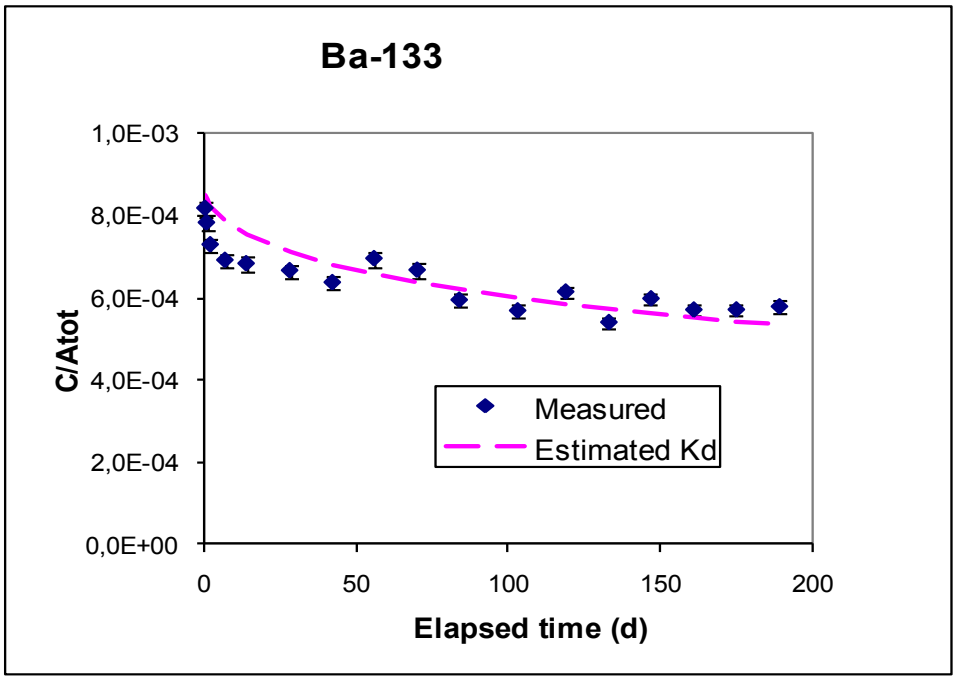

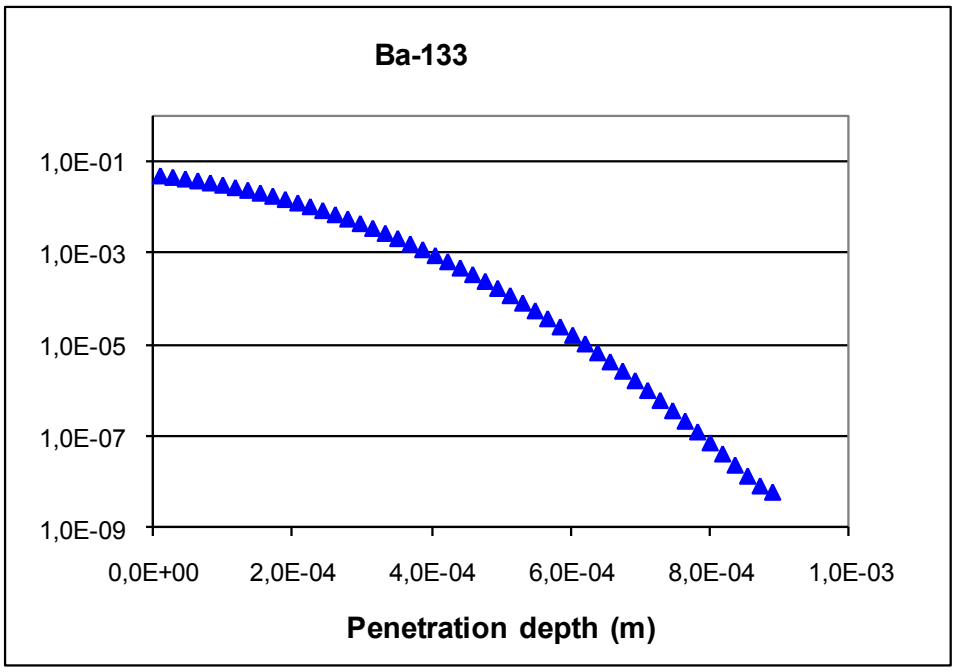

Figure A11-2. *^{133}Ba estimations, sorption addressed by only using a K_d.*

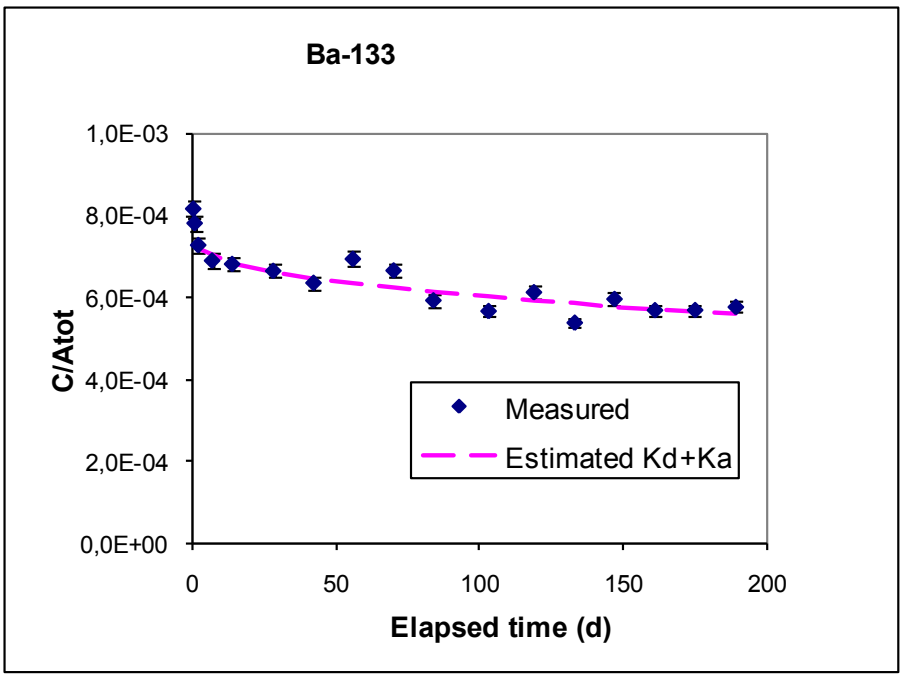

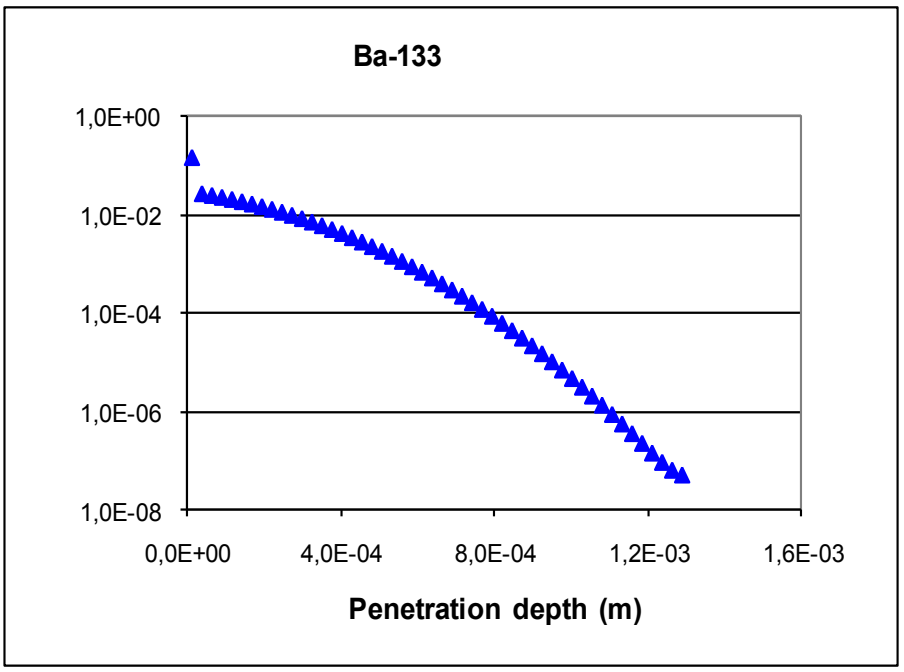

Figure A11-3. *^{133}Ba estimations, sorption addressed by only using both a K_d and a K_a.*

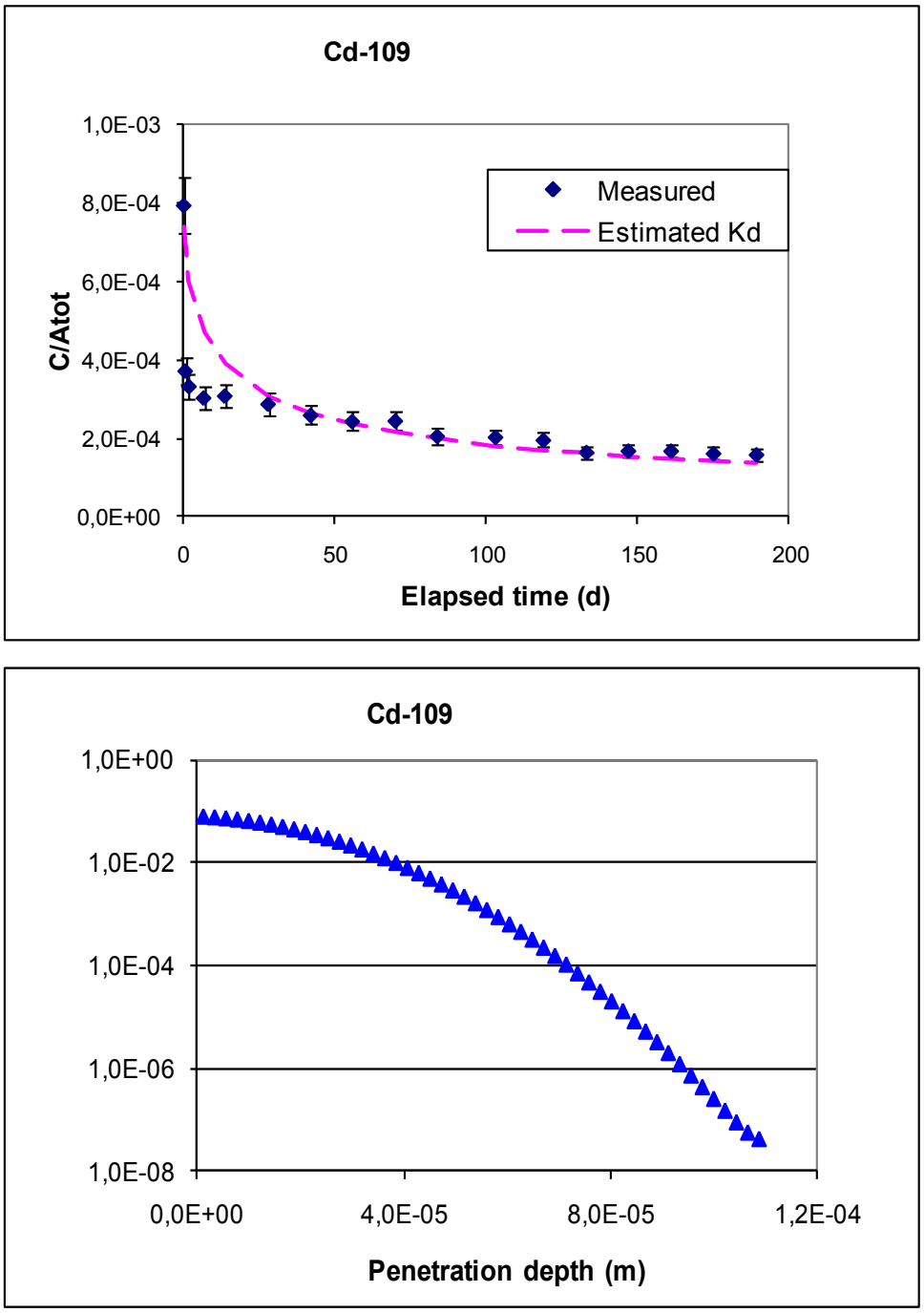

Figure A11-4. *^{109}Cd estimations, sorption addressed by only using a K_d.*

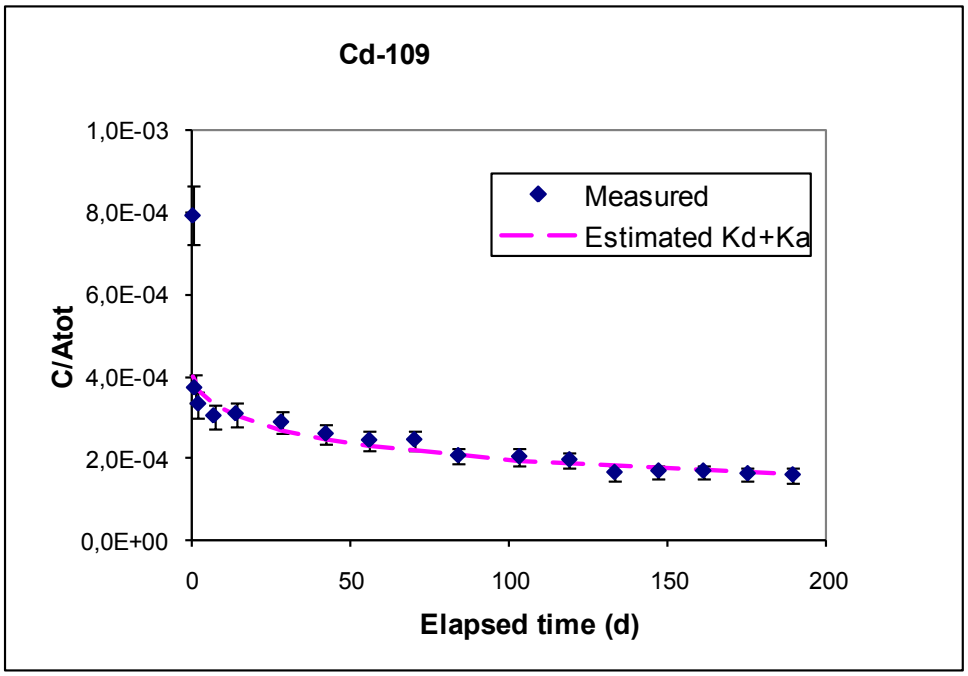

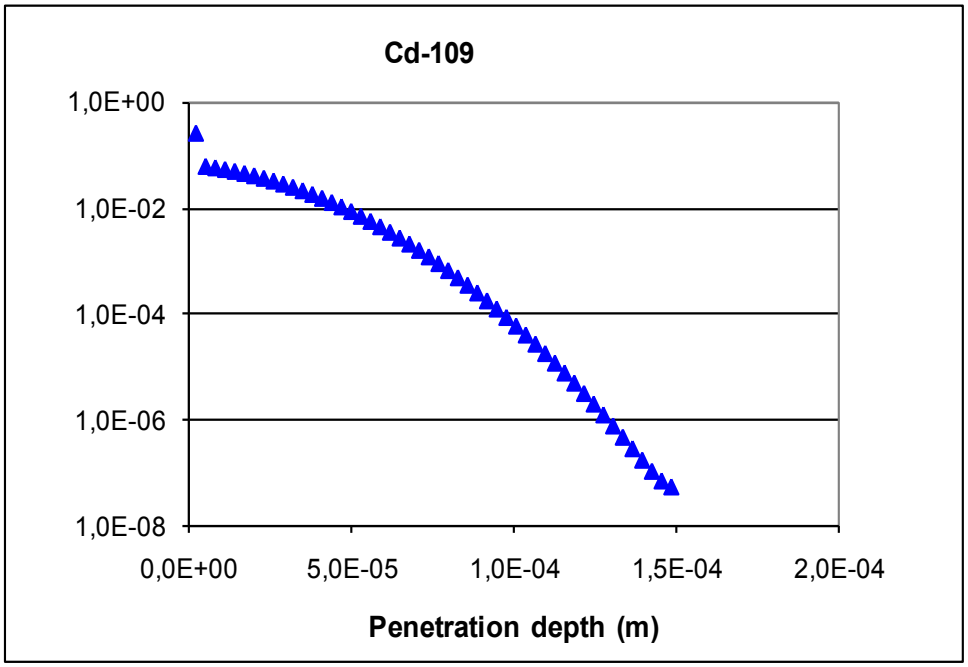

Figure A11-5. *^{109}Cd estimations, sorption addressed by only using both a K_d and a K_a.*

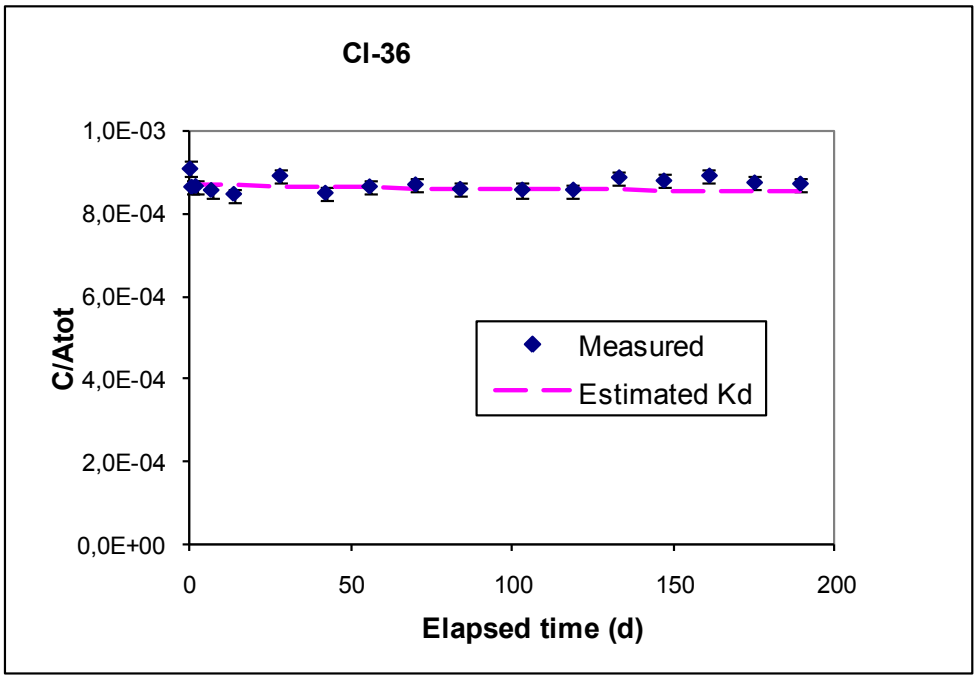

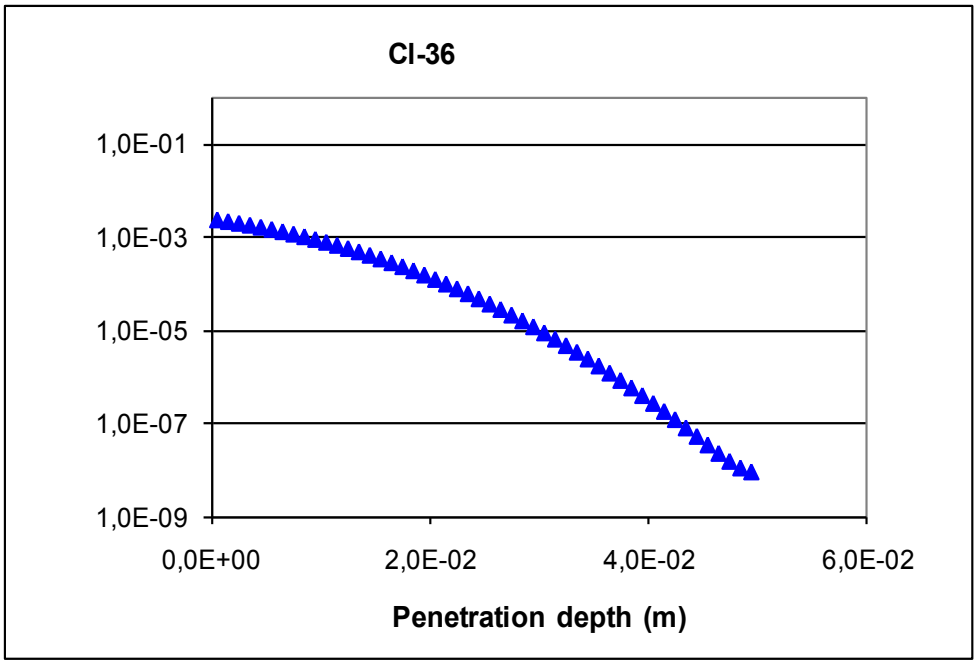

Figure A11-6. *^{36}Cl estimations, sorption addressed by only using a K_d.*

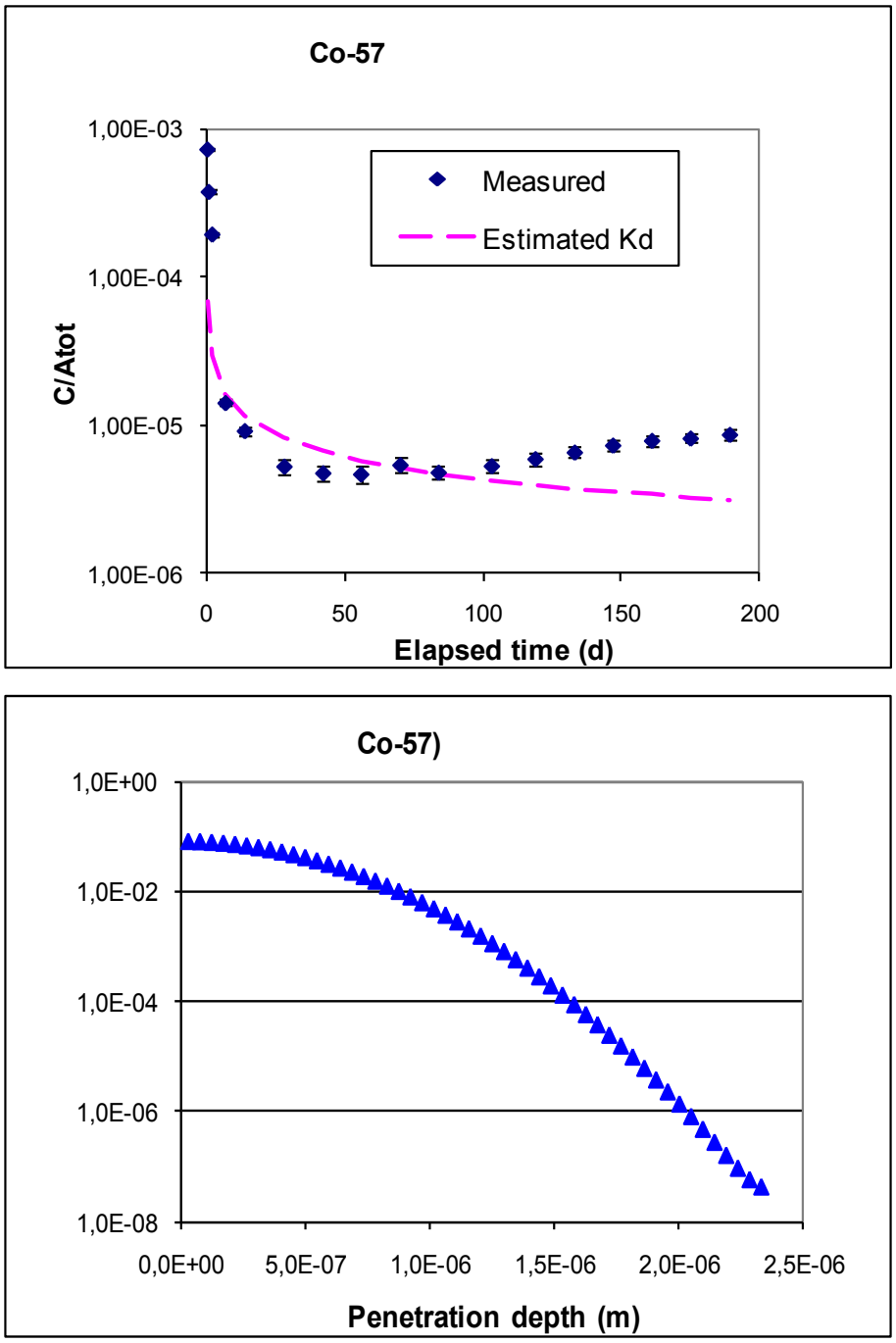

Figure A11-7. *^{57}Co estimations, sorption addressed by only using a K_d.*

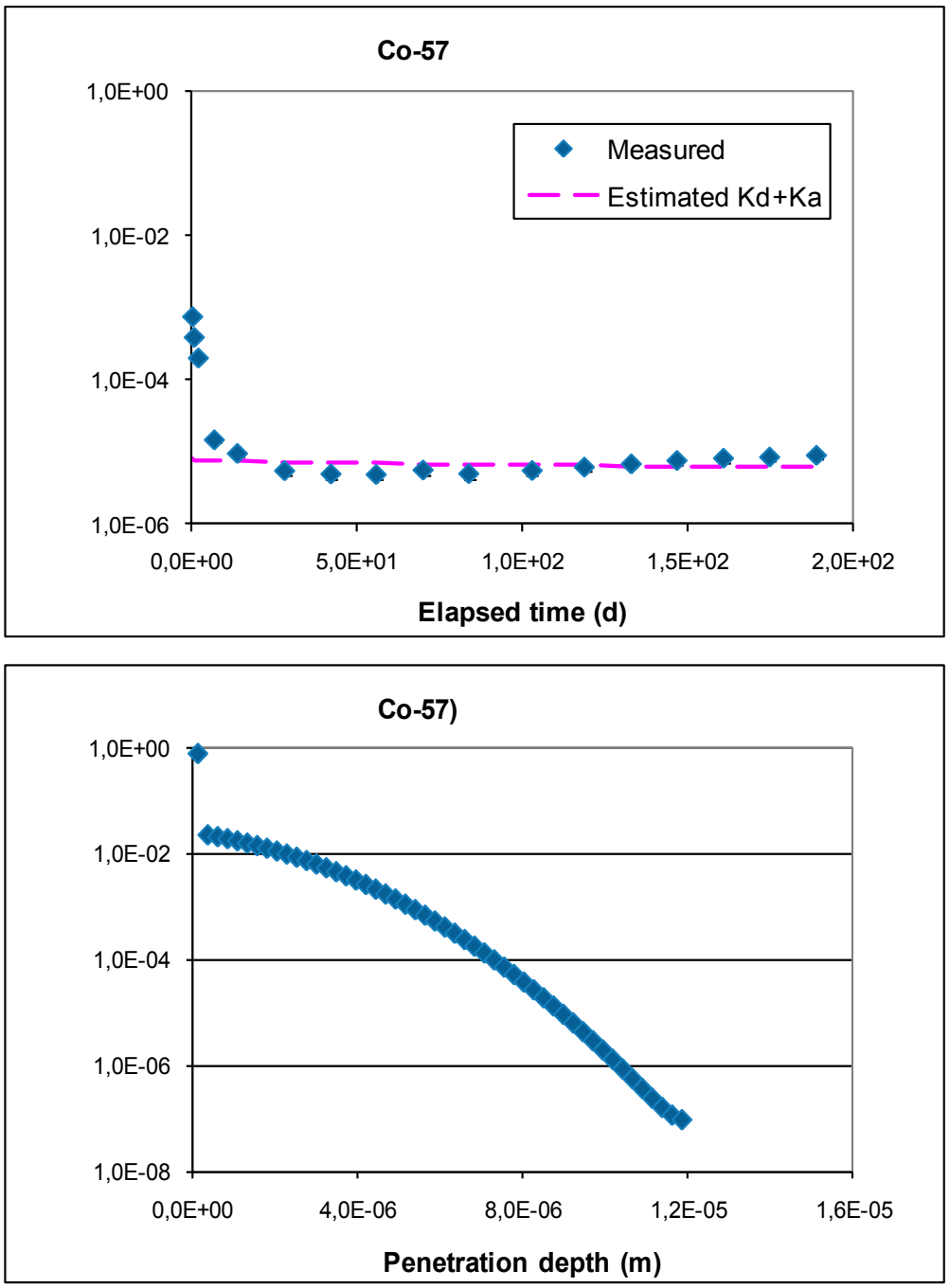

Figure A11-8. *^{57}Co estimations, sorption addressed by only using both a K_d and a K_a.*

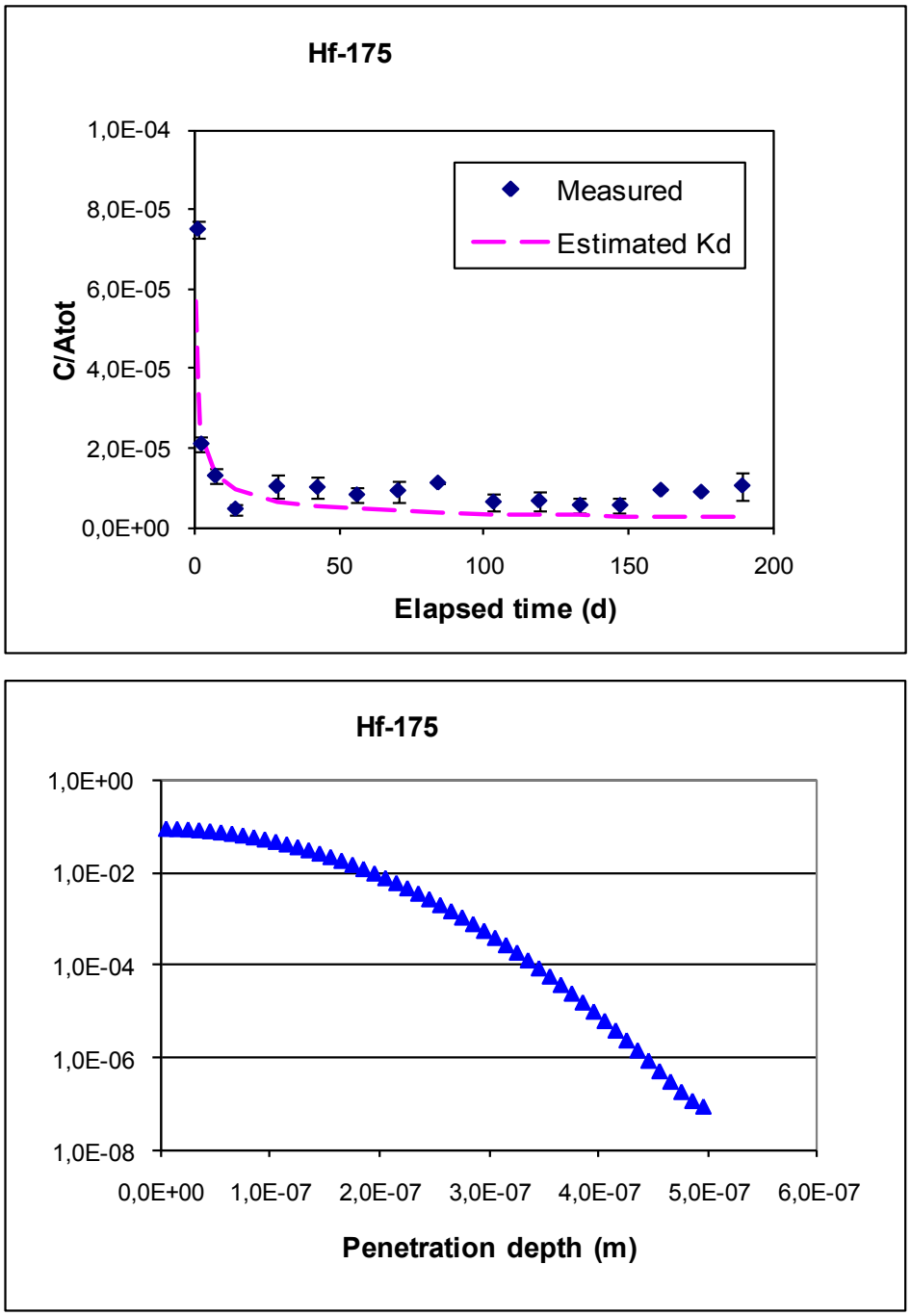

Figure A11-9. *^{175}Hf estimations, sorption addressed by only using a K_d.*

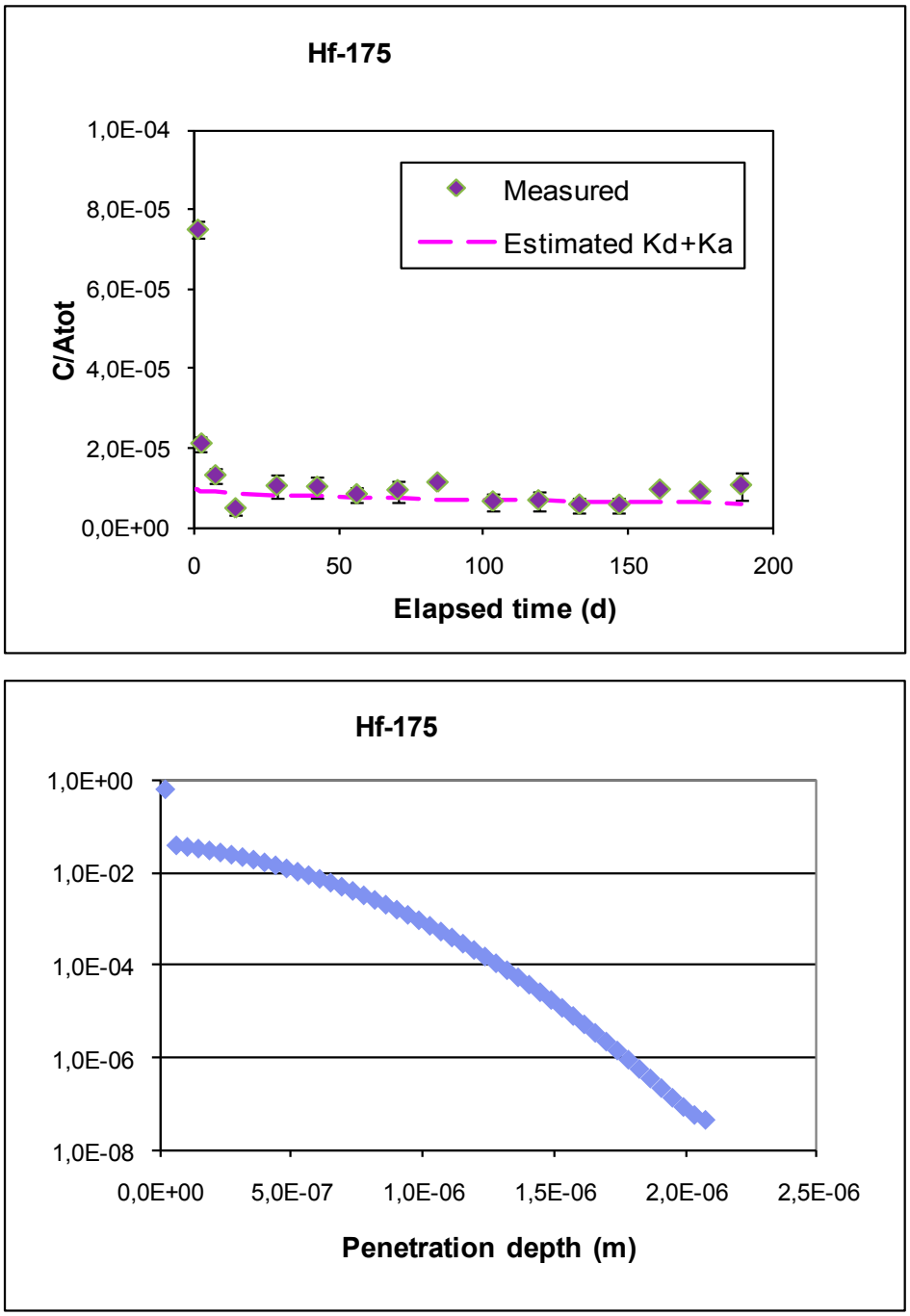

Figure A11-10. *^{175}Hf estimations, sorption addressed by only using both a K_d and a K_a.*

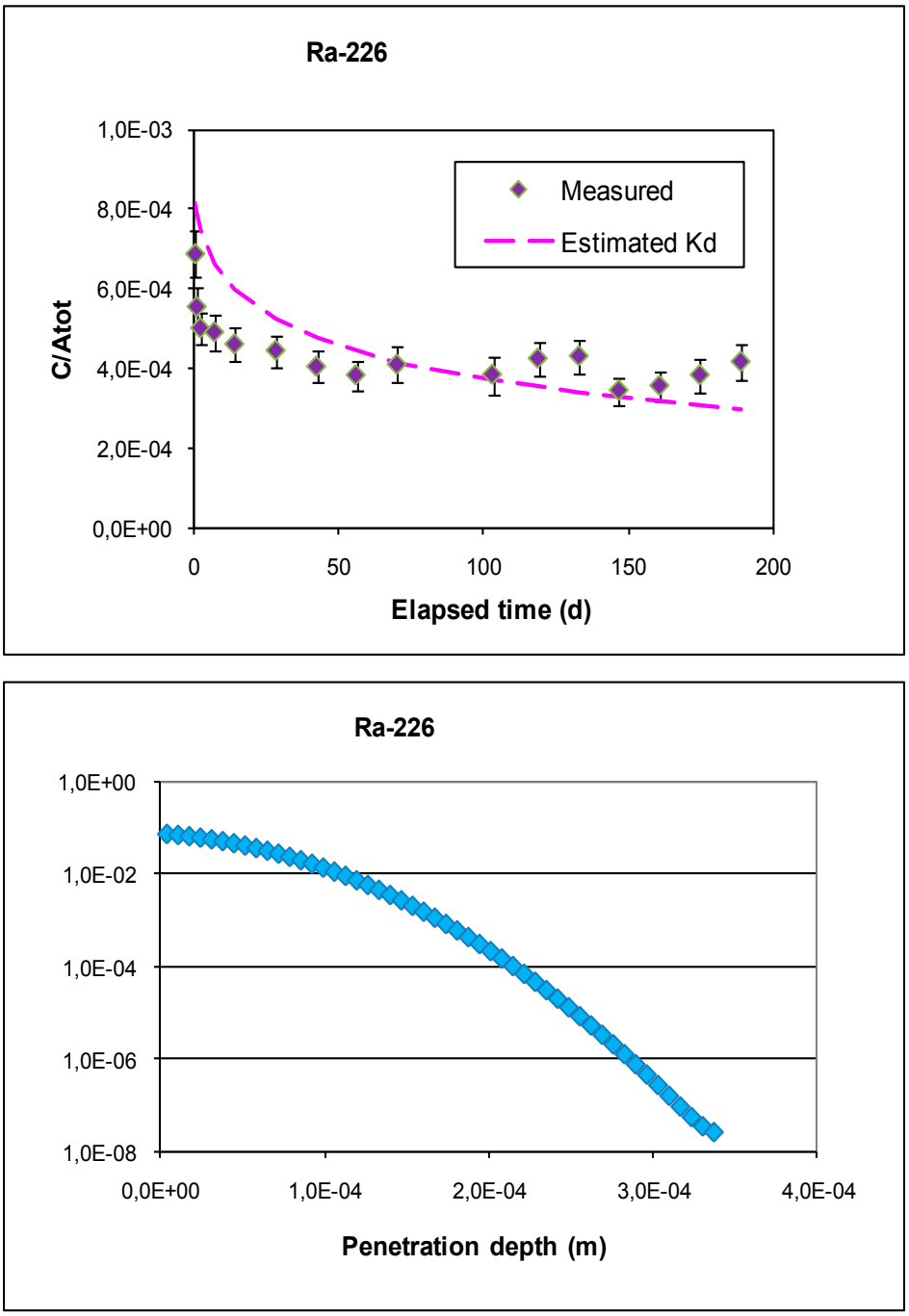

Figure A11-11. *^{226}Ra estimations, sorption addressed by only using a K_d.*

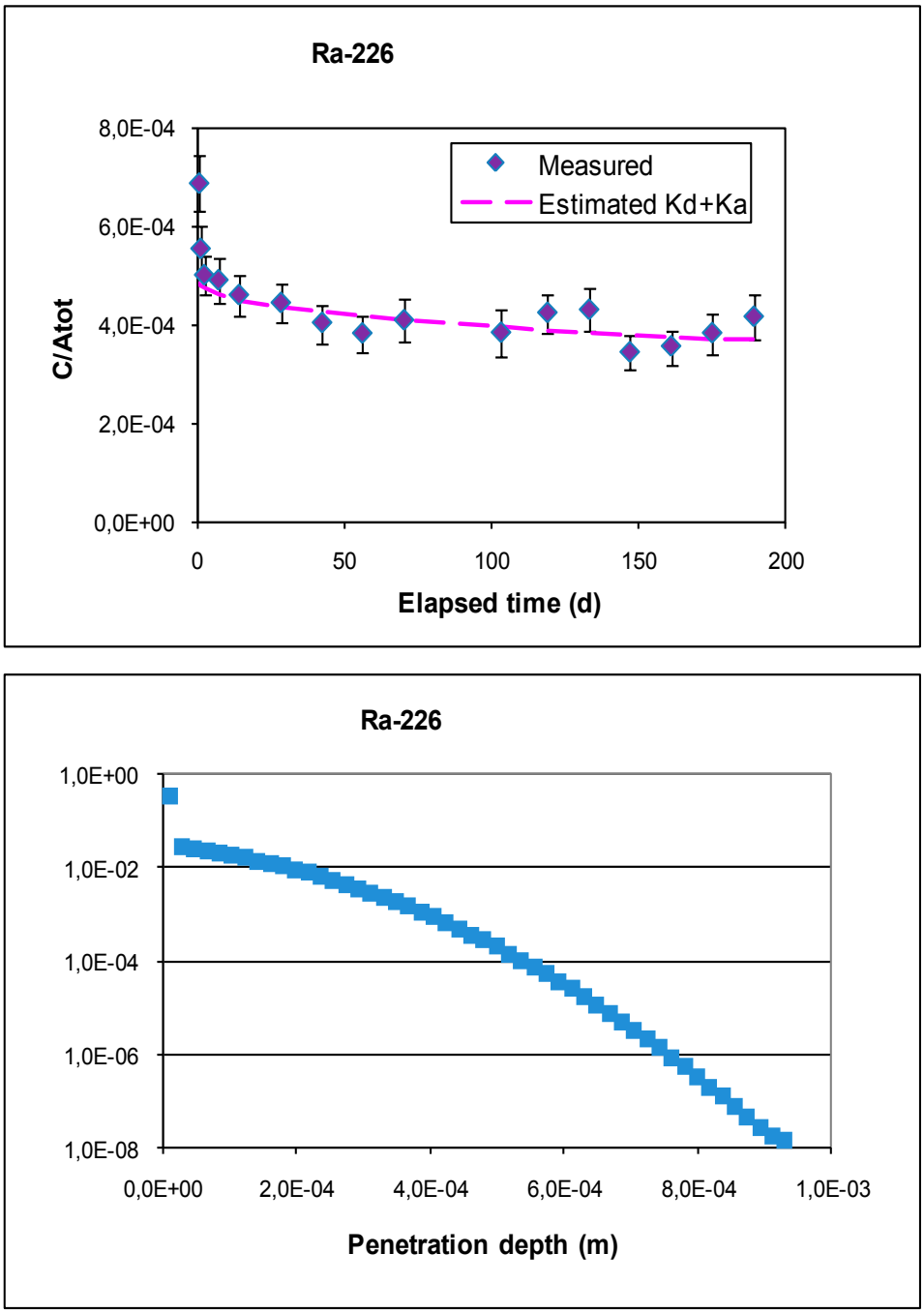

Figure A11-12. *^{226}Ra estimations, sorption addressed by only using both a K_d and a K_a.*

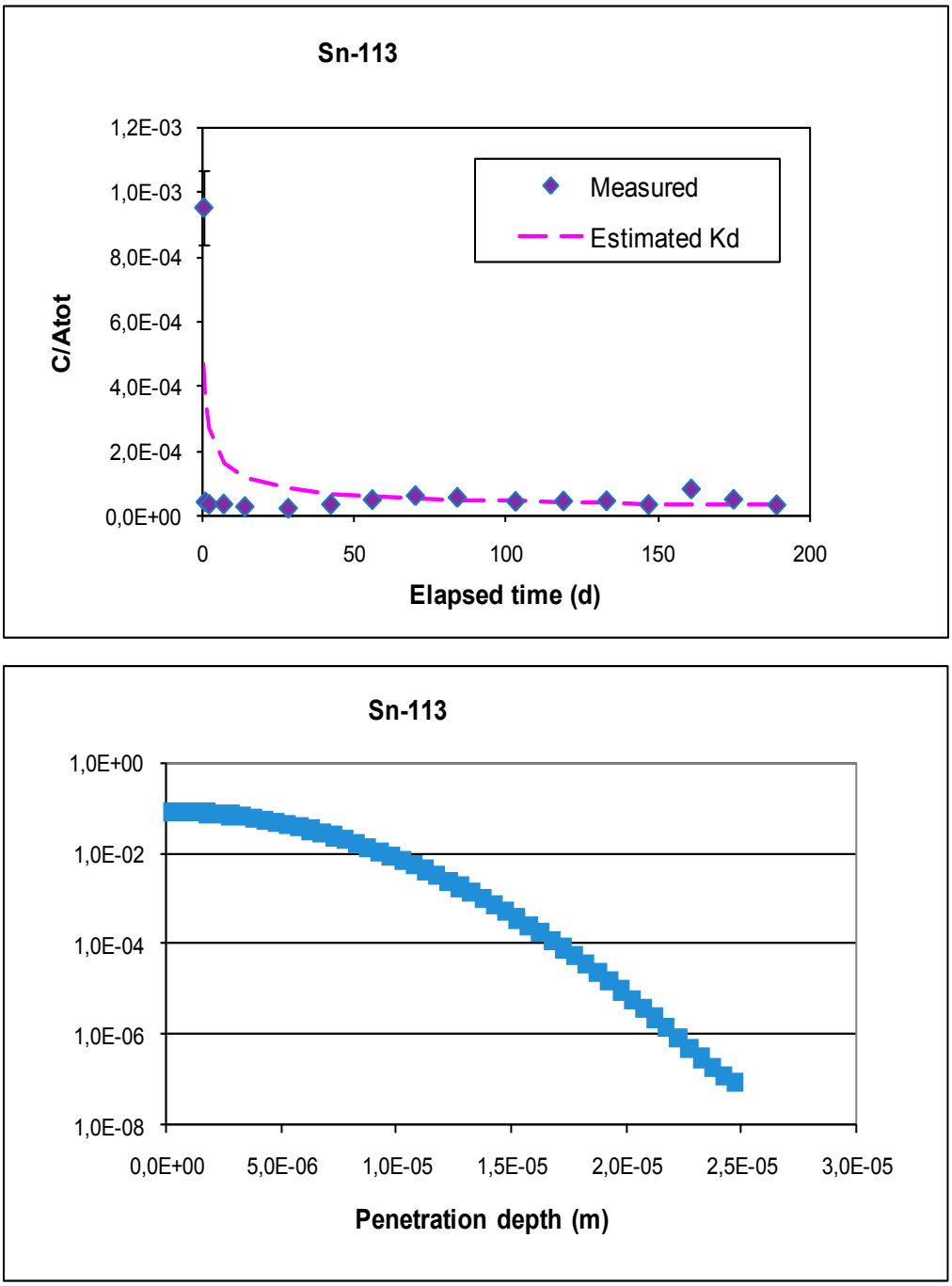

Figure A11-13. *^{113}Sn estimations, sorption addressed by only using a K_d.*

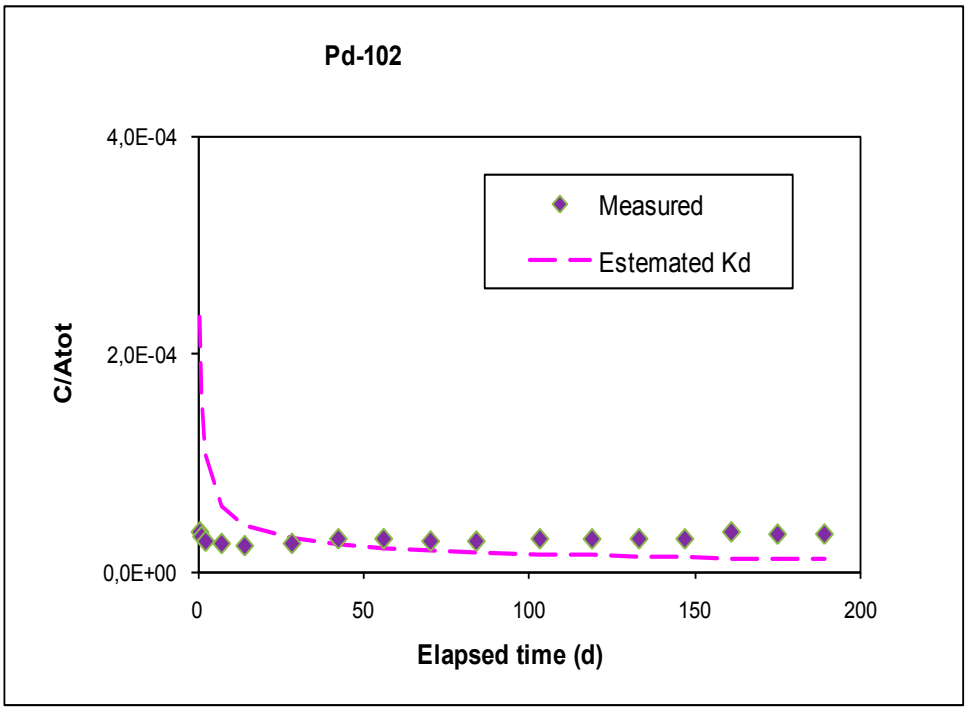

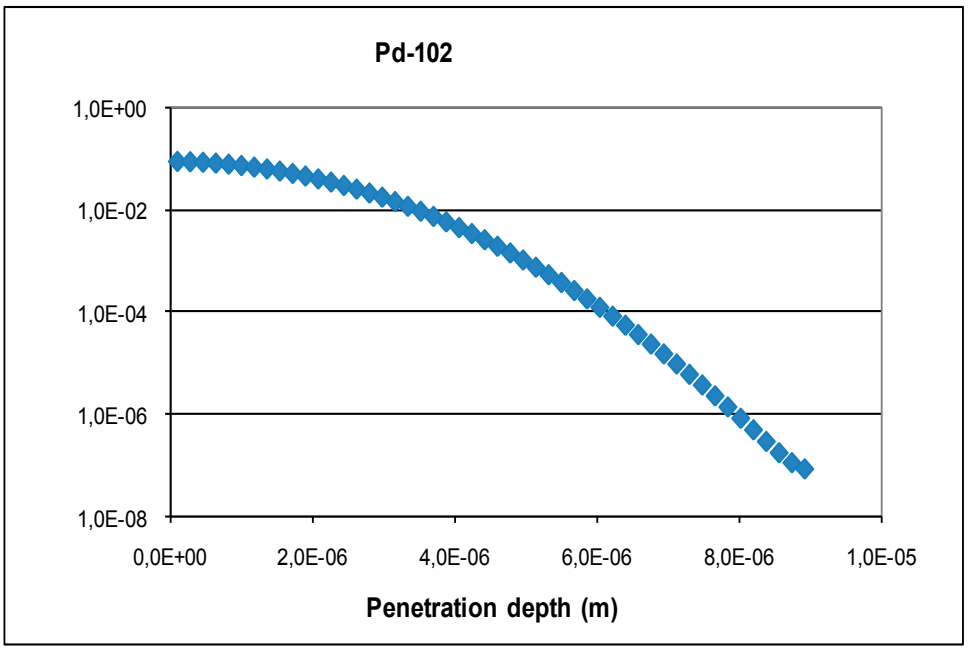

Figure A11-14. *^{102}Pd estimations, sorption addressed by only using a K_d.*

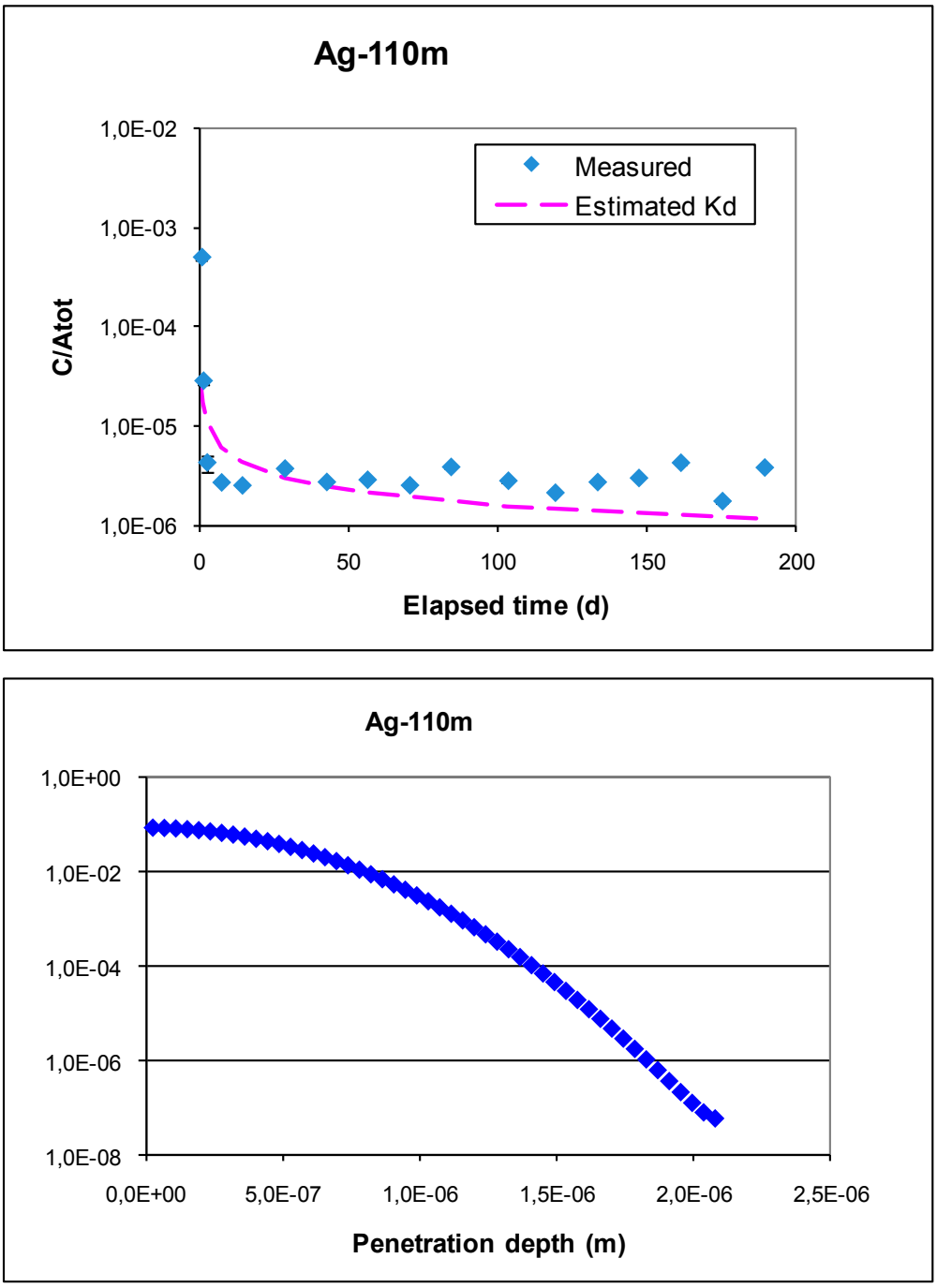

Figure A11-15. *^{110m}Ag estimations, sorption addressed by only using a K_d.*

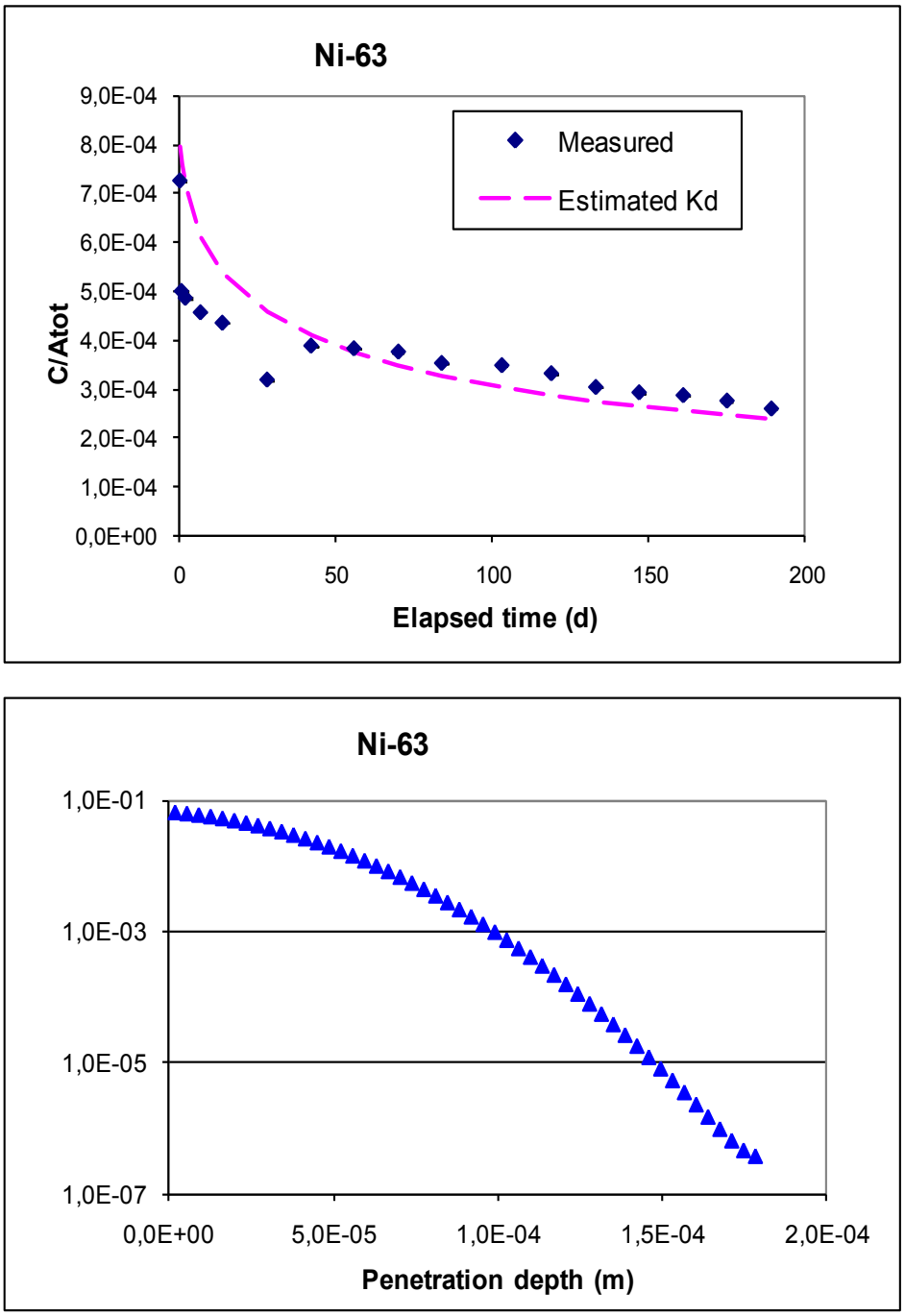

Figure A11-16. *^{63}Ni estimations, sorption addressed by only using a K_d.*

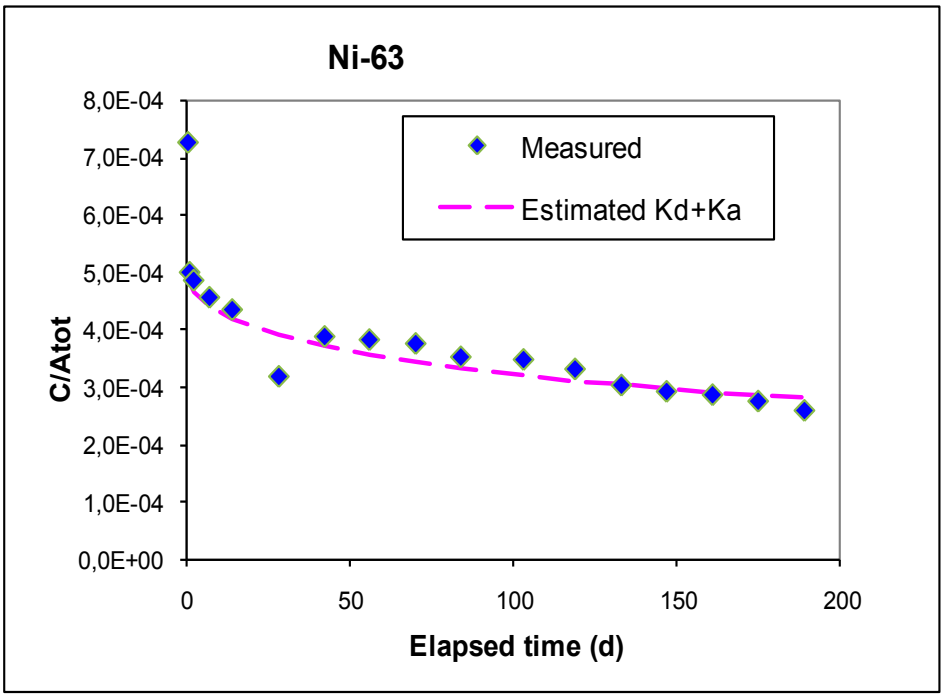

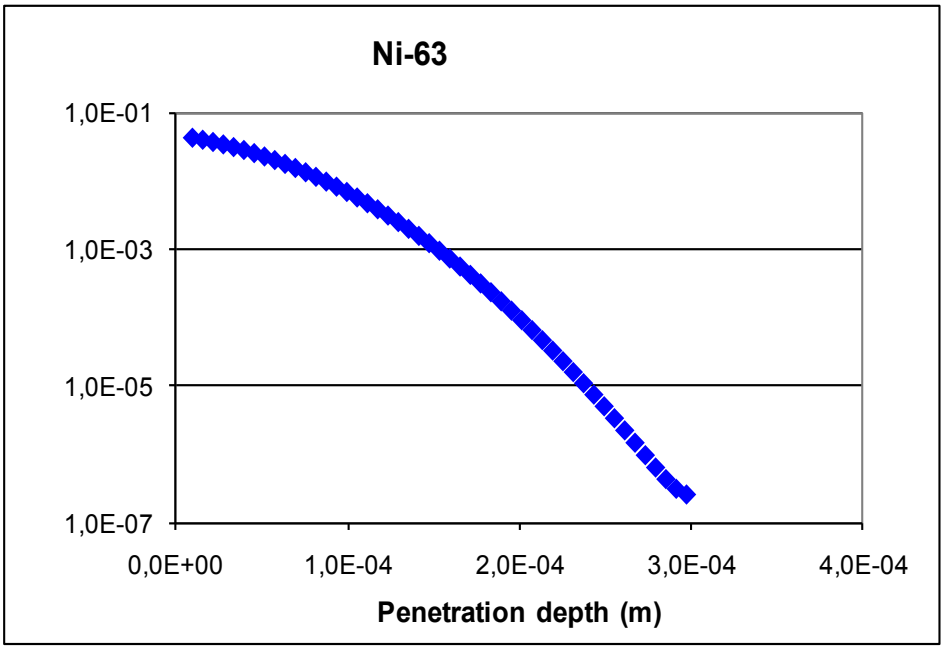

Figure A11-17. *^{63}Ni estimations, sorption addressed by only using both a K_d and a K_a.*

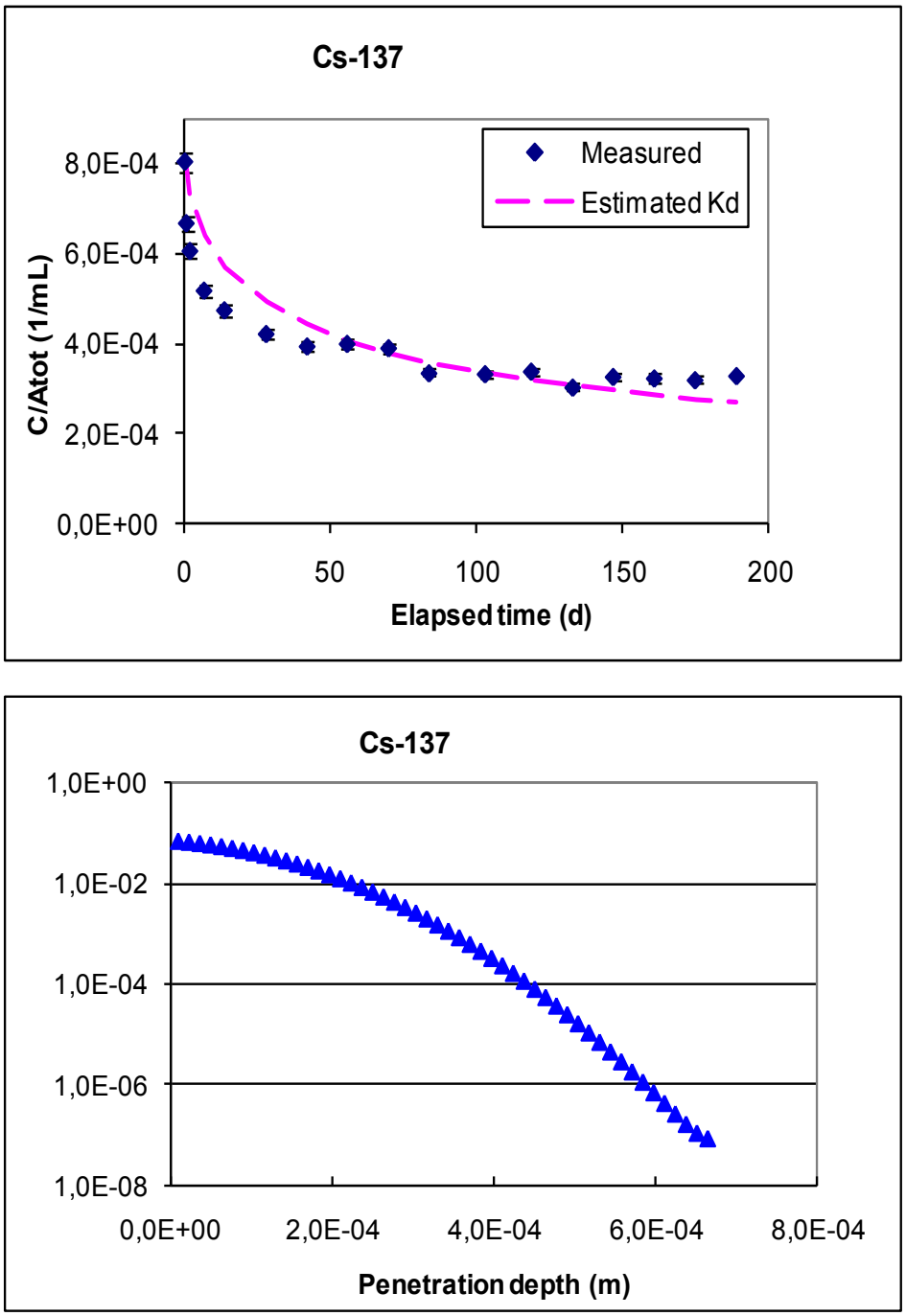

Figure A11-18. *^{137}Cs estimations, sorption addressed by only using a K_d.*

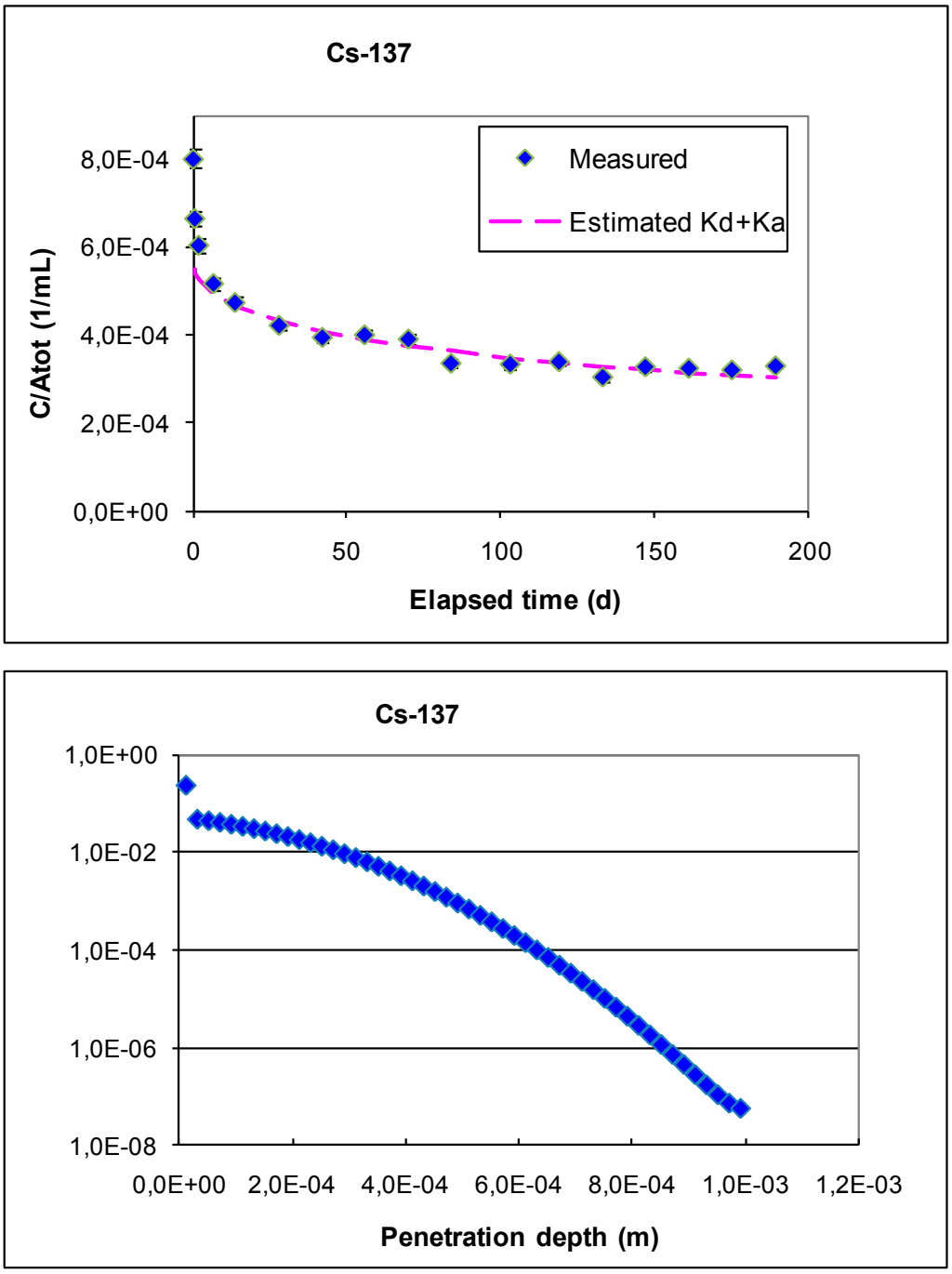

Figure A11-19. *^{137}Cs estimations, sorption addressed by only using both a K_d and a K_a.*

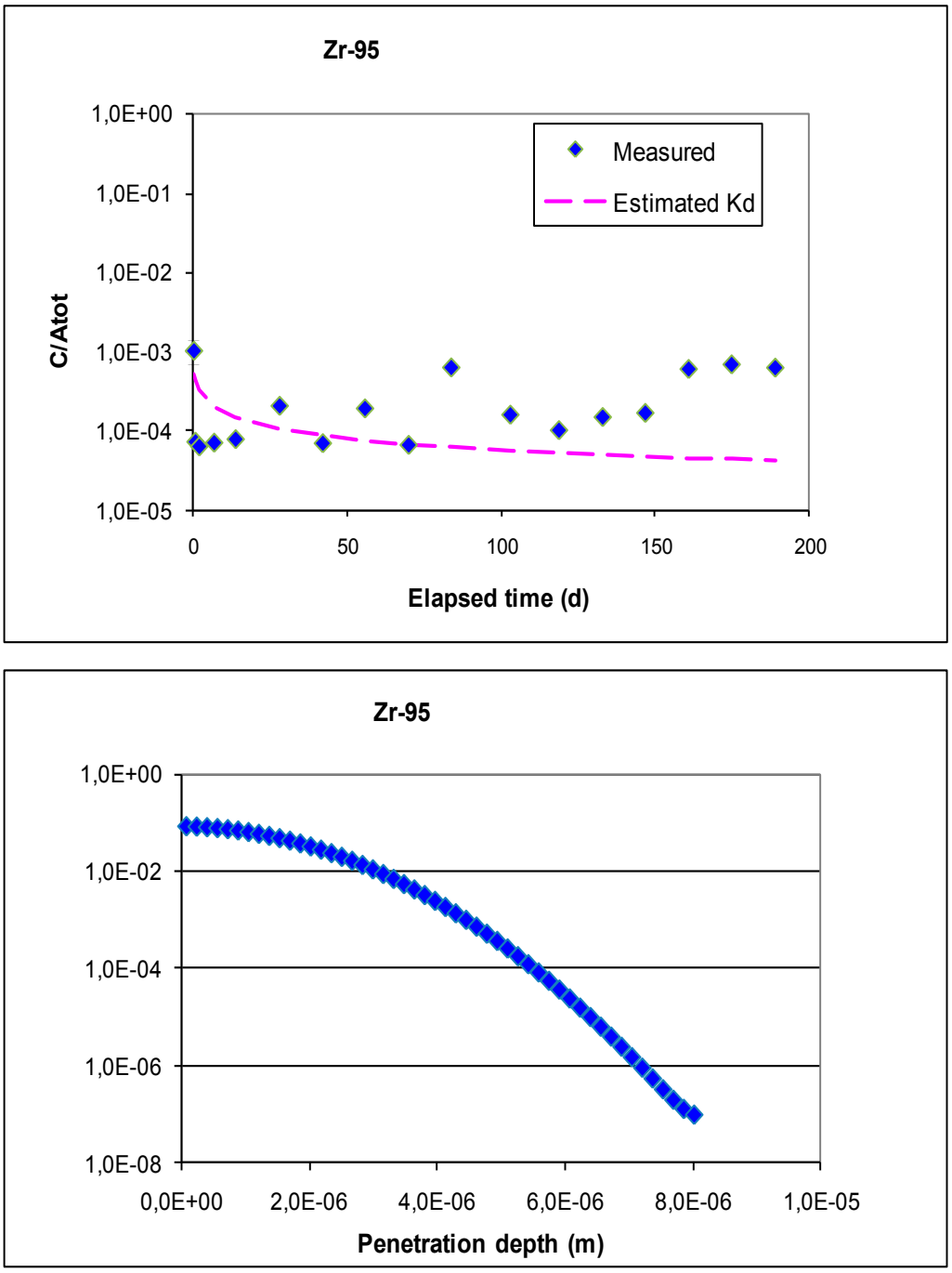

Figure A11-20. *^{95}Zr estimations, sorption addressed by only using a K_d.*

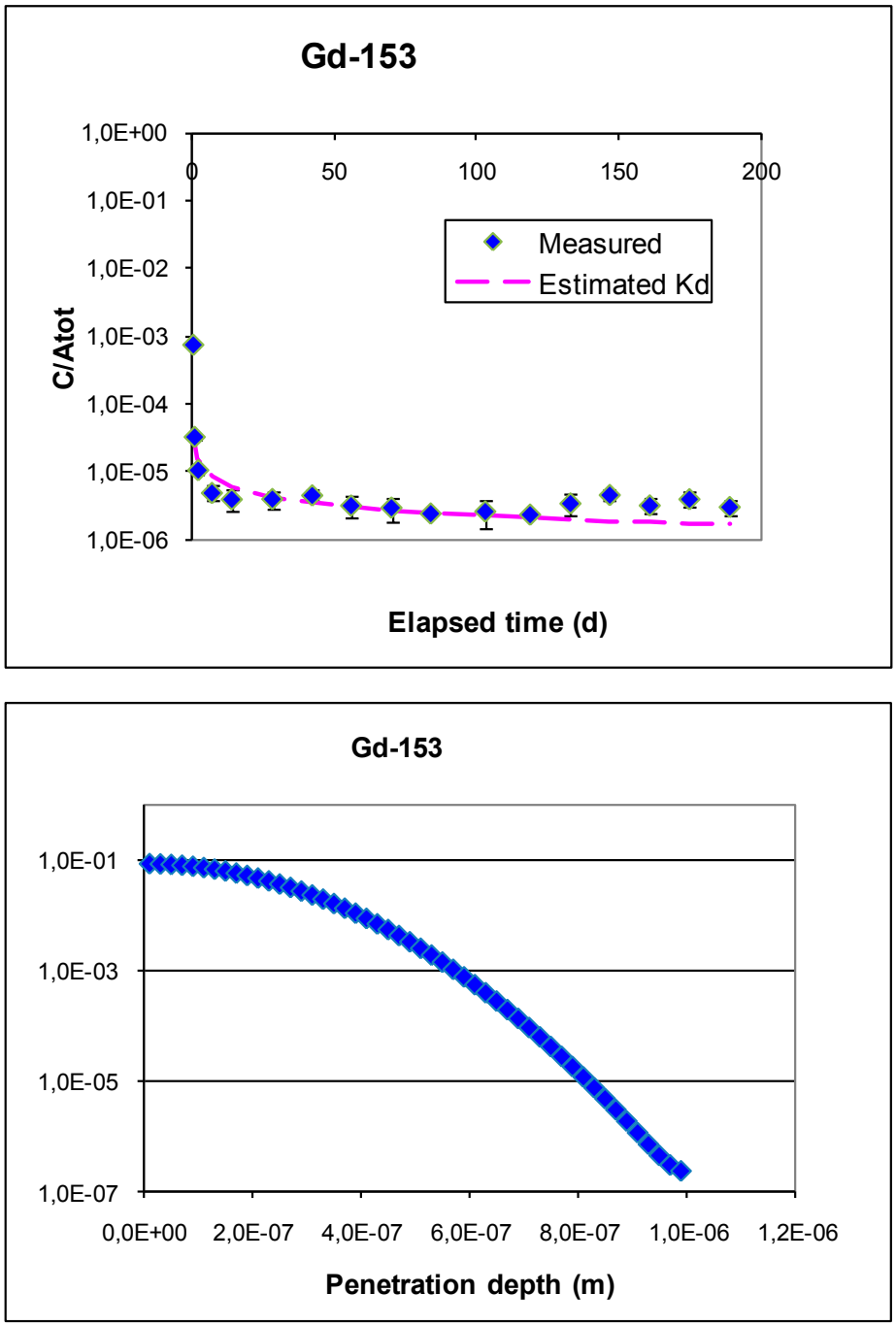

Figure A11-21. *^{153}Gd estimations, sorption addressed by only using a K_d.*

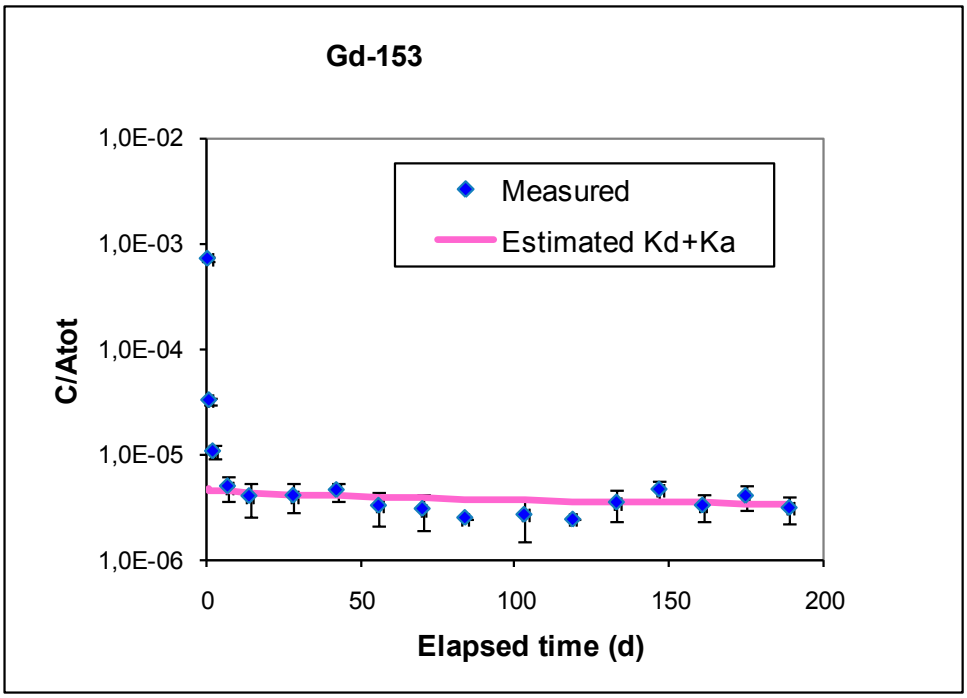

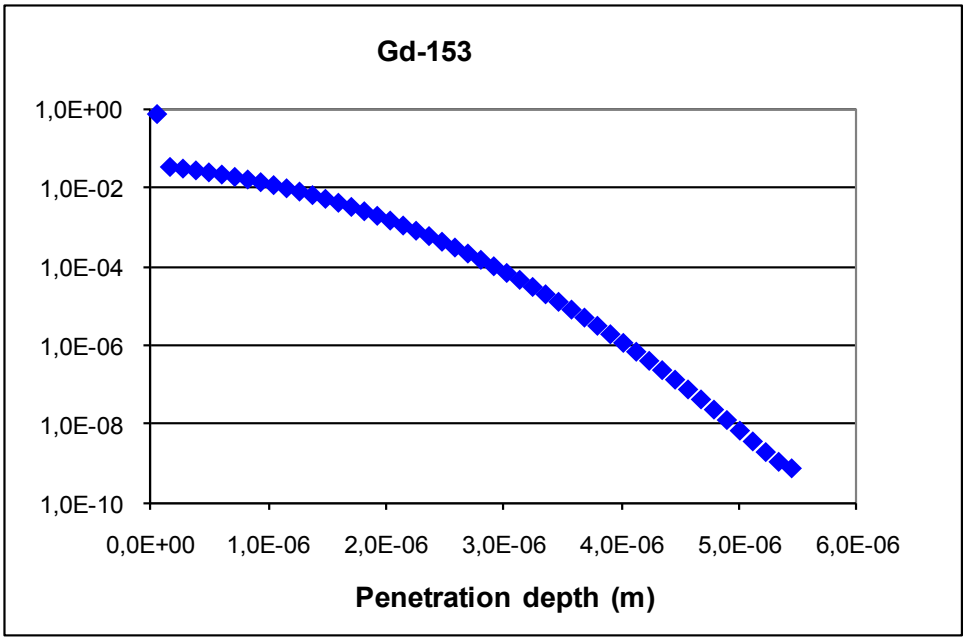

Figure A11-22. *^{153}Gd estimations, sorption addressed by only using both a K_d and a K_a.*

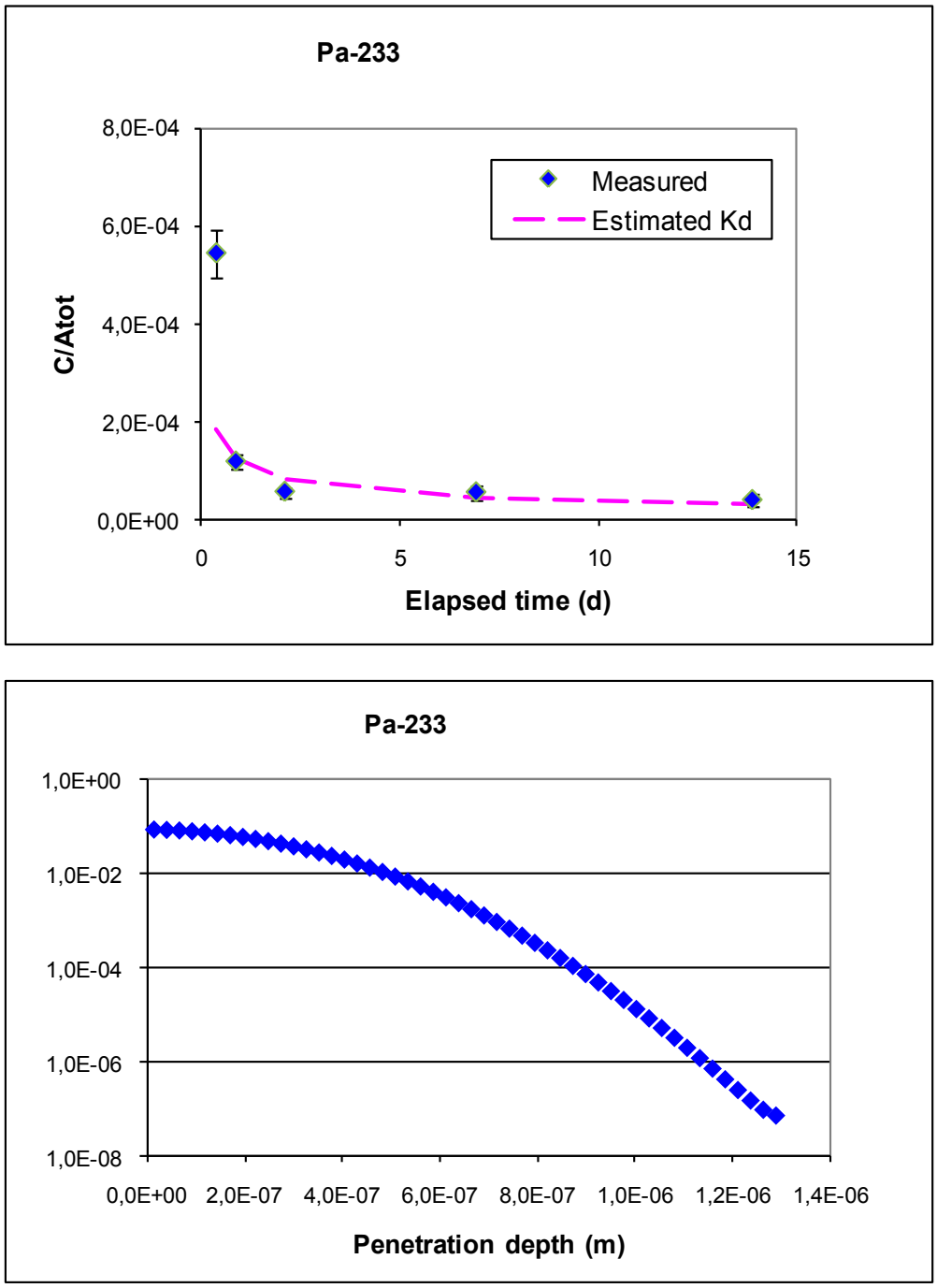

Figure A11-23. *^{233}Pa estimations, sorption addressed by only using a K_d.*

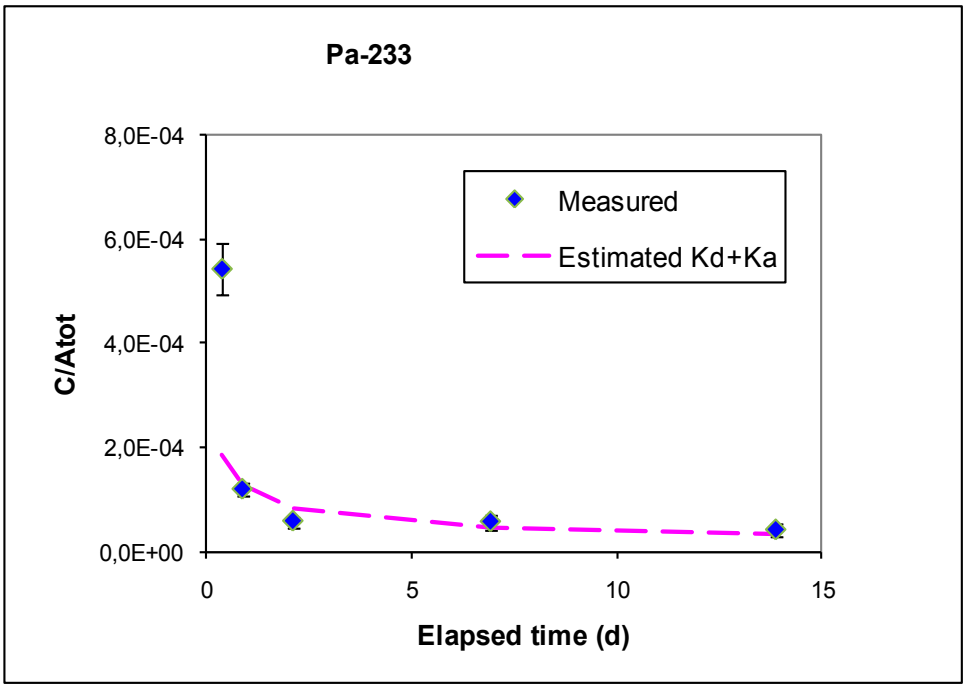

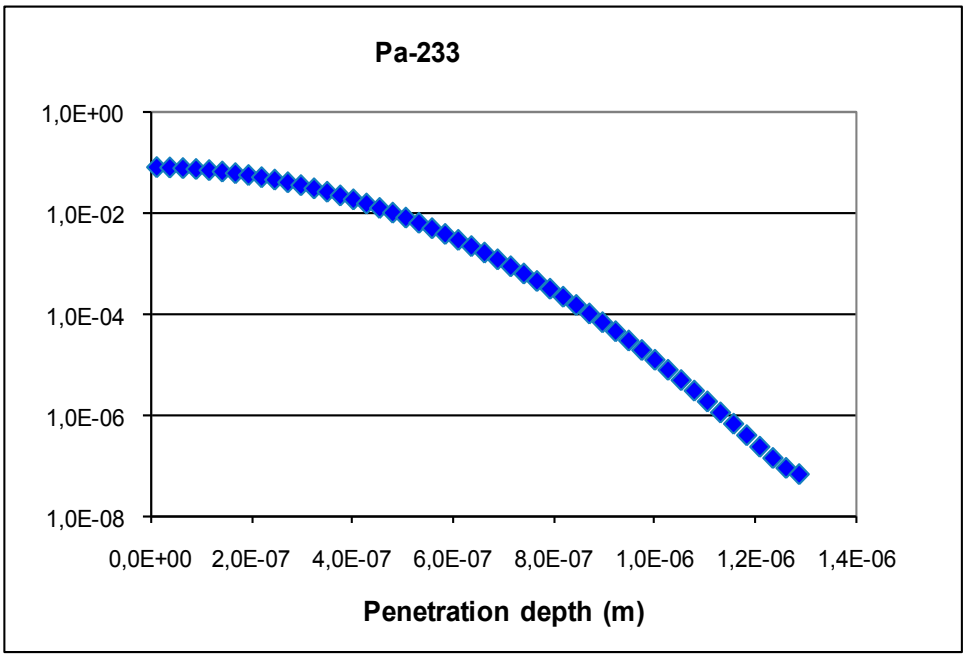

Figure A11-24. *^{233}Pa estimations, sorption addressed by only using both a K_d and a K_a.*

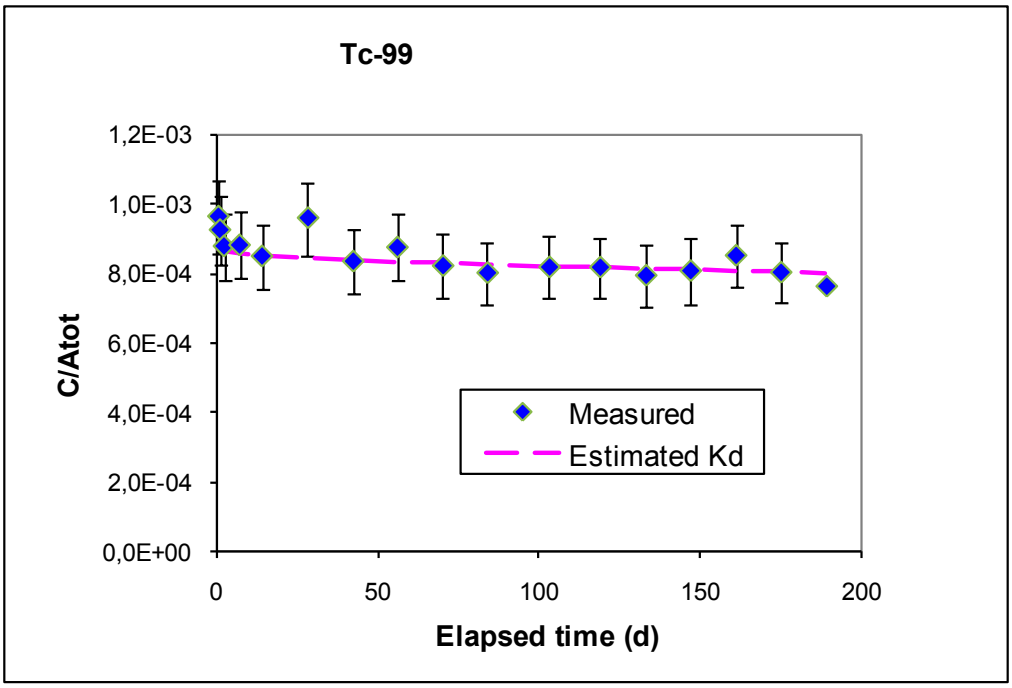

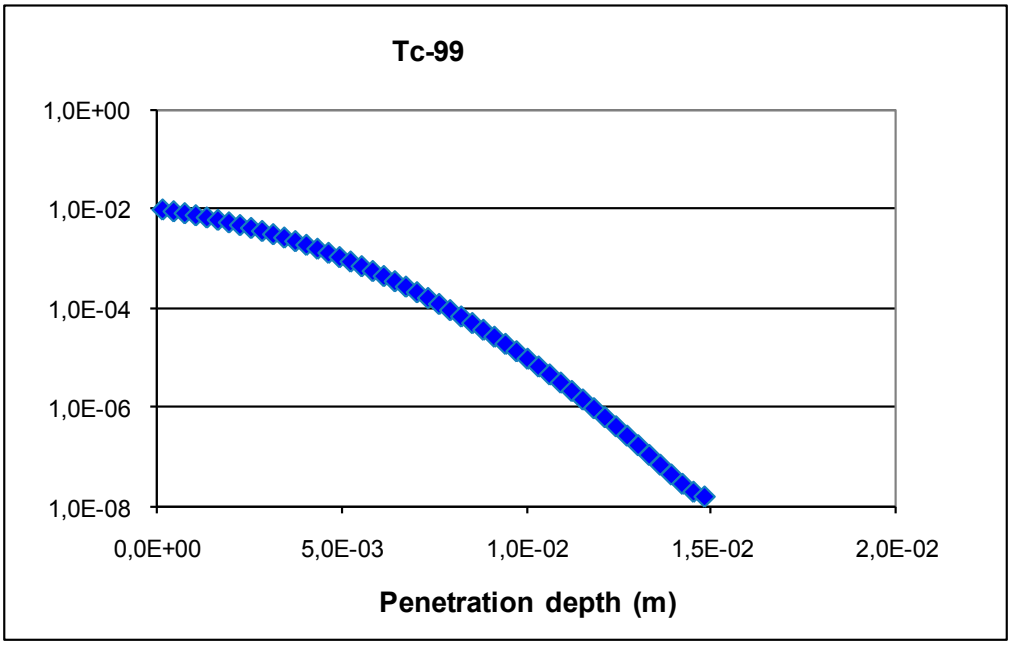

Figure A11-25. *^{99}Tc estimations, sorption addressed by only using a K_d.*

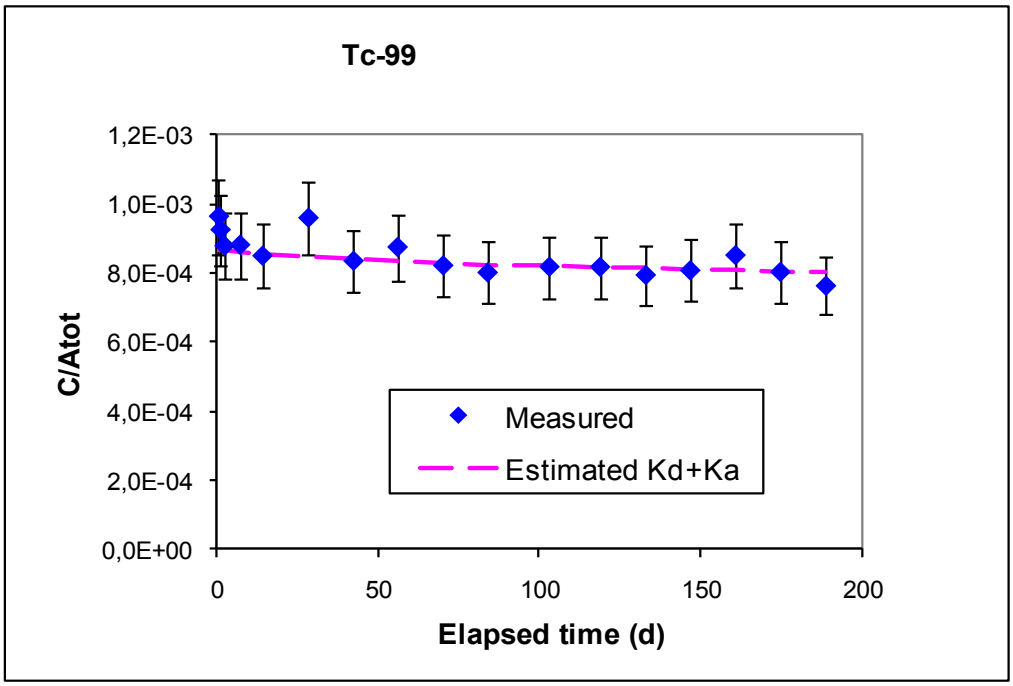

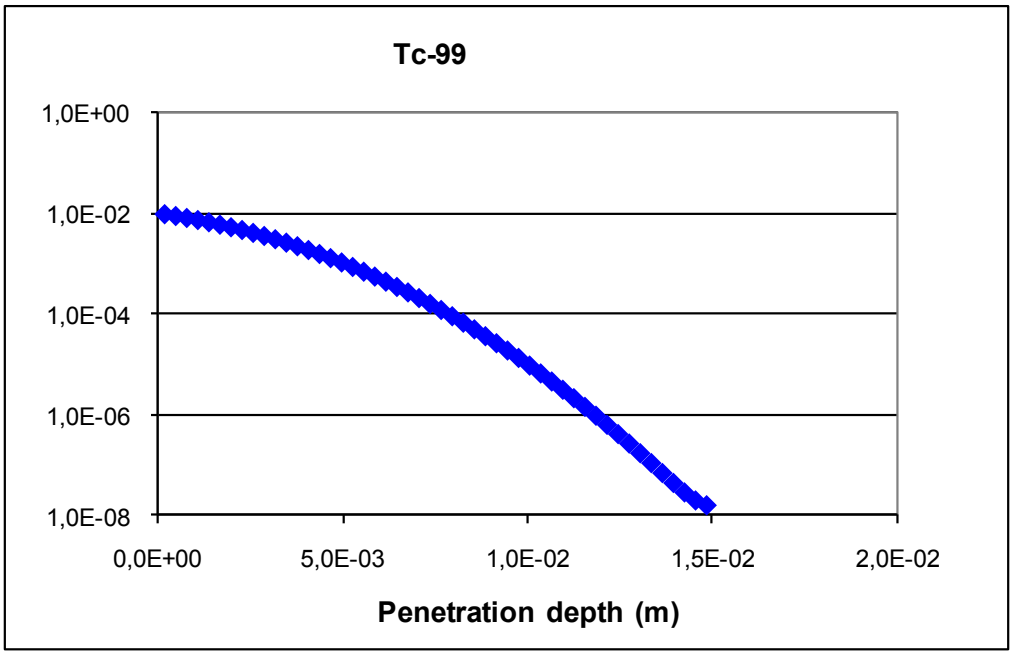

Figure A11-26. *^{99}Tc estimations, sorption addressed by only using both a K_d and a K_a.*

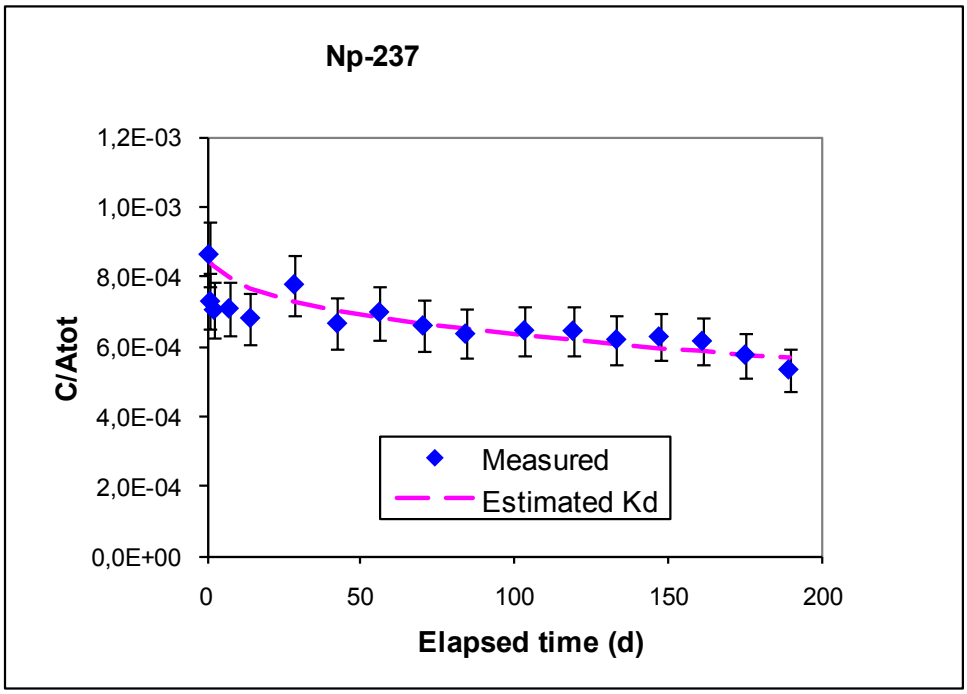

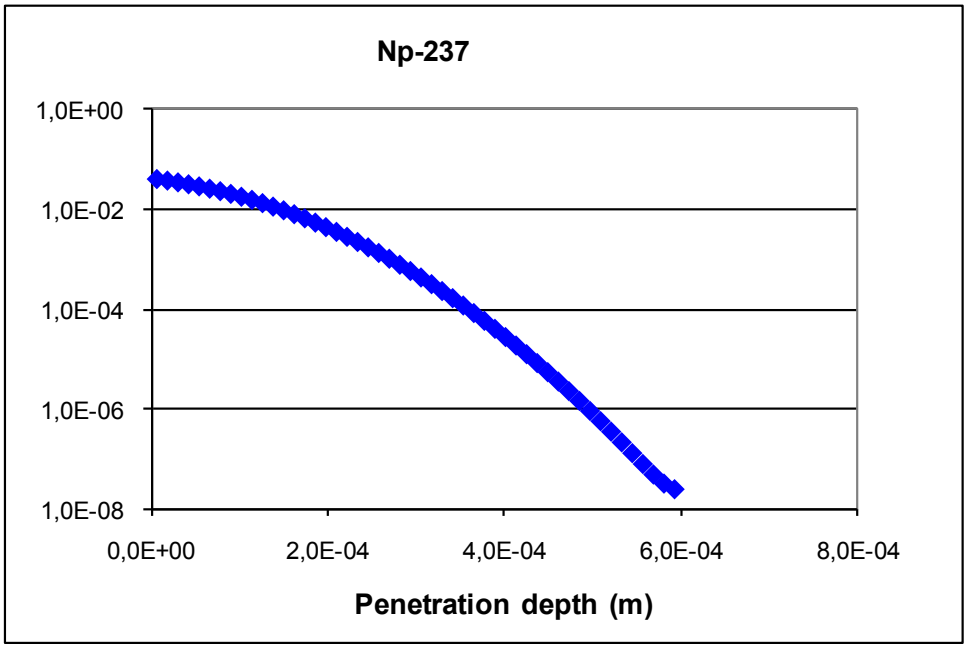

Figure A11-27. *^{237}Np estimations, sorption addressed by only using a K_d.*

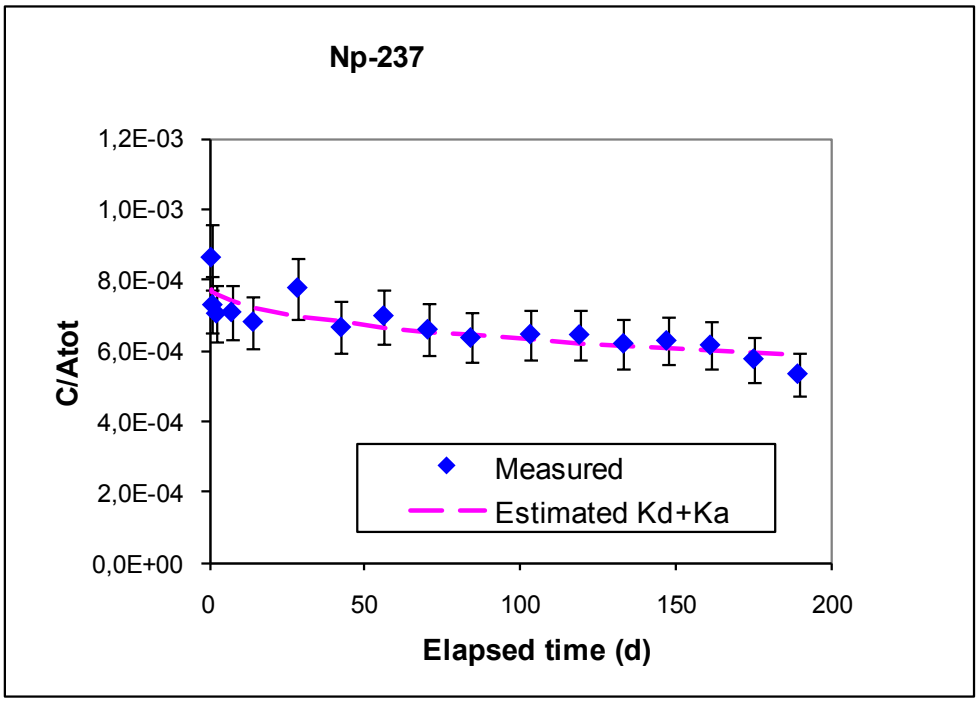

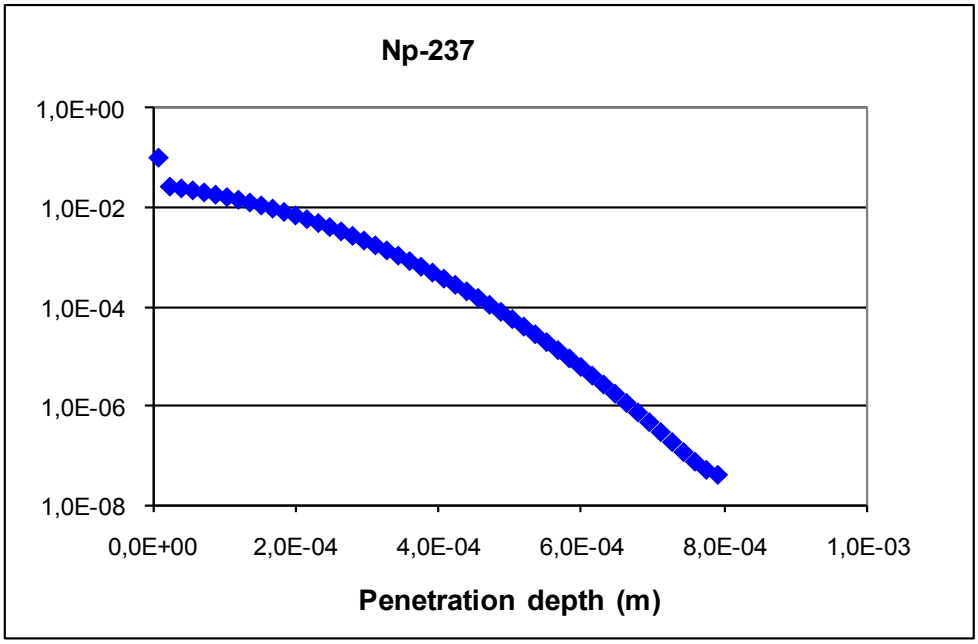

Figure A11-28. *^{237}Np estimations, sorption addressed by only using both a K_d and a K_a.*

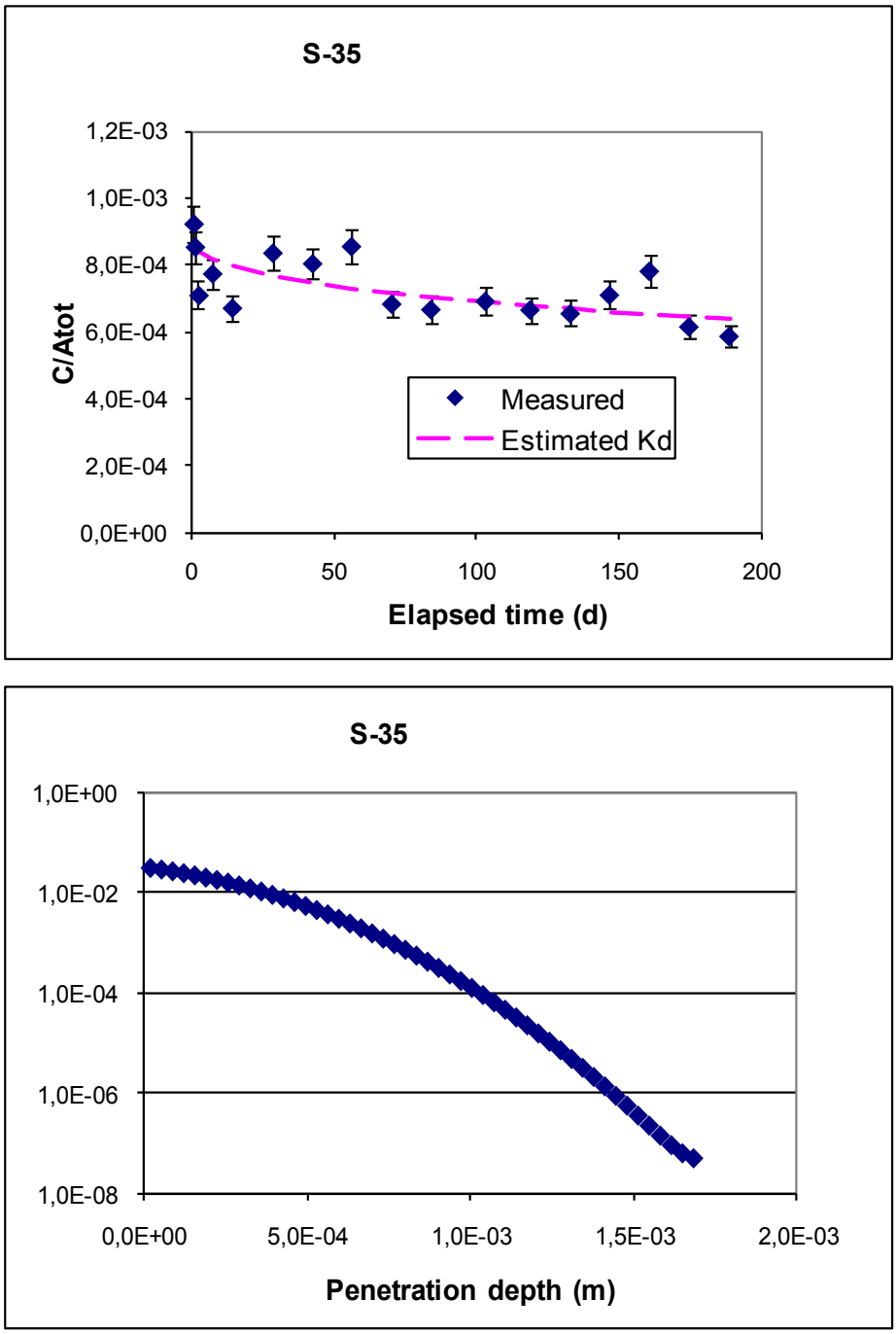

Figure A11-29. *^{35}S estimations, sorption addressed by only using a K_d.*

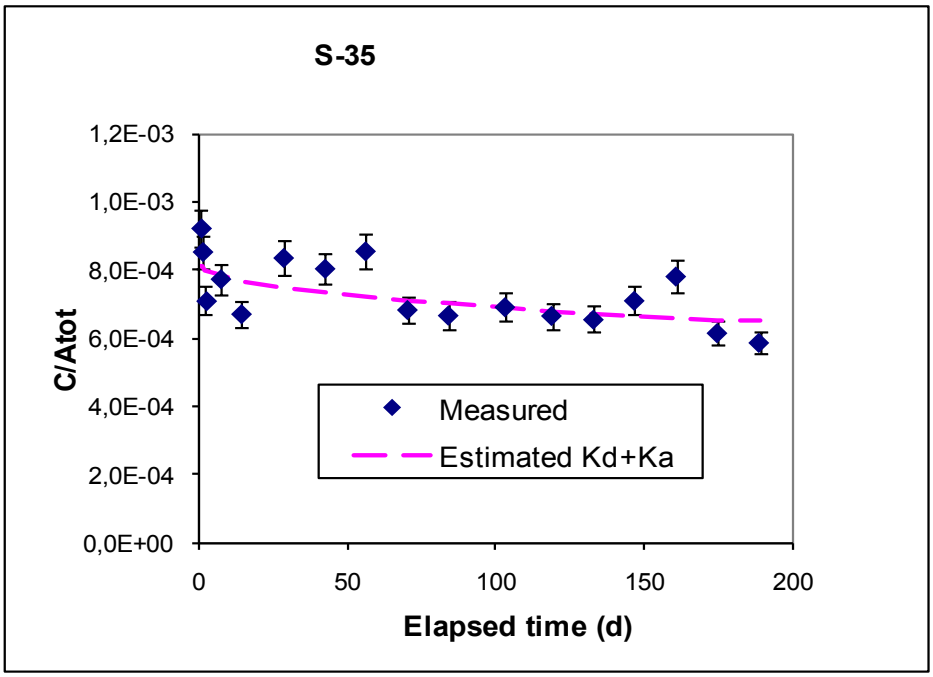

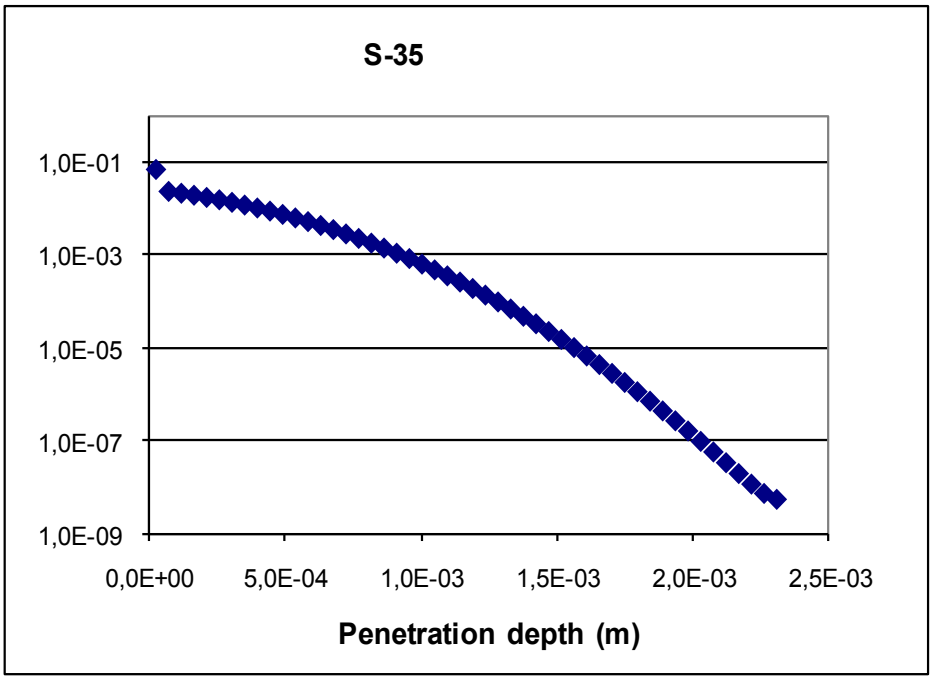

Figure A11-30. *^{35}S estimations, sorption addressed by only using both a K_d and a K_a.*

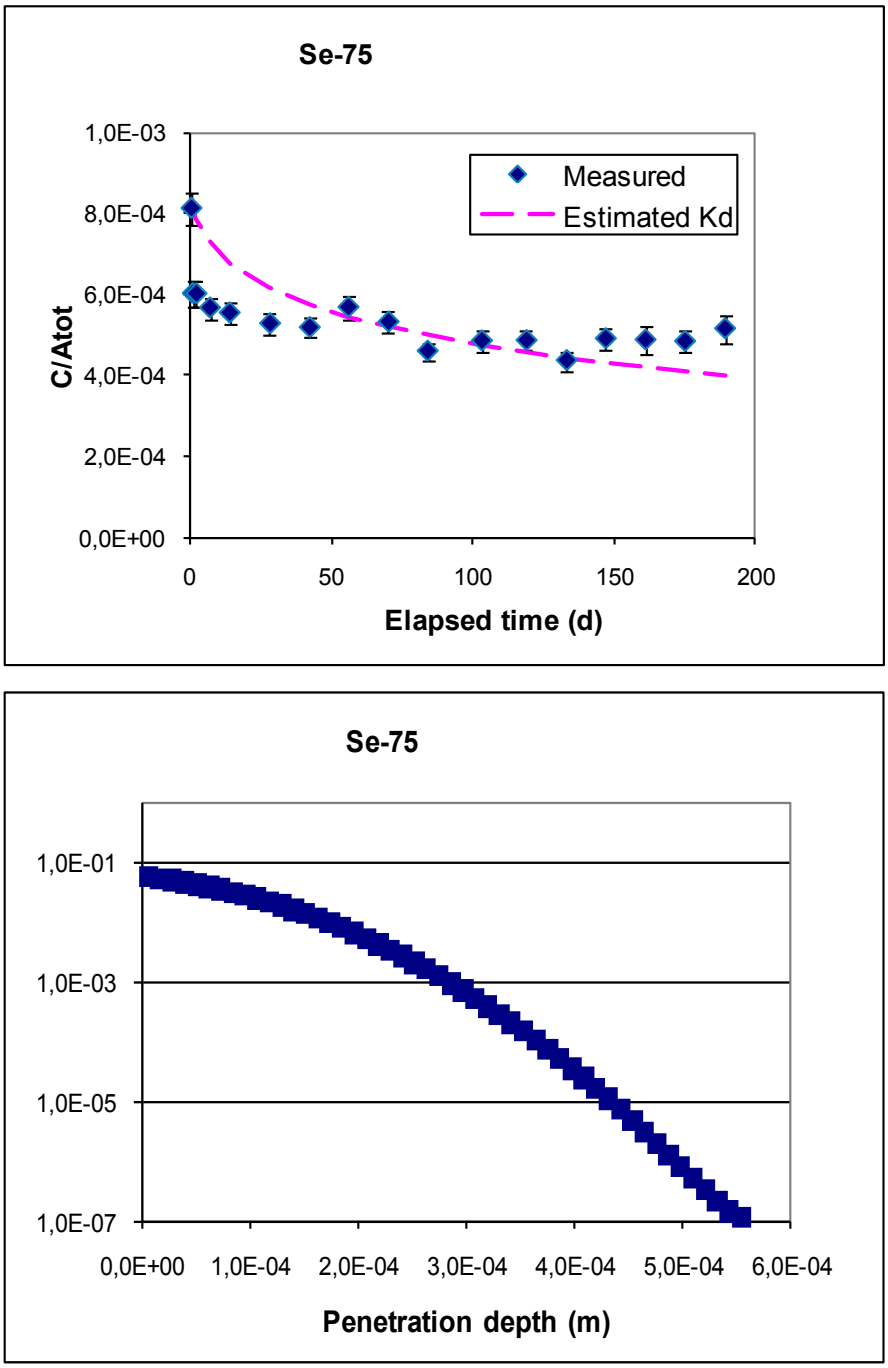

Figure A11-31. *^{75}Se estimations, sorption addressed by only using a K_d.*

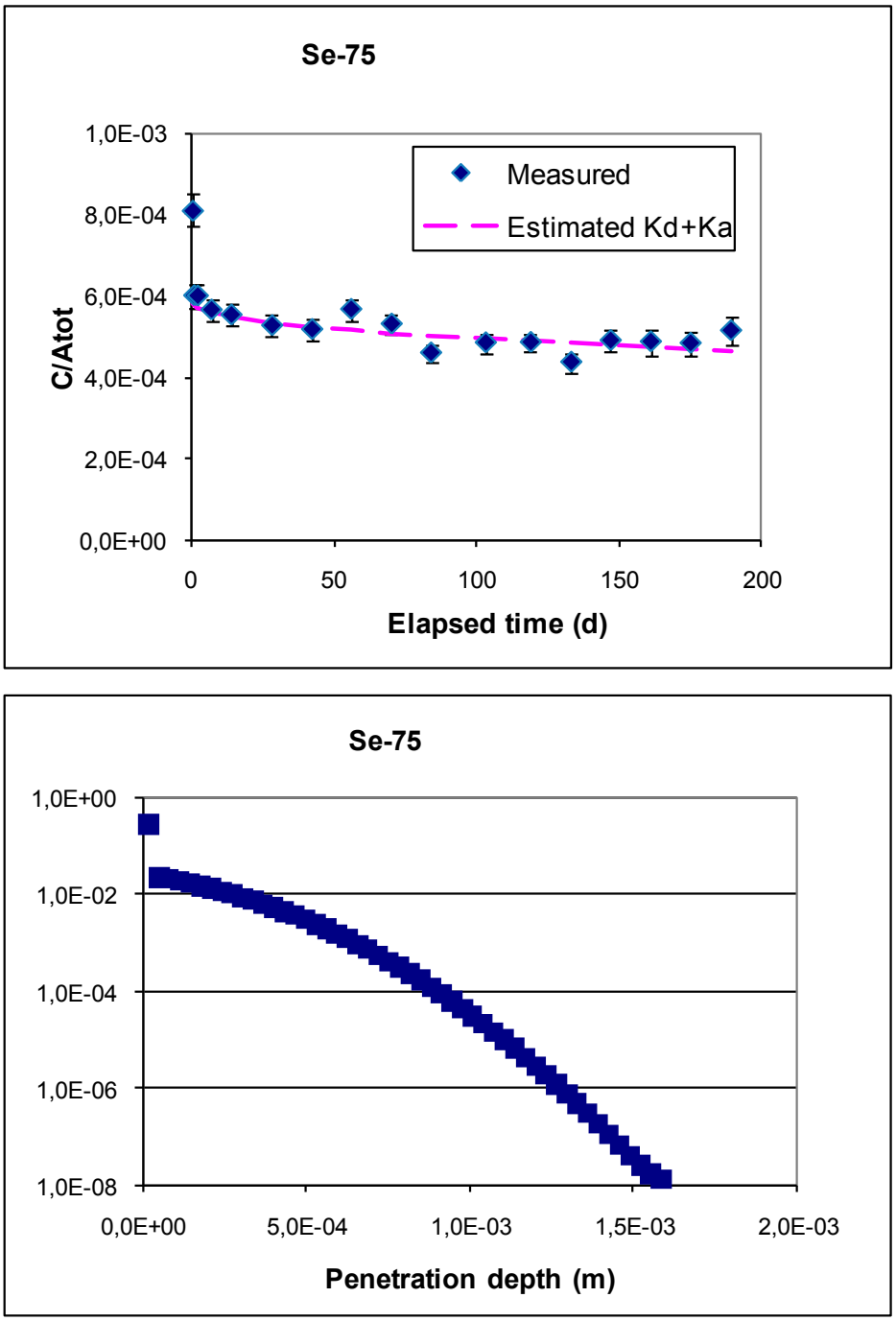

Figure A11-32. *^{75}Se estimations, sorption addressed by only using both a K_d and a K_a.*

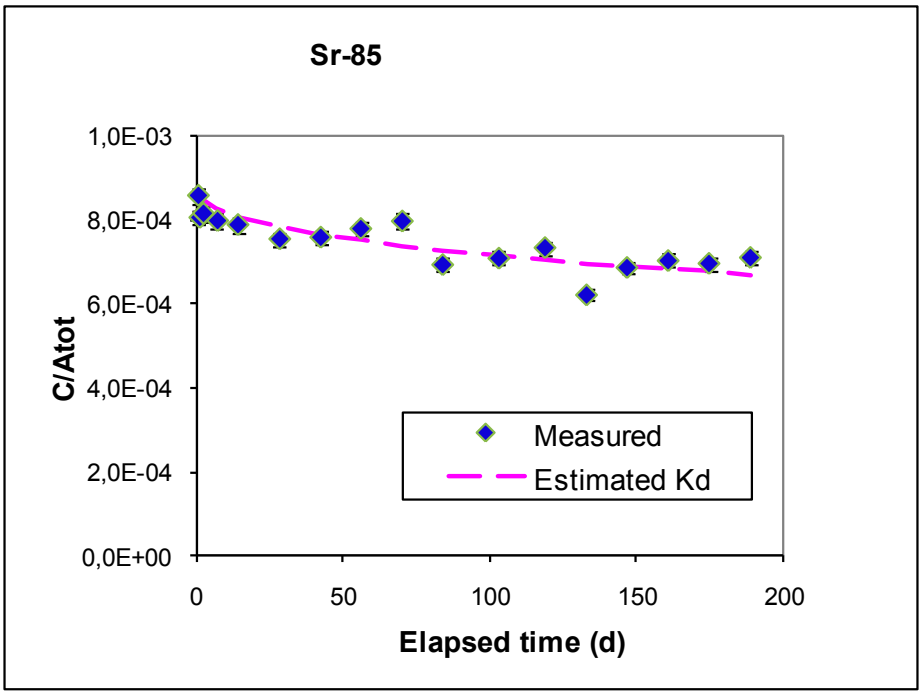

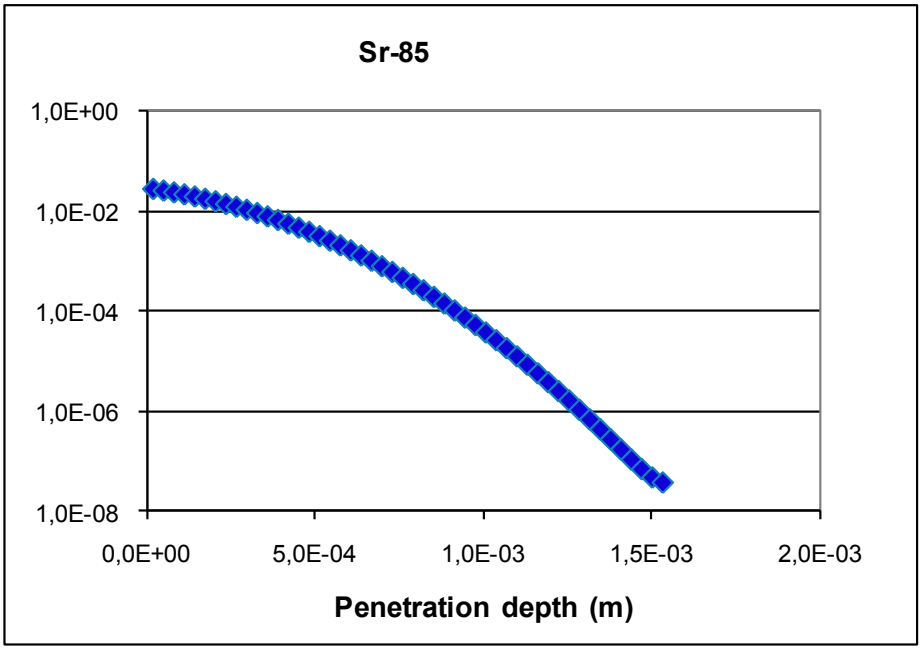

Figure A11-33. *^{85}Sr estimations, sorption addressed by only using a K_d.*

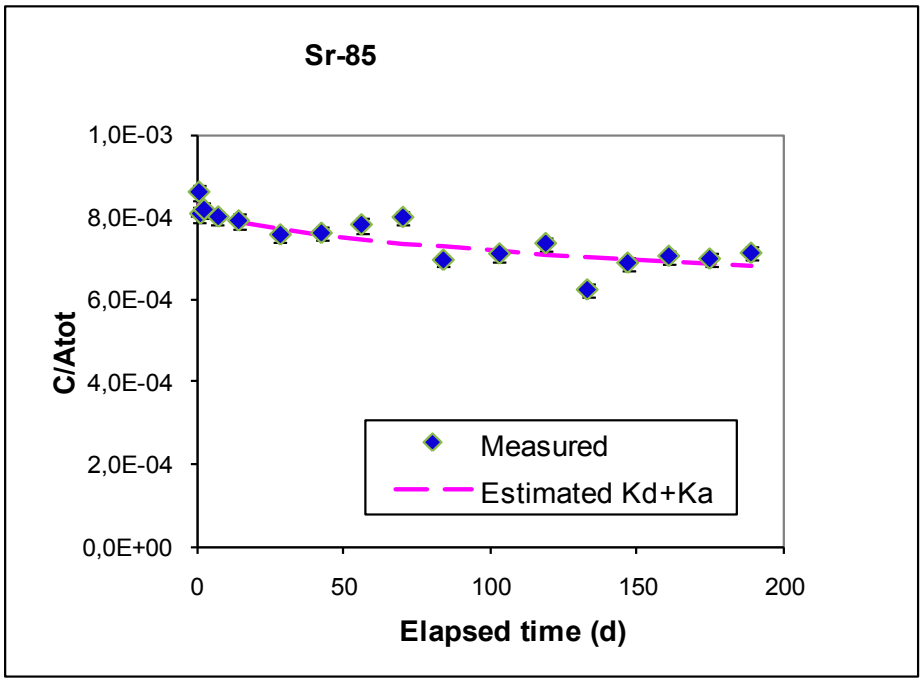

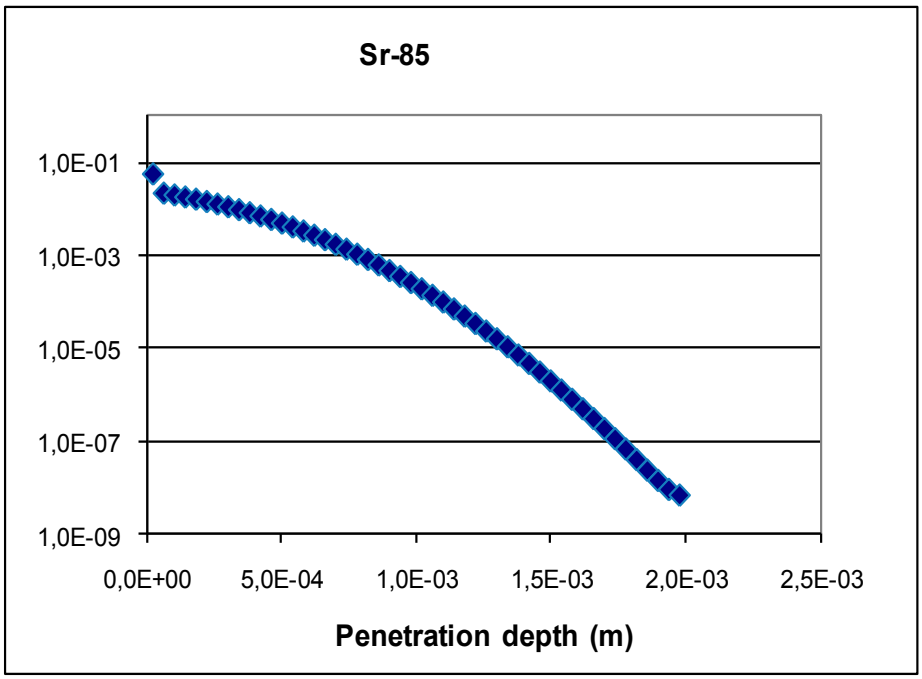

Figure A11-34. *^{85}Sr estimations, sorption addressed by only using both a K_d and a K_a.*

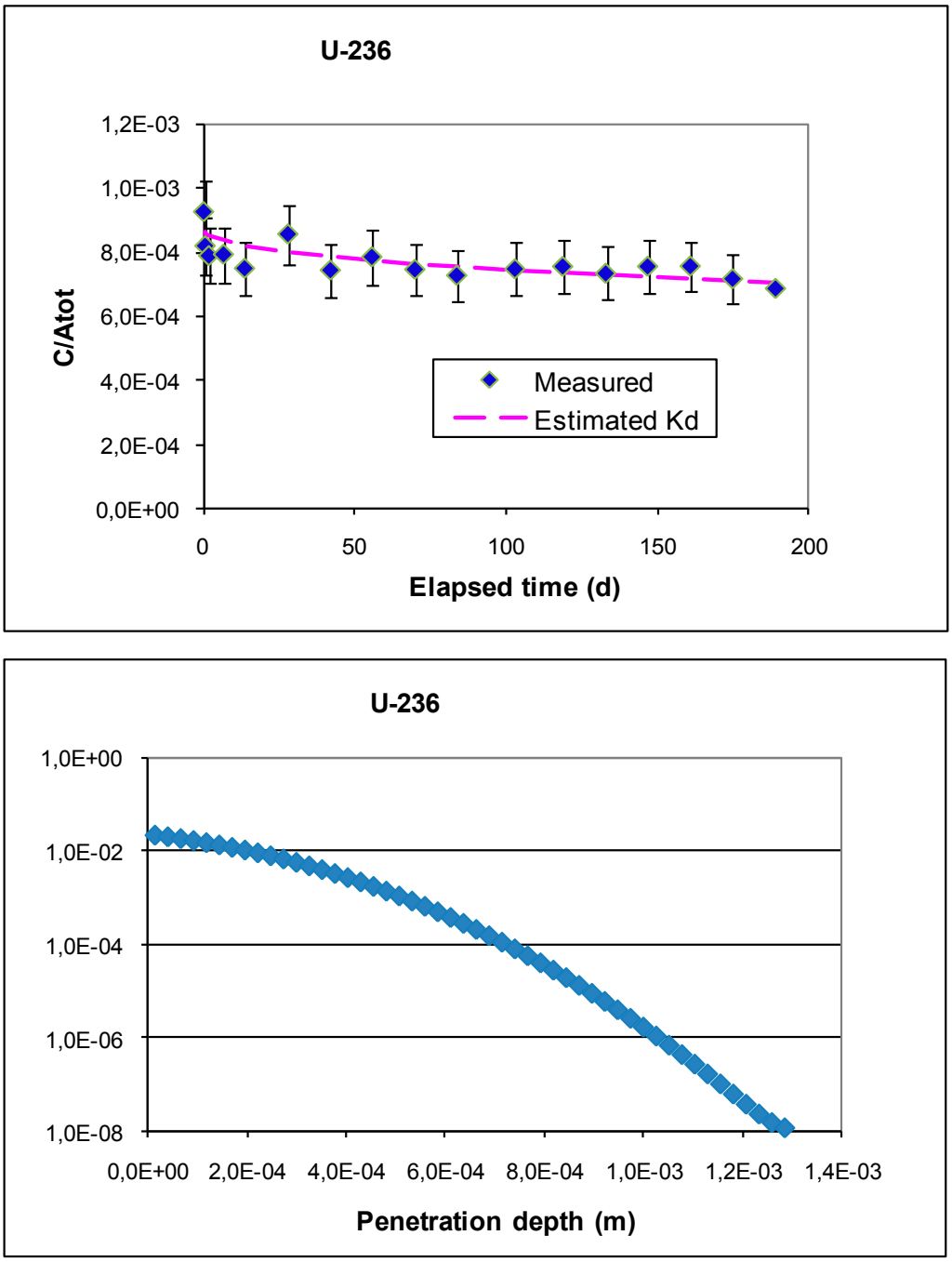

Figure A11-35. *^{236}U estimations, sorption addressed by only using a K_d.*

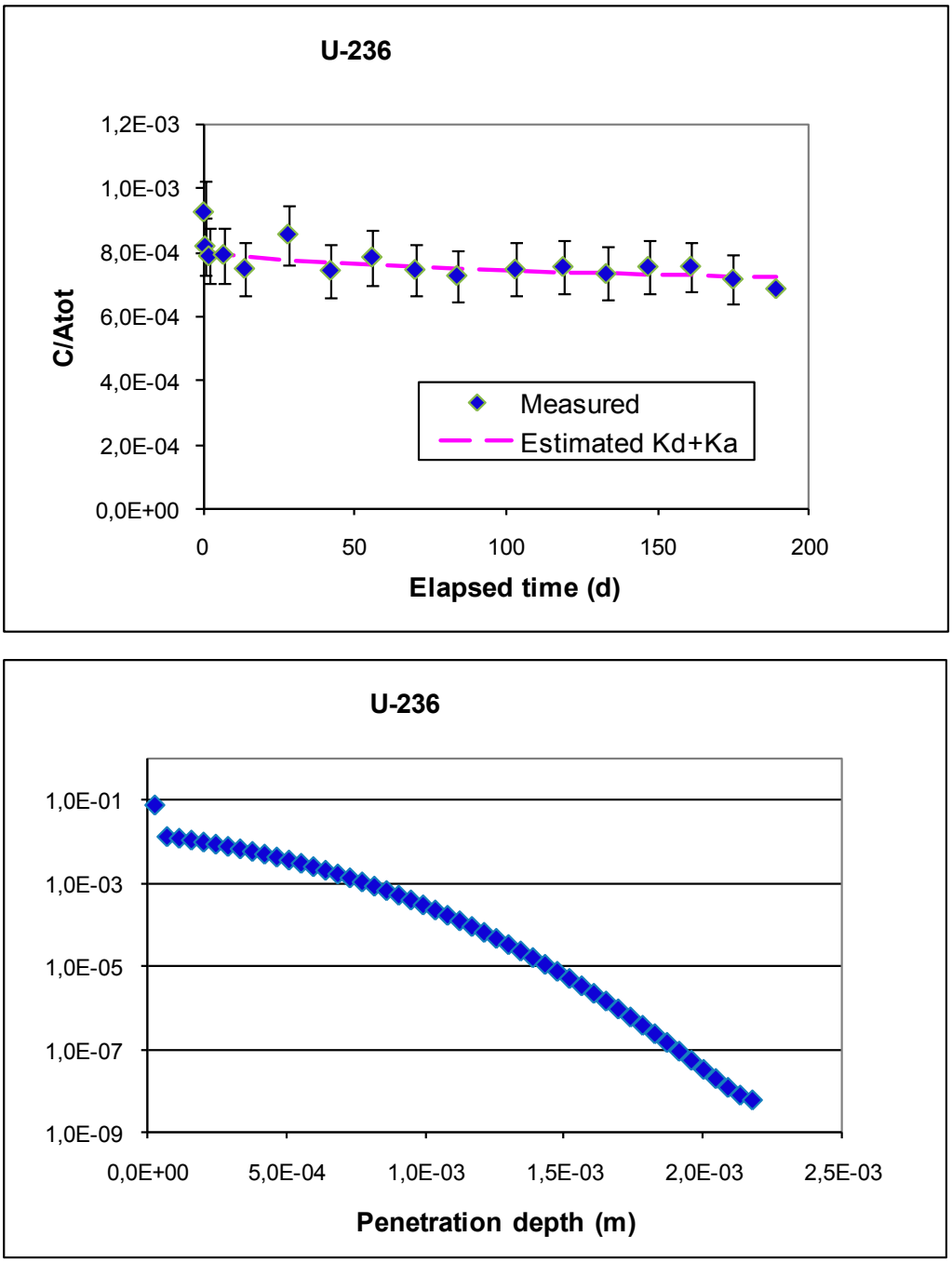

Figure A11-36. *^{236}U estimations, sorption addressed by only using both a K_d and a K_a.*